Molecular Characterisation of the Candidate Region for *bronx waltzer* : a Mouse Model of Hearing Impairment

Amy Taylor

Thesis submitted to the University of Nottingham for the degree of Doctor of Philosophy

September 2005

Wellcome Trust Sanger Institute
Wellcome Trust Genome Campus
Hinxton
Cambridge
CB10 1SA

Declaration

I declare that this thesis is the result of my own work and has not, whether in the same or different form, been presented to this or any other university in support of an application for any degree other than that for which I am now a candidate

Acknowledgements

First and foremost my thanks go to my supervisor Karen Steel. Thank you for giving me the opportunity to carry out this research, for your advice, guidance and support throughout, as well as for your life-saving "open-door" policy. If I ever work for anyone half as skilful, as dedicated, as assertive and yet as compassionate as you I shall consider myself very lucky.

I owe so much gratitude to so many of my labmates that I hardly know where to begin. Actually that's a lie, of course I have to start with Sarah. From being my sole companion when we moved from Nottingham, through reassuring me and listening to me (and occasionally even feeding me!) during the "lost months" of writing up, right up to *voluntarily* reading and commenting on my *entire* thesis – you have been more than I ever wished for or deserved in a friend. The rest of Team 27 have all helped to keep me sane in their own ways, but I am especially grateful to Andy Penn for his help with the vast number of PCR reactions required to resequence all my candidate gene exons.

I would also like to thank the members of the "old lab" at the IHR in Nottingham, in particular Alex Erven, Liz Quint, Kelvin Hawker, Ralph Holme and Angela Lucas for patiently teaching me the techniques and ways of the lab, as well as Kathy Davies and Neil Glenn for taking such excellent care of my crazy little mice. Going even further back, my thanks go to the people who worked on various aspects of this exciting project before me – Tracy Bussoli, Mikey Cheong, Annemarie Kelly and Claudia Noguiera.

For assistance with my zebrafish work I thank Derek Stemple, Matthew Clark, Elizabeth Busch and Christian Söllner, as well as Agnieszka Rzadzinska for help with phalloidin staining and using the confocal microscope. I also thank the ExoSeq and Sequencing groups for help with exon resequencing.

Finally, I am deeply indebted to my family, who are almost but not entirely as crazy as my mice, and to whom this thesis is dedicated. To Grandma and Grandad, to Nanna and Mossy, and to my parents Debby and Jeff who have always supported me unwaveringly in everything I've wanted to do, so long as they believed it would make me happy. Well, making you proud will make me happy. To the imminently future Dr. Keith Taylor: "Ha! I did it first!", and to the possibly future Dr. Aidan Taylor: "Are you *really* sure you want to put yourself through this?!" I love you all so very much. xxx

Abbreviations

ABR	Auditory brainstem response
AHCs	Auditory hair cells
BAC	Bacterial artificial chromosome
bHLH	basic Helix Loop Helix
BLAST	Basic local alignment search tool
bp	Base pairs
CAPs	Compound action potentials
cDNA	Complementary DNA
cM	centiMorgan
CMs	Cochlear microphonics
CO_2	Carbon dioxide
dATP	2'-deoxyadenosine-5'-triphosphate
dbSPL	Decibels sound pressure level
dCTP	2'-deoxycytidine-5'-triphosphate
ddH_2O	Double distilled deionised water
dGTP	2'-deoxyguanosine-5'-triphosphate
DMSO	Dimethyl sulfoxide
DNA	Deoxyribonucleic acid
dNTP	Deoxynucleoside triphosphate
dpc	days *post coitum*
dpf	days post fertilisation
DPOEs	Distortion product otoacoustic emissions

ds	Double stranded
dTTP	2'-deoxythymidine-5'-triphosphate
E	Embryonic day
EDTA	Ethylenediaminetetraacetic acid
EMBL	European molecular biology laboratory
ENU	N-ethyl-N-nitrosourea
ESTs	Expressed sequence tags
EUCIB	European collaborative interspecific backcross mapping panels
g	Grams
GER	Greater epithelial ridge
HCl	Hydrochloric acid
HMM	Hidden Markov model
hpf	hours post fertilisation
HPLC	High performance liquid chromatography
HTGS	High throughput genome sequence
IHCs	Inner hair cells
IVF	*in vitro* fertilisation
K^+	Potassium ion
Kb	Kilobase
L	Litres
LB	Luria-Bertani medium
LER	Lesser epithelial ridge
LOD	Log of odds
Mb	Megabase
mg	milligrams

$MgCl_2$	Magnesium chloride
ml	millilitres
MO	Morpholino oligonucleotide
MRC	Medical Research Council
mRNA	Messenger RNA
Na^+	Sodium ion
NaCl	Sodium chloride
NaOH	Sodium hydroxide
NCBI	National center for biotechnology information
OD	Optical density
OHCs	Outer hair cells
OMIM	Online Mendelian Inheritance in Man
OTOTO	Osmium tetroxide-thiocarbohydrazide procedure
P	Post-natal day
PBS	Phosphate buffer saline solution
PCR	Polymerase chain reaction
pg	picograms
pH	potential of Hydrogen
QTL	Quantitative trait locus
RFLP	Restriction fragment length polymorphism
RNA	Ribonucleic acid
RNAi	RNA interference
RNase	Ribonuclease
rpm	Revolutions per minute
RT-PCR	Reverse transcription-PCR

s.e.	standard error
SCs	Supporting cells
SDS	Sodium dodecyl sulphate
SEM	Scanning electron microscopy/microscope
SNP	Single nucleotide polymorphism
SPs	Summating potentials
ss	Single stranded
SSCP	Single strand conformation polymorphism
ssDNA	Single stranded DNA
SSLP	Simple sequence length polymorphisms (microsatellites)
STS	Sequence tagged sites
T0.1E	10mM Tris/0.1mM EDTA buffer
TBE	Tris/borate/EDTA buffer
TE	10mM Tris/1mM EDTA buffer
TEM	Transmission electron microscopy/microscope
Tris	Tris(hydroxymethyl)aminomethane
U	Enzyme units
μg	micrograms
μl	microlitres
μm	micrometre
UTR	Untranslated region
UV	Ultraviolet
WGS	Whole genome shotgun
YAC	Yeast artificial chromosome

Table of Contents

Declaration ..... **ii**

Acknowledgements ..... **iii**

Abbreviations ..... **iv**

Table of Contents ..... **viii**

Abstract **1**

CHAPTER 1: GENERAL INTRODUCTION **2**

1.1 Functional anatomy of the ear **4**

1.1.1 The auditory system *4*
1.1.1.1 The external ear 5
1.1.1.2 The middle ear 5
1.1.1.3 The inner ear 7

1.1.2 The cochlea *8*
1.1.2.1 The organ of Corti 10
1.1.2.2 Auditory transduction 12

1.1.3 The vestibular system *13*
1.1.3.1 The semicircular canals 13
1.1.3.2 The otolithic organs 14

1.2 Development of the ear **16**

1.2.1 Development of the external ear *16*

1.2.2 Development of the middle ear *16*

1.2.3 Development of the inner ear *16*
1.2.3.1 Development of the organ of Corti 20
1.2.3.2 Development of hair cell stereocilia 21
1.2.3.3 Development of the semicircular canals 21
1.2.3.4 Development of the maculae 23
1.2.3.5 Development of the cupulae and cristae ampullares 23
1.2.3.6 Genetics of hair cell development 24

1.3 Pathology of deafness **27**

1.3.1 Pathology of the auditory system *27*
1.3.1.1 Morphogenetic defects 27
1.3.1.2 Cochleosaccular defects 28
1.3.1.3 Neuroepithelial defects 28

1.3.2 The mouse as a model in hearing research *29*

1.4 The bronx waltzer (*bv*) mouse mutant **30**

1.4.1 Electrophysiology of bronx waltzer *30*
1.4.1.1 Round window response recordings 30
1.4.1.2 Auditory brainstem recordings 32
1.4.1.3 Otoacoustic emissions 32

1.4.2 Ultrastructural studies of the bronx waltzer inner ear *33*
1.4.2.1 Ultrastructural studies of the cochlea 33
1.4.2.2 Ultrastructural studies of the vestibular system 35

1.4.3 Cochlear innervation in bronx waltzer *38*

1.4.4 Previous mapping of the bronx waltzer mutation *38*
1.4.4.1 Genetic mapping of the bv locus 38
1.4.4.2 Physical mapping of the *bv* locus 40

1.5 This thesis 41

CHAPTER 2: GENERAL MATERIALS AND METHODS 42

2.1 Mice 43

2.2 DNA preparation from tissue 43

2.3 Estimating nucleic acid concentrations 44

2.4 Polymerase Chain Reaction 45

2.4.1 Design and synthesis of oligonucleotides for PCR *45*

2.4.2 General PCR protocols *46*

2.5 Agarose gel electrophoresis 48

2.6 RNA preparation 49

2.7 Reverse transcription 50

2.8 DNA sequencing 51

CHAPTER 3: REFINEMENT OF THE BV CRITICAL REGION USING THE EXISTING BACKCROSS 54

3.1 Introduction 55

3.1.1 Genetic mapping *55*
3.1.1.1 Establishing a backcross 56
3.1.1.2 Haplotype analysis 58
3.1.1.3 Markers for genetic mapping 58
3.1.1.4 Phenotypic analysis 60

3.1.2 The existing bv/101 genetic map *61*

3.1.3 Identifying new markers *64*

3.1.4 Previous physical mapping *64*

3.2 Methods 66

3.2.1 Bacterial Artificial Chromosomes (BACs) *66*

3.2.1.1 Storage of BAC clones 69
3.2.1.2 Preparation of plasmid DNA from BAC clones 69
3.2.1.3 Building a BAC contig to span the region 70

3.2.2 Investigating potential new polymorphisms 71
3.2.2.1 Mouse SNP Database 71
3.2.2.2 Sequence sampling 72
3.2.2.3 Tandem repeats 72
3.2.2.4 SNPs from published sequence 73

3.3 Results 75

3.3.1 A physical map of the bronx waltzer candidate region 75
3.3.1.1 Placement of genetic mapping markers 77
3.3.1.2 Estimating the physical size of the region 79

3.3.2 Identifying new polymorphic markers 80
3.3.2.1 Publicly available SNPs 80
3.3.2.2 Sequence sampling 84
3.3.2.3 Tandem repeat sequences 97
3.3.2.4 SNPs from published sequence 99

3.4 Discussion 103

CHAPTER 4: A NEW INTRASPECIFIC INTERCROSS TO NARROW THE BRONX WALTZER CRITICAL REGION 107

4.1 Introduction 108

4.1.1 Choosing an outcross strain 108

4.1.2 Choosing a breeding strategy 109

4.2 Methods 114

4.2.1 Inbred strain DNA 114

4.2.2 Microsatellite markers 115

4.2.3 Phenotyping F_2 intercross offspring 115

4.2.4 Tissue collection 116

4.3 Results 117

4.3.1 Strain selection 117

4.3.2 An intraspecific intercross 122
4.3.2.1 Statistical analysis 124
4.3.2.2 Genotyping F_2 mice 124

4.4 Discussion 128

4.4.1 Strain selection 128

4.4.2 The origins of the bronx waltzer genetic background 129

4.4.3 Transmission ratio analysis 130

4.4.4 Interpretation of intercross data 132

CHAPTER 5: ASSESSMENT OF GENES LOCATED WITHIN THE CANDIDATE REGION 135

5.1 Introduction 136

5.1.1 What makes a good candidate gene? 136
5.1.1.1 A potential role in pathways known to be required for hearing 137
5.1.1.2 Expression in the inner ear during development 141
5.1.1.3 The eye and the ear 143

5.1.2 Assessing genes with known or predicted functions 145

5.1.3 Assessing novel and predicted genes 145

5.2 Methods 147

5.2.1 Data mining of inner ear expression databases 147

5.2.2 Expression studies using inner ear cDNA 149
5.2.2.1 Obtaining inner ear cDNA 149
5.2.2.2 Primers designed for amplification from cDNA 149
5.2.2.3 PCR from cDNA 153

5.3 Results 154

5.3.1 Assessment of previously characterised genes 154

5.3.2 Gene expression in the inner ear – published data 161

5.3.3 Gene expression in the inner ear – RT-PCR data 165

5.4 Discussion 176

5.4.1 Analysis of inner ear expression data 176
5.4.1.1 Inner ear expression databases 176
5.4.1.2 RT-PCR data 178

5.4.2 Assessment of candidacy based on the evidence gathered 181

5.4.3 Selection of candidate genes for further analysis 188

CHAPTER 6: GENE KNOCKDOWN IN ZEBRAFISH AS AN ASSESSMENT OF CANDIDATE GENE FUNCTION 187

6.1 Introduction 188

6.1.1 The zebrafish ear 189

6.1.2 Hearing and vestibular phenotypes in zebrafish 192

6.1.3 Conservation of function in the mouse and the zebrafish 193

6.1.4 Disrupting gene function in zebrafish 195

6.1.5 Morpholinos 196
6.1.5.1 Advantages of morpholinos 197
6.1.5.2 Blocking translation (targeting start sites) 199
6.1.5.3 Blocking nuclear processing (targeting splice junctions) 201

6.2 Methods 204

6.2.1 Selection of target genes 204

6.2.2 Identification of orthologous genes *204*
6.2.2.1 Morpholinos targeted to start sites 205
6.2.2.2 Morpholinos targeted to splice junctions 205

6.2.3 Morpholino design *207*
6.2.3.1 Designing morpholinos to start sites 207
6.2.3.2 Designing morpholinos to splice junctions 207

6.2.4 Administration of morpholinos *208*
6.2.4.1 Morpholino preparation 208
6.2.4.2 Morpholino injection 210

6.2.5 Negative and positive controls *211*

6.2.6 Zebrafish *211*
6.2.6.1 Zebrafish oocytes 212

6.2.7 Assessment of phenotype *212*
6.2.7.1 Observing development 212
6.2.7.2 Assessing hearing and vestibular defects 213
6.2.7.3 Tissue collection 213
6.2.7.4 Phalloidin staining of actin bundles 213

6.3 Results 214

6.3.1 Orthologous genes *214*
6.3.1.1 Morpholinos targeted to start sites 214
6.3.1.2 Morpholinos targeted to splice junctions 216

6.3.2 Morpholino injections *219*
6.3.2.1 Morpholinos targeted to start sites 219
6.3.2.2 Morpholinos targeted to splice junctions 224
6.3.2.3 Phalloidin staining of actin bundles 229

6.4 Discussion 231

6.4.1 Analysis of negative and positive controls *231*
6.4.1.1 Negative control: injection of MO buffer 231
6.4.1.2 Positive control: injection of cadherin 23 morpholinos 232

6.4.2 Phalloidin staining of actin filaments *233*

6.4.3 Comparison of start site and splice site morpholinos *234*

6.4.4 Confirmation of splice-blocking MOs *236*

6.4.5 Conclusions *238*

CHAPTER 7: EXON RESEQUENCING OF GENES WITHIN THE BRONX WALTZER CANDIDATE REGION 242

7.1 Introduction 243

7.1.1 Large scale mutation detection *243*
7.1.1.1 WAVE analysis 244
7.1.1.2 High-throughput exon resequencing 245

7.1.2 The mouse genome sequence *246*
7.1.2.1 Sequence quality in the *bv* candidate region 247
7.1.2.2 Gene annotation 250

7.2 Methods **251**
7.2.1 Template DNA samples *251*
7.2.2 Large-scale primer design *253*
7.2.3 Nested PCR amplification *253*
7.2.4 Sequence analysis *255*

7.3 Results **256**
7.3.1 Sequence coverage *256*
7.3.2 Sequence polymorphisms *267*

7.4 Discussion **271**
7.4.1 Sequence coverage *271*
7.4.2 Candidacy of genes following re-sequencing *272*
7.4.3 Sequence polymorphisms *274*

CHAPTER 8: MODIFIERS OF THE BRONX WALTZER MUTATION **278**

8.1 Introduction **279**
8.1.1 Variability in the bronx waltzer phenotype *279*
8.1.2 A backcross to Mus castaneus *280*
8.1.3 Linkage analysis of behavioural trait modifiers *282*
8.1.4 Hair cells in backcross mutants *285*

8.2 Methods **287**
8.2.1 Phenotypic extremes *287*
8.2.2 Cochlear dissection *287*
8.2.3 Preparation of samples for scanning electron microscopy *288*
8.2.4 Hair cell counts *289*

8.3 Results **290**
8.3.1 Hair cells in backcross mutants *290*
8.3.2 Linkage analysis of hair cell modifiers *294*

8.4 Discussion **296**

CHAPTER 9: GENERAL DISCUSSION **299**

9.1 Summary of results **300**
9.1.1 Mapping and sequencing progress *300*
9.1.2 Critical evaluation of candidate genes *301*
9.1.2.1 Forkhead box protein N4 (*Foxn4*) 303
9.1.2.2 Myosin 1H (*Myo1h*) 303
9.1.2.3 Potassium channel tetramerization domain-containing 10 (*Kctd10*) .. 305

9.1.2.4 Ubiquitin protein ligase E3B (*Ube3b*) 306
9.1.2.5 Transient receptor potential cation channel V4 (*Trpv4*)..... 307
9.1.2.6 G protein-coupled receptor kinase- interactor 2 (*Git2*) 308
9.1.2.7 Calcium-binding protein 1 (*Cabp1*)..... 309
9.1.2.8 Dynein light chain 1, cytoplasmic (*Dnclc1*) 310
9.1.2.9 Paxillin (*Pxn*)..... 311
9.1.2.10 Citron (*Cit*) 313

9.1.3 Tissue specific expression 315

9.2 Further work..... 316

9.2.1 Further mapping..... 317

9.2.2 Further sequencing..... 317

9.2.3 Further expression studies 318

9.2.4 Gene knockdowns and knockouts..... 320

9.3 *Bronx waltzer* as a model of hereditary deafness 321

REFERENCES 323

APPENDICES ..... on data CD

Abstract

bronx waltzer is an autosomal recessive mouse mutation causing abnormalities in the inner ear which result in mutant mice having deficiencies in both the auditory and vestibular systems. Homozygous mice exhibit hyperactivity, circling behaviour, head tossing and failure to respond to sound. Hearing loss in these mice is due to degeneration of the inner hair cells in the organ of Corti, while the vestibular phenotype is a result of sensory hair cell degeneration in the maculae and cristae. This phenotype is visible from E17.5, shortly after the hair cells differentiate, making *bronx waltzer* an interesting model for the understanding of the molecular basis of development and function of the inner ear as well as for hereditary deafness.

The mutation was previously localised to a 2.8Mb region of chromosome 5 using a backcross of 1073 mice to the inbred strain 101/H. There remained 17 backcross mice with recombinations within this interval, and thus new polymorphic markers have been sought in order to reduce the size of the candidate region. With the identification of two new proximal flanking markers, the size of the critical region has been reduced to 2.45Mb, with the exclusion of seven candidate genes.

The remaining 52 genes currently annotated within the region have been systematically assessed and functional studies carried out on those thought most likely to be the causative agent for *bronx waltzer*. These have included expression screening using inner ear cDNA and gene knockdown using morpholinos designed to target zebrafish orthologs. In addition, large scale exon resequencing of all the coding regions within the interval has been carried out and 90.63% coverage achieved overall, with complete coding sequence obtained for 23 candidate genes. These new data have provided a means of critically evaluating the candidacy of genes within the *bronx waltzer* critical region.

Chapter 1:

General Introduction

CHAPTER 1

GENERAL INTRODUCTION

Deafness is the most common of the sensory disorders with approximately one in every 850 children born suffering a permanent hearing impairment (Fortnum *et al.* 2001), and progressive deafness affecting 16% of the adult population (Davis *et al.* 1995; Steel and Kros 2001). Syndromes which include deafness as part of their collection of symptoms also contribute to the number of people affected, with over 430 different syndromes currently listed in the Online Mendelian Inheritance in Man (OMIM) database.

A number of aetiologies can contribute to hearing impairment, including environmental factors, exposure to ototoxins, genetic effects and developmental complications. However, it is estimated that half of all instances of deafness can be attributed to a genetic cause (Resendes *et al.* 2001; Morton 2002). Thus the study of the genes involved in the molecular mechanisms of hearing not only has the potential of elucidating the pathways and interactions which operate within the auditory system allowing us to hear, but also of identifying candidates for deafness disorders.

1.1 FUNCTIONAL ANATOMY OF THE EAR

1.1.1 The auditory system

The mammalian peripheral auditory system is composed of three distinct parts, the outer ear, the middle ear and the inner ear (see Figure 1.1).

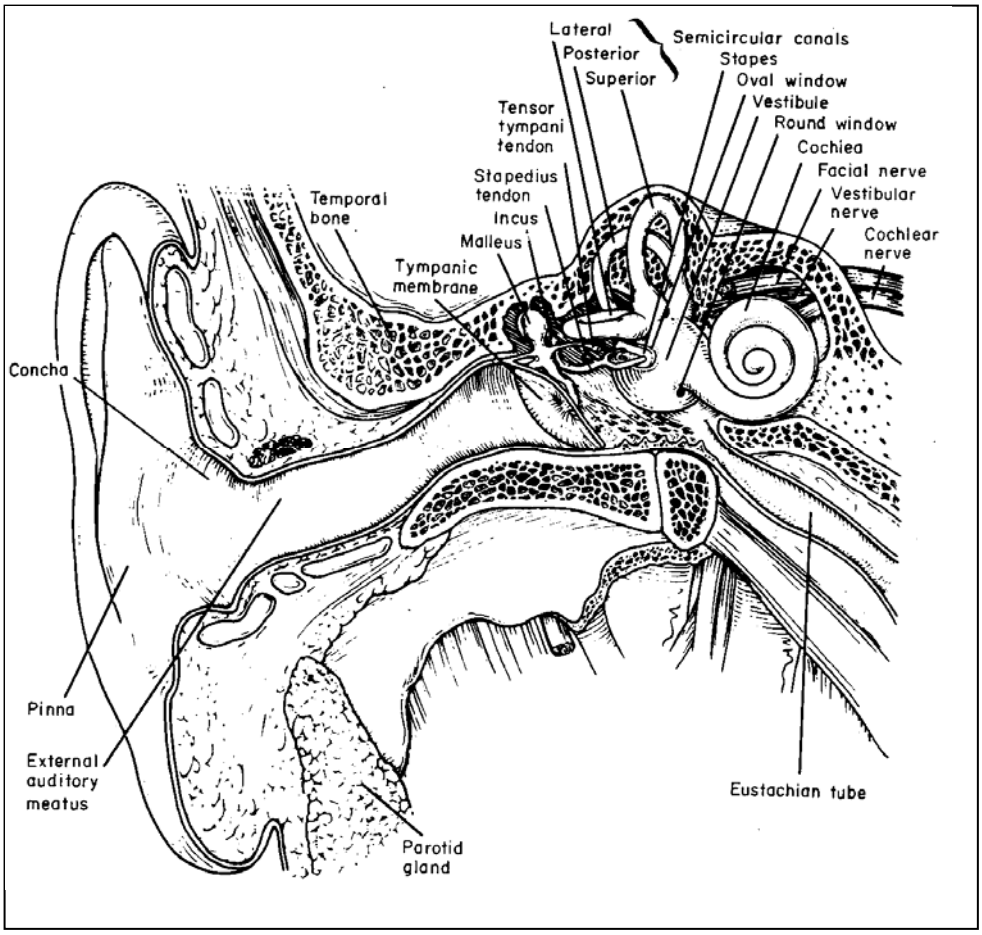

Figure 1.1: The structure of peripheral auditory system, comprising the external, middle and inner ears (from Pickles, 1988).

1.1.1.1 The external ear

The outer ear is formed by the fleshy auricle (in humans) or pinna (in animals) and the external auditory meatus (ear canal). The shape of the auricle allows airborne sound vibrations to be channelled into the ear canal, as well as enhancing high frequency sounds and aiding our ability to identify the directional origin of sound (Pickles 1988). The ear canal then conveys vibrations towards the tympanic membrane where they are transferred to the middle ear.

1.1.1.2 The middle ear

The middle ear is an air-filled recess within the temporal bone. Within this cavity are located the three auditory ossicles, the malleus, incus and stapes, as well as the tensor tympani and stapedius – the muscles which hold them in place. The remainder of the middle ear is made up by the Eustachian tube and the tympanic membrane.

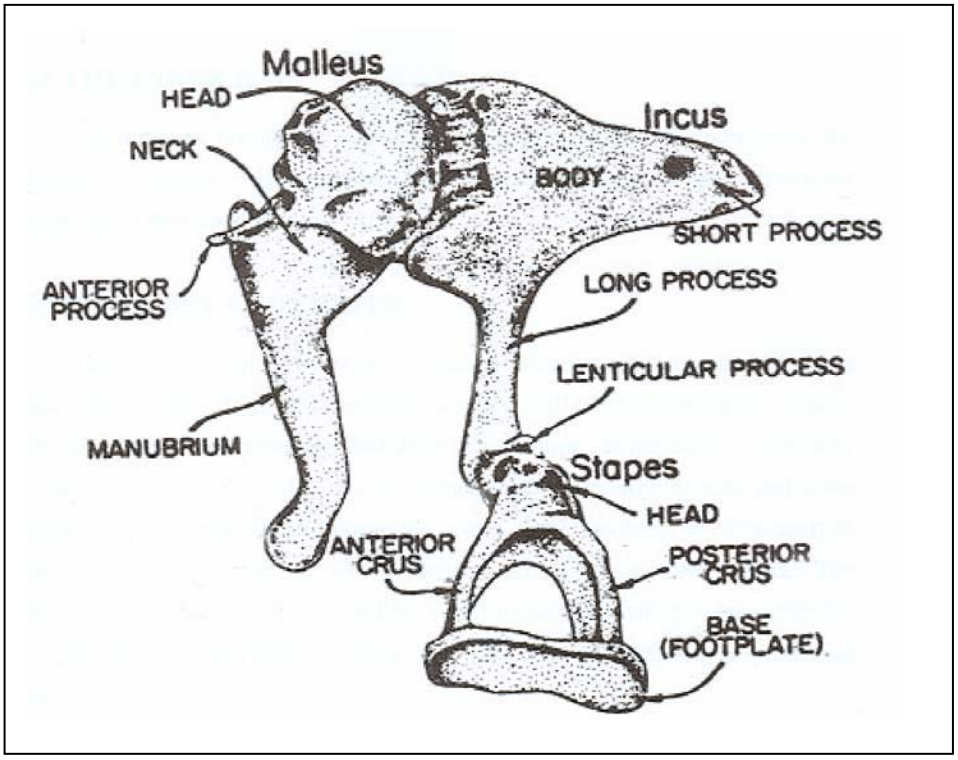

Figure 1.2: Schematic of the human ossicular chain of the middle ear showing the anatomical landmarks of each bone. The ossicles form a continuous chain spanning the middle ear cavity with the manubrium of the malleus contacting the tympanic membrane and the footplate of the incus inserting into the oval window of the cochlea (from Schuknecht 1974).

The tympanic membrane is a tri-laminar structure, consisting of an outer layer of ectoderm, an internal lining of mesoderm and an inner layer of endoderm. Its external surface is in contact with the outside environment via the external auditory meatus, whilst its inner surface connects with the manubrium of the malleus (Figure 1.2). The head of the malleus articulates with the body of the incus, and the lenticular process of the incus connects with the head of the stapes. The ossicular chain spanning from the outer ear to the inner ear is completed by the insertion of the footplate of the stapes into the oval window of the cochlea. Thus vibrations carried through the external auditory meatus to the tympanic membrane are transmitted to the inner ear. In addition, the lever action of the ossicular chain, combined with the transfer of vibrations from the large, low impedance tympanic membrane to the smaller, higher impedance oval window results in an amplification of the sound as it reaches the cochlea (Pickles 1988).

1.1.1.3 The inner ear

The inner ear is made up of two labyrinths – the bony labyrinth and the membranous labyrinth, both of which are encased by a protective bony shell called the otic capsule. The bony labyrinth can be divided into 3 distinct areas: the vestibule; the three semi-circular canals and the cochlea (Figure 1.3a). Within these lie the separate areas of the membranous labyrinth: the saccule; the utricle; the semicircular ducts and the cochlear duct or scala media (Figure 1.3b). Functionally, the inner ear can be divided into two systems. The vestibular system which is concerned with the mechanisms of balance comprises the semicircular canals, the vestibule and the membranous sacs and ducts they enclose. The snail-like cochlea forms part of the auditory system, with the oval window of the bony labyrinth situated at its base to allowing transmission of sound from the outer and middle ears. The development of the inner ear is discussed in Section 1.2.3.

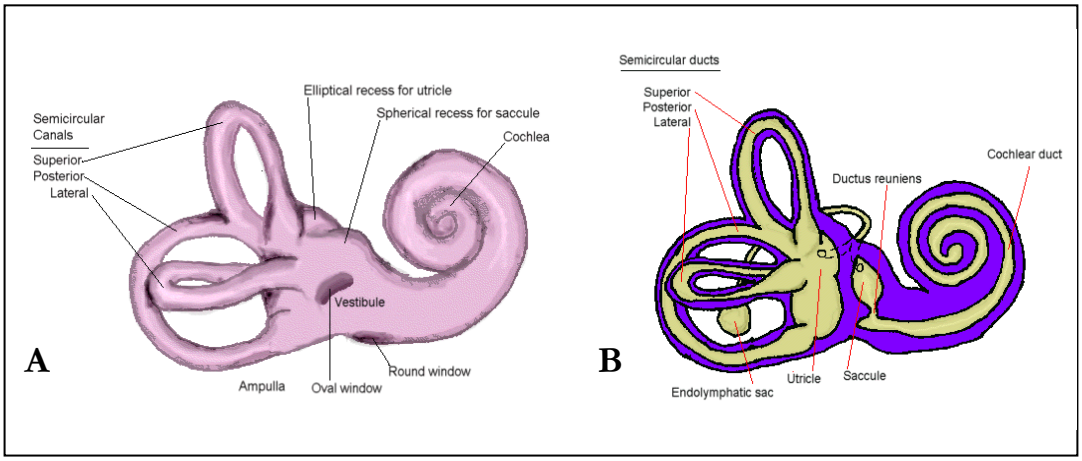

Figure 1.3: The gross structure of the inner ear, showing the bony labyrinth (A) and the membranous labyrinth (B)
From http://medic.med.uth.tmc.edu/Lecture/Main/ear.htm

1.1.2 The cochlea

The cochlear duct is a spiral-shaped bony tube surrounding a central core called the modiolus. In humans the spiral is two and three quarter turns in length, in the mouse it is one and three quarters. The cochlear duct is divided along its length into three chambers, the scala vestibuli, the scala tympani and the scala media (Figure 1.4). The scala vestibuli and scala tympani form the outer layers of the duct and both contain perilymph which is high in sodium ion (Na^+) concentration and low in potassium ion (K^+) concentration like most other extracellular fluids. Between them lies the scala media, a cavity which is triangular in cross section and filled with endolymph high in K^+ concentration and low in Na^+ concentration, similar to the intracellular fluids of neurons.

The division between the scala media and the scala tympani below it is formed by the basilar membrane. This structure is composed of connective tissue, with a distinct basement membrane separating it from the overlying organ of Corti. Above the scala media the boundary is formed by Reissner's membrane, while the external wall attaches to the wall of the bony labyrinth and is termed the lateral wall. This wall includes the spiral ligament and stria vascularis which play important roles in recycling endolymph and maintaining the ion gradients within the scala media.

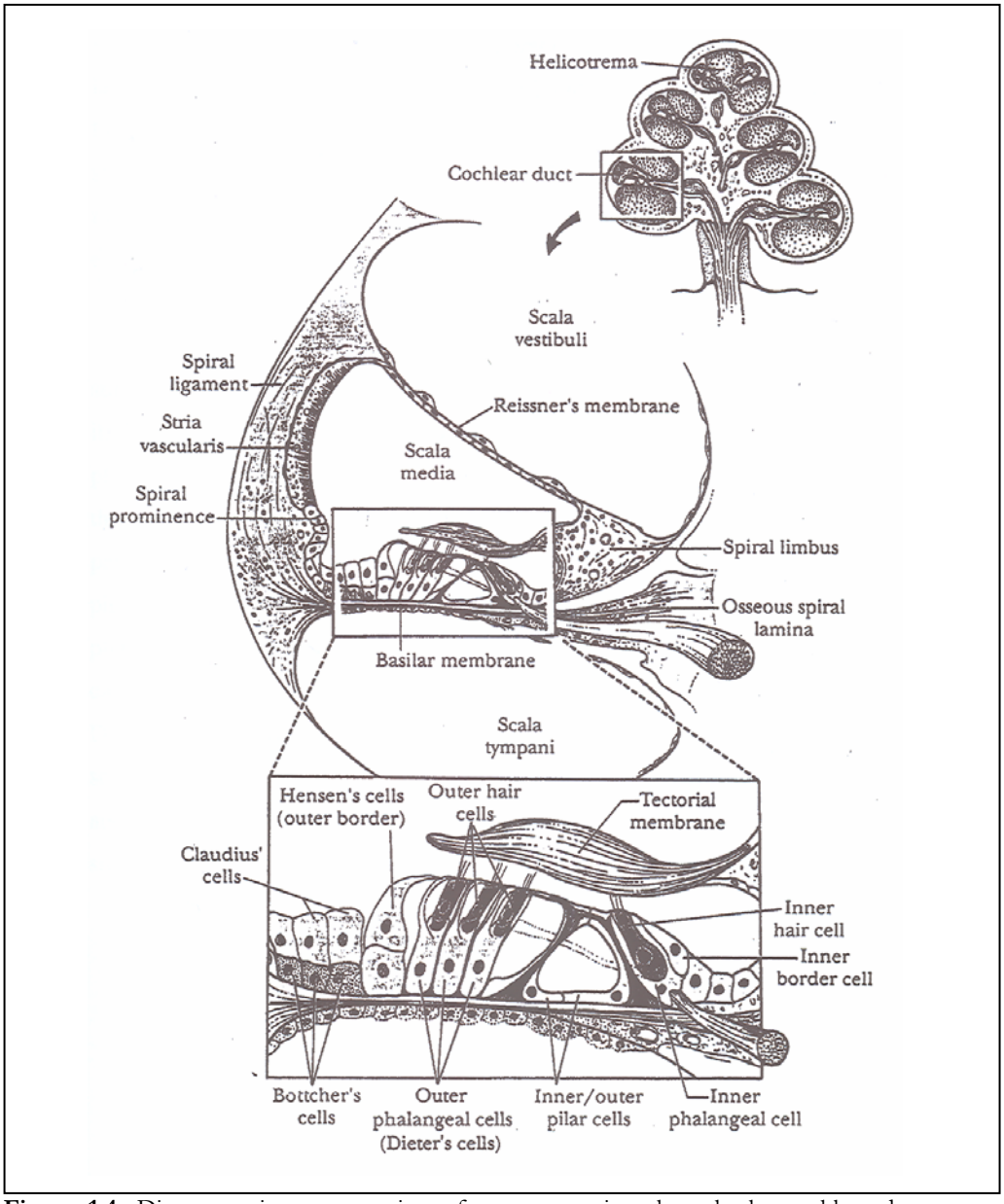

Figure 1.4: Diagrammatic representation of a cross section through the cochlear duct emphasising the location of the organ of Corti (from Goodhill 1979).

1.1.2.1 The organ of Corti

The organ of Corti is the highly specialised sensory patch of the cochlea and is composed of sensory hair cells and supporting cells. It rests on the basilar membrane and extends through the length of the cochlea within the scala media (Figure 1.4). Hair cells can be distinguished by the bundles of stereocilia on their apical surfaces and form two distinct types; the inner hair cells (IHCs) and outer hair cells (OHCs). The IHCs are arranged in a single row towards the modiolar edge of the organ of Corti, while the OHCs are ordered in three parallel rows (sometimes up to four rows in the apex) slightly further away from the central core of the cochlea (Figure 1.5). IHCs have a flask-shaped cellular body and a centrally located nucleus and account for 90-95% of the afferent innervation leading to the cochlear nucleus (Spoendlin 1972). The OHCs are longer and cylindrical in shape, and have an abundant efferent nerve supply. However, the most noticeable difference between the two types of hair cells is the arrangement of the stereocilia on their surface. The IHCs have their stereocilia arranged in a slightly crescent manner, whilst the stereocilia on OHCs are arranged in a distinctive "v" shape in the apex, widening to form a "w" shape in the base. In general the stereocilia of IHCs are longer and of larger diameter than those of the OHCs, which tend to be short and narrow. The stereocilia of both hair cell types form a "staircase" gradient with the tallest stereocilia at the outer edge of the cell. Stereocilia are composed of tightly packed actin filaments, making them relatively strong and rigid. Between the rows of stereocilia exist tip links and numerous lateral links which preserve the integrity of the bundle and also mean that the stereocilia in a bundle all move together. The deflection of the stereocilia bundle towards the tallest stereocilia row produces an excitatory response, as discussed later.

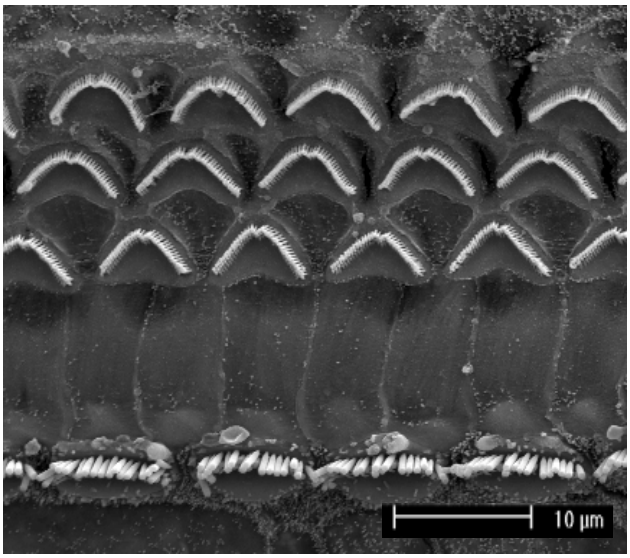

Outer hair cells

Inner hair cells

Figure 1.5: Scanning electron micrograph showing the apical surface of an adult mouse organ of Corti. Outer hair cells are arranged in three parallel rows and possess thin-shafted stereocilia which are arranged in a characteristic "V" or "W" formation. Inner hair cells form a single row and have thicker stereocilia organised into a slight crescent shape.

The sensory hair cells in the organ of Corti are surrounded by a variety of different supporting cells. Lying between the single row of IHCs and the first row of OHCs are two rows of microtubule-packed inner and outer pillar cells. As well as separating the two hair cell types, these cells give the organ of Corti rigidity along its length. The upper ends of the pillar cells form a plate called the reticular lamina which forms the division between the endolymph of the scala media and the perilymph of the scala tympani below. Surrounding the pillar cells are phalangeal cells. Inner phalangeal cells surround the inner IHCs, while outer phalangeal cells (also called Deiter's cells) support the OHCs, forming a cup at their base and extending fine microtubule-filled processes towards the reticular lamina which serve to separate the three rows of OHCs. Hensen's cells form the outer border external to the OHC rows, while inner border cells are situated between the row of IHCs and the modiolus.

The tallest stereocilia of the OHCs are embedded in the fibrous and gelatinous tectorial membrane. This structure is anchored to the spiral limbus

and forms a flap which covers the organ of Corti. The IHCs are not embedded in this matrix, but instead fit loosely into a groove on its under surface (Pickles 1988).

1.1.2.2 Auditory transduction

Auditory transduction refers to the transformation of the tiny vibrational movements of the basilar membrane and the organ of Corti which rests upon it into electrical impulses. The sound waves that enter the cochlea via the outer and middle ear at the oval window cause the displacement of endolymph in the scala media which is accommodated by the round window. This movement of the fluid surrounding the basilar membrane causes it to be displaced, with the frequency of the sound determining the pattern of movement. Sounds of a low frequency result in a vibration pattern which peaks in the apex of the cochlea, while high frequency tones produce more vibration in the basal region. This arrangement is described as tonotopic organisation.

The movement of the basilar membrane in turn causes displacement of the stereocilia bundles on the surfaces of the sensory hair cells. This displacement occurs because the tectorial membrane in which their tips are embedded has a different pivot point from the basilar membrane which forms their base. Thus when the membranes are displaced, the stereocilia also undergo displacement.

Mechanical stimuli applied to a hair bundle elicit electrical responses by causing transduction channels to open or close. When the stereocilia bundle is deflected towards the tallest row of stereocilia, tension in the tip-links which connect adjacent stereocilia exerts force on the transducer channels and causes more of them to open, thus allowing an influx of extracellular K^+ and Ca^+ which causes depolarisation of the cell. A stimulus which brings about a movement of the stereocilia towards the short edge of the bundle has the opposite effect, causing the transducer channels to close and hyperpolarising

the cell. The degree of polarisation in turn affects the rate of release of a synaptic transmitter which causes the transmission of a pattern of action potentials to the brain. These are carried along an afferent nerve fibre which contacts the base of the cell, and encodes information regarding the intensity, time course and frequency of the sound stimulation.

1.1.3 The vestibular system

The vestibular system is concerned with the perception of static and dynamic equilibrium which is necessary for balance and spatial orientation. Static equilibrium relates to the position of the body in relation to gravity, while dynamic equilibrium is concerned with the maintenance of body position in response to movement. It comprises the semicircular canals and the otolithic organs, the saccule and the utricle, as well as the endolymphatic sac and duct (Figure 1.3). The endlymphatic duct joins the endolymphatic sac to the utricle and plays a role in fluid homeostasis; the anatomy and function of the remaining components are described below.

1.1.3.1 The semicircular canals

Within the bony semicircular canals lie the lateral, anterior and posterior semicircular ducts (Figure 1.3). Both ends of each canal join to the vestibule, while the rostral end opens out into an ampulla, an expanded cavity containing a sensory patch known as the crista ampullaris. Each of these is an elongated epithelial structure situated on a ridge of supporting tissue arising from the wall of the ampulla, with its surface populated by three distinct cell types. The first of these are supporting cells, characterised by a tall columnar shape and short microvilli on the apical surface. The other two cell types are sensory hair cells, which are classified as type I or type II depending on their morphology and innervation. Type I cells are flask shaped, with an afferent nerve chalice and some efferent nerve fibres surrounding the baso-lateral

region. Type II cells are cylindrical in shape, and possess both efferent and afferent innervation at their base.

Both type I and type II cells possess stereocilia on their apical surface. These are stiff actin-filled microvilli which are organised into a "staircase" shape, with taller projections at the back, gradually decreasing in height towards the front. The stereocilia of the hair cells project into a cone-shaped gelatinous membrane called the cupula. Each cell also has a single kinocilium – a cilium containing the classic 9+2 arrangement of microtubules at its core – which is always located on the utricular side of the hair cell.

The semicircular ducts and their associated cristae are responsible for the detection of changes in the direction and rate of movement of the head, known as rotational acceleration and deceleration. In order to account for all planes of movement, the superior and posterior canals are in vertical planes perpendicular to each other, while the lateral canal is in a near-horizontal plane. Each crista is located perpendicular to the plane of the duct with which it is associated. Rotation of the head in the plane of that semicircular canal causes movement of the endolymph within it, which in turn displaces the cupula. This causes movement of the embedded stereocilia bundles towards or away from the kinocilium, resulting in depolarising or hyperpolarising receptor potentials respectively and the release of a neurotransmitter at varying rates, initialising neural impulses towards the central vestibular system.

1.1.3.2 The otolithic organs

The utricle and saccule are dilated regions of the central vestibule, each containing a sensory patch termed a macula. The two maculae are located perpendicular to each other and are composed of supporting cells and type I and type II sensory hair cells similar to those found in the cristae. The stereocilia of the hair cells are embedded in a gelatinous layer of glycoprotein called the otolithic membrane, a sheet-like structure which is thought to be

secreted by the supporting cells. The upper surface of this membrane contains minute crystalline bodies composed of calcium carbonate and protein which are known as otoconia.

The maculae are responsible for the maintenance of static equilibrium – the detection of gravity – which is of particular importance when other cues as to spatial orientation are lacking, such as when the eyes are closed, or in the dark or under water. Movement of the head causes the otolithic membrane, weighed down by the otoliths, to move in relation to the hair cells beneath them, giving rise to displacement of the stereocilia. As in the cristae and the cochlea, this causes increased excitation when the movement is towards the kinocilium and reduced excitation when the movement is away from the kinocilium.

1.2 DEVELOPMENT OF THE EAR

1.2.1 Development of the external ear

The pinna of the external ear arises from the ectoderm of the first and second pharangeal arches. During the fifth week of human development three pairs of auricular hillocks arise from these tissues. These then proceed to enlarge, differentiate and fuse to give the final shape of the pinna. The external auditory meatus is derived from a deepening of the first pharangeal cleft during the sixth week. This is followed by cell proliferation and canalization of the deepening tube.

1.2.2 Development of the middle ear

Beginning at the seventh week of gestation (E13.5 in mice), the ossicles develop from neural crest derived cells from the first and second arches which condense to form cartilage before being converted to bone by the process of endochondral ossification. During the ninth month of development pharangeal endoderm expands to enclose the ossicles, forming the tympanic cavity, with the connection to the pharynx being maintained by the Eustachian tubes. Meanwhile, the pharangeal membrane separating the tympanic cavity from the external auditory meatus develops into the tympanic membrane, a structure composed of an outer layer of ectoderm, an internal lining of mesoderm and an inner layer of endoderm. Once the ossicular chain has been established, the ventral end of the malleus becomes attached to the eardrum and the footplate of the stapes becomes attached to the oval window of the bony labyrinth, thus forming a continuous connection between the outer and inner ears.

1.2.3 Development of the inner ear

In the mouse the first sign of inner ear development is seen between embryonic day E8 and E8.5, corresponding to four weeks of development in

the human embryo. This takes the form of a thickening in the ectoderm adjacent to the rhombomeres 5 and 6 of the embryonic hindbrain which is termed the otic placode (Figure 1.6C). The derivation of this structure has been the subject of much and varied research. It is thought to be of ectodermal origin, although in the absence of surrounding tissues ectoderm has been found to be unable to develop an otic placode (Jacobson 1963). Hence the role of the surrounding tissues in inducing its formation has been considered, the main candidates for this role being the mesoderm, neural plate, endoderm and notochord. The main mode of study employed was that of transplantation and in this way the tissues necessary for the specification of the ectoderm have been characterised.

The most likely ectoderm to form ear vesicles was that taken from tissue between mid and late gastrulation and from near the site where they would be expected to form, thus implying that there exists a specified otic field before the otic placode becomes visible. Jacobson (1963) also suggested that this could be pre-empted by a broader placodal field, including the tissue which will later differentiate to become ear, nose and lens placode.

It was found that several of the surrounding tissues were capable of inducing an otocyst when transplanted individually with ectoderm. However, the most successful induction occurred when several tissues were present, indicating a more complicated mechanism of induction than was previously assumed.

Following the establishment of the otic placode, the structure begins to invaginate, forming an otic cup or pit (Figure 1.6D). This pit continues to deepen until it is completely closed off and an otic vesicle or otocyst is formed (Figure 1.6E). During this time the cochlear and vestibular neurons are formed by delamination from the otic cup, initially existing as a combined cochleo-vestibular ganglion but later splitting to form separate ganglia. There follows a period of much proliferation and the structure becomes enlarged, soon after which there begins the process of differentiation when

morphogenesis and patterned development of specific cell types will take place (Figure 1.6F).

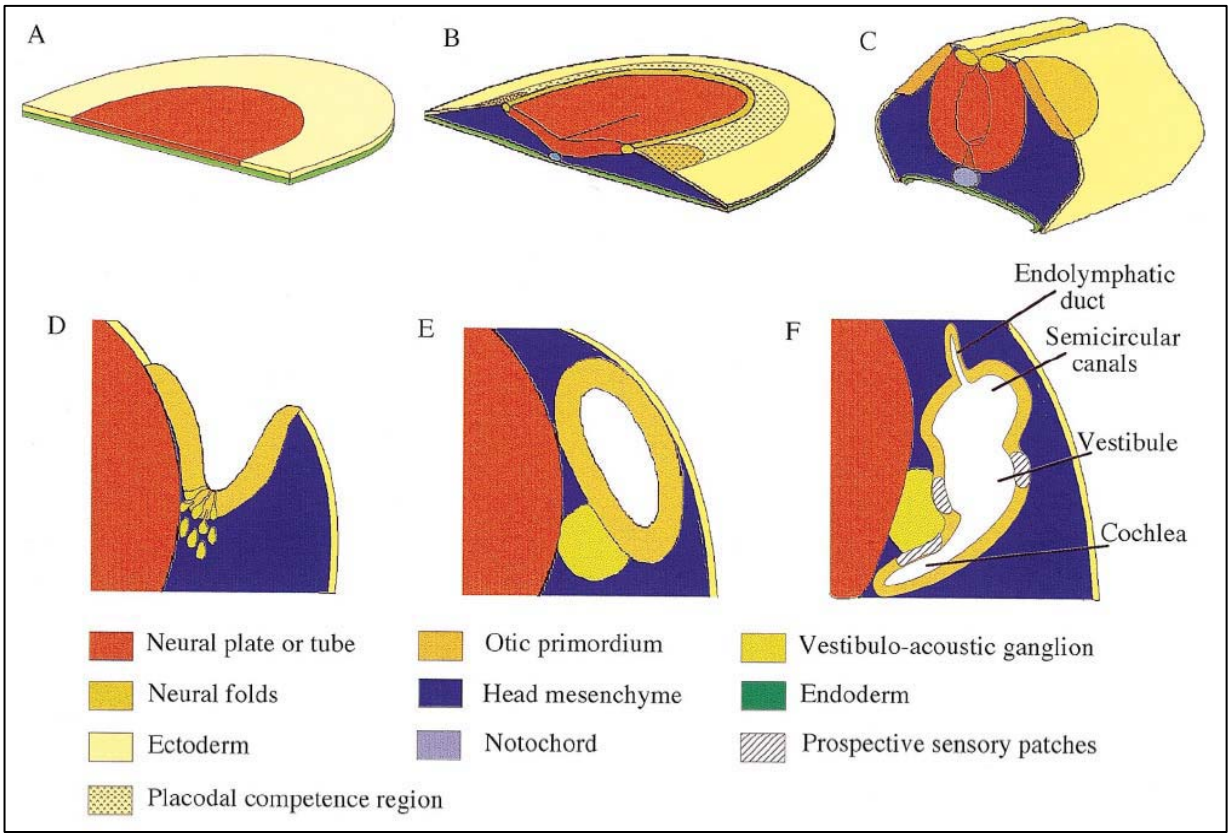

Figure 1.6: Summary of inner ear early development (from Torres and Giraldez 1998)

A) Pregastrula, the prospective neural plate is indicated in red.
B) Head fold, the prospective otic placode is indicated in orange and the prospective multiplacodal ectoderm stripe is stippled.
C) Otic placode.
D) Otic cup, neuroblast appears differentiating from the otic epithelium.
E) Otic vesicle.
F) Otocyst differentiation, the primordia of the different anatomical regions are as indicated.

1.2.3.1 Development of the organ of Corti

The organ of Corti forms a part of the cochlear duct which coils around inside the cochlea. At embryonic day E11.5 in the mouse, the cochlear duct begins to form from a tubular pouch which extends from the otocyst. The cochlear duct develops thickened epithelial areas, the greater and lesser ridges, from which the organ of Corti develops. It is thought that the greater epithelial ridge will give rise to the inner hair cells (IHCs), and the lesser epithelial ridge to the outer hair cells (OHCs).

The base of the organ of Corti is first to develop, and the tube continues to coil around so that by E13.5 in the mouse 1.75 turns have been made, but no cellular differentiation can yet be observed. Between E14.5 and E18.5 the tectorial membrane begins to form and the epithelial cells begin to specialise and mature so that eventually the IHCs and OHC s can be distinguished from the supporting cells by their stereocilia which first become apparent at E17.5.

When the mouse is born following approximately 20 days of gestation the organ of Corti is not yet fully formed. At birth the tunnel of Corti and Nuel spaces – the fluid-filled spaces between the pillar cells and surrounding the OHC cell bodies respectively – are absent. At postnatal day 6 the tunnel of Corti begins to open at the base as pillar cells devlop, slowly progressing up to the apex so that it is fully open by P10. Nuel spaces also develop during this time.

The IHCs and OHCs are themselves immature at birth, and undergo further maturation up to P14. Microvilli shorten or are resorbed, kinocilia disappear, synapses with nerve endings develop and the inner pillar cells expand between the rows of IHCs and OHCs to give them their distinctive mature appearance.

1.2.3.2 Development of hair cell stereocilia

The stereocilia first develop in the mouse at E16.5 as short, thick microvilli covering the surface of the hair cells with over 200 per cell. This is far more than would be expected in a mature hair cell and indeed many of these subsequently regress. The stereocilia vary in height, with the tallest being near the kinocilium and the rest forming graduations down towards the cell surface. Tip links and side links between the stereocilia are thought to develop as this staircase pattern evolves, with the remaining unlinked stereocilia being reabsorbed by the cell. Mature-looking stereocilia are visible at P14, when the kinocilium has also been reabsorbed. By P20, the stereocilia are fully mature.

1.2.3.3 Development of the semicircular canals

The semicircular canals initially develop from bilayered outpocketings of epithelium from the otic vesicle at embryonic day E11.5 in the mouse. The superior and posterior semicircular canals will develop from a single dorsally directed outpocketing, while the horizontal canal develops later and from a separate laterally directed outpocketing. The two layers of epithelium in the central regions of these pockets, termed canal plates, join each other and fuse. This movement is thought to be brought about by the production of glycosaminoglycan by the canal plate epithelial cells which is secreted onto the underlying mesenchyme (Haddon and Lewis 1991). During this fusion the epithelium appears to vanish, leaving a hollow rim of epithelium surrounding the periphery of the original outpocketing (Figure 1.7). Martin and Swanson (1993) showed that the disappearance of these cells is due to their retraction into the canal epithelium adjacent to the fusion site in the mouse, whereas in chick it is thought to be due to programmed cell death. The crucial developmental stages of the semicircular canals are over by embryonic day E13.5, by which time the inner ear labyrinth is fully formed in miniature.

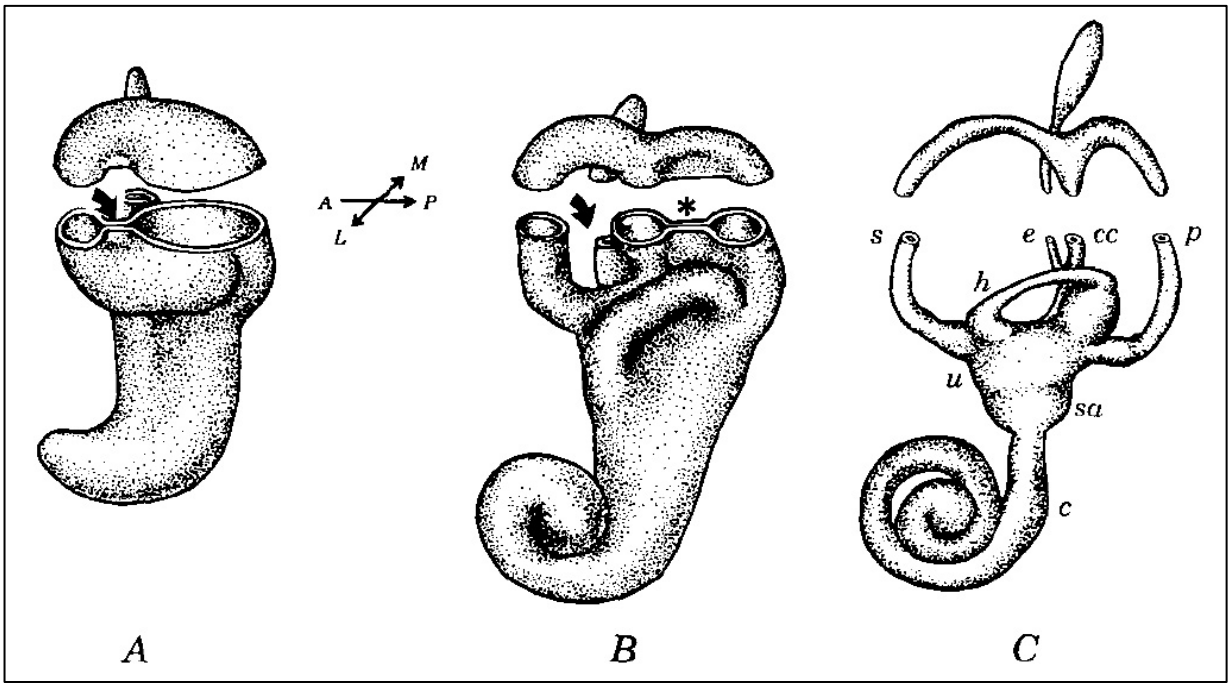

Figure 1.7: Inner ear morphogenesis during semicircular canal development (Martin and Swanson 1993)
A - The walls of the canal plate have met in the region of the superior semicircular canal (arrow).
B - The fused layer of canal plate epithelium has disappeared, posterior canal walls have come together and are opposed.
C - The superior and posterior semicircular canals are no longer fused but are united by the shared crus commune.

Key:
s - superior semicircular canal
p - posterior semicircular canal
h - horizontal semicircular canal
cc - crus commune
e - endolymphatic duct
u - utricle
sa - saccule
c - cochlea

M - medial
L - lateral
A - anterior
P - posterior

1.2.3.4 Development of the maculae

At embryonic day E13.5 the maculae can be distinguished from the remaining epithelium of the membranous labyrinth by the microvilli on their surface. Each hair cell also possesses a single kinocilium which is distinct from the microvilli in its exaggerated length and thickness. By E14.5 the hair cells have developed ciliary tufts and the kinocilium has become polarised slightly off centre on the hair cell surface. The maculae then begin to grow in surface area, a change thought to be due to the migration of the supporting cells from a multi-layered structure to a monolayer. Alongside this change the number of ciliary tufts increases so that by E16.5 it is possible to see well-developed tufts in the central striolar zone and more immature tufts at the periphery. The otoconia also appear at this stage, and continue to increase in number until birth. From this stage onwards the maculae continue to increase in size, while the central-peripheral gradient of development persists.

1.2.3.5 Development of the cupulae and cristae ampullares

At around E13.5 in the embryonic stage of mouse development the epithelial ridge, which will later be the site of the crista ampularis, becomes identifiable. At this time the ampullae may also be distinguished as a small dimple on the surface of the epithelium. Between E14.5 and E16.5 the gelatinous membranes which form the cupulae begin to develop via the secretion of material from the surface cells until by E16.5 they span the space between the cristae and the roofs of the ampullae.

Meanwhile the ampullae acquire a coating of microvilli, with the central region of the cristae also exhibiting polarised ciliary tufts. Kinocilia are also present. At E15.5 the size of the cristae and the number of hair bundles have both increased. In the cristae of the superior and posterior canals the torus can be seen beginning to form in the shape of a bulge separating the cristae into two parts. The crista itself is also altering in morphology, becoming

cylindrical from its previous flat appearance, and the ciliary tufts continue to spread and to enlarge. There are fewer tufts at the base than at the apex of the crista, and at birth this pattern is still seen, but with additional new immature tufts at the top of the cristae.

1.2.3.6 Genetics of hair cell development

The hair cells in the organ of Corti, the maculae and the cristae all develop from an initial sensory primordium which becomes distinct from the surrounding cells (reviewed by Fekete 1996). From this sensory primordium will arise both the auditory hair cells (AHCs) and the various types of supporting cells (SCs) which together make up the sensory epithelia. The fate of these cells is thought to be specified by lateral inhibition mediated by Delta-Notch signalling. Evidence suggests that the *Delta/Serrate/Lag2* (DSL) family ligands *Delta* and *Jagged1* signal to Notch transmembrane receptors on adjacent cells within the sensory primordium. One cell begins to express higher levels of *Delta1*, making it a nascent hair cell. This causes the upregulation of *Notch* expression in neighbouring cells which in turn inhibits further *Delta1* expression in these cells and destines them to become supporting cells. This mechanism of lateral inhibition allows the development of the initially homogenous cell population into the precise mosaic of hair cells and supporting hair cells seen in the fully developed sensory patches. Expression studies in the cochlea have shown that *Delta* is expressed from E13.5 initially in a single row corresponding to the inner hair cells, indicating that these may be specified slightly earlier than the outer hair cells, where *Delta* expression is seen from E16.5 (Morrison *et al.* 1999). By contrast *Jagged1* is initially expressed throughout the sensory primordium but as *Delta1* becomes upregulated in the nascent hair cells it becomes restricted to the supporting cells, making it another candidate for a role in lateral inhibition.

The mouse atonal homologue *Math1* has also been identified as a key player in the development of auditory hair cells. *Math1* knockout mice fail to develop

any AHCs (Bermingham *et al.* 1999), while overexpression leads to supernumerary hair cells (Zheng and Gao 2000). Unlike atonal which is expressed prior to the differentiation of the sensory primordium and is thought to play a role in its specification, *Math1* expression occurs after the sensory precursor domain has been established (Chen *et al.* 2002). This suggests that while not playing a role in hair cell precursor selection, *Math1* is essential for the early differentiation of hair cells.

The basic helix-loop-helix (bHLH) genes *Hes1* and *Hes5* (mammalian hairy and Enhancer-of-split homologs) are thought to play a role in hair cell production. They are expressed in the developing mouse cochlea from E14, with *Hes1* showing expression in the greater epithelial ridge (GER) and the lesser epithelial ridge (LER) while *Hes5* expression was seen most strongly in the supporting cells of the LER and in a narrow band of cells within the GER (Zine *et al.* 2001). Histological studies suggest that inner hair cells are derived from progenitor cells within the GER and outer hair cells from the LER (Lim and Rueda 1992; Zheng *et al.* 2000). In correlation with this, *Hes1* knockout mice showed an increase in the number of IHCs, whilst *Hes5* knockout mice had increased numbers of OHCs (Zine *et al.* 2001). In both cases the supernumary cells showed upregulation of *Math1*, indicating that *Hes1* and *Hes5* participate in hair cell formation via inhibition of *Math1*.

The cyclin dependent kinase inhibitor $p27^{Kip1}$ is expressed in the organ of Corti between E12 and E14, coinciding with the exit from the cell cycle (Chen and Segil 1999), and is localised to the supporting cells. Homozygous $p27^{Kip1}$ knockout mice possess supernumary AHCs but also retain SCs, implying a role in suppression of AHC development but not one in absolute differentiation. Interestingly, heterozygous knockout mice only develop additional IHCs, suggesting some form of dosage-dependent or time-dependent specificity.

A number of transcription factor genes have been implicated in the survival of hair cells late in embryonic development. When *Pou4f3* is knocked out the hair cells are specified normally but fail to mature and later degenerate (Erkman *et al.* 1996). Mutations in *Gfi1*, the mouse ortholog of the Drosophila gene senseless, give a very similar phenotype (Wallis *et al.* 2003) and expression of *Gfi1* is directly dependent on *Pou4f3* (Hertzano *et al.* 2004).

It is clear that although some of the mechanisms underlying hair cell fate specification and maturation have been elucidated, the process is far from being fully understood. The study of mouse mutants with phenotypes indicating that the process has been somehow disrupted is a useful approach to identifying further genes which may be involved, and the *bronx waltzer* mouse is one such mutant. None of the genes described above lie within the candidate region for *bronx waltzer*, and none give the same specific phenotype (see Section 1.4) when mutated or knocked out.

1.3 PATHOLOGY OF DEAFNESS

1.3.1 Pathology of the auditory system

Defects of the auditory system can be broadly grouped into two main types based on the region of the ear which is affected. Conductive defects occur when abnormalities in the outer or middle ears affect the transmission of sound to the inner ear. In the outer ear these may take the form of malformations which are severe enough to affect the conduction of sound. In the middle ear, abnormalities include disruption of the ossicular chain which impairs transmission of vibration to the oval window, or the condition of otosclerosis which causes progressive conductive hearing loss due to excess ossification.

The second class of auditory defect are those described as sensorineural, encompassing any anomalies in either cochlear function or neural responses. Neural defects may occur either in the peripheral neurons if the function or survival of primary inner ear neurons is affected, or in the central nervous system if processing of auditory information is impaired. Cochlear defects, which account for the vast majority of cases of genetic hearing impairment, can be further divided into three main classes which reflect different mechanisms of interference in the normal development and function of the ear. These three categories – morphogenetic, cochleosaccular and neuroepithelial defects – are discussed in the following paragraphs.

1.3.1.1 Morphogenetic defects

Morphogenetic defects are characterised by early disruption of the normal development of the inner ear, causing structural malformations which vary widely in severity. In some cases only the semicircular canals are affected, with defects ranging from a slight constriction in a single canal (most frequently the lateral canal) to the truncation of one or more canals such as in the mouse mutants with mutations in the *Chd7* gene on chromosome 4 (Bosman *et al.*

2005). In more severe cases, the inner ear can develop into a grossly misshapen cyst which is hardly reminiscent of the normal inner ear shape, such as in the *Dreher* mice (Bergstrom *et al.* 1999).

1.3.1.2 Cochleosaccular defects

Cochleosaccular defects are characterised by abnormality of the stria vascularis which tend to manifest in one of two ways. Either Reissner's membrane collapses onto the organ of Corti suggesting disruption of fluid homeostasis or there is a significant reduction in endocochlear potential, both of which imply strial malfunction and can lead to secondary hair cell degeneration. Many cochleosaccular abnormalities are accompanied by pigmentation defects caused by a lack of melanocytes. This lends support to the implication of the stria in such cases since melanocytes are present in the stria of the normal inner ear (Steel and Brown 1994) but are absent in the stria of some animals which lack a measurable endocochlear potential (Steel *et al.* 1987). Some cochleosaccular defects may be caused by defects in cell types other than melanocytes but these are less well understood.

1.3.1.3 Neuroepithelial defects

Neuroepithelial defects concern the sensory patches of the inner ear – the maculae and cristae in the vestibular system and the organ of Corti in the cochlea. The architecture of the sensory hair cells, and particularly the stereocilia on their surface, is vital to their function (see Section 1.1.2.1), so if their development or maintenance is disrupted then inner ear function can be severely impaired. Hair cell degeneration is often seen in mutants with neuroepithelial defects but this is likely to be a secondary effect of the mutation caused by a failure to be specified or develop or mature normally.

Neuroepithelial defects are thought to be the most common cause of human hearing impairment and as such represent an interesting area of investigation. This is because the identification of genes involved in hair cell development

and function hold the promise of a fuller understanding of the mechanisms of hearing. They may even provide the possibility of regenerating lost hair cells in an effort to restore hearing in the future. In addition, the majority of these defects manifest as autosomal recessive traits with a uniform penetrance and symmetry between the two ears, making them good models for the most common mode of transmission of genetic deafness in humans, that of autosomal recessive inheritance.

1.3.2 The mouse as a model in hearing research

The study of deafness in humans is difficult, with the usual complications of human pedigrees compounded by the fact that the ear is for the most part inaccessible, making detailed clinical analysis challenging. Gross deformities may be identified by means of computed tomography (CT) scanning, but the more common sensorineural forms of hearing impairment cannot be analysed in this way. Thus a model system is required in order to facilitate the study of auditory pathologies.

The mouse lends itself well as a model organism, being small in size, relatively easy to maintain in the laboratory and similar to man in terms of developmental and biochemical pathways, physiology and genetic conservation. Mice are particularly suited to genetic studies since they have a short generation time and can produce large litters, facilitating the construction of high resolution genetic maps. Crucially, the auditory and vestibular systems of mice and men are extremely similar. With the exception of the shape of the pinna/auricle, the structure of the mouse inner ear is almost identical to that of humans. These factors make the mouse an ideal model for the study of auditory physiology and pathology.

1.4 THE BRONX WALTZER (*bv*) MOUSE MUTANT

Bronx waltzer (*bv*) is an autosomal recessive mouse mutation causing abnormalities in the inner ear which result in mutant mice having deficiencies in both the auditory and vestibular systems. It takes its name from the place of its discovery – the Albert Einstein College of Medicine in the Bronx, New York – and the circling behaviour of mice homozygous for the mutant gene which has been described as "waltzing".

The mutation arose spontaneously on an unknown genetic background and was first described by Deol and Gluecksohn-Waelsch (1979). They examined sectioned mutant cochleas under the light microscope and found that the great majority of the inner hair cells (IHCs) were absent and that those which were present were almost all of abnormal appearance, while the outer hair cells (OHCs) seemed morphologically normal. They also noted that the neurones in the spiral ganglion underwent a rapid process of degeneration.

Following these initial observations it was felt that the *bronx waltzer* mouse represented an interesting model for hereditary deafness and for the development and function of the inner ear. As a result many studies have since been carried out in order to further characterise the mutation and the findings of some of these are outlined in the ensuing paragraphs.

1.4.1 Electrophysiology of bronx waltzer

1.4.1.1 Round window response recordings

Using round window response recordings in mice, three different responses can be determined.

The compound action potential (CAP) provides information concerning the activity of the auditory nerve. Since these signals originate from the inner hair cells, the CAP can be taken to be an indication of IHC function. To produce

a recordable signal it is expected that the IHCs are capable of afferent innervation and additionally that their response to sound is synchronous (Steel and Harvey 1992). In *bronx waltzer* the CAP was shown to be very small or absent in homozygotes (Bock *et al.* 1982), possibly a result of the reduced numbers of IHCs seen in the mutant cochlea and/or the reduction in the number of spiral neurons innervating the cells. In heterozygous mice the CAP thresholds were much higher than control mice at 10 kHz. This led to the suggestion that the mutated *bronx waltzer* gene may not be fully recessive in its effect on hearing.

Cochlear microphonics (CM) are thought to be an indicator of OHC function. They take the form of an alternating current response which mimics the waveform of the stimulus and a normal response indicates functional OHCs. In *bronx waltzer* homozygotes CM were present but greatly reduced when compared to wild type responses. As described later in this chapter, ultrastructural studies have shown that the OHCs in *bronx waltzer* mice appear normal, so these CM results are somewhat unexpected. Bock and Yates (1982) suggested that OHC function may be dependent upon IHC function, which is impaired in *bronx waltzer*. It is also possible that the OHCs are affected by the mutation in some way not visible by electron microscopy. Lenoir and Pujol (1984) observed an abnormal abundance of smooth endoplasmic reticulum (ER) which they speculated may be an indication of metabolic problems, although they did not study any control mice. In contrast, Takeno *et al.* (1994) studied CM amplitudes in chinchilla cochleae with selective IHC loss and found them to be close to normal. They also reported that under the light microscope (LM) the OHCs appeared normal and proposed that the IHCs and OHCs work independently of each other in the cochlear transduction process.

Summating potentials (SP) are offsets in the response sustained for the duration of the stimulus. Their polarity can be either negative or positive and they are thought to represent the intracellular direct current (dc) response of

both inner and outer hair cells (Steel and Harvey 1992). Bock *et al.* (1982) recorded both positive and negative summating potentials in *bronx waltzer* and in control CBA mice. Positive SPs were found to be reduced in the mutants but negative SPs were comparable with controls except at low frequencies. It was suggested that the OHCs which appear normal in the mutant are capable of producing both positive and negative dc potentials, although summating potentials are not well understood and are therefore difficult to interpret.

1.4.1.2 Auditory brainstem recordings

Auditory brainstem responses (ABRs) are recorded using differential pin electrodes situated beneath the skin at the vertex of the mouse head behind the pinna on the side to be recorded. The response is recorded as the difference between the signals from the two electrodes when a stimulus is presented and consists of several waves. It is thought that the first negative wave of deflection represents the neuronal activity of the cochlear nerve, and that the later waves reflect the functioning of the central auditory pathway. Schrott *et al.* (1989) found ABRs in bronx waltzer mice to be elevated by ~20dB SPL compared to CBA controls, a surprisingly small difference. It was suggested that the surviving IHCs, being morphologically intact and evenly spread throughout the length of the cochlea, provide a sufficient response so that the ABRs are relatively unaffected. In addition, since the OHCs appear normal, it is possible that their amplification of the basilar membrane movements enhances the stimulation of those IHCs which are present.

1.4.1.3 Otoacoustic emissions

Spontaneous emissions are recordable in a functioning ear canal but may also be associated with OHC loss. Conversely, evoked emissions are detectable in response to acoustic stimuli and include distortion product otoacoustic emissions (DPOEs). These can be recorded in both humans and rodents and are thought to reflect OHC activity. Studies of DPOEs in *bronx waltzer*

(Schrott *et al.* 1991) showed markedly raised thresholds, a surprising finding since the OHCs appear morphologically normal. Possible explanations of this result are that the OHC row disorganisation affects DPOEs, or that DPOEs rely on there being sensory input into the nervous system from functioning IHCs.

1.4.2 Ultrastructural studies of the bronx waltzer inner ear

As has been previously mentioned, the *bronx waltzer* mutant mice exhibit circling behaviour which is consistent with abnormalities in the vestibular system. They are also almost completely deaf, indicating problems with the auditory system which have been shown to be located in the cochlea (Deol and Gluecksohn-Waelsch 1979). Hence the structural studies of *bronx waltzer* mice have focussed on these two areas of the ear.

1.4.2.1 Ultrastructural studies of the cochlea

Following on from the studies of Deol and Gluecksohn-Waelsch, Lenoir and Pujol (1984) conducted a scanning electron microscopy (SEM) study of the cochleas of postnatal *bronx waltzer* mice. At birth, they found that the IHCs appeared to be either absent completely, rounded with the absence of stereocilia, or of normal appearance. At postnatal day P9 approximately 20-25% of the IHCs appeared normal, while the rest were absent or degenerated. It has also been noted that the pillar cells which lie adjacent to the row of IHCs in the normal mouse ear were malformed or missing in *bronx waltzer* mice (Deol 1981) and this was confirmed by Lenoir and Pujol who described disorganised pillar cells and OHCs in the region of the degenerated IHCs.

A more recent and detailed study of the *bronx waltzer* organ of Corti was carried out by Bussoli (1996) utilising scanning electron microscopy (SEM) and transmission electron microscopy (TEM). The mice examined ranged in age from E16.5 to P30 and much information was gained pertaining to the series of events leading to the previously observed phenotype.

At E16.5 there was no evidence of hair cell formation in either control or *bronx waltzer* mice. At E17.5 the control mice showed the early stages of IHC development in the middle coil, while the mutant IHCs appeared to have shrunk to one third of their usual size and had taken on a rounded appearance. At E18.5 stereocilia could be seen to be differentiating in the control mice, initially in the basal end and followed by differentiation in the middle coil and apex as would be expected. The *bronx waltzer* IHCs in contrast now had a disorganised appearance and few showed signs of developing stereocilia. TEM at E19.5 also revealed vacuolation and nuclear condensation with rounded mitochondria, observations which are consistent with controlled cell death.

During the first few days after birth – P0 and P1 – the affected IHCs in the mutant mice were seen to be reabsorbed into the neuroepithelium. Following this event the OHCs start to become disorganised, although their individual appearance remains normal. From this stage onwards the observations were of depleted IHCs, with many missing or degenerated and a few appearing relatively normal. The disorganisation occasionally seen in OHCs is attributed to the disruption to the row of pillar cells caused by missing IHCs (see Figure 1.8). Occasionally atypical cells similar in appearance to OHCs were observed in positions normally occupied by IHCs.

In summary, it was found that the IHCs in *bronx waltzer* mice degenerate from E17.5, soon after their development would be expected to begin. It is possible that this process is due to a form of controlled cell death and it appears to lead after birth to disorganisation of the OHCs and pillar cells. The pattern of degeneration follows the pattern of normal hair cell differentiation in the organ of Corti, that is, from the basal end of the cochlea progressing towards the apex.

1.4.2.2 Ultrastructural studies of the vestibular system

The sensory patches of the vestibular system in *bronx waltzer* mice were first examined using light microscopy by Deol (1981) who found that the hair cells in both the cristae and the saccule were markedly reduced, had a rounded appearance and possessed malformed stereocilia. In the maculae the appearance of the hair cells degenerates rapidly after birth so that at P12 the saccular macula has none visible. In the utricular macula the same process occurs but less quickly. In the cristae more of the hair cells survive to adulthood, but many of these are degenerated. The vestibular ganglion has also been seen to exhibit some loss of cells.

Dêmemes and Sans (1985) carried out postnatal SEM and TEM studies of the cristae, utricular macula and vestibular ganglion. The first stage studied was P3, at which point the hair cells in the sensory patches already showed considerable signs of degeneration. Many cells had a bulging appearance and lacked stereocilia and ciliary tufts. The stereocilia which were present had an unusual morphology, being at varying stages of development and never attaining the normal staircase arrangement. By adulthood there is sometimes a complete absence of sensory cells and it was observed that those which remain resemble type II cells, but could in fact be developing type I cells which pass though a developmental stage similar to type II cells. It was therefore proposed that the *bronx waltzer* mutation may cause a halt to vestibular hair cell differentiation.

In order to understand the process leading up to the degeneration of the hair cells in the vestibular system, Cheong (2000) carried out a prenatal SEM study of the utricular macula and the superior crista (Figure 1.8). Observations made in these two sensory patches were extrapolated to include the saccular macula and the posterior and lateral cristae as the mutation has previously been shown to affect these regions in the same way (Deol 1981; Dememes and Sans 1985).

Control and *bronx waltzer* maculae and cristae were studied qualitatively at 4 stages of development – at E17.5, E19.5, P0 and P2. Some degeneration of the hair cells was observed at E17.5, indicating that the effect of the *bronx waltzer* mutation may be manifested in the vestibular system at an earlier stage than was studied here. Indeed, the observation of depleted hair cells may not represent the first event in the action of the mutation and in order to determine this a different approach would need to be used as intracellular events are not visible using SEM. It was observed that the density of stereocilia-bearing hair cells decreases over time between E17.5 and P2. The vestibular hair cells have never been observed to mature beyond this stage, since they appear to die prior to the final steps in differentiation.

In comparisons between the two sensory patches studied it was found that the utricular macula had a greater prevalence of degenerated cells at each stage studied, suggesting that the mutation takes effect here prior to affecting the superior crista (Cheong and Steel 2002). As it is thought that the maculae develop before the cristae this also follows the reported temporal pattern of differentiation, lending support to the idea that the *bronx waltzer* mutation takes effect at the time of hair cell differentiation as proposed in the organ of Corti (Bussoli *et al.* 1997).

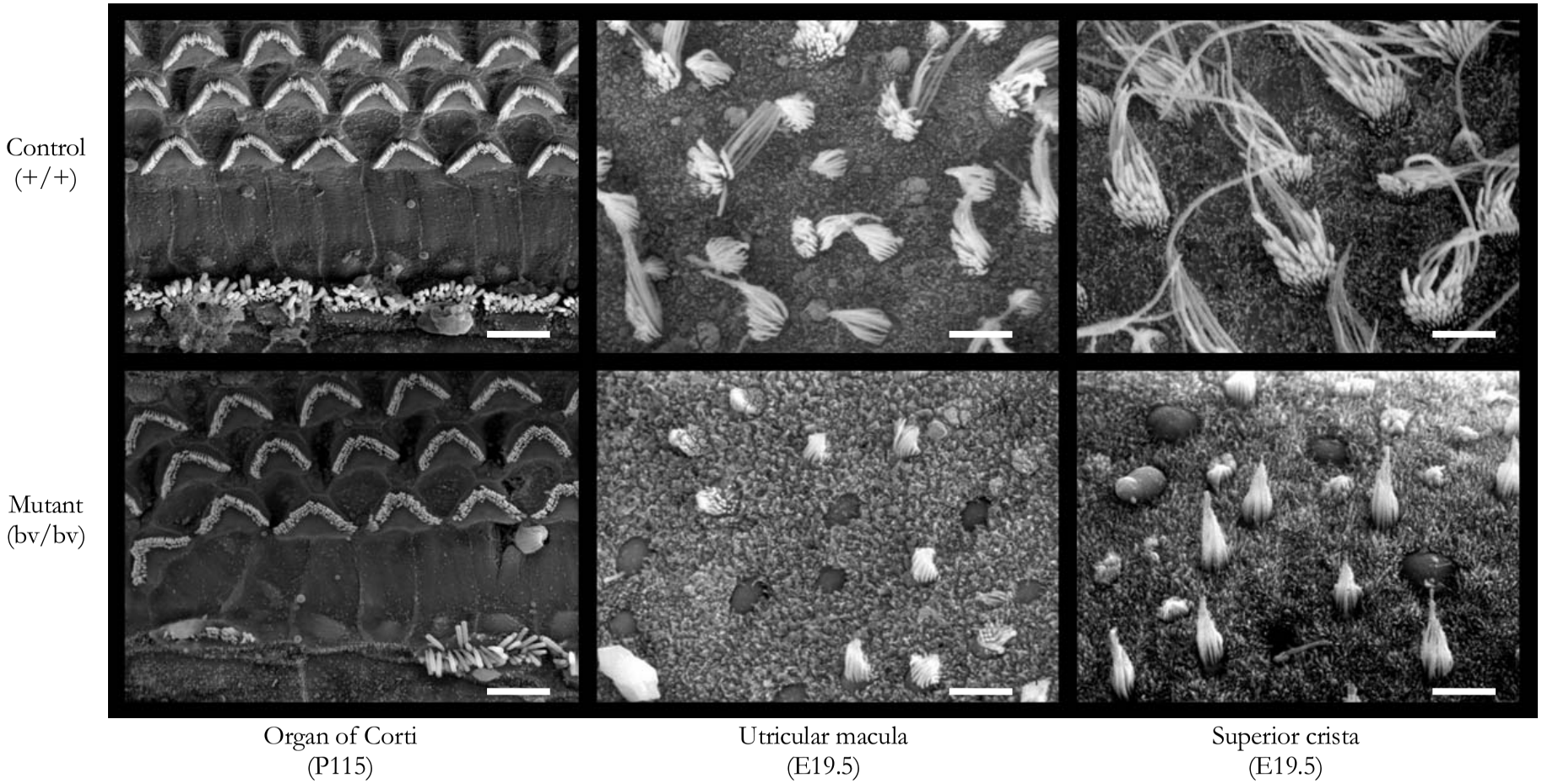

Figure 1.8: Scanning electron micrographs showing the apical surfaces of sensory patches in the wild type and *bronx waltzer* ear.
In the *bv* organ of Corti many inner hair cells are missing or degenerating. Outer hair cells appear normal, although their orientation is somewhat affected by the disorganised supporting cells. In the *bv* utricular macula and superior crista hair cells are underdeveloped with stereocilia much shorter than the wild type cells. In addition, many are seen to be in the process of being resorbed into the epithelium. Scale bar = 5μm (E19.5 images from Cheong, 2000).

1.4.3 Cochlear innervation in *bronx waltzer*

As previously mentioned, Deol and Gluecksohn-Waelsch (1979) reported a depletion in the cells of the spiral ganglion beginning at birth. However this finding was later contradicted by Lenoir and Pujol (1984) whose TEM study revealed no such degeneration.

Following on from these conflicting observations further studies have been made of the innervation of the cochlea, although the results are still somewhat contradictory. Observations made of the synapses at the bases of IHCs by Lenoir and Pujol (1984) found them to be present but abnormal, having no presynaptic densities and their afferent endings contained cytoplasm with a woolly appearance. Sobkowicz *et al.* (1988) found that surviving IHCs fail to be recognised by nerve fibres, and that the synapses with these IHCs are rarely formed. Schrott *et al.* (1989) obtained results which differed again, finding that remaining IHCs had synapses of normal appearance. It should be noted that these studies were carried out on *bronx waltzer* mice of differing genetic background and hence the variation in observations may possibly be attributed to the differing effects of modifier genes.

1.4.4 Previous mapping of the bronx waltzer mutation

1.4.4.1 Genetic mapping of the bv locus

A positional cloning approach was adopted to identify the *bronx waltzer* gene and an intraspecific backcross between the *bronx waltzer* mice and the mouse strain 101/H was established (Bussoli *et al.* 1997). This strain was chosen as a result of the higher degree of polymorphisms observed between it and the *bronx waltzer* background as compared with a number of other inbred strains. A mapping panel consisting of 1085 mice was established and used to position polymorphic markers in relation to the *bronx waltzer* locus. This work

led to the localisation of the *bronx waltzer* gene to a 1.86cM region of mouse chromosome 5, between flanking markers *D5Mit209* and *D5Mit188*.

Using the markers identified as being close to the *bv* locus and mapping these on a well characterised panel – the BXD recombinant inbred strains (Schadt *et al.* 2003) - it was possible to elucidate additional markers and previously identified genes which mapped to the same region of chromosome 5 and hence may represent candidate genes for *bronx waltzer*. In addition, the identification of nearby genes allowed comparison of the mouse map to the human map as many genes are conserved between the two species. Using this approach the candidacy of genes in the region was assessed by consideration of the role of the molecules they encode, but no obvious candidates were identified.

This work was continued by Cheong (2000), who refined the genetic map by mapping the flanking set of markers on two more recombinant panels – the BSS (Jackson Laboratory) and EUCIB (European Collaborative Interspecific Backcross; Breen *et al.* 1994) backcross panels. Once a region had been established on these panels by the placement of known markers, other polymorphic markers which had previously been mapped to the same region could be mapped back to the *bv*/101 backcross panel in the hope that they would map closer to the *bv* locus than the established flanking markers, thereby narrowing down the candidate region for the *bronx waltzer* gene. Unfortunately this was not the case. However, the further characterisation of the region in terms of markers, expressed sequence tags (ESTs) and genes allowed the identification of a region of conserved synteny on human chromosome 12q24.2. As the human sequence was then becoming available this provided a rich source of information about the possible constitution of the homologous mouse region, including the *bv* gene. The known genes from this region were assessed for their candidacy, but again no obvious candidates were identified.

1.4.4.2 Physical mapping of the *bv* locus

Cheong (2000) also carried out physical mapping in order to establish a contiguous set of clones across the candidate region. To accomplish this a yeast artificial chromosome (YAC) library was screened by PCR pool screening using the markers localised to the region. Clones identified as being positive for these markers were ordered according to the known order of the markers from the genetic map.

Using this method 2 YAC clones were identified which appeared to span the region between D5Mit25 and D5Mit209. However, these YACs displayed gaps in their STS content consistent with deletions or chimerism which are not uncommon in YACs, making them poor candidates for further study. Even so, the mapping of ESTs and STSs onto this physical map enabled the identification of further markers which were assessed as candidates for *bv*. None were considered particularly strong candidates.

1.5 THIS THESIS

At the outset of this work the *bronx waltzer* mutation had been localised to a 1.86cM region of mouse chromosome 5 using a mapping backcross consisting of 1085 mice. Of these there still remain 19 backcross mice exhibiting recombinations between the flanking markers. Therefore this backcross holds the potential to narrow the *bv* candidate region further if novel polymorphic markers can be found which map between the markers *D5Mit25* and *D5Mit209*. Hence the first aim of this work is to make use of the now readily available mouse genome sequence data as well as the facility to sequence large numbers of samples easily to identify new polymorphisms between bronx waltzer and the inbred strain used for the backcross, 101/H. This refinement of the critical interval should lead to a smaller number of candidate genes to be considered as causative agents for the mutation.

The second major aim of this project is to characterise the genes which localise to the *bronx waltzer* candidate region with the intention of identifying those most likely to give rise to the observed phenotype. The methods employed include an analysis of background literature and expression data, functional studies using the zebrafish as an alternative model and large-scale exon re-sequencing. The collation of these various forms of data regarding the candidate genes will allow them to be prioritised for further analysis, with the aim of discovering the gene which encodes *bronx waltzer* and thus further the understanding of its role in the ear.

Finally, since variability in the *bronx waltzer* phenotype has been reported on different genetic backgrounds, further investigations are to be carried out with the aim of identifying genes which may act as modifiers of the *bv* mutation. These could prove interesting since building up a picture of the molecules which interact with *bv* could aid in both its identification and subsequent characterisation.

Chapter 2:

General Materials and Methods

CHAPTER 2

GENERAL MATERIALS AND METHODS

This chapter describes the materials and methods common to much of the work contained within this thesis, more specific methods can be found within the chapter to which they are unique.

Unless otherwise stated, all materials and reagents were obtained from Sigma.

2.1 MICE

Mice carrying the *bv* mutation were originally obtained from Professor M.S Deol at University College London in 1982. Details of the genetic background were unknown and the mice were maintained at the MRC Institute of Hearing Research in Nottingham on their original background. In 2003 the stock was successfully rederived at the Wellcome Trust Sanger Institute in Cambridgeshire. However, poor breeding performance necessitated the use of IVF using oocytes from the inbred strain CBA/Ca and as a result the *bv* mutation is currently maintained on a 50% CBA/Ca background. In addition, to ensure the survival of the *bv* allele, sperm samples from *bv* affected males have been frozen and are currently stored at the MRC Mammalian Genetics Unit, Harwell, UK.

2.2 DNA PREPARATION FROM TISSUE

Mouse DNA samples were prepared by phenol/chloroform extraction and sodium acetate precipitation. Tissue for DNA extraction was obtained from the tail and pinnae. Tail tissue was removed from the tail bone by cutting down the length of the tail and peeling away the skin. This tissue, together with the pinnae, was cut into fragments of approximately $5mm^2$ and divided between two 1.5ml tubes and one screw-capped microcentrifuge tube (Eppendorf), with the latter snap frozen in liquid nitrogen and later removed for storage at -70°C. During tissue collection from backcross mice, the liver,

spleen, kidneys, heart, lungs and testis were also removed. These were divided between two 2ml cryotubes (Nunc), snap frozen in liquid nitrogen and stored at -70°C.

To the tissue in each of the two 1.5ml microcentrifuge tubes (Eppendorf) containing tail/ear tissue was added 1.0ml tail mixture (100mM EDTA, pH 7.5; 0.5% SDS; 50mM Tris-HCL, pH 7.5; 1.0mg/ml Proteinase K) and they were incubated at 55°C overnight. One of these tubes was then stored long term at 4°C while the other was processed immediately for DNA extraction. After being spun at 14,000 rpm in an Eppendorf 5415C microcentrifuge for three minutes in order to remove undigested hair and tissue, the supernatant was removed to a fresh tube. An equal volume of equilibrated phenol (pH 7.9) was added and gently mixed by inversion for one minute, then centrifuged for a further three minutes at 14,000 rpm and the aqueous layer removed to another fresh tube. This step was repeated twice more, then an equal volume of 24:1 chloroform:isoamyl alcohol (IAA) was added, mixed by inversion for one minute and centrifuged at 14, 000 rpm for three minutes. The aqueous layer was again removed and this step repeated once more. DNA was precipitated with two volumes of 100% ethanol and one tenth volume of 3M sodium acetate, pH 4.8. The precipitate was spooled out using the sealed and hooked end of a glass Pasteur pipette, washed in 70% ethanol and allowed to air-dry before being resuspended in 100µl TE and melted at 65°C for one hour.

2.3 ESTIMATING NUCLEIC ACID CONCENTRATIONS

DNA concentrations of prepared samples were estimated using first a Cecil 2020 spectrophotometer and later an Eppendorf Biophotometer. In both cases optical density (OD) readings were taken at wavelength (λ) 260nm to measure DNA concentration, and λ 280nm to measure protein concentration. The ratio between these two readings was calculated as a means of assessing the purity of the sample, with an $OD_{\lambda 260}/OD_{\lambda 280}$ ratio of 1.8 to 2.0 being considered adequately pure for subsequent PCR reactions. DNA

concentration was calculated on the basis that an $OD_{\lambda 260}$ of 0.1 corresponds to 1μg/μl of double stranded DNA. Samples were generally diluted 1:500 for this measurement, and the final concentrations adjusted to reflect this dilution factor.

2.4 POLYMERASE CHAIN REACTION

The polymerase chain reaction (PCR) is a method which allows the amplification of a specific region of DNA (Saiki *et al*; 1985). Two short oligonucleotides, or primers, are designed to match DNA sequence at either end of the region of interest. One of these is designed to complement the + (plus) strand of the DNA molecule, whilst the other matches the – (minus) strand. In the presence of the thermostable enzyme *Taq* polymerase I, derived from the thermophilic bacterium *Thermus aquaticus*, and under the correct conditions, the portion of DNA lying between these two primers is amplified.

The first stage of PCR is a denaturation step at about 94°C in order to melt apart the two strands of the DNA template and so render them accessible for the primers to adhere. Second is an annealing step, carried out at around 55°C, which allows the primers to bind to the section of template DNA they have been designed to complement. Third is an extension phase at 72°C which enables the *Taq* enzyme to synthesise new strands of DNA complementary to the template, beginning at the points where primers have bound. This is followed by further cycles of the three temperature phases, resulting in an exponential increase in the number of copies of the amplified DNA fragment

2.4.1 Design and synthesis of oligonucleotides for PCR

Oligonucleotides were designed using the Primer3 design package hosted by the Whitehead Institute for Biomedical Research at http://frodo.wi.mit.edu/primer3/. Criteria for choosing primers were set as follows: Primer size – minimum 18, optimum 20, maximum 27; Melting point – minimum 57, optimum 60, maximum 63; GC content – minimum 20,

optimum 50, maximum 80. In addition, a GC clamp of one base at the internal end of each primer was preferred and the mispriming library for rodent and simple sequences was used to check for repetitive sequences which might anneal in multiple locations. All the remaining options were left as defaults, including those designed to discard primers with self-complementarity which might form hairpins, and those to check complementarity between primer pairs which could give rise to primer dimers.

Primers were synthesised initially by MWG Biotech (Milton Keynes, Bedfordshire, UK) and later by Sigma-Genosys (Haverhill, Essex, UK). In both cases, primers arrived lyophilised and were diluted according to their supplied optical density readings to a stock concentration of 100μm. Working dilutions were then made to a concentration of 10μm.

2.4.2 General PCR protocols

Throughout the project two different PCR systems were utilised. The first, ABgene Thermoprime Plus PCR ReddyMix™ was used for the majority of PCR reactions carried out. The second, BioLine BIO-X-ACT™ High Fidelity Long DNA Polymerase was used for reactions where a larger fragment was to be amplified or where proofreading capability in the enzyme was thought to be beneficial.

ABGene ReddyMix™ is supplied at 2X final concentration, with the final reaction concentrations as follows: 0.025units/μl Thermoprime Plus DNA Polymerase; 75mM Tris-HCL (pH 8.8 at 25°C); 20mM $(NH_4)_2SO_4$; 0.01% Tween 20; 200μm of each dATP, dCTP, dGTP, dTTP; 1.5mM $MgCl_2$. To this were added forward and reverse primers at a final concentration of around 1mM each, and template DNA at approximately 5ng/μl. The exact concentrations of primers and templates were adjusted to optimise the reaction. The remainder of the reaction volume was made up with sterile

ddH_2O. An example of the volumes used a typical reaction using ABGene ReddyMix™ is shown in Table 2.1.

Stock Solution	**Volume per 10µl reaction (µl)**	**Final reaction concentration**
2X ReddyMix™	5	1X
Forward primer (10µM)	1	1µM
Reverse primer (10µM)	1	1µM
DNA template (25-100ng/µl)	1	2.5-10ng/µl
Sterile ddH_2O	2	-

Table 2.1: Preparation of a 10µl PCR reaction using ABGene ReddyMix™

Bioline BIO-X-ACT™ reactions were comprised of 10X OptiBuffer (constituents not disclosed), with the addition of 200µM each of dATP, dCTP, dGTP, dTTP; 1.1mM $MgCl_2$; 300nM of each forward and reverse primer and 0.5-2ng/µl template DNA. A typical reaction using Bioline BIO-X-ACT™ is shown in Table 2.2.

Stock Solution	**Volume per 50µl reaction (µl)**	**Final reaction concentration**
10X OptiBuffer	5	1X
DNA template (25-100ng/µl)	1	0.5-2ng/µl
Forward primer (10µM)	1.5	300nM
Reverse primer (10µM)	1.5	300nM
dNTP (2mM)	5	200µM
$MgCl_2$ (50mM)	2.2	1.1mM
BIO-X-ACT Long DNA Polymerase (4u/µl)	0.5	0.04u/µl
ddH_20	33.3	-

Table 2.2: Preparation of a 50µl PCR reaction using Bioline BIO-X-ACT™

PCR reactions were performed in ABGene 96-well polypropylene PCR plates, heat-sealed with foil, and run on an M.J. Research PTC-225 Tetrad DNA Engine thermocycler. PCR conditions were adjusted to optimise different reactions but all were based on the standard protocol shown in Table 2.3.

Step	PCR phase	Temperature	Time
1	Initial denaturation	95°C	2 minutes
2	Denaturation	95°C	30 seconds
3	Annealing	2°C below T_M of primers	30 seconds
4	Extension	72°C – ReddyMix™ 68°C – BIO-X-ACT™	1 minute/1Mb of expected product
5	Thermocycling	Repeat steps 2-4, 34 times	–
6	Cooling	4°C	Indefinitely

Table 2.3: PCR conditions used for DNA amplification

2.5 AGAROSE GEL ELECTROPHORESIS

Size determination of DNA fragments was carried out by agarose gel electrophoresis using Hybaid Electro4 gel tanks. Agarose (UltraPURE, GIBCO BRL) was added to 0.5X TBE buffer (44mM Tris, 45mM boric acid, 1mM EDTA, pH 8) at concentrations varying from 2-4% depending on the expected product size. This was melted using a microwave on medium power and ethidium bromide was added at a concentration of 0.4μg/ml in order to allow visualisation of DNA fragments under long-wave ultraviolet light. Gels were cast in perspex gel trays with appropriate combs inserted for the loading of samples. In general, 2% gels were used to resolve fragments ranging from 100-600bp in length. Where higher resolution was required for small fragments or when screening for small differences in product size, 3-4% gels were used. To provide a reference for size and for concentration, DNA molecular weight marker was loaded on each row of samples to be run. Marker VIII (Boehringer Mannheim) was used initially, later being replaced by Hyperladder IV (Bioline). PCR samples from ReddyMix reactions could be loaded directly into agarose gels since the 2X master mix includes a loading buffer. Samples from BIO-X-ACT reactions were prepared for loading by the addition of 6X loading buffer (0.25% bromophenol blue, 12.5mM EDTA,

40% sucrose). Electrophoresis was carried out at 80-150 volts for 1-2 hours depending on the percentage of the gel and the size of products being resolved. Lower voltages were used for lower percentage gels, higher voltages for higher percentage gels. Following electrophoresis gels were visualised on a UV transilluminator and images captured using initially a video capture system (Herolab E.A.S.Y. 429K) and later a digital capture device (SynGene).

2.6 RNA PREPARATION

Preparation of RNA was achieved using TRIzol (Invitrogen), a solution of phenol and guanidine isothiocyanate which maintains the integrity of the RNA, while disrupting cells and dissolving cell components. In the case of mouse and fish tissue, samples were homogenised before the addition of 1ml TRIzol. In the case of ES cells, TRIzol was added directly and homogenisation achieved by passing the lysate through a pipette several times. Samples were incubated at room temperature for 5 minutes to allow full lysis to occur, then 200µl chloroform was added, mixed vigorously by hand for 15 seconds and incubated for a further 2-3 minutes at room temperature. Following centrifugation at no more than 12,000g for 15 minutes at 2 to 8°C, the colourless aqueous upper phase was transferred to a fresh tube. RNA was precipitated from the supernatant by addition of 500µl isopropyl alcohol, mixing and incubation at room temperature for 10 minutes before centrifugation at no more than 12,000g for 15 minutes at 2 to 8°C. The supernatant was then removed and discarded, and the RNA pellet washed with 1ml of 75% ethanol (prepared using RNase-free water). This was mixed by vortexing and centrifuged at no more than 7.500g for 5 minutes at 2-8°C before being allowed to partially air-dry. Resuspension was carried out by the addition of RNase-free water, mixing by pipette and incubation at 55-60°C for 10 minutes. Quantification of RNA was carried out using an Eppendorf Biophotometer with readings being taken at $OD_{\lambda 260}$ and a conversion factor of 1 OD unit being equal to 38µg of single-stranded DNA or RNA used to calculate concentration.

Optionally, the extracted RNA could be treated with DNase in order to remove genomic DNA contamination prior to reverse transcription. In this case, 1 unit of amplification grade DNase I, (Invitrogen) was added for each 1 μg of RNA sample to be treated. To this was added an appropriate volume of 10X DNase I reaction buffer, and the remaining volume made up with DEPC-treated water. Samples were incubated at room temperature for 15 minutes and a one tenth volume of 25mM EDTA was then added to inactivate the enzyme. Heat inactivation was carried out at 65°C for 10 minutes, after which the samples were ready to be used for reverse transcription.

2.7 REVERSE TRANSCRIPTION

Reverse transcription (RT-PCR) utilises the ability of the enzyme reverse transcriptase to synthesise DNA from an RNA template. The resulting complementary DNA (cDNA) fragments represent the population of genes which are expressed in the tissue from which the RNA was extracted. Since the messenger RNA molecules will have been processed and introns excised from the sequence, cDNA can be used to study the transcripts present in a given tissue type.

cDNA was prepared using the SuperScript™ II First-Strand Synthesis System for RT-PCR (Invitrogen). To 5μg of RNA sample was added 1μl 10mM dNTP and 1μl 50mM Oligo$(dT)_{20}$ primers. The reaction volume was made up to 10μl with RNase-free water and the sample incubated at 65°C for five minutes in order to allow annealing of primers to the template RNA, before being placed on ice for at least one minute. A cDNA synthesis mix consisting of 2μl 10X RT buffer, 4μl 25 mM MgCl2, 2μl 0.1M DTT and 1μl RNaseOUT™ (40 U/μl) was made up and added to the RNA/primer mixture. This was gently mixed and collected by brief centrifugation before being incubated ate 42°C for two minutes. At this point 1μl SuperScript™ II RT (50 U/μl) was added and the sample incubated at 42°C for a further 50 minutes before the reaction was terminated at 70°C for 15 minutes and chilled

on ice. RNA was then removed by the addition of 1µl RNase H (2 U/µl) and incubation at 37°C for 20 minutes. The reaction volume was made up to 50µl by the addition of 30µl ddH_2O and 1µl used as the template in subsequent PCR reactions.

2.8 DNA SEQUENCING

Sequencing of DNA samples was carried out using the dideoxy chain termination method described by Sanger *et al.* (1977). In this process, DNA polymerase I is utilised to synthesise complementary copies of a template DNA molecule in the presence of an ample quantity of deoxy-NTPs and a limited amount of differently fluorescence-labelled dideoxy-NTPs. DNA synthesis continues until a dideoxy nucleotide residue is incorporated, at which point the chain is terminated. In a given sequencing reaction, different chains will be terminated at different points, giving a population of DNA molecules carrying fluorescent labels denoting which nucleotide constitutes the terminal residue. When these are separated on a polyacrylamide gel, the differently-sized molecules migrate at different rates, giving a series of fluorescent bands which can be read as the sequence of the DNA molecule.

DNA fragments to be sequenced were obtained by PCR and their specificity verified by agarose gel electrophoresis before proceeding. They were then purified using an AMPure™ PCR Purification kit (Agencourt) which utilises magnetic beads to separate PCR products from remaining reaction ingredients which might disrupt subsequent processes. To each reaction in a 96-well PCR plate was added 1.8X the reaction volume of AMPure™ and the solution mixed thoroughly before being placed onto a SPRIplate96-R magnetic plate. After 5-10 minutes separation time, cleared solution was removed and discarded while the magnetic beads to which PCR products have adhered remained attached to the sides of the well. The beads were washed twice by the addition of 90µl of 70% ethanol and after the removal of the second wash they were allowed to air-dry. Elution was carried out by the addition of 25µl 1X T0.1E (10mM Tris-HCL; 0.1mM EDTA) and the plate

sealed and vortexed before collection by brief centrifugation. The PCR plate was then returned to the magnetic plate and separation of the beads allowed to occur once more, at which point the eluate was removed to a fresh plate. A small amount of the purified product was run out on an agarose gel in order to determine concentration before being used as the template for sequencing reactions.

Sequencing reactions were set up using the BigDye Terminator v3.1 Cycle Sequencing Kit (Applied Biosystems). Each reaction consisted of 1.5µl Sanger BigDye Dilution buffer (0.3M Tris HCl, pH9; 6mM MgCl2; 10% tetramethylene sulphone), 0.5µl BigDye terminator v3.1, 5-15ng template DNA, 1µM forward or reverse primer, and was made up to a total volume of 9µl with ddH2O. Cycle sequencing was then carried out on an M.J. Research PTC-225 Tetrad DNA Engine thermocycler using the conditions shown in Table 2.4.

Step	Cycle	Temperature	Time
1	Initial denaturation	96°C	30 seconds
2	Denaturation	92°C	15 seconds
3	Annealing	52°C	15 seconds
4	Extension	60°C	2 minutes
5	Thermocycling	Repeat steps 2-4, 44 times	-
6	Cooling	10°C	Indefinitely

Table 2.4: Thermocycling conditions used for sequencing reactions

DNA precipitation was used to purify the amplified samples from the remaining reaction components. This was achieved by the addition of 50µl precipitation mix (100mM sodium acetate in 96% ethanol) and 10µl water. Following centrifugation at 4000rpm and 4°C for 40 minutes, the supernatant was removed and the pellet washed with 100µl cold 70% ethanol. Samples were again centrifuged at 4000rpm and 4°C for 10 minutes, the supernatant was removed and the pellet allowed to dry. They were then loaded onto an ABI 3700 capillary sequencer (Applied Biosystems). Analysis of the resulting

sequence files was carried out initially using the software suite Vector NTI (InforMax) and later the software package Gap4 (Staden).

Chapter 3:

Refinement of the bv critical region using the existing backcross

CHAPTER 3

REFINEMENT OF THE *BV* CRITICAL REGION USING THE EXISTING BACKCROSS

3.1 INTRODUCTION

This chapter describes the work carried out to characterise and refine the candidate region for the *bronx waltzer* gene as defined by a pre-existing intraspecific backcross of [(*bv*/*bv* x 101/H)F1 x *bv*/*bv*]. It also includes the determination for the first time of the physical size of the critical interval.

3.1.1 Genetic mapping

Recombination events which occur between sister chromatids during meiosis are the phenomena that make genetic mapping possible. Genetic mapping determines the linkage between two given markers based on the frequency with which they recombine. The closer they are to each other, the lower the probability that a crossover will occur between them. Hence a marker which is seen to co-segregate closely with a phenotype can be an indication that the allele responsible for the phenotype is located close to the marker. The second requirement for genetic mapping is a means of distinguishing between copies of a marker inherited from each parent. The markers used must be polymorphic – be able to exist as multiple variations within a given population. In human genetic mapping this is achieved by assessing the haplotypes of different family members in order to establish which portions of the genome have been inherited from each parent. In the mouse, it is made simpler by the ability to control matings and so introduce polymorphisms into a population by crossing the mutant mouse with a wild type mouse carrying different alleles of the genetic markers to be used. The most common strategy, and the one used here, is the backcross.

3.1.1.1 Establishing a backcross

The first stage of the backcross is to mate the mutant strain with a different strain, known as an outcross. In this case the outcross was between *bronx waltzer* (*bv*/*bv*) and the inbred strain 101/H (+/+ at the *bronx waltzer* locus). The resulting F_1 offspring will all be +/*bv*, carrying one chromosome from each parent. Since the *bronx waltzer* mutation is recessive, these are then mated with homozygous *bv*/*bv* mice so as to give backcross progeny which may be either +/*bv* or *bv*/*bv* and allow phenotyping according to their behaviour. Each backcross mouse will carry one chromosome purely from the *bronx waltzer* background and one from the outcross parent. This chromosome from the F_1 parent may have undergone recombination between *bv* and 101/H DNA, allowing the position of polymorphic markers to be mapped in relation to the phenotype of the mouse. This backcross strategy is illustrated in Figure 3.1.

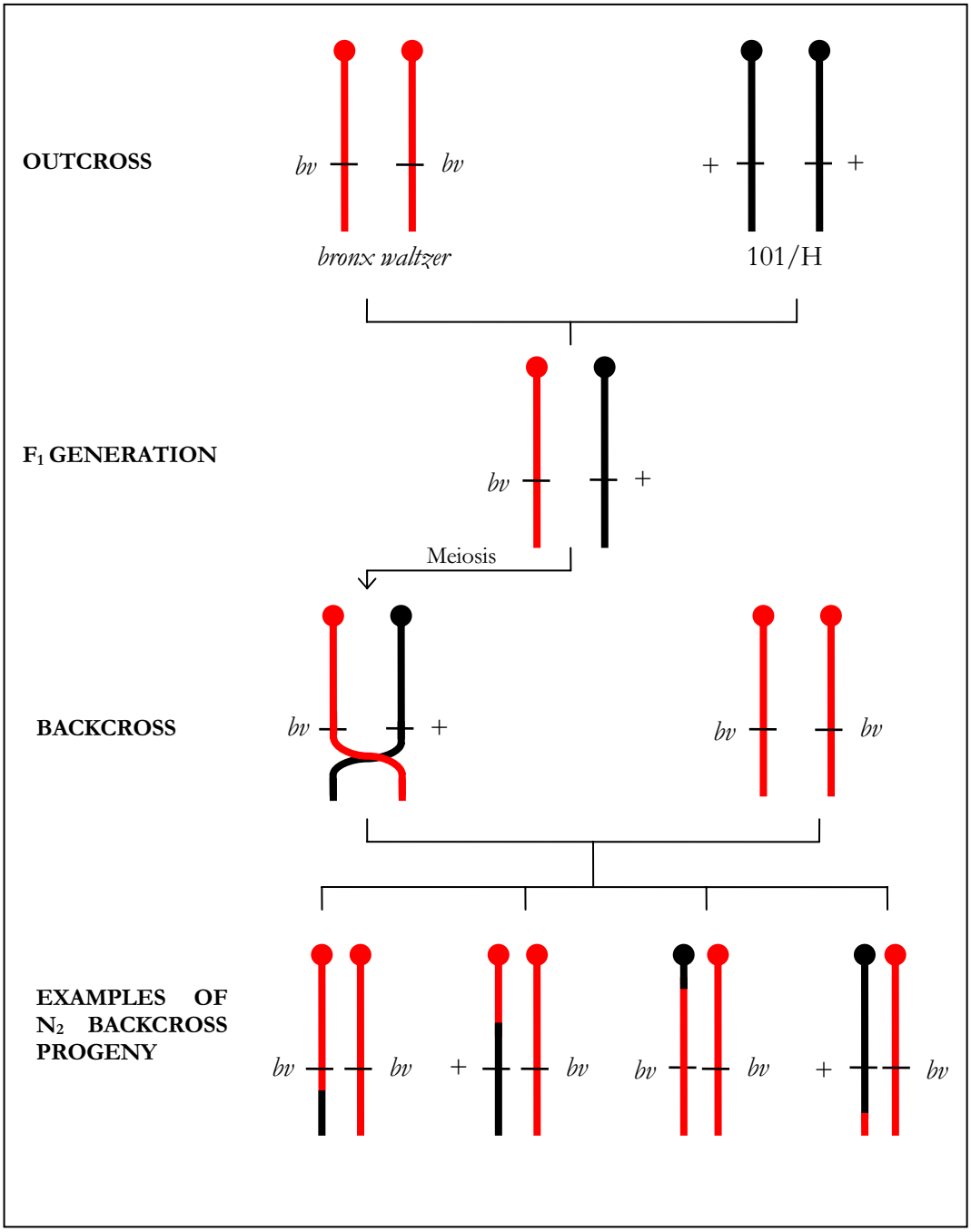

Figure 3.1: The backcross strategy employed in the genetic mapping of the *bronx waltzer* locus. Chromosomes derived from *bronx waltzer* are shown in red while those from the inbred strain 101/H are in black. During gamete formation in the F1 generation, recombination may occur between the two parental chromosomes at the prophase I phase of meiosis. These recombinant chromosomes are inherited by the backcross offspring along with one set of *bronx waltzer* chromosomes, giving a variety of possible progeny as shown in the bottom row.

3.1.1.2 Haplotype analysis

Study of the recombined chromosomes inherited from the F_1 generation mice by backcross offspring is known as haplotype analysis. The frequency of recombination between two markers is used to calculate the relative genetic distance between them and the *bronx waltzer* allele, as indicated by the phenotype of the mouse, can be placed amongst them. Relative genetic distances are expressed as centiMorgans (cM), where two loci are said to be one centiMorgan apart if recombination is observed between them in 1% of meioses.

3.1.1.3 Markers for genetic mapping

In order to be informative within the context of a genetic mapping approach, markers must exhibit discernable differences between the genetic backgrounds being utilised, a property known as polymorphism. Polymorphic markers allow the parental origin of each portion of an individual's genetic make-up to be determined, thus enabling the linkage of different portions of the genome to the phenotypic trait in question to be traced.

The simplest form of polymorphism to detect is one where a stretch of sequence varies in length between strains. This is generally due to the presence of a repeat sequence which is non-coding and can exist in varying copy numbers (Hamada *et al.* 1982). Such sequences, often referred to as microsatellites or simple sequence length polymorphisms (SSLPs), are di-, tri-, or tetra-nucleotide repeats which exist at high frequency within the genome. Their varying sizes between different individuals allow simple analysis by PCR using primers designed to sequence flanking the repeat region, making them very useful as genetic markers. An example of an SSLP is shown in Figure 3.2.

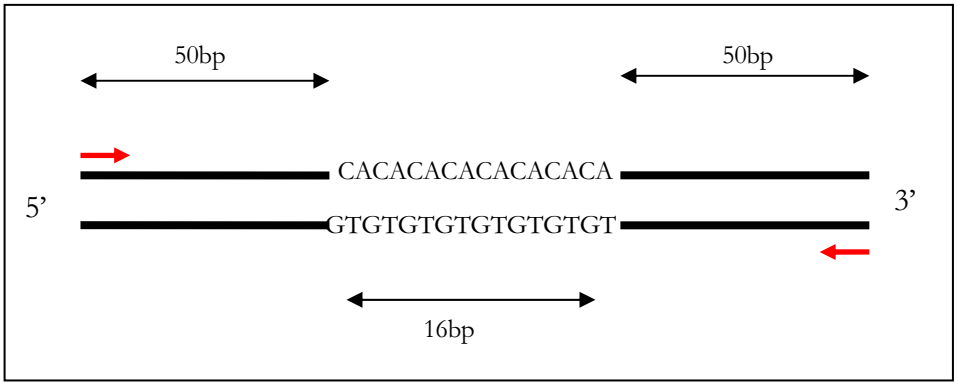

Figure 3.2: Diagram showing a typical simple sequence length polymorphism (SSLP). The example given is a di-nucleotide repeat. The number of CA units varies between individuals, giving differently sized fragments when the region is amplified by PCR using the primers shown in red.

A genetic linkage map placing 6580 such markers to a resolution of 0.2cM within the mouse genome was constructed by Dietrich *et al.* (1996). This framework map of markers greatly simplifies the process of identifying a candidate region for a given gene, since backcross mice can be quickly screened with a panel of markers chosen to cover the whole genome to initially locate a region of linkage. Markers can then be chosen at higher density from within that region in order to narrow the area of interest.

A second form of polymorphism which can be useful for genetic mapping is the single nucleotide polymorphism (SNP). These single base substitutions are present at varying densities throughout the mouse genome and may be found in both coding and non-coding regions. The more distantly two strains of mice are related, the more SNPs with differing alleles can be expected to be found. In general SNP discovery is achieved by sequence analysis, and once detected large numbers of samples can be screened for the different alleles in a number of ways. If the base change occurs within the recognition site of a restriction enzyme and disrupts its ability to bind, it is possible to rapidly assay it by performing a restriction digest and analysing the pattern of fragment sizes obtained. An alternate method of SNP screening is to perform an Oligo Ligation Assay (OLA), which requires a perfect sequence match between a pair of oligos and the target sequence in the amplified fragment to give a

band. If the polymorphic base is present at the point where the two oligos touch, the oligos can be ligated together and produce a band of the expected size. Additionally, the assay can be designed to give various different sized bands by using several sets of oligo probes, and different fluorescent tag colours can also be incorporated.

3.1.1.4 Phenotypic analysis

Mice were typed phenotypically at the *bronx waltzer* allele by assessment of their behaviour. Two behavioural parameters were analysed – the presence or absence of the Preyer reflex as an indicator of basic auditory function and manifestation of shaker-waltzer behaviour as a measure of vestibular dysfunction. Prior to sacrificing the backcross offspring for DNA preparation, these tests were performed to determine the phenotype of each mouse and so to establish which copy of the *bv* allele had been inherited from the F_1 parent. Since all mice inherit one mutant copy of the *bv* gene from the backcross parent, manifestation of the *bronx waltzer* phenotype can be interpreted to mean that the mouse must have inherited a second mutant copy from the F_1 parent. Conversely, mice with normal behaviour and responses must have inherited a wild type copy of the gene, making them heterozygous at the locus.

In the course of this backcross the Preyer reflex test was administered by striking a large pair of metal forceps on a metal surface out of sight and away from the cage so as to minimize vibration. A positive result was recorded if the mouse retracted their pinnae in response to this broad frequency band of sound. In the absence of this response a negative result was recorded. Shaker-waltzer behaviour was assessed by observing the mice and a positive result was recorded if the mouse demonstrated rapid upward flicking motions of the head and periodic circling within the cage. In cases where the phenotype was questionable, a reaching response test was administered. Here, the mouse was held by the tail above the cage and its behaviour observed. Mice exhibiting

shaker-waltzer behaviour curl their heads towards their belly and/or revolve around their body axis while normal mice stretch their limbs and reach out towards the ground.

Mice thought to be homozygous for *bv* were removed from the cage first in order to prevent their hyperactive behaviour from disturbing their heterozygote littermates and causing them to behave atypically as a result of nervousness. The backcross progeny were all culled by cervical dislocation and their tissue taken and stored as described in Section 2.2.

3.1.2 The existing *bv*/101 genetic map

The backcross between *bronx waltzer* and 101/H was originally established by Bussoli (1996). The inbred strain 101/H was chosen as the outcross background following analysis of 33 SSLP markers mapping to mouse chromosome 5, to which the mutation had previously been localised (R. Brister, *pers. comm.*). 101/H showed 52% polymorphism with *bronx waltzer*, making it the most polymorphic of the inbred strains tested. In an initial typing of 701 backcross mice, the mutation was mapped to a 1.28cM region between the markers *D5Mit25* and *D5Mit188* (Bussoli *et al.* 1997).

Following subsequent breeding and work by Cheong (2000), a final total of 1085 backcross mice arose from this cross. Twelve of these mice were excluded from further analysis as a result of either discrepant or difficult phenotyping, leaving 1073 for haplotype analysis. During the course of this study, the single mouse (T672) which had positioned the *bv* locus distal of the marker *D5Mit209* was retyped and its breakpoint found to lie instead between *D5Mit367* and *D5Mit95*. As a result, and with the inclusion of data arising from the new backcross mice, the new candidate region for *bronx waltzer* was described as a 1.86cM region flanked by the markers *D5Mit25* and *D5Mit209*. The haplotype diagram representing these results is shown in Figure 3.3, and the genetic map arising from these data is shown in Figure 3.4.

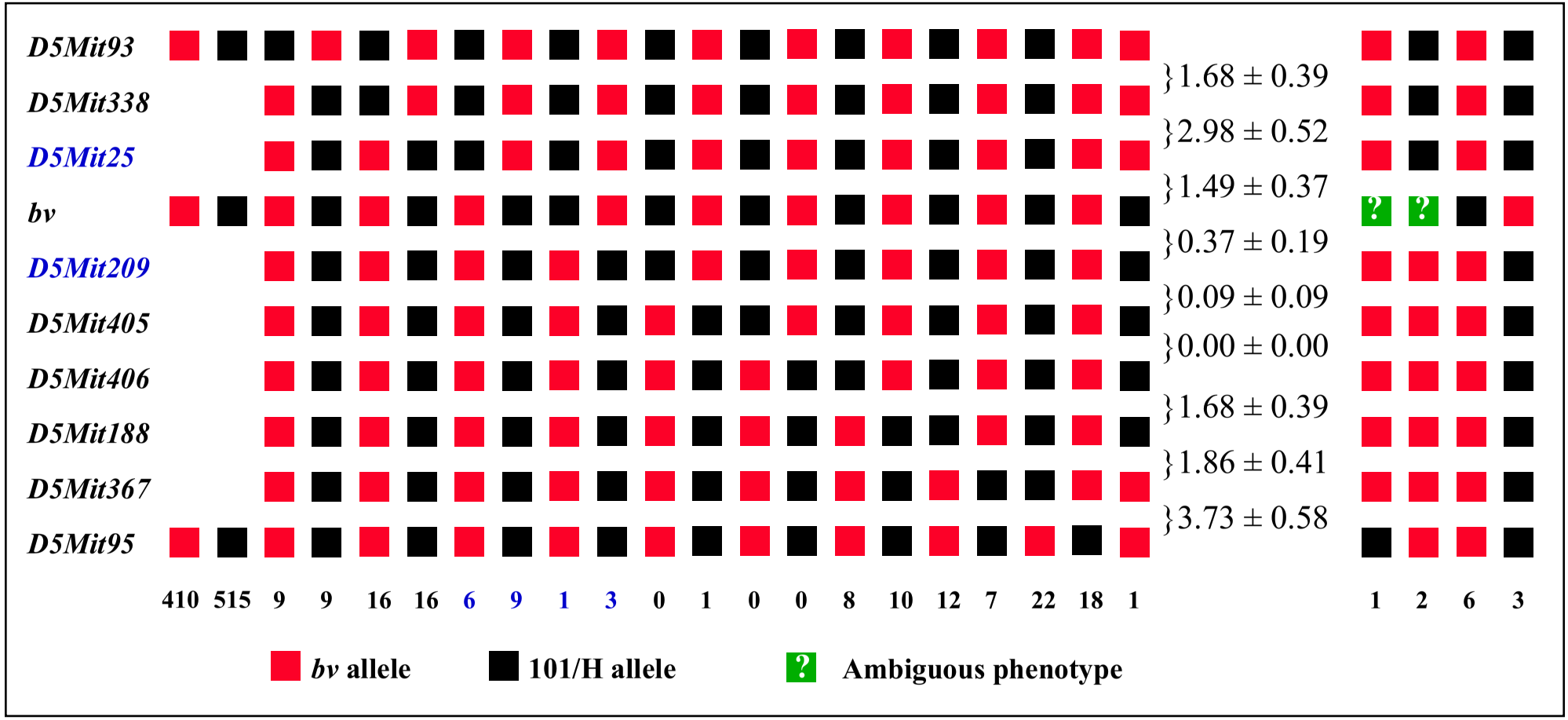

Figure 3.3: Haplotype analysis of the total 1085 progeny arising from the *bv*/101/H intraspecific backcross. Genetic markers used in the mapping are listed on the left, and numbers of mice typed with each pattern of recombination are shown along the bottom. Genetic distances calculated between the markers based on the number of recombinations occurring between them are given to the right. Mice excluded from the analysis as a result of discrepant or difficult phenotyping are shown on the far right of the diagram. Flanking markers and mice exhibiting recombinations between them are highlighted in **blue**. Adapted from Cheong (2000).

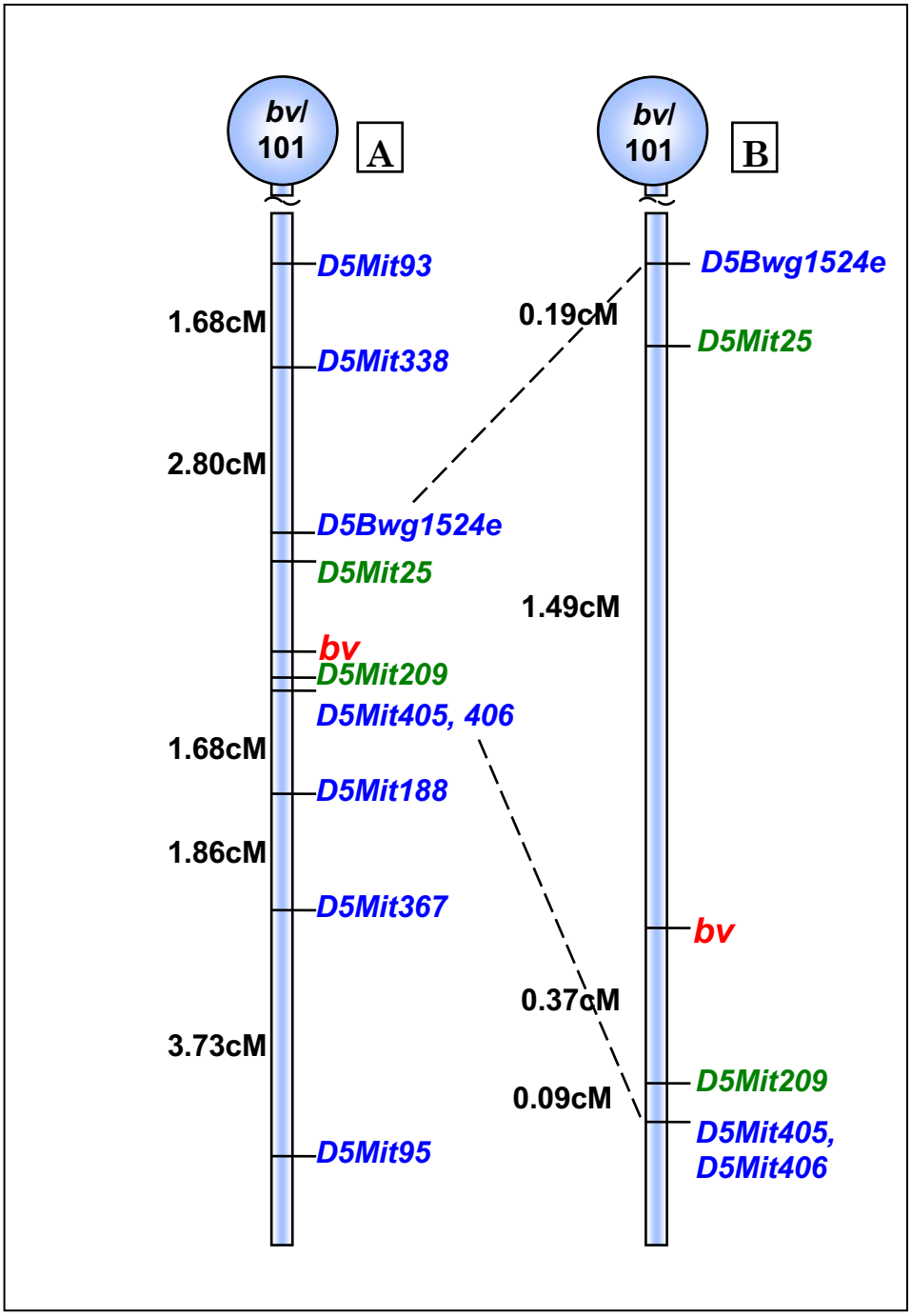

Figure 3.4: The mouse genetic map as elucidated using the 1073 backcross mice typed from the *bv*/101 cross. [A] depicts the region on chromosome 5 surrounding the *bv* locus, the markers closest to *bv* are shown on an enlarged map in [B].Genetic loci are drawn to the right of the diagrams, with the *bronx waltzer* locus shown in red, flanking markers in green and other genetic markers in blue. Genetic distances determined by the number of recombinations observed between markers are given in black to the left of the diagrams.

3.1.3 Identifying new markers

As shown by the haplotype diagram in Figure 3.3, there remain 19 backcross mice exhibiting recombinations between D5Mit25 and D5Mit209. Therefore this backcross still holds the potential to narrow the *bv* candidate region further if novel polymorphic markers can be found which map between the flanking markers. Previous attempts made at identifying such markers have included the screening of the European Collaborative Interspecific Backcross (EUCIB) mapping panel and the Jackson Laboratory mapping panels BSB and BSS in order to identify ESTs or genes which may include polymorphisms (Cheong 2000). This work also helped to identify a region of conserved synteny on human chromosome 12, from which gene sequence was obtained. One of the markers identified in this manner, D5Bwg1524e, proved to be polymorphic for *bv* and 101, but on screening the backcross panel it was found to map proximal to D5Mit25 and therefore lies outside the critical region as shown in Figure 3.4.

The paucity of markers in the region and the potential remaining in the backcross are addressed in this chapter with a continuation of the search for new markers using resources and sequence that were only made available more recently.

3.1.4 Previous physical mapping

Using the genetic map determined by the *bv*/101 backcross, the next stage of positional cloning began with the construction of a physical map to cover the critical interval (Cheong 2000). The genetic markers which mapped close to the *bronx waltzer* locus were first used to screen a YAC library but the clones identified in this way were suspected of harbouring deletions and chimerisms and further work was abandoned. The second library screen was of the CITB Mouse BAC library but this too was problematic and resulted in a large number of false positives. A map was built using the data obtained and the distances between markers estimated based on the sizes of the BACs for

which they were positive. Using this methodology the physical distance between the flanking markers *D5Mit25* and *D5Mit209* was determined to span under 1Mb since both markers were found to be positive for, and therefore present within a single 91Kb clone, BAC42I5. Given the 1.86cM genetic distance separating these markers, this physical distance seemed remarkably small and the results were called into question. In the mouse genome 1cM is thought to equate to roughly 2Mb of sequence so the critical interval might be expected on average to be 3.72Mb. This discrepancy could potentially be explained by the presence of a recombination hotspot located between the markers causing a higher than average recombination rate. Further physical mapping as described within this chapter allows the comparison of these data to those arising from the public mouse mapping and sequencing project.

3.2 METHODS

Some of the methods employed in this chapter are described in Chapter 2. The following procedures are specific to this chapter.

3.2.1 Bacterial Artificial Chromosomes (BACs)

The BACs used form part of the Mouse C57BL/J6 Female RPCI-23 and Mouse C57BL/J6 Male RPCI-24 BAC libraries originating from the Roswell Park Cancer Institute, Buffalo, New York. The RPCI-23 library was constructed in the pBACe3.6 vector shown in Figure 3.5 (Frengen *et al.* 1999)from *Eco*RI-digested C57BL/6J genomic DNA (Osoegawa *et al.* 2000). The RPCI-24 library is made up of size-selected *Mbo*I fragments cloned into the pTARBAC1 vector (Zeng *et al.* 2001) between the *Bam*HI sites (see Figure 3.6). Both vectors are hosted in the *Escherichia coli* substrain DH10B and include chloramphenicol resistance genes allowing for selection by growth on media containing the antibiotic. Clones originating from the RPCI-23 library are generally identified by the prefix bM, and those from the RPCI-24 library by the prefix bN.

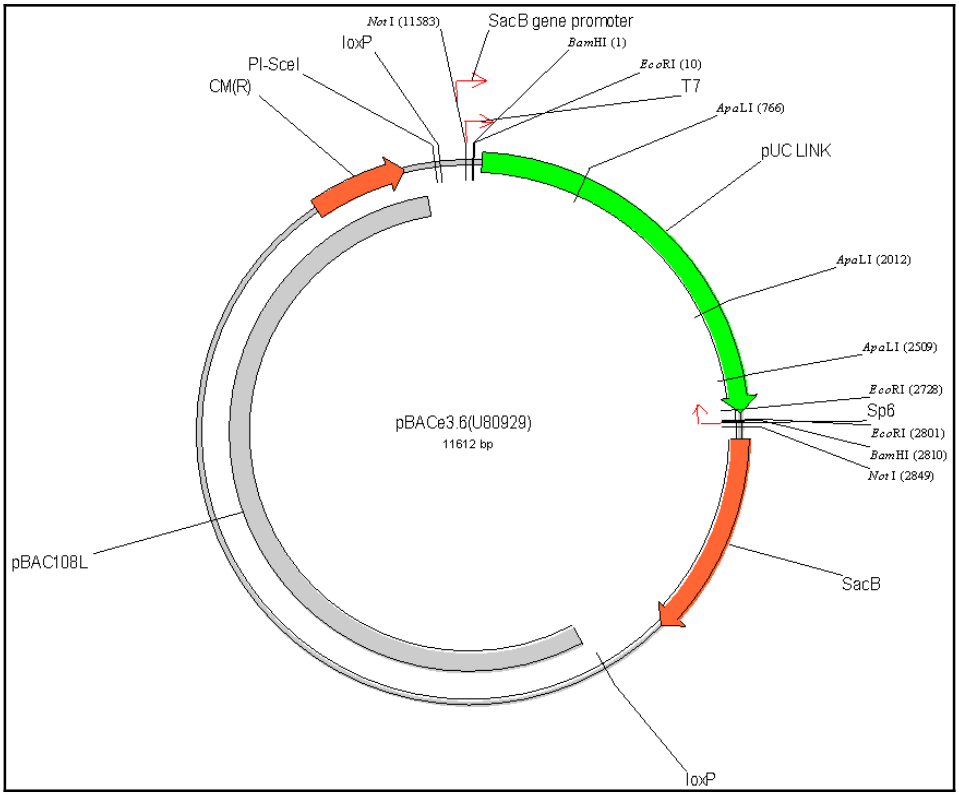

Figure 3.5: Diagrammatic representation of the cloning vector pBACe3.6 used in the construction of the female mouse C57BL/6J BAC library RPCI-23 (Frengen *et al.* 1999).

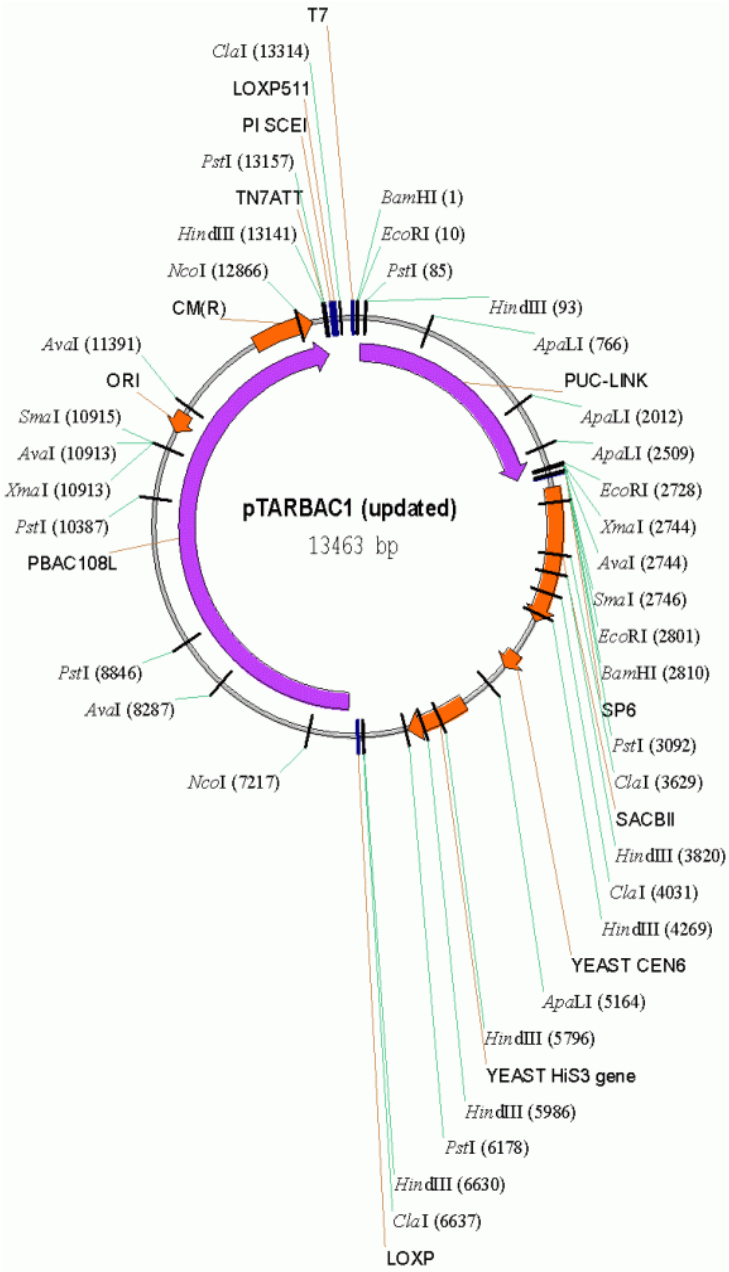

Figure 3.6: Diagrammatic representation of the cloning vector pTARBAC1 used in the construction of the male mouse C57BL/6J BAC library RPCI-24 (Zeng *et al.* 2001).

Clones were obtained from the BACPAC Resources Center (BPRC) at Children's Hospital Oakland Research Institute in Oakland, California and arrived as bacterial stab cultures. On arrival these were streaked onto LB agar (10 g/l bacto-tryptone; 5 g/l yeast extract; 10 g/l NaCl; 15 g/l agar; pH7.4) containing 20µg/ml chloramphenicol and incubated overnight at 37°C. A single colony from each culture was then used to inoculate 11ml LB broth (10 g/l bacto-tryptone; 5 g/l yeast extract; 10 g/l NaCl; pH7.4) containing 20µg/ml chloramphenicol and incubated overnight at 37°C with vigorous shaking (300rpm). These cultures were then used for the preparation of plasmid DNA as well as for long-term storage of the clones.

3.2.1.1 Storage of BAC clones

From each LB culture grown from a single bacterial colony, two aliquots of 400µl were removed to two separate 1.5ml microcentrifuge tubes labelled with the name of the clone from which they were derived. To each of these was added 100µl sterile 50% glycerol, giving a final glycerol concentration of 10%. These were then stored separately at -80°C, with one set of tubes being used to inoculate subsequent cultures and one set being reserved as archive copies.

3.2.1.2 Preparation of plasmid DNA from BAC clones

Plasmid DNA was obtained by alkaline lysis of the bacterial culture prepared as described in Section 3.2.1. The remaining 10ml culture was centrifuged at 12,000g and 4°C for 10 minutes and the supernatant removed and discarded. The cell pellet was then resuspended in 200µl Solution I (50mM glucose; 25mM Tris-HCl, pH8; 1mM EDTA), transferred to a 1.5ml microcentrifuge tube and incubated on ice for 5 minutes. Cells were lysed by the addition of 400µl briefly cooled Solution II (0.2M NaOH; 1% SDS) and mixed by inversion before being incubated on ice for a further 10 minutes. Precipitation of cellular debris and genomic DNA was achieved by the addition of 300µl

ice cold solution III (3M potassium acetate; 11.5% glacial acetic acid, pH4.8), mixing by inversion and centrifugation at 12,000g and 4ºC for 10 minutes. The supernatant was then removed to a fresh tube to which was added 600µl ice cold isopropanol in order to precipitate plasmid DNA. Samples were incubated on ice for 10 minutes before being centrifuged at 12,000g and 4ºC for 15 minutes. The supernatant was then discarded and the pellet resuspended in 200µl T0.1E (10mM Tris-HCL; 0.1mM EDTA). Plasmid DNA was purified by the addition of 200µl 50:50 phenol:chloroform, vigorous shaking and centrifugation at 12,000g and 4ºC for 5 minutes. The aqueous layer was removed to a fresh tube and DNA re-precipitated by the addition of 20µl 3M sodium acetate and 200µl isopropanol. Samples were then incubated on ice for 10 minutes before being centrifuged at 12,000g and 4ºC for 15 minutes. The supernatant was removed and the pellet washed by the addition of 200µl 70% ethanol followed by centrifugation at 12,000g and 4ºC for 5 minutes. Following removal of the supernatant, pellets were allowed to air dry completely before being resuspended in 50µl T0.1E (10mM Tris-HCL; 0.1mM EDTA). RNA was removed by the addition of 1µl 10mg/ml RNase and incubation at 37ºC for 1 hour. DNA was then quantified using a UV spectrophotometer (see Section 2.3) and dilutions made for use as template DNA in subsequent PCR reactions. Remaining DNA was stored at -20ºC.

3.2.1.3 Building a BAC contig to span the region

The following work was carried out prior to the publication of the map of the mouse genome (Gregory *et al.* 2002) but was enabled by access to the raw mapping data during assembly by the authors. These data consisted of clones from the BAC libraries RPCI23 and RPCI24 (see Section 3.2.1) positioned primarily using *Hin*dIII fingerprints of the clone inserts (Marra *et al.* 1997; Soderlund *et al.* 2000) alongside comparison of BAC end sequences (Zhao *et al.* 2001) to the tile path of sequenced human clones. These together were used to assemble the clones into contiguous series where neighbouring clones

shared significant restriction fragment lengths on digestion with *Hin*dIII, and where the order of BAC end sequences matched that found in the human sequence. This process of contiguation was carried out using the software package FPC (Soderlund *et al.* 2000) which is currently available from the Arizona Genomics Institute website (http://www.genome.arizona.edu/fpc/). Markers were added to the map by electronic PCR (Schuler 1997) or by hybridisation with overgo probes (Han *et al.* 2000).

The flanking markers *D5Mit25* and *D5Mit209* were localised to the pre-publication map by sequence identity. Using the raw mapping data, a tile path of 32 BACs was selected which, judging from their restriction fingerprints, would represent the complete region between the flanking markers. This was achieved by ensuring that adjacent tile path clones shared a number of restriction fragments of the same length.

3.2.2 Investigating potential new polymorphisms

A number of different approaches were used in order to garner information regarding new regions of polymorphism between the *bv* stock genetic background and that of the chosen backcross strain 101/H.

3.2.2.1 Mouse SNP Database

The first of these was the employment of the Mouse SNP Database (http://mousesnp.roche.com/cgi-bin/msnp.pl) – a database holding records of reported single nucleotide polymorphisms between inbred strains which predated the more extensive SNP data now available through Mouse Ensembl (http://www.ensembl.org/Mus_musculus/). This database is searchable using the genetic distances determined by the MIT F2 Intercross (Dietrich *et al.* 1996) and available on the Whitehead Institute/MIT Center for Genome Research website (http://www.broad.mit.edu/cgi-bin/mouse/sts_info). The positions of the flanking markers *D5Mit25* and *D5Mit209* are 49.5cM and 49.2cM respectively, and these values were used to

obtain records from within the database which may lie within the critical region. Because the *bronx waltzer* mutation is not maintained on in inbred strain background the database could not be used to determine whether the SNPs would be polymorphic within the backcross samples, but was instead used as an indicator of potential polymorphism to be determined by PCR (see Section 2.4) or by sequencing (see Section 2.8). The SNPs obtained from this database and the sequences of primers used to screen for them are given in Appendix A.1.

3.2.2.2 Sequence sampling

The second approach used was one of sequence sampling within the critical region. This effort also predated the release of the mouse genome sequence and so was limited to those areas where sequence was known and hence primers could be designed. Sequences utilised included 20 from 3' untranslated regions (UTRs) of genes mapping genetically within the region and 43 BAC end sequences obtained using primers placed within vector sequence to amplify part of the cloned insert (Kelley *et al.* 1999; Zhao *et al.* 2001) and available via the NCBI Clone Registry (http://www.ncbi.nlm.nih.gov/genome/clone/). Where a sequence was too large to be amplified by a single set of primers, several pairs of primers were designed to amplify overlapping regions of the sequence and so cover its full length. These short sequences were screened first for size polymorphisms between *bv* and 101/H by PCR and agarose gel electrophoresis and later for smaller polymorphisms by sequencing. The primers used to amplify 3' UTRs are in Appendix A.2, and those used to assay BAC ends are given in Appendix A.3.

3.2.2.3 Tandem repeats

With the publication of the first draft of the mouse genome (Gregory *et al.* 2002), new methods became available in the search for novel polymorphisms.

The third approach used an algorithm designed to find regions of tandem repeats within a specified sequence (Benson, 1999), in the hope that some of these would prove to be SSLPs. Software based on this algorithm was obtained from the Boston University website (http://tandem.bu.edu/trf/trf.html) and sequence lying between the flanking markers was processed using this program. Regions showing tandem repeats of large size and high repeat conservation were selected as being most likely to be polymorphic. Of these, 18 were chosen which were distributed throughout the candidate region. Primers were designed around each tandem repeat (see Appendix A.4) and used to amplify fragments from *bv* and 101/H templates which could then be compared for size differences using agarose gel electrophoresis. Later, they were also sequenced in an effort to detect smaller size differences which may not be resolved by electrophoresis.

3.2.2.4 SNPs from published sequence

A growing number of SNPs from various strains in comparison to the published C57BL/6J sequence have been reported by researchers and collated by the NCBI in dbSNP (http://www.ncbi.nlm.nih.gov/SNP/index.html). These have also been annotated onto the published sequence and can be accessed using Mouse Ensembl (http://www.ensembl.org/Mus_musculus/). Once again, primers were designed in the flanking sequence of 70 such SNPs which lay within the candidate region (see Appendix A.5 for primer sequences) and used to amplify fragments from *bv* and 101 templates by PCR, followed by sequencing of the products and comparative analysis to assess their polymorphism.

Recently, a new resource of potential SNPs became available as a result of the comparison of sequence from the strain 129S5/SvEv^{Brd} to the published sequence for C57BL/6J. This sequence sampling of 129S5/SvEv^{Brd} was a result of the Mutagenic Insertion and Chromosome Engineering Resource (MICER) (Adams *et al.* 2004), a publicly available library of insertional

targeting vectors. In order to determine the position of the clones, their ends were sequenced and compared to the published C57BL/6J sequence with an identity of over 100bp with >95% identity required to confirm a location. The differences between them were then annotated as SNPs. Primers were designed to flank 119 such SNPs which lay within the *bv* region of interest (primer sequences are listed in Appendix A.6) and used to amplify fragments from *bv* and 101 templates. The products were then sequenced in order to determine whether they were also polymorphic between these strains.

3.3 RESULTS

3.3.1 A physical map of the *bronx waltzer* candidate region

Through the selection of BAC clones based on their restriction digest fingerprints, a preliminary tiling path across the region was established. Clones which had end sequences available were prioritised in order to simplify the subsequent verification of the tile path. Overlaps were tested by PCR amplification using primers designed within the end sequences of a given BAC. These were used to amplify fragments from template DNA prepared from the inserts of the BACs thought to neighbour the one being tested. DNA from the two clones on each side of each BAC was used in order to check that no clones were redundant in the tile path. This strategy is illustrated in Figure 3.7 and examples of the products obtained in these amplification assays are shown in Figure 3.8.

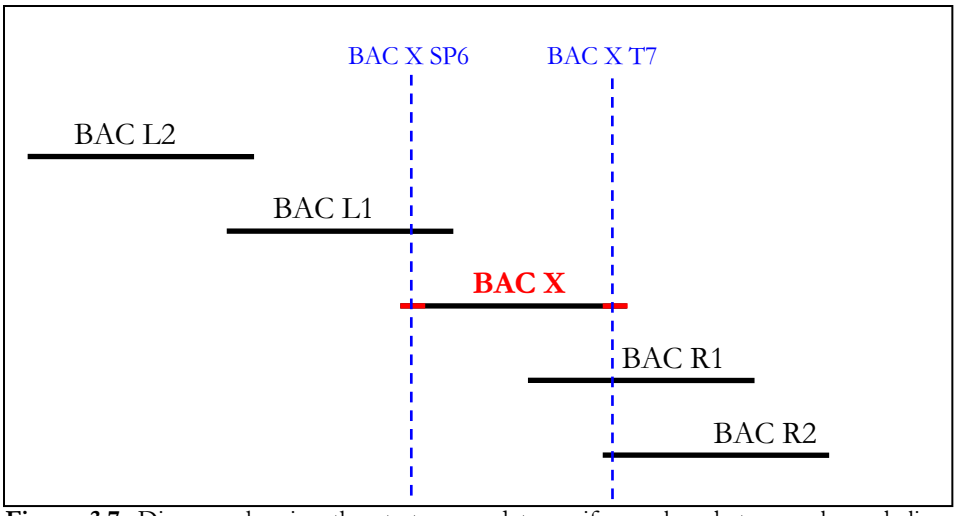

Figure 3.7: Diagram showing the strategy used to verify overlaps between clones believed to be contiguous. In this example the overlaps of BAC X are being verified. Red bars represent the end sequences of the BAC insert obtained by sequencing using primers designed to the flanking vector sequences, either SP6 or T7. The primers BACXSP6 and BACXT7 are designed within these sequences and used to amplify fragments from template DNA prepared from the proposed neighbouring clones. Successful amplification is taken as a positive result, meaning that the two clones overlap and shown here by blue dashed lines. In this case, BAC X overlaps BAC L1 to the left and BACs R1 and R2 to the right, making BAC R1 redundant.

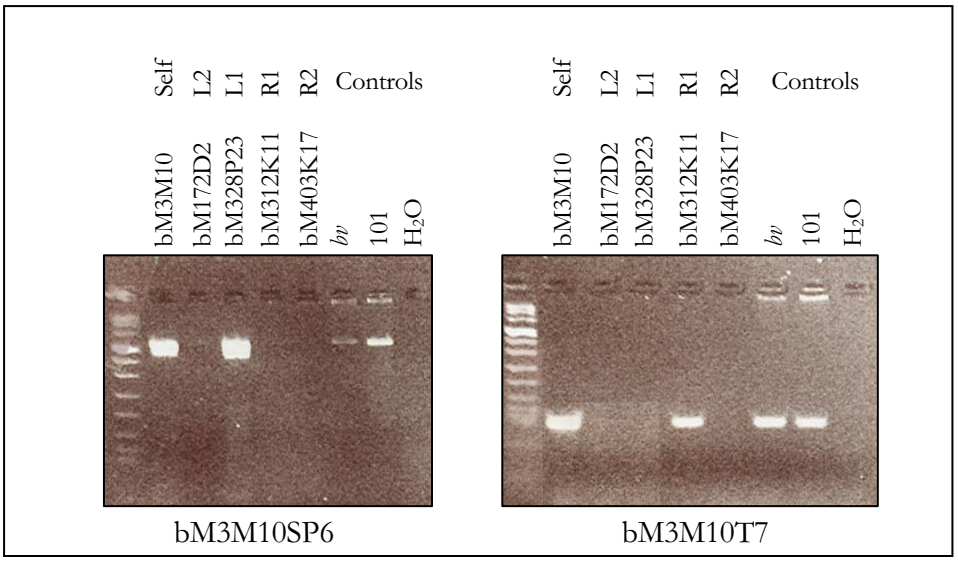

Figure 3.8: An example of the assay used to confirm BAC overlaps, showing the results for clone bM3M10. Primers designed to the SP6 end sequence are positive for the L1 clone bM328P23, while those designed to the T7 end sequence are positive for the R1 clone bM312K11. The L2 and R2 clones give negative results, showing that no clones in this portion of the tile path are redundant.

3.3.1.1 Placement of genetic mapping markers

Once the overlaps had been verified and the clones confirmed to be contiguous but non-redundant, the panel of DNA from each BAC insert was tested by PCR amplification with each of the known markers from the genetic map in order to define physical size of the critical region. Amplified products visualised by agarose gel electrophoresis were taken as evidence that a given marker was contained within the clone which gave a positive result. Some examples of this assay are shown in Figure 3.9 and the completed physical map showing confirmed overlaps and marker positions is presented in Figure 3.10.

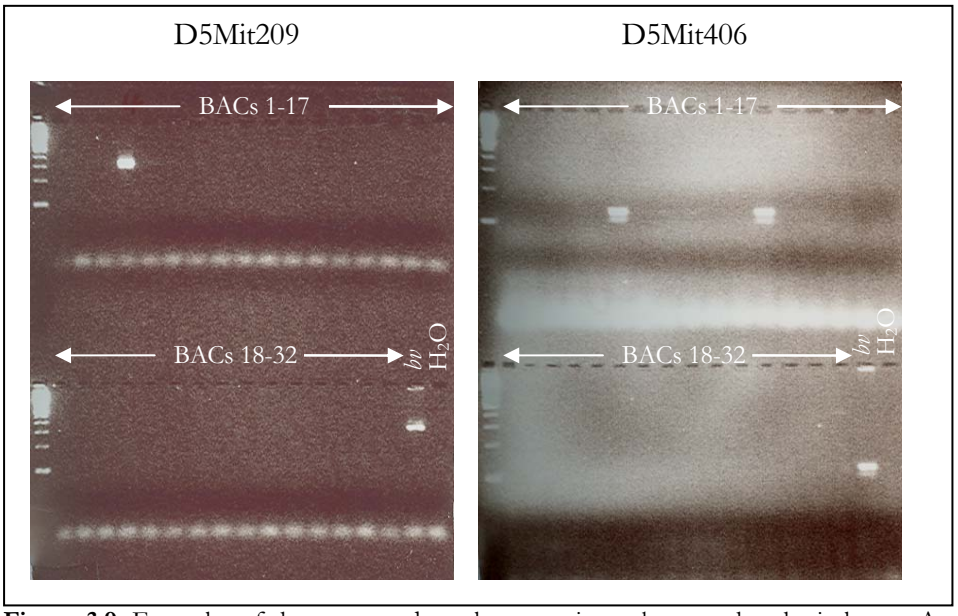

Figure 3.9: Examples of the assay used to place genetic markers on the physical map. A panel of DNA prepared from BAC clones in the minimum tiling path was screened by PCR using primers designed to the markers. A positive result for a clone suggests that it contains that marker. *D5Mit209* was positive for clone bM75L23, while D5Mit406 hits overlapping clones bM79M23 and bM231H24.

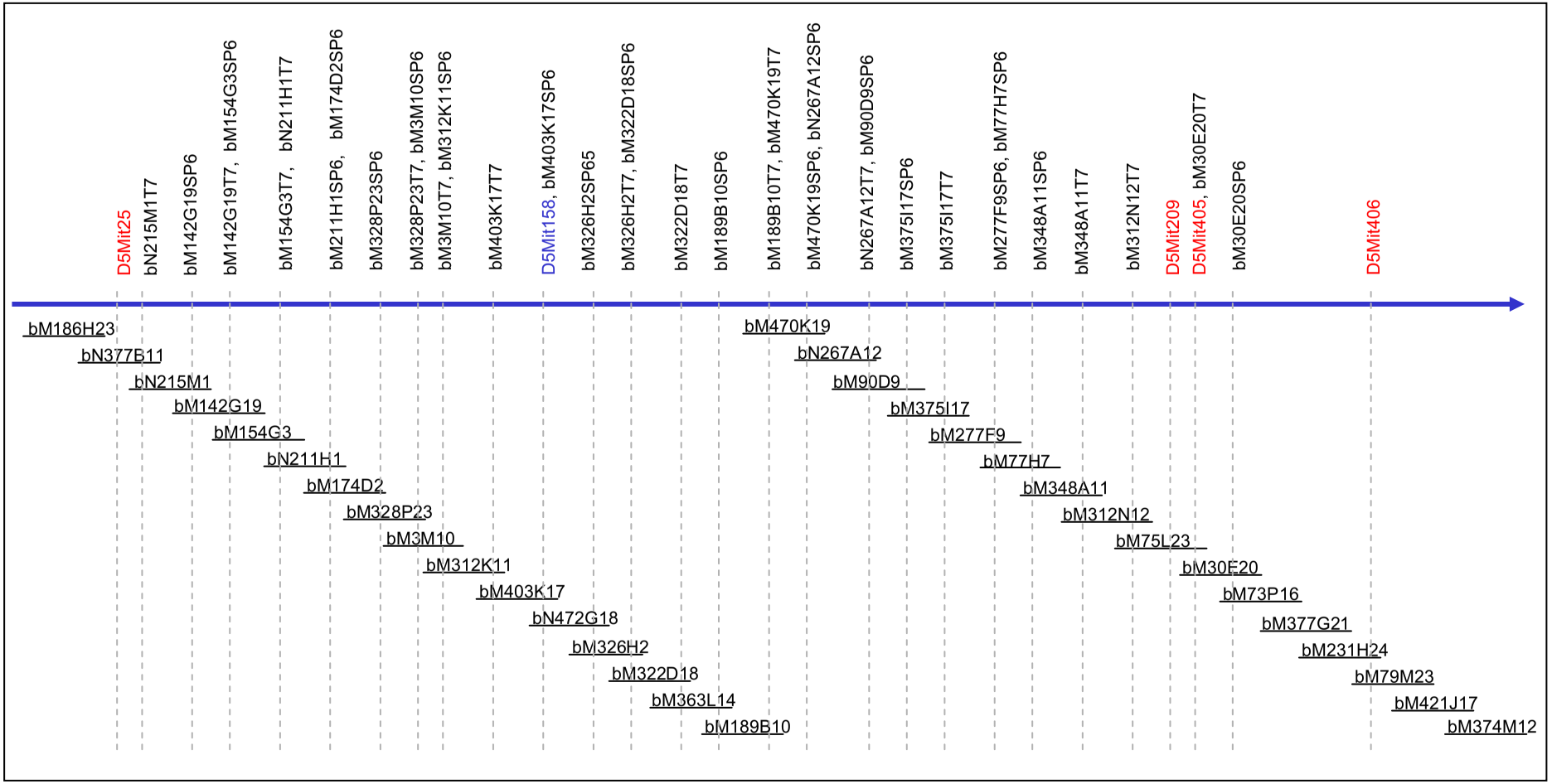

Figure 3.10: A contiguous BAC physical map of the *bronx waltzer* candidate region. BAC end sequences (shown in black) were used as markers to confirm overlaps, positive results are represented as dashed grey lines. Genetic markers polymorphic for *bv* and 101/H are shown in **red**, those not polymorphic are shown in **blue**.

3.3.1.2 Estimating the physical size of the region

With the flanking markers shown to be contained within clones bN377B11 (*D5Mit25*) and bM75L23 (*D5Mit209*) and the mapping between them proven to be contiguous, it became possible to estimate the physical distance between them. This was initially achieved using the software FPC (see Section 3.3.1.1) which is able to estimate distances based on the cumulative size of fragments in the *Hin*dIII fingerprints of clones within a given region. The distance obtained by this method between the flanking markers *D5Mit25* and *D5Mit209* was 2.6Mb. Later, as the mouse sequence became available, the physical distance was calculated as 2.8Mb, showing the mapping estimate to be quite accurate.

3.3.2 Identifying new polymorphic markers

In order to be informative within the context of the existing and still powerful panel of 1073 mice from the *bv*/101 backcross, markers must be distinguishable from one background to the other so that it can be determined from which parent a mouse has inherited that marker. This section details the outcome of the approaches used to identify such markers and reduce the size of the candidate region, thus also reducing the number of genes to be considered as candidates for *bronx waltzer*.

3.3.2.1 Publicly available SNPs

The first source of polymorphisms to be investigated was the Mouse SNP Database. Three markers were found to map close to the *bv* region and these were tested for polymorphism between *bv* and 101/H by PCR assay. Of the three markers, two were shown to be polymorphic between the two strains. M09391, a SNP represented by a G in *bv* and an A in 101/H, was detected using allele-specific PCR primers. Two reverse primers were designed to the sequence where the SNP was located, one including the G-allele and the other incorporating the A-allele. Using a common forward primer, these gave amplification only when the included allele was present, as shown in Figure 3.11. M26940, a short polymorphic repeat, was shown to be slightly longer in 101 than in *bv*, as shown in Figure 3.12. The third marker obtained from the Mouse SNP database, M11668, was tested by PCR assay but was found not to be polymorphic between the two strains used in this cross (data not shown).

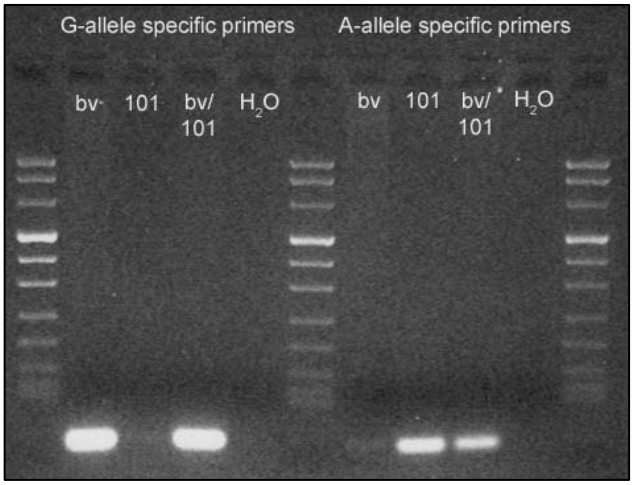

M09391

AACACCAG**[A/G]**ACTGAAT

Figure 3.11: Publicly available SNP M09391, showing allele-specific amplification and demonstrating polymorphism between *bv* and 101/H. The marker lane contains Molecular Marker VIII (Roche).

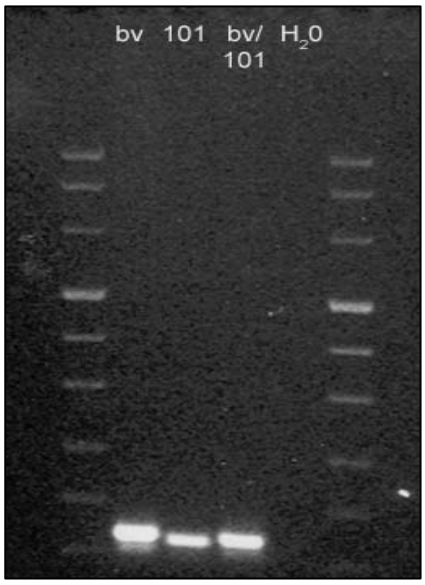

M26940

ATCTAT**[CTAT/]**TTATTT

Figure 3.12: Polymorphic repeat M26940 showing differing sizes on amplification from *bv* and 101/H templates. The marker lane contains Molecular Marker VIII (Roche).

The markers obtained from the Mouse SNP database were mapped close to the *bv* locus according to genetic distances from the MIT F2 Intercross (http://www.broad.mit.edu/mouse_rh/) but their precise positions in relation to the existing flanking markers were not known. Therefore, before screening the backcross panel of recombinant mice with these newly identified markers, their position within the region was determined by screening the panel of BAC inserts which make up the physical map described in Section 3.3.1. The resulting position of the markers is shown in Figure 3.13. This screen demonstrated that the two polymorphic markers lie distal of *D5Mit209*, are outside the candidate region and therefore cannot be used to narrow the region further. The marker M11668 does lie within the critical region but cannot be used for genetic mapping purposes because *bv* and 101 alleles do not demonstrate polymorphism and therefore cannot be differentiated.

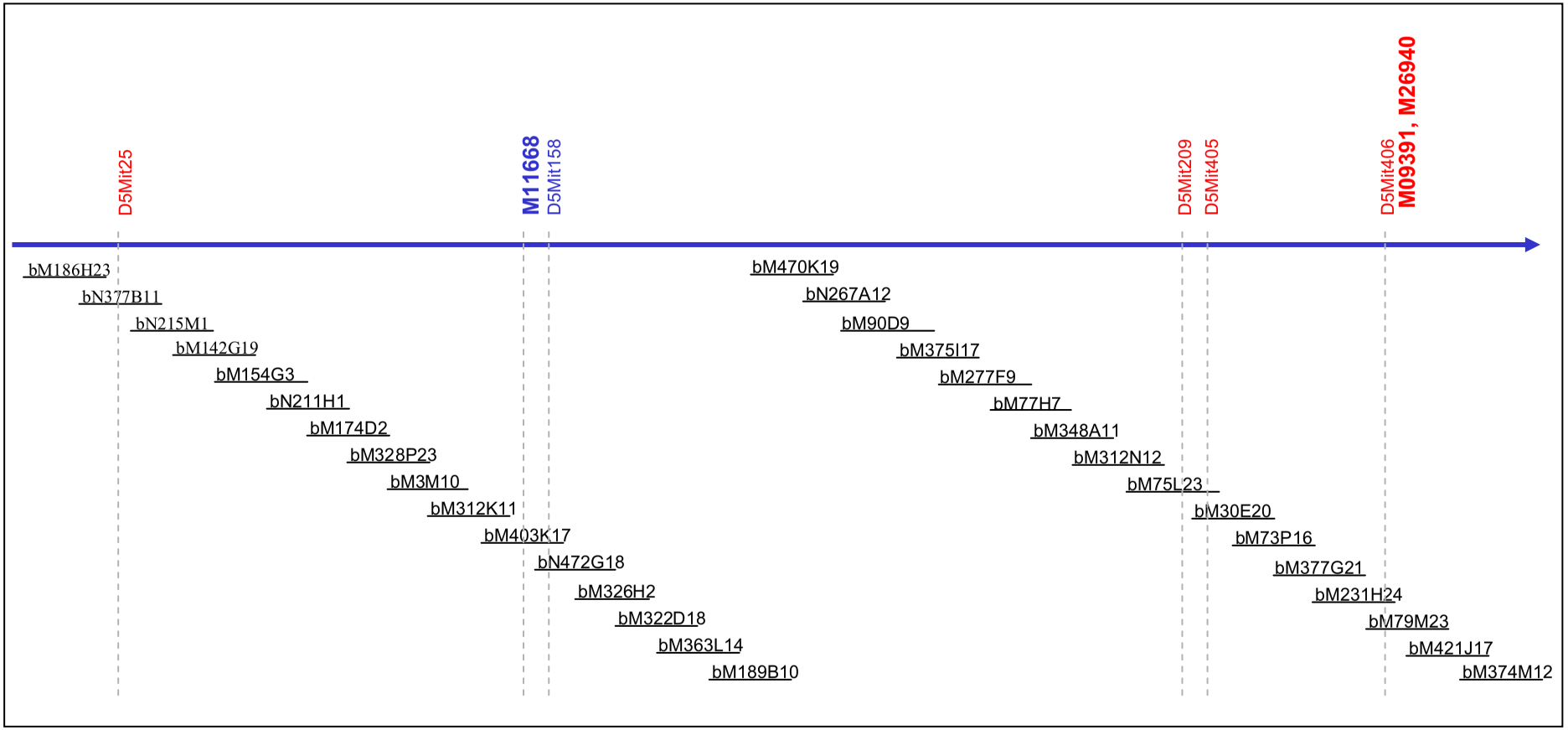

Figure 3.13: Physical BAC map of the *bronx waltzer* candidate region showing the positions of new markers obtained from the Mouse SNP Database in bold. Markers polymorphic for *bv* and 101 are in **red**, non-polymorphic markers are in **blue**.

3.3.2.2 Sequence sampling

As a means of searching out new regions of sequence which harbour differences between the two strains used in the backcross, a number of sources of sequence were employed, both before and after the publication of the mouse genome sequence.

3.3.2.2.1 BAC end sequences

The first set of sequences to be investigated for potential polymorphisms were the BAC end sequences used in the physical mapping of the region. Amplification of these by PCR using *bv* and 101 DNA as templates gave products which could be compared for size polymorphism by agarose gel electrophoresis. Of the 43 end sequences tested, only one showed a size differential between the two strains which could be detected using this method. Figure 3.14 illustrates the polymorphism identified using primers designed to the SP6 end sequence of the BAC bM277F9 (bM277F9SP6).

As an existing anchor on the physical map, bM277F9SP6 was known to lie within the critical region, situated proximal to *D5Mit209* (see Figure 3.16). Therefore the new marker was screened against the panel of mice from the *bv*/101 backcross which showed recombination between the known flanking markers. Examples of the results of this screen are shown in Figure 3.15 and a revised haplotype diagram showing its position is given in Figure 3.17.

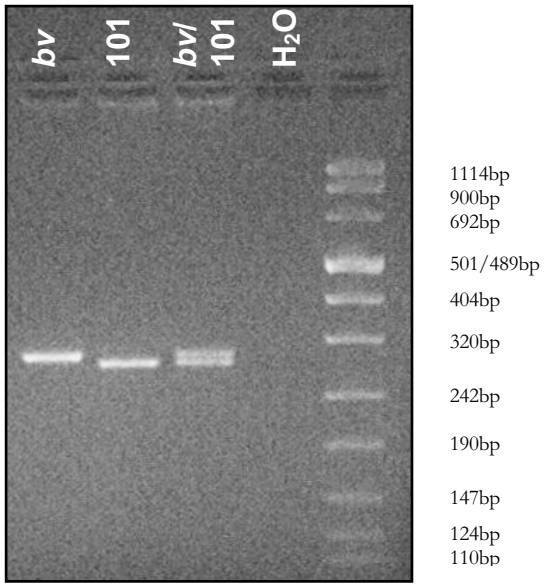

Figure 3.14: Agarose gel showing size polymorphism between *bv* and 101 within the sequence amplified by primers design to the SP6 end sequence of the clone bM277F9. The marker lane contains Molecular Marker VIII (Roche).

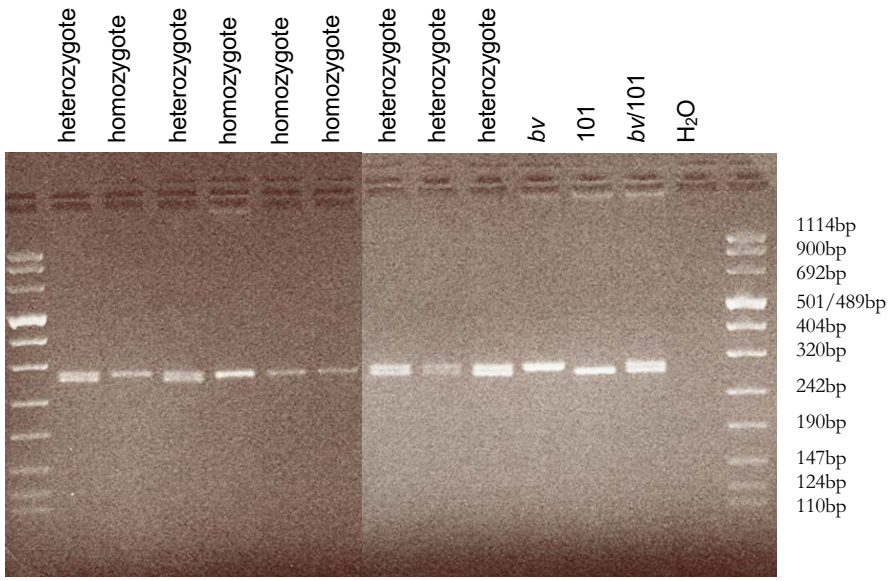

Figure 3.15: Examples of the results obtained by screening the recombinant animals from the *bv*/101 backcross with new polymorphic marker bM277F9SP6. Animals homozygous for the *bronx waltzer* background at this locus give a single larger-sized band. Animals heterozygous for *bv* and 101 give a double band and can be scored as having inherited 101 DNA from the F1 parent at this locus. The marker lane contains Molecular Marker VIII (Roche).

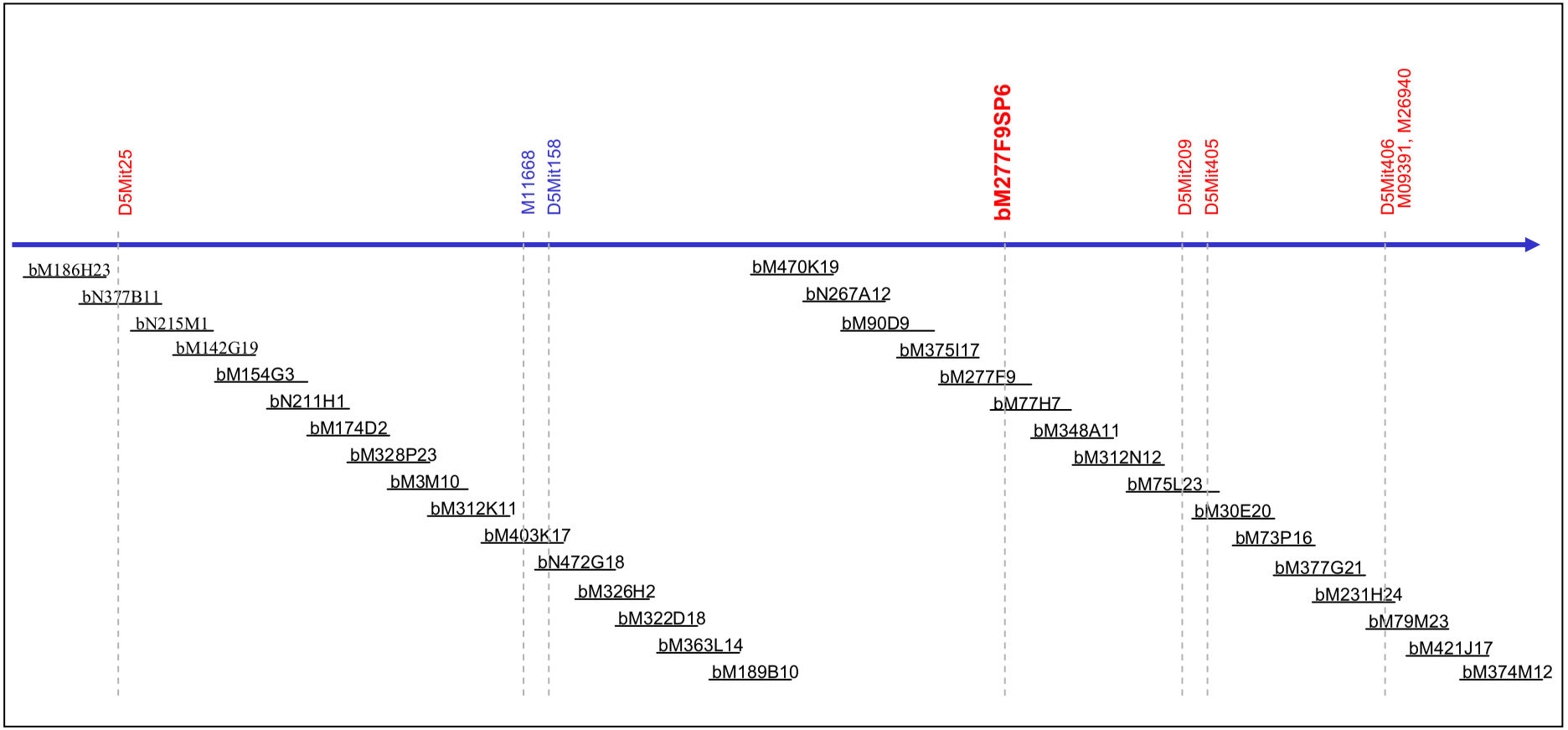

Figure 3.16: Physical BAC map of the *bronx waltzer* candidate region showing the position of the newly identified polymorphic marker bM277F9SP6. Markers polymorphic for *bv* and 101/H are in **red**, non-polymorphic markers are in **blue**.

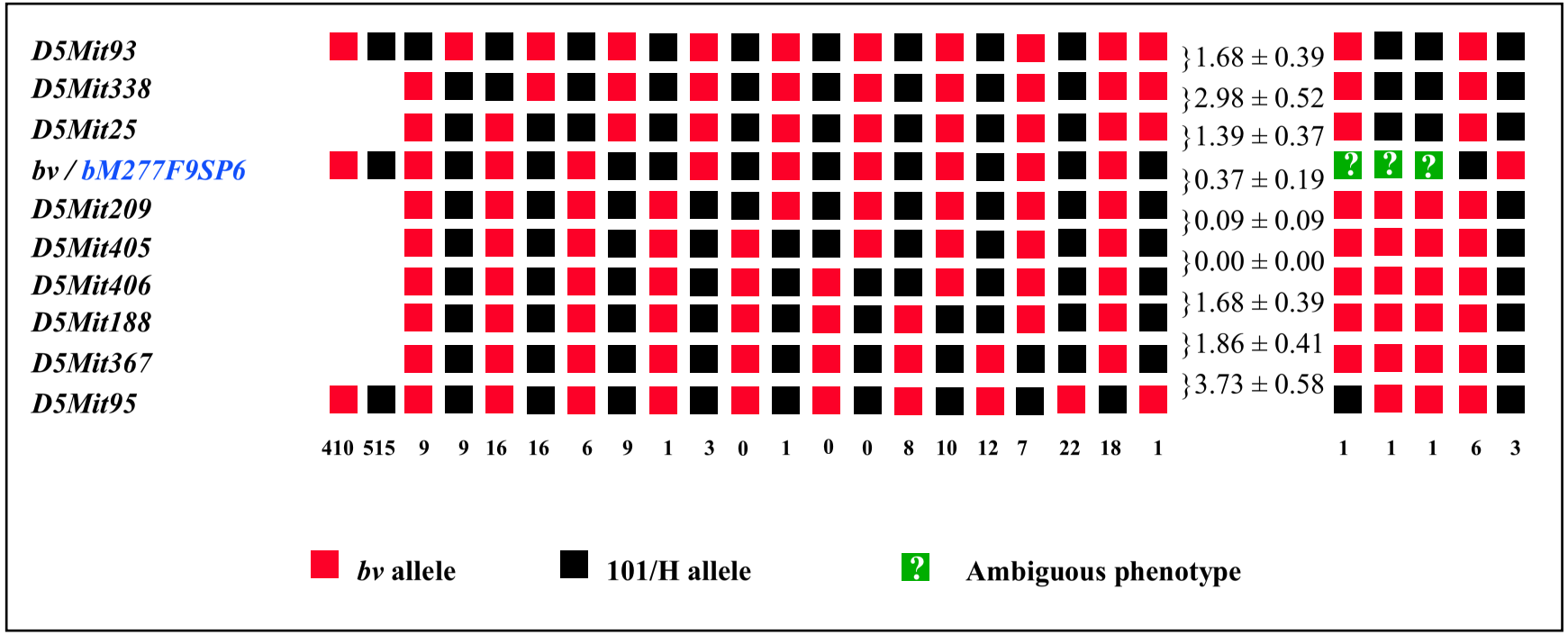

Figure 3.17: Haplotype analysis of the total 1085 progeny arising from the *bv*/101/H intraspecific backcross, showing the position of the newly mapped marker bM277F9SP6 (highlighted in blue). Genetic markers used in the mapping are listed on the left, mice typed with each pattern of recombination are shown along the bottom. Genetic distances calculated between the markers based on the number of recombinations occurring between them are given to the right. Mice excluded from the analysis as a result of discrepant or difficult phenotyping are shown on the far right of the diagram.

The new marker bM277F9SP6 was found to be non-recombinant with the *bv* locus, having in every case the same genotype as the phenotype of the backcross mouse. This result suggests that the marker lies in very close proximity to the gene responsible for the *bronx waltzer* phenotype, since for two markers to co-segregate consistently in over 1000 meioses there must have occurred no recombination between them, implying either a very short distance or a region of extremely low recombination. The recombination rate can be compared to the average rate for mouse chromosome 5, which at 150Mb (Ensembl Build 33) and 92cM (Mouse Genome Database) has an average of 1.6Mb/cM. The *bv* candidate region, at 2.8Mb and 1.86cM has an average of 1.5Mb/cM, making it very similar to the average recombination rate. Thus it is likely that bM277F9SP6 represents a very near marker for *bv*.

However, since there are no recombinations between bM277F9SP6 and *bv*, the new marker is mapped to the same place as *bv* on the genetic map (see Figure 3.18) and thus does not represent a new flanking marker. Therefore the size of the candidate region has not been reduced by the discovery of this marker, though it is possible to say that the gene is more likely to be situated in close proximity to bM277F9SP6.

One of the mice which were excluded from the original haplotype analysis, T901, appeared to show recombination between *bv* and bM277F9SP6 if the tentative phenotype is to be believed. The phenotyping notes for this mouse state that it exhibited slight head bobbing, a small Preyer reflex, reached out on landing and did not circle. At the time it was thought to most likely to be a heterozygote, meaning that it carried a 101/H copy of the *bv* allele from the F1 parent. If this were the case then the new marker bM277F9SP6 would represent a new distal marker on the genetic map, mapping just 0.09cM of the *bv* locus and reducing the size of the candidate region by 0.28cM to 1.67cM. However, should the mouse in fact carried a mutant *bv* copy of the allele then bM277F9SP6 would be mapped proximal of the *bv* locus and since the phenotype could not definitively be recorded, the mouse must be discounted from the results.

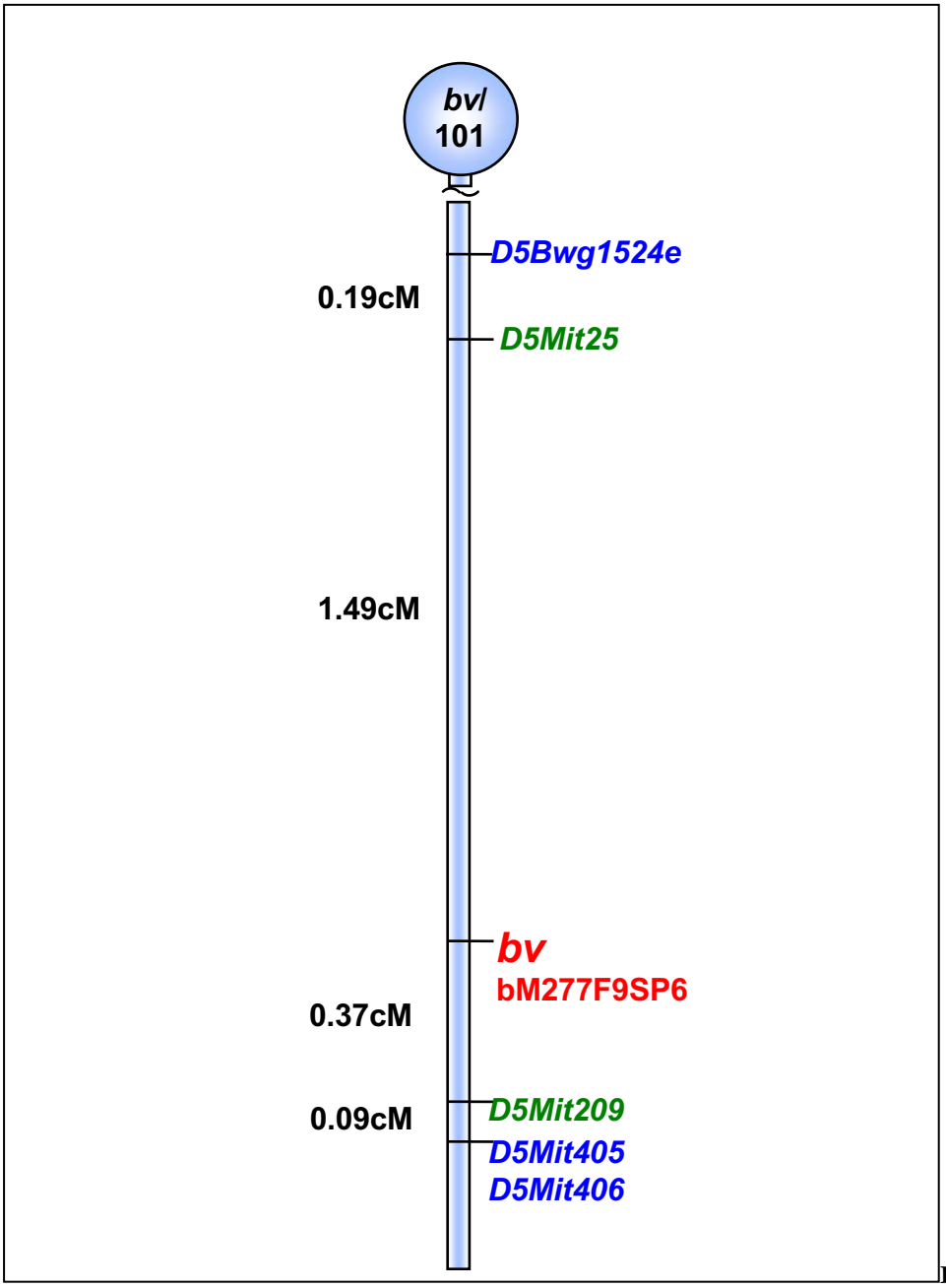

Figure 3.12: Genetic map of the *bv*/101 backcross showing the position of the newly mapped marker bM277F9SP6 which co-segregates with *bronx waltzer*. Genetic loci are drawn to the right of the diagram, with the *bronx waltzer* locus shown in red, flanking markers in green and other genetic markers in blue. Genetic distances determined by the number of recombinations observed between markers are given in black to the left of the diagram.

3.3.2.2.2 3' untranslated regions

The second source of sequences sampled prior to the release of the sequence of the mouse genome were untranslated regions of genes annotated within the critical interval. Once again, these were amplified by PCR using *bv* and 101 templates and the sizes of the products compared by agarose gel electrophoresis. Twenty such sequences originating from 14 different genes were compared in this way, of which one proved to be polymorphic. The visible size differential between fragments amplified using primers designed to part of the untranslated region of the gene *Uracil-DNA Glycosylase* (*UNG*) is illustrated in Figure 3.19.

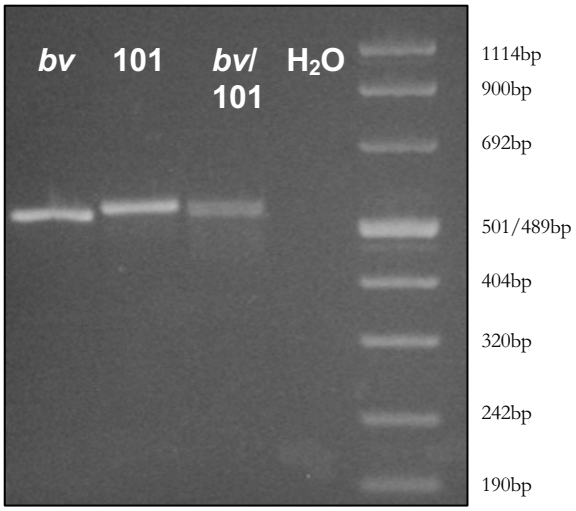

Figure 3.19: Agarose gel showing different sized bands resulting from amplification of the marker UNG-utr1 using *bronx waltzer* and 101/H template DNA. The marker lane contains Molecular Marker VIII (Roche).

This new polymorphic marker was used to screen the panel of recombinant mice from the *bv*/101 backcross in order to determine its position relative to the existing genetic markers (Figure 3.20). A single mouse was found to have a recombination breakpoint between the existing proximal marker *D5Mit25* and UNG-utr1, as shown in the haplotype diagram in Figure 3.21. Using this data the marker was plotted on the genetic map (Figure 3.22), as well as being tested against the panel of BAC insert

DNA so that its physical position within the region could be established. (Figures 3.23 and 3.24).

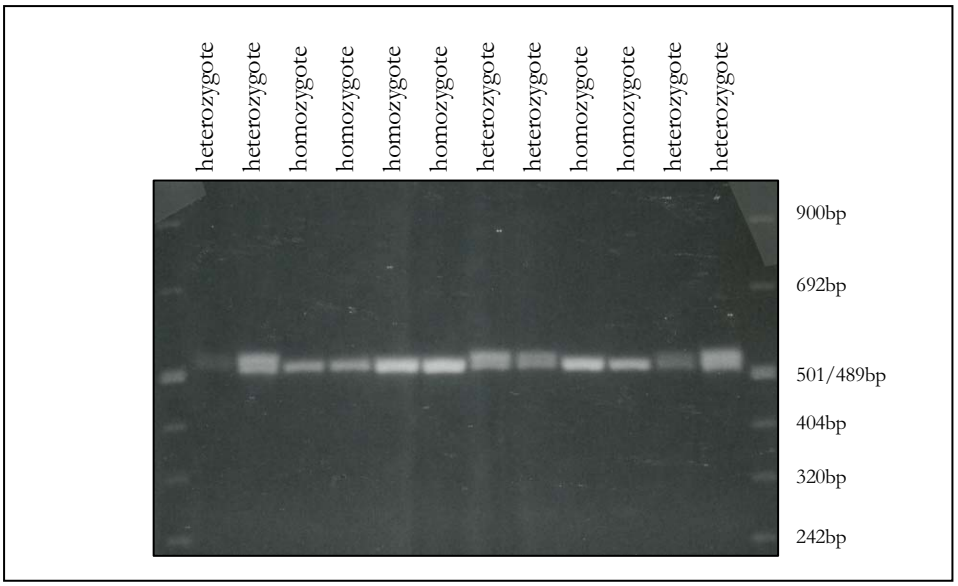

Figure 3.20: Agarose gels showing examples of bands amplified from backcross panel DNA using the marker UNG-utr1 to distinguish between mice homozygous or heterozygous at the locus. The marker lane contains Molecular Marker VIII (Roche).

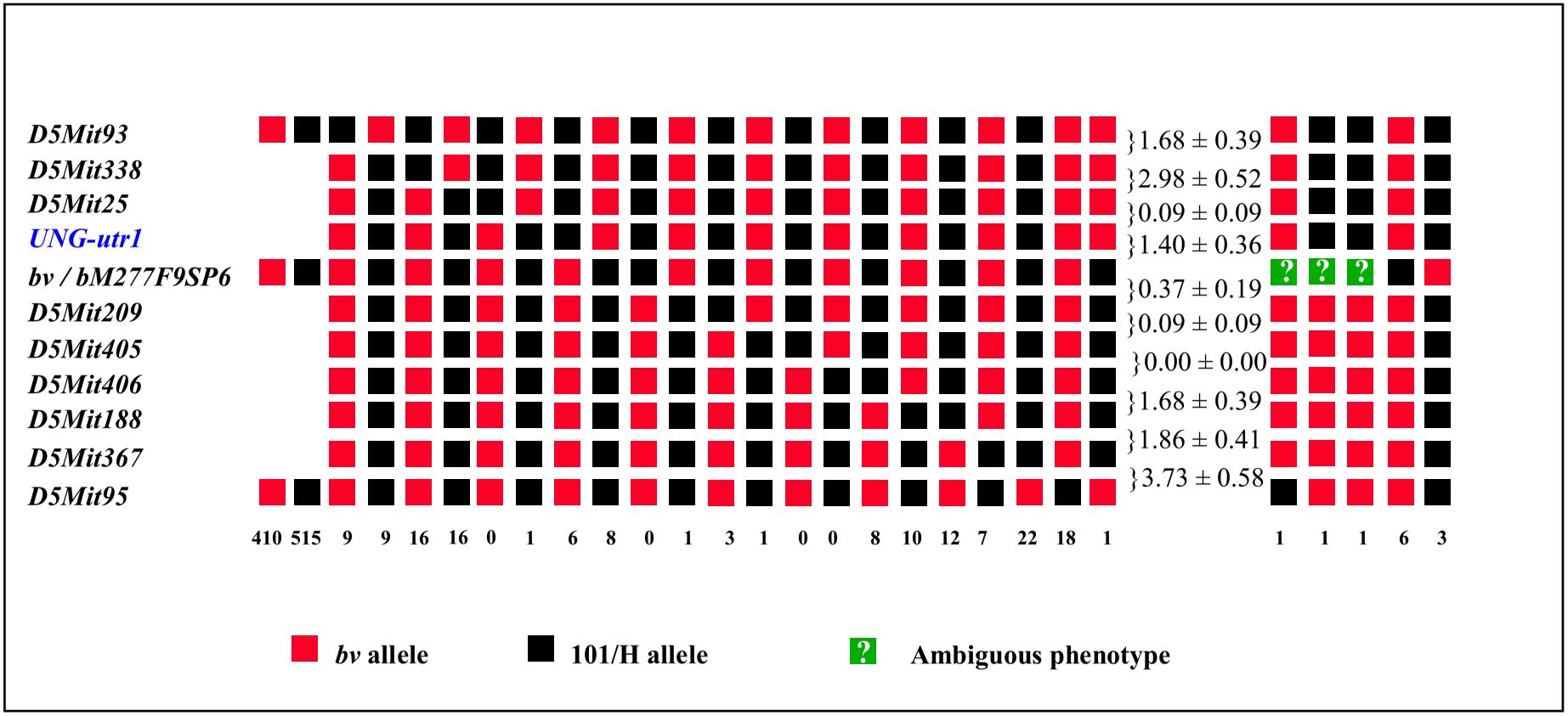

Figure 3.21: Haplotype analysis of the total 1085 progeny arising from the *bv*/101/H intraspecific backcross, showing the position of the newly mapped marker UNG-utr1 (in blue). Genetic markers used in the mapping are listed on the left, the number of mice typed with each pattern of recombination are shown along the bottom. Genetic distances calculated between the markers based on the number of recombinations occurring between them are given to the right. Mice excluded from the analysis as a result of discrepant or difficult phenotyping are shown on the far right of the diagram.

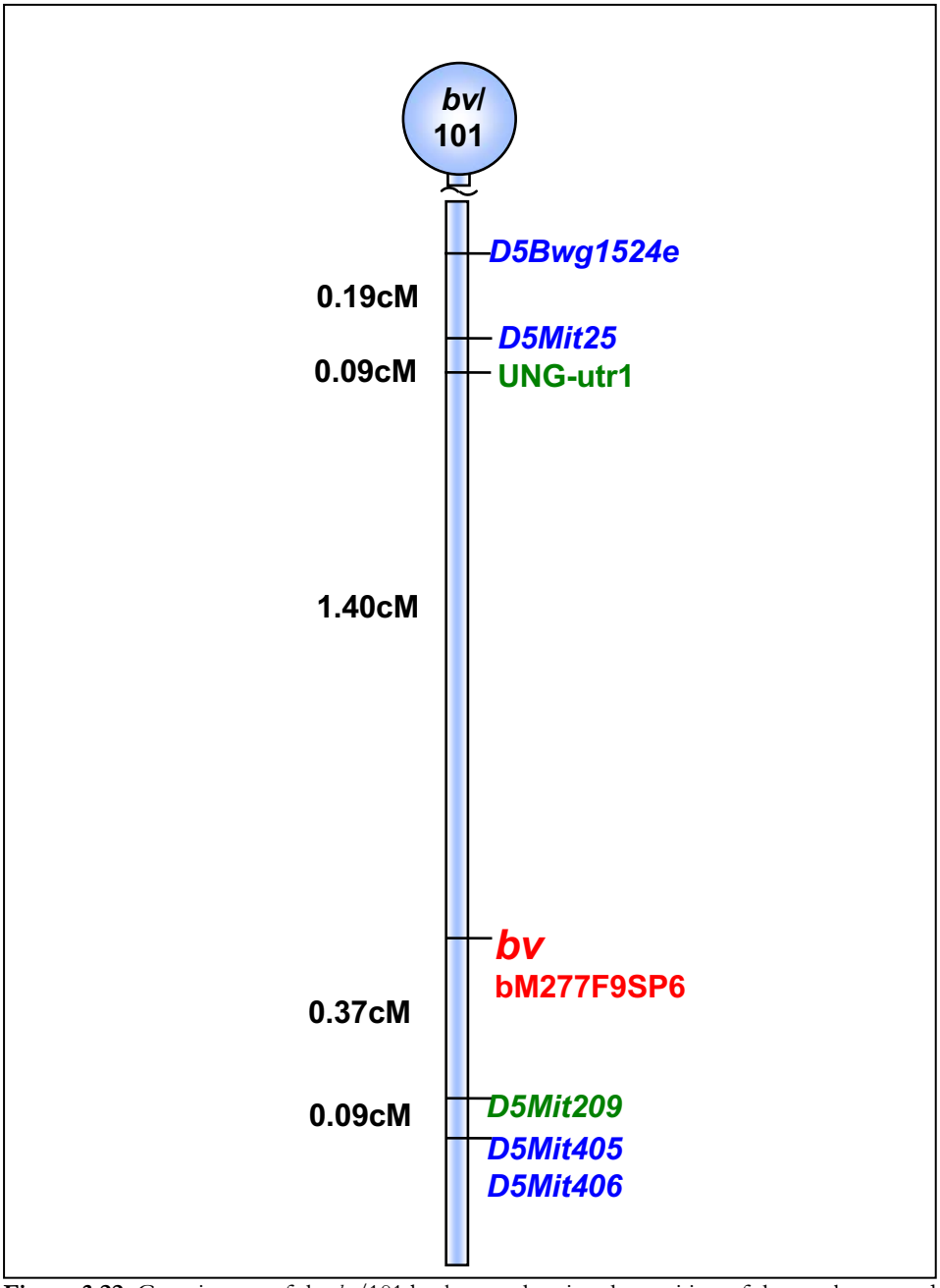

Figure 3.22: Genetic map of the *bv*/101 backcross showing the position of the newly mapped marker UNG-utr1. Genetic loci are drawn to the right of the diagram, with the *bronx waltzer* locus shown in **red**, flanking markers in **green** and other genetic markers in **blue**. Genetic distances determined by the number of recombinations observed between markers are given in black to the left of the diagram.

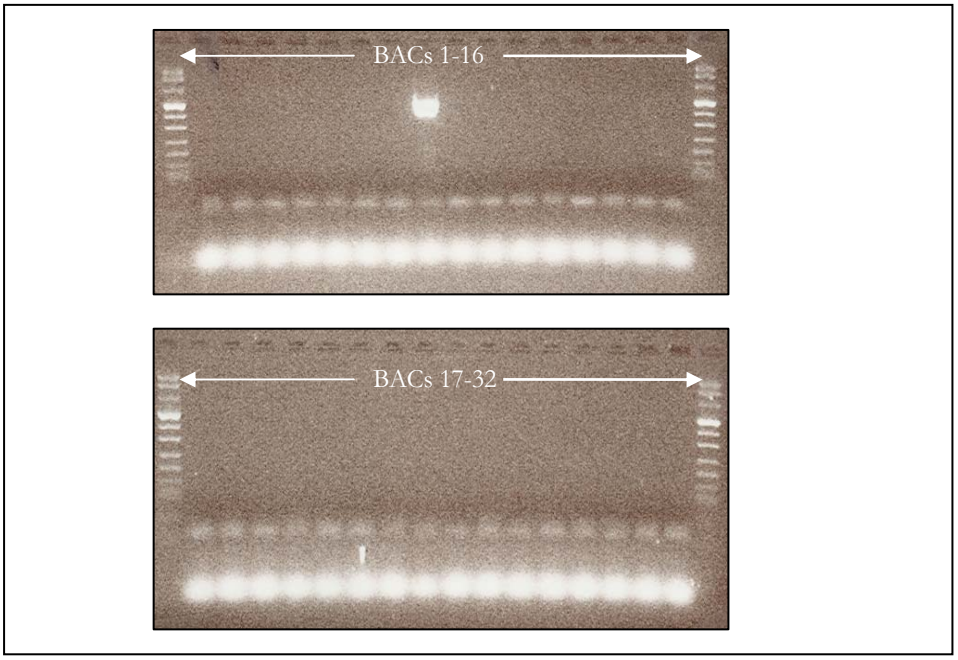

Figure 3.23: Agarose gels showing BAC inserts screened for the marker UNG-utr1. The positive clone is bM142G19, which is situated distal of the flanking marker D5Mit25 (see Figure 3.24).The marker lanes contain Molecular Marker VIII (Roche).

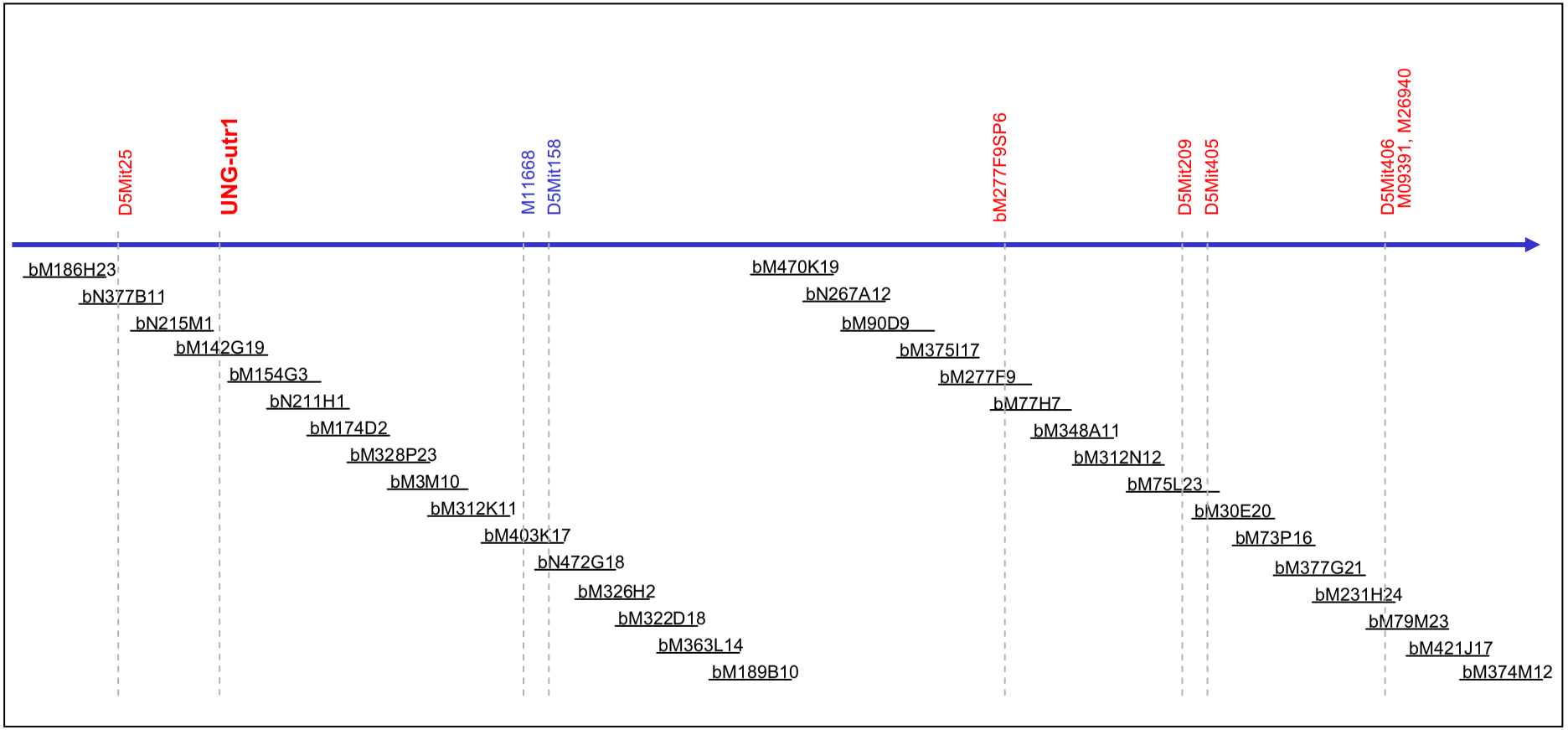

Figure 3.24: Physical BAC map of the bronx waltzer candidate region showing the position of the newly identified polymorphic marker UNG-utr1. Markers polymorphic for *bv* and 101 are in **red**, non-polymorphic markers are in **blue**.

UNG-utr1 was found to map between *D5Mit25* and the *bv* locus, thus establishing it as a new flanking marker for the *bronx waltzer* candidate region. Its discovery resulted in a reduction of the size of the genetic interval by 0.09cM to 1.77cM. When placed on the Mouse Ensembl physical map as shown in Figure 3.25a, it was found to reduce the physical interval by 257Kb to 2.5Mb. The establishment of this new proximal flanking marker resulted in the exclusion of seven genes from the candidate region as illustrated in Figure 3.25b. Since UNG is located on the forward strand and this marker is situated in its 3' untranslated region, the coding region and any upstream transcriptional control elements lie outside of the region defined by the new marker, and thus it too is unlikely to be a candidate gene for *bronx waltzer*.

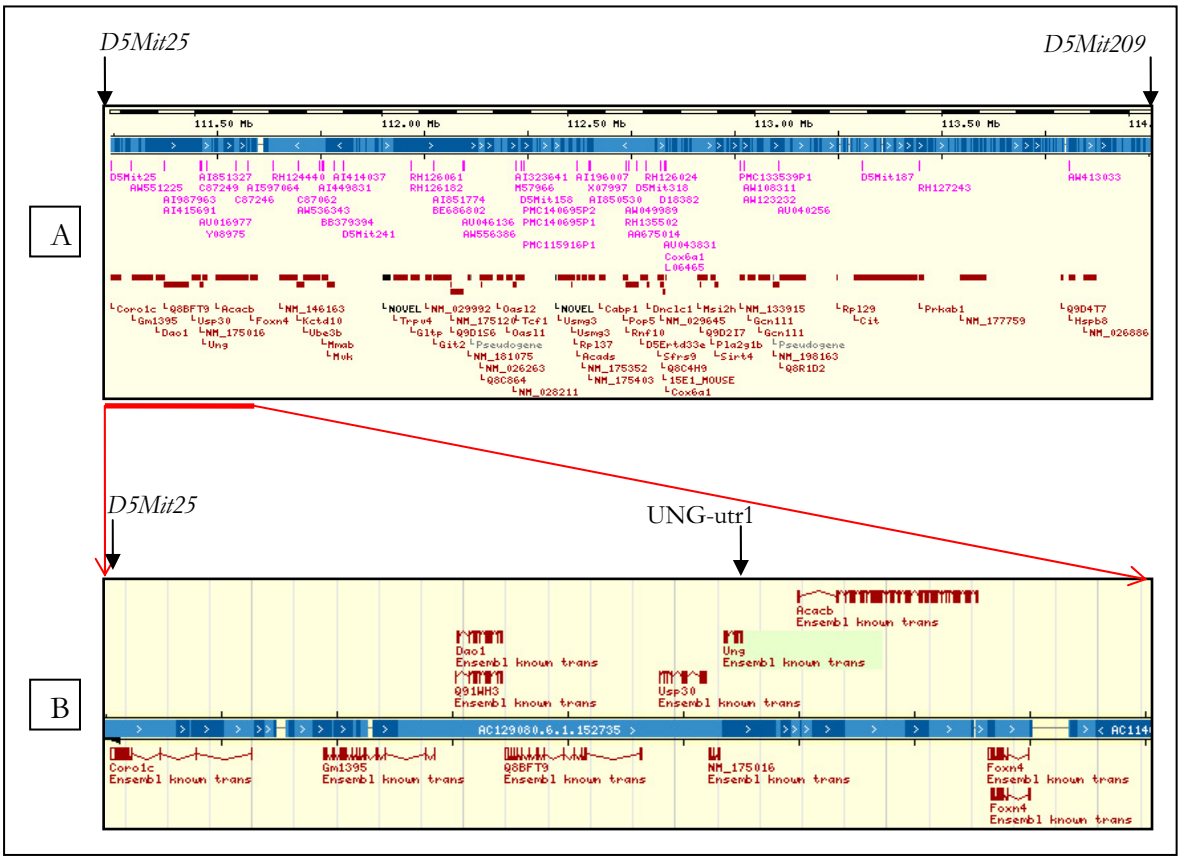

Figure 3.25: Screenshots from Mouse Ensembl showing the location of the newly characterised proximal flanking marker UNG-utr1. [A] depicts the original candidate region, spanning 2.8Mb from *D5Mit25* to *D5Mit209*. [B] shows the proximal end of the region in greater detail, including the placement of UNG-utr1 which reduces the size of the region by 257Kb and excludes seven genes from candidacy.

3.3.2.3 Tandem repeat sequences

With the publication of the draft sequence of the mouse genome (Gregory *et al.* 2002), new sources of potential polymorphisms became available. The first of these to be exploited was the ability to locate new tandem repeats within the region, since these often vary in length between different mouse strains (Hamada *et al.* 1982). The Tandem Repeat Finder software (Benson 1999) was used to detect such sequences in the region between the flanking markers UNG-utr1 and *D5Mit209*. The data produced consisted of a repeat table containing information about each repeat, including its location, size, number of copies and nucleotide content. An example of the output is given in Figure 3.26. Using this information, repeat regions with a low period size, high copy number and high fidelity between adjacent copies were identified as being most likely to prove polymorphic since they are most likely to undergo errors in replication. A selection of 18 such repeats were chosen from areas distributed throughout the region and primers were designed to amplify these repeats. Amplification by PCR with *bv* and 101 DNA templates allowed comparison of the product sizes obtained. Examples of the results obtained in this screen are shown in Figure 3.27.

Since no obvious size differences were observed between the fragments amplified from different DNA samples, sequencing of the products was carried out in order to detect any small differences but none were identified.

Indices	Period Size	Copy Number	Consensus Size	Percent Matches	Percent Indels	Score	A	C	G	T	Entropy (0-2)
207577--207629	3	17.7	3	100	0	106	0	32	33	33	1.58
208116--208185	2	35.0	2	82	0	77	44	1	54	0	1.09
210862--210906	14	3.2	14	83	0	54	15	2	33	48	1.57
210942--211033	10	9.4	10	73	4	53	9	4	36	48	1.56
212461--212514	4	12.5	4	98	2	72	0	0	44	55	0.99
212509--212538	7	4.3	7	100	0	60	0	0	26	73	0.84
213458--213483	1	26.0	1	100	0	52	0	0	0	100	0.00
214190--214223	11	3.2	11	83	8	52	55	23	0	20	1.43
214276--214449	8	21.4	8	70	14	88	51	19	2	26	1.58
215964--216007	2	22.0	2	100	0	88	50	0	0	50	1.00
221664--221713	2	25.0	2	100	0	100	50	0	0	50	1.00
224104--224170	12	5.6	12	80	0	62	29	58	0	11	1.34
227640--227723	4	21.0	4	95	0	114	67	0	32	0	0.91
230326--230371	8	6.0	8	85	10	51	50	15	34	0	1.44
230341--230373	4	8.3	4	93	0	57	51	21	27	0	1.48
230668--230700	2	16.5	2	100	0	66	51	48	0	0	1.00
234119--234182	19	3.4	19	85	8	94	7	32	32	26	1.85
235820--235981	21	7.8	19	79	16	153	15	62	0	22	1.32
239107--240044	9	105.1	9	69	22	357	9	49	19	21	1.76
239062--240064	4	232.8	4	73	14	707	9	49	19	21	1.77
239065--240077	13	76.6	13	77	13	827	9	49	19	21	1.77
241636--241662	1	27.0	1	100	0	54	100	0	0	0	0.00

Figure 3.26: Example of the output obtained when analysing the candidate region for potential polymorphic repeat regions using Tandem Repeat Finder software. Repeats were selected to have a period size of between 2 and 4, a copy number great than 20 and a high percentage match between adjacent repeats. Those meeting these criteria are marked by red arrows.

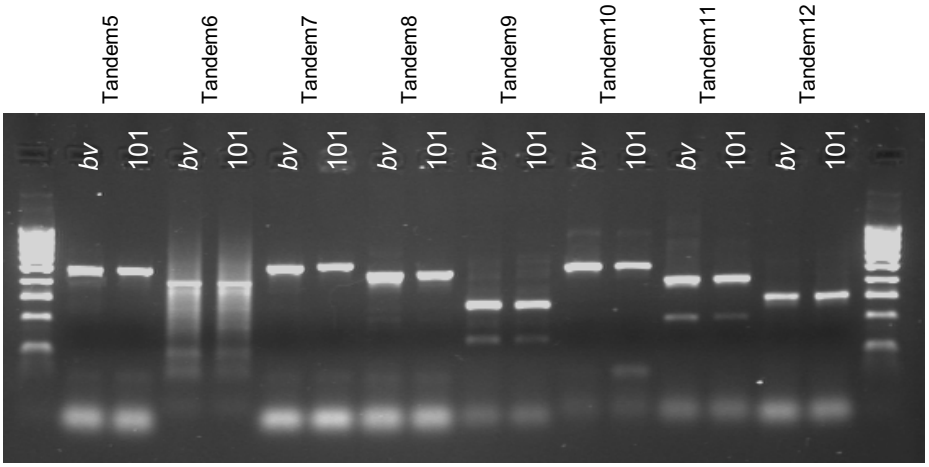

Figure 3.27: Examples of the sizes of products amplified from *bv* and 101 DNA using primers designed around tandem repeat sequences. Although Tandem 7 appears to give slightly different sized bands, no difference was identified when the products were sequenced. The marker lanes contain 1Kb ladder.

3.3.2.4 SNPs from published sequence

3.3.2.4.1 Annotated SNPs

SNPs reported between the published sequence from C57BL/6J and other strains were investigated as a potential source of SNPs between *bv* and 101/H. A total of 292 such SNPs were identified from Ensembl Build32 between the flanking markers of the *bronx waltzer* region and these were amplified using 70 sets of primers designed to flank them. In most cases a single set of primers could be used to amplify several annotated SNPs where they were clustered together. Of these, 68 were successfully amplified from *bv* and 101/H templates and 56 gave sequence of a suitable quality for analysis. However, none of them showed polymorphism between the strains.

3.3.2.4.2 MICER SNPs

Another resource which became available subsequent to the publication of the genome sequence was a set of SNPs identified between the mouse strain C57BL/6J which was the subject of the public sequencing effort and the strain 129S5/SvEv^{Brd} which was used in the creation of the Mouse Insertion and Chromosome Engineering Resource. A total of 187 of the SNPs highlighted in this way were found to lie between the flanking markers of the *bv* critical region and 119 sets of primers were used to amplify them. Of the amplicons sampled, 87 were successfully sequenced and of these one was shown to contain a SNP between the two strains. Sequence traces illustrating this SNP are shown in Figure 3.28.

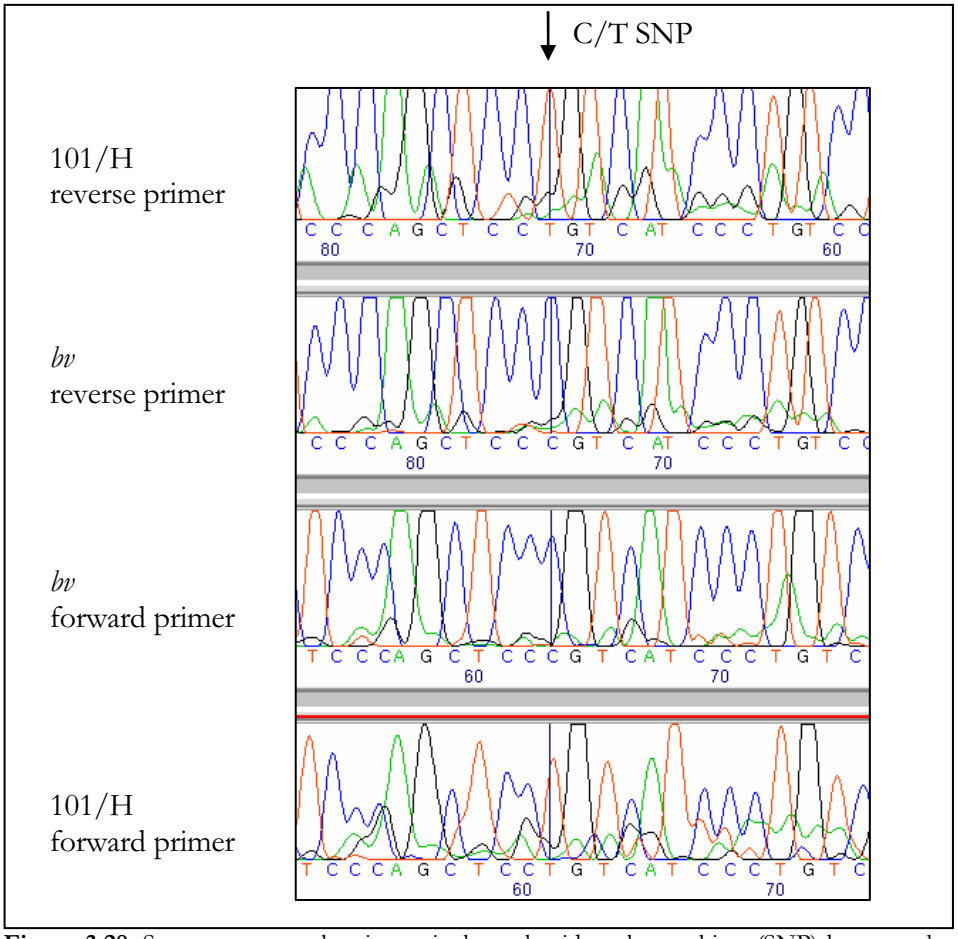

Figure 3.28: Sequence traces showing a single nucleotide polymorphism (SNP) between the mouse strains *bronx waltzer* and 101/H. The fragment was amplified using primers designed to a SNP identified by the MICER project, designated DASNP3.

The marker containing the SNP, DASNP3 was used to screen the backcross recombinant panel by sequencing products amplified from each mouse sample and was found to be positioned on the genetic map in the same place as UNG-utr1 (Figure 3.29).

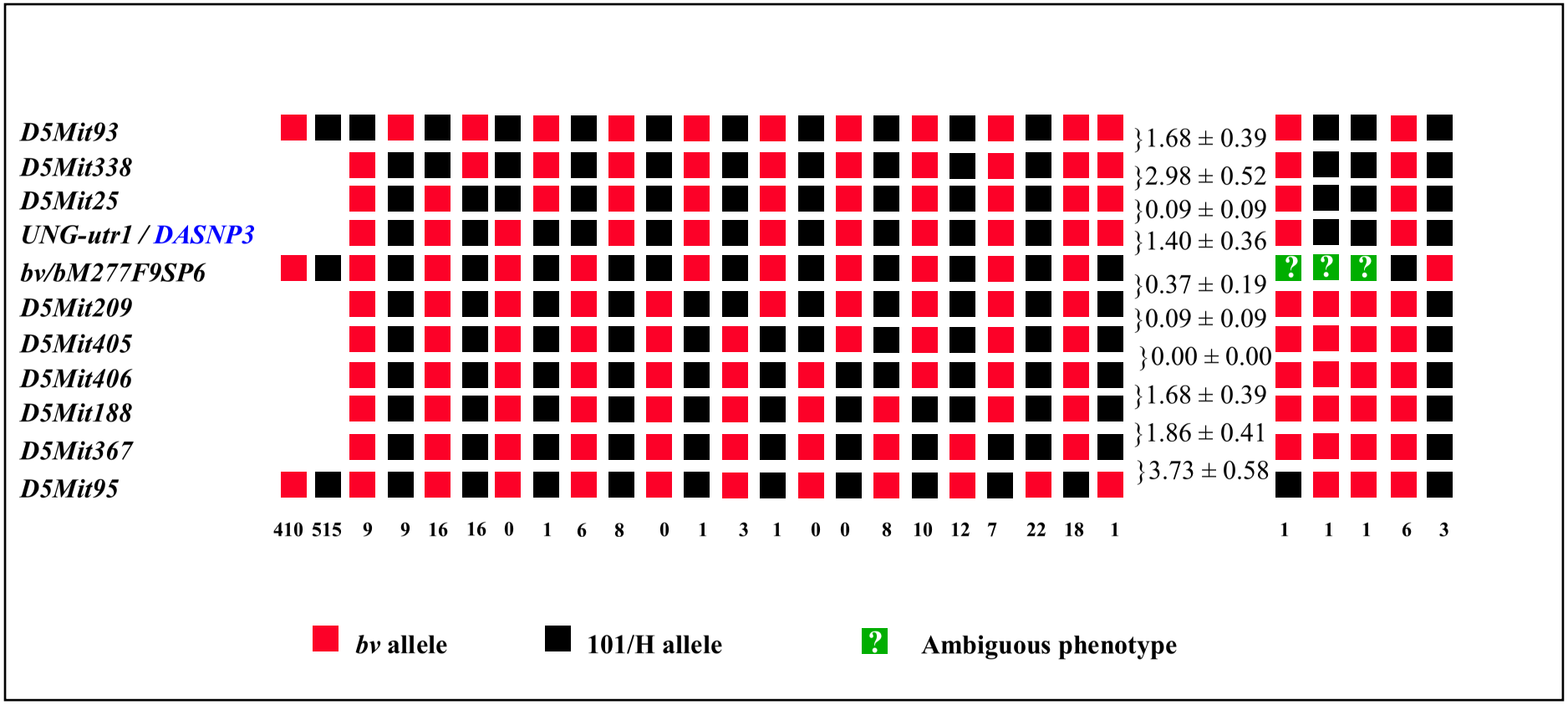

Figure 3.29: Haplotype analysis of the total 1085 progeny arising from the *bv*/101/H intraspecific backcross, showing the position of the newly mapped marker DASNP3 highlighted in **blue**. Genetic markers used in the mapping are listed on the left, numbers of mice typed with each pattern of recombination are shown along the bottom. Genetic distances calculated between the markers based on the number of recombinations occurring between them are given to the right. Mice excluded from the analysis as a result of discrepant or difficult phenotyping are shown on the far right of the diagram.

Although the placement of this marker does not alter the size of the candidate region on the genetic map, physically it is situated distal of UNG-utr1 (Figure 3.30), making it a new proximal flanking marker and reducing the size of the critical region by 78Kb. The marker lies within an intron of the gene *Acacb*, the most proximal gene in the region. As such, it does not fully exclude any further genes from candidacy since the mutation could still lie in an exon further downstream, but it does strengthen the case for the exclusion of *UNG*.

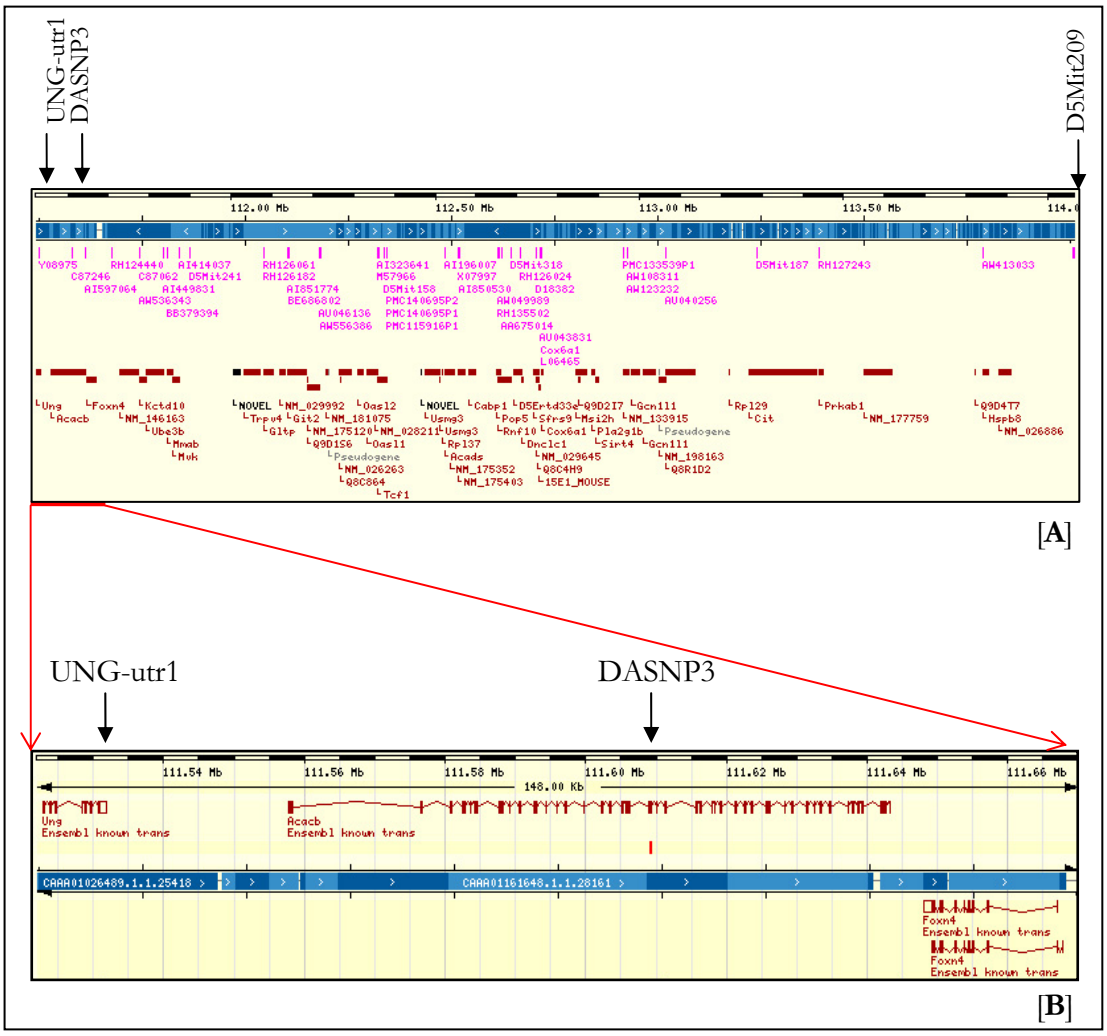

Figure 3.30: Screenshots from the Mouse Ensembl database illustrating the positions of markers flanking the *bv* candidate region. The entirety of the region is illustrated in [A], while [B] shows an enlarged section of the region depicting more accurately the placement of markers UNG-utr1 and DASNP3

3.4 DISCUSSION

Over the course of this project, much more information has become available concerning the genomic composition of the mouse. As these data were released they have been incorporated into the approaches used to further characterise and refine the candidate region for the *bronx waltzer* gene. This began with the use of physical mapping data to establish a contiguous series of BAC clones spanning the region, allowing the first estimate of its physical size. Later, newly available sequence data was employed in efforts to identify new markers polymorphic for *bronx waltzer* and 101/H. During the course of this study, a total of 422 amplicons from within the *bv* candidate region were analysed for polymorphisms between *bronx waltzer* and the backcross strain 101/H. These covered 563 potential polymorphisms, including 482 reported SNPs and 81 other sequences which carried the possibility of variation between strains. Of these only three were found to exhibit polymorphisms, of which two cosegregate and form a new proximal flanking marker reducing the size of the region by 0.09cM to 1.77cM and by 334Kb to 2.45Mb with the exclusion of seven candidate genes. The third marker is non-recombinant with the *bv* locus and therefore cannot be used to reduce the size of the region, but does carry the implication that the gene responsible for the *bronx waltzer* phenotype is likely to be situated very close by. A final version of the genetic map showing the placement of these novel markers is given in Figure 3.31, while the physical positions are illustrated in Figure 3.32.

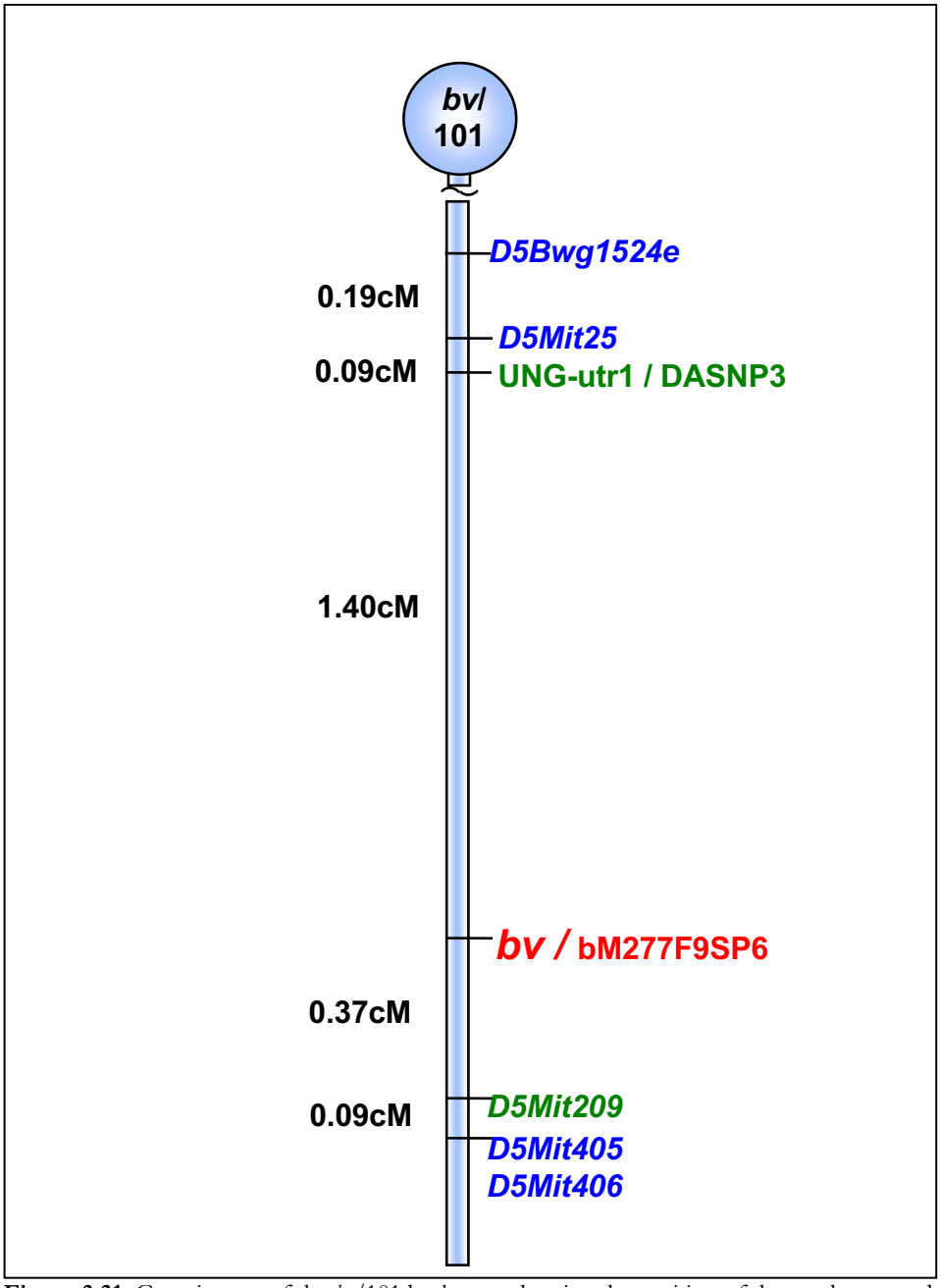

Figure 3.31: Genetic map of the *bv*/101 backcross showing the position of the newly mapped polymorphic markers. Genetic loci are drawn to the right of the diagram, with the *bronx waltzer* locus shown in **red**, flanking markers in **green** and other genetic markers in **blue**. Genetic distances determined by the number of recombinations observed between markers are given in black to the left of the diagram.

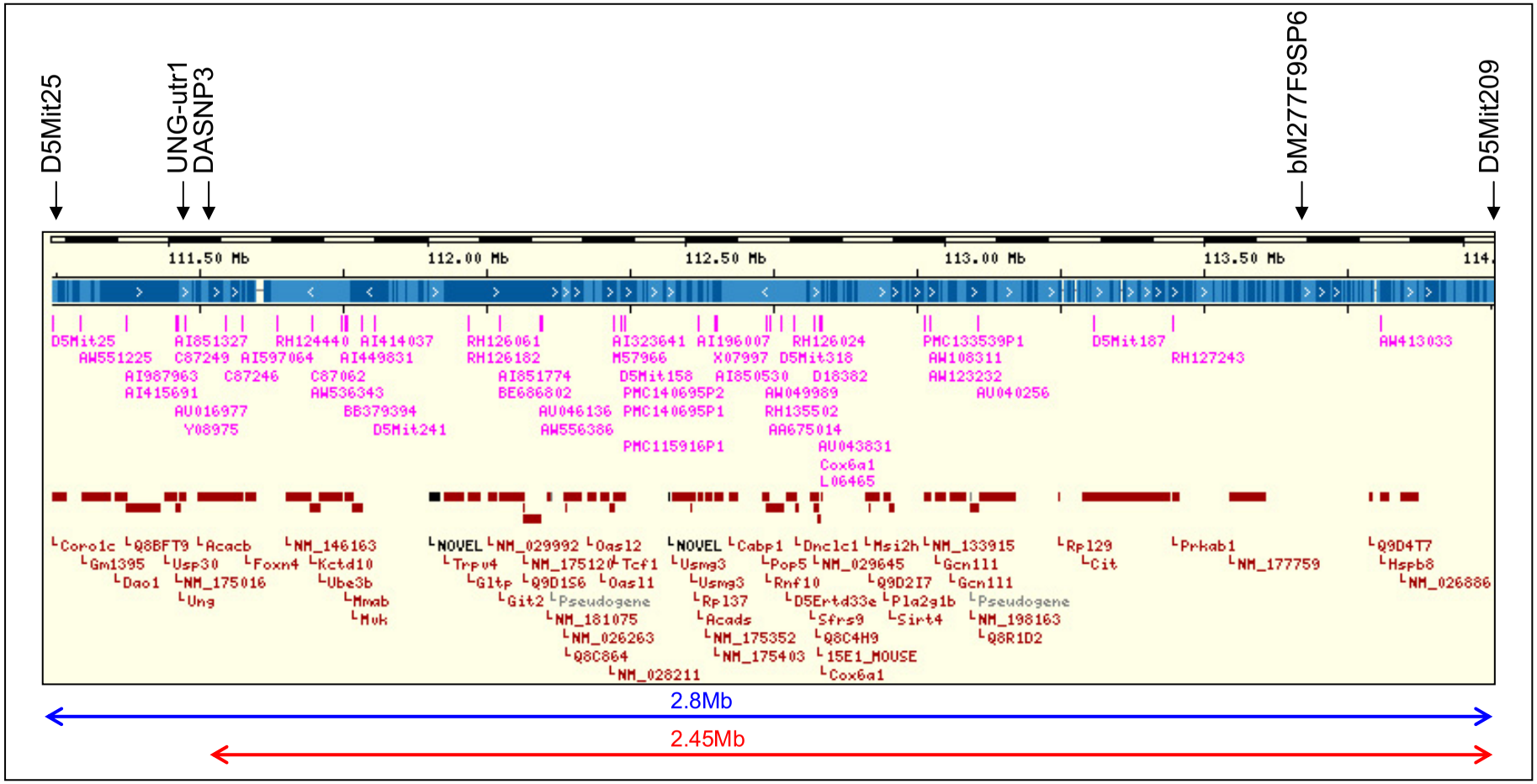

Figure 3.32 Screenshot from Mouse Ensembl Build 33 depicting the final candidate region for the bronx waltzer locus and showing the locations of existing and newly determined markers polymorphic for *bv* and 101/H. The original candidate region was delineated by the markers D5Mit25 and D5Mit209 and is marked by the blue arrow. The new proximal marker DASNP3 reduces the size of the region by 0.35Mb and excludes seven genes from the region as shown by the red arrow. bM277F9SP6 is non-recombinant with the *bv* locus, making it unsuitable for use as a flanking marker but suggesting that the gene encoding bronx waltzer is likely to be in its vicinity.

The very low rate of polymorphisms in this region despite the high level of sequence sampling suggests that the area is conserved between the two strains being investigated, *bronx waltzer* and 101/H. Even though the inbred strain was chosen from a panel as being the most polymorphic when typed against 33 SSLP markers from mouse chromosome 5 (Bussoli *et al.* 1997), the region close to the *bv* locus will have been inherited by almost all mutant mice and so been selected for during normal breeding for maintenance of the colony, and therefore may not be representative of the rest of the chromosome. Since the background on which the *bv* mutation arose and is maintained is unknown, it is possible that this portion of its genome was inherited from a mouse strain closely related to 101/H. The degree of polymorphism between *bronx waltzer* and a number of inbred strains within this small region is investigated further in Chapter 4 as a means of choosing a more polymorphic strain for a subsequent cross, and of providing clues as to which mouse inbred strain background the *bv* mutation may have arisen on.

Chapter 4:

A new intraspecific intercross to narrow the bronx waltzer critical region

CHAPTER 4

A NEW INTRASPECIFIC INTERCROSS TO NARROW THE *BRONX WALTZER* CRITICAL REGION

4.1 INTRODUCTION

At the commencement of this project, significant attempts had already been made to identify new markers which could be used to refine the existing *bronx waltzer* map based on the backcross with the inbred strain 101/H (see Section 3.1.3). Since these had so far proved fruitless and evidence was mounting that the strains may harbour a low polymorphism rate within the defined interval, it was decided that the establishment of a new mapping cross with a different inbred strain would be beneficial.

In order for an additional cross to be informative for linkage mapping purposes and allow the size of the candidate region to be reduced, it must fulfil three criteria. First, the phenotype must be distinguishable on the new genetic background with maximum penetrance. Secondly, the strain chosen for the outcross should contain polymorphisms which make it distinguishable from the *bronx waltzer* background within the critical region and finally, it must result in offspring possessing genetic breakpoints between the current flanking markers. The measures taken to ensure the greatest likelihood of these conditions being met are outlined below.

4.1.1 Choosing an outcross strain

At the time of the establishment of this cross, a physical map of the mouse genome had been published and sequence was becoming available. The physical positions of the flanking markers *D5Mit25* and *D5Mit209* were known, and therefore it was possible to isolate markers which mapped between them. These could then be screened against a panel of prepared

genomic DNA samples from a variety of inbred strains in order to determine which had the largest number of informative polymorphisms with *bronx waltzer* within the region, making it a suitable candidate for the outcross. Additionally, this study may provide information regarding the genetic background on which the *bv* mutation first arose, with any strain demonstrating few or no polymorphisms being a potential candidate or close relative of that on which the original *bv* mutation initially arose.

4.1.2 Choosing a breeding strategy

The simplest and most commonly employed breeding strategy for linkage mapping is that of the backcross (see Section 3.1.1.1). This operates on the principle that each mouse resulting from the cross represents a single isolated meiotic recombination event. One complete set of chromosomes are inherited from each inbred parent, making it possible to distinguish at each locus whether the individual has inherited the mutant allele from its F1 parent or that from the wildtype outcross strain. Thus a haplotype map of the recombinant chromosome can be constructed relatively easily.

A second approach sometimes used for mapping is that of the intercross. Here, an outcross is carried out in the same way as for a backcross, but the resulting mice from the F_1 generation are then mated together instead of being crossed back to one of the parental inbred strains. As a result, the F_2 intercross offspring will carry two recombinant chromosomes, as illustrated in Figure 4.1.

The main advantage of this strategy is the occurrence of meiotic recombination events in each parent effectively doubling the number of potentially informative breakpoints in each F_2 animal. However this same feature is also responsible for the major disadvantage of the intercross, since the inheritance of two recombinant chromosomes makes analysis of the data significantly more complex than for a backcross. Each animal carries two

separate haplotypes for each linkage group, making it impossible to assign alleles to one or the other haplotype. At every locus, each allele may have been inherited from either parent. Thus, when generating *de novo* linkage maps from large-scale intercross experiments it is essential to use software designed to carry out multilocus maximum likelihood analysis such as Mapmaker (Lander *et al.* 1987).

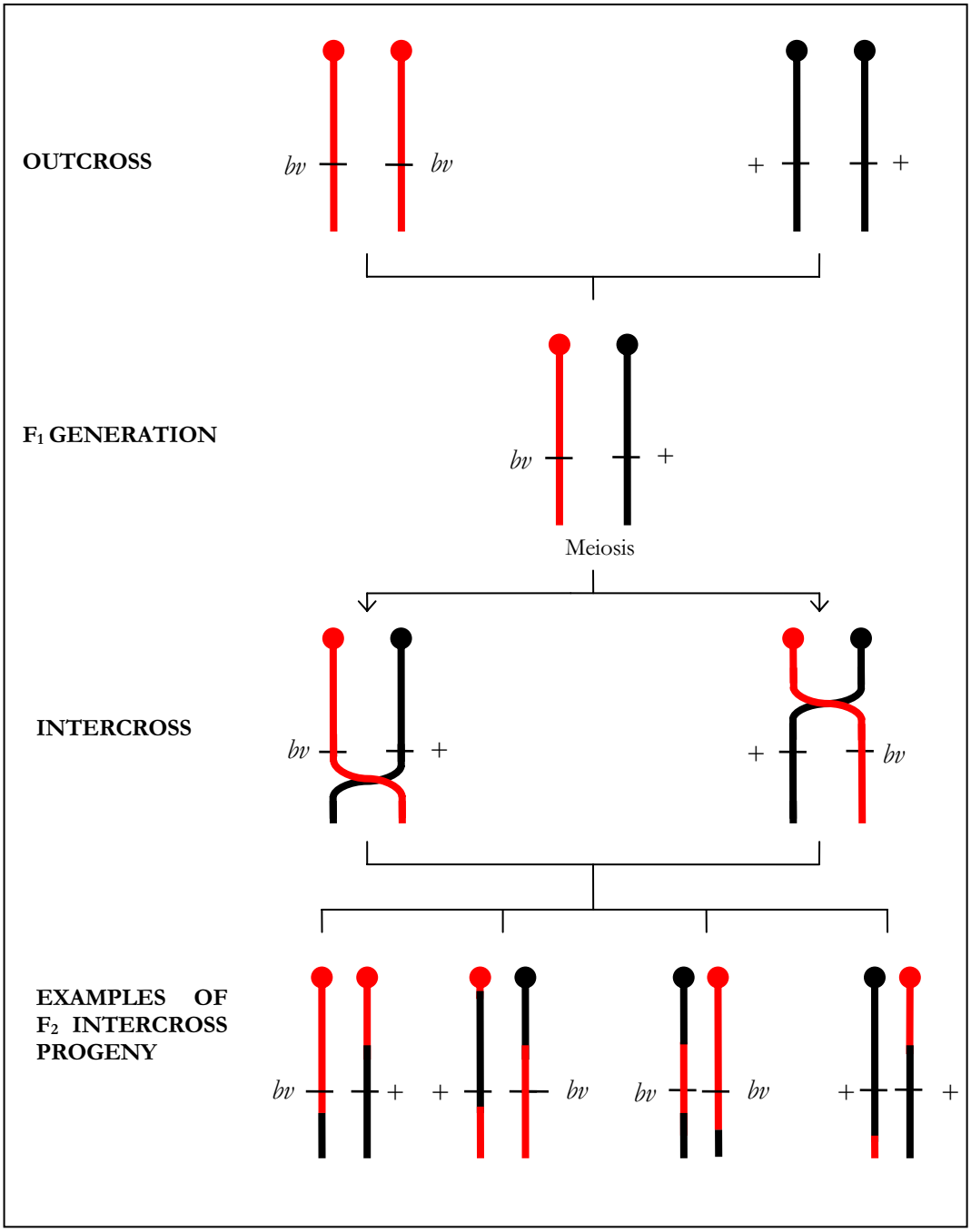

Figure 4.1: Diagram illustrating the breeding strategy employed in the generation of an intercross. Chromosomes derived from *bronx waltzer* are shown in red while those from the selected inbred strain are in black. During gamete formation in the F_1 generation, recombination may occur between the two parental chromosomes at the prophase I phase of meiosis. These F_1 mice are then bred together, producing intercross offspring in possession of two sets of recombinant chromosomes. The expected Mendelian ratios for the F_2 progeny of such a cross are 1:2:1 of wild type, heterozygotes and homozygous mutants.

Despite the difficulties inherent in analysing the data, the intercross strategy is still the most suitable in certain circumstances. The first is in the case of recessive deleterious mutations where animals homozygous for the mutation either die before adulthood or are rendered infertile. Since backcrossing the F_1 generation to an affected mutant is unfeasible, an intercross becomes the only available option for linkage mapping. However, since it is not possible to discern heterozygote carriers from wild type animals, only the affected mutant offspring can be used for analysis.

Although *bronx waltzer* is not deleterious in the homozygous form, the phenotype does have an impact on breeding strategy which needs to be taken into account. Mice homozygous for the mutant *bv* allele exhibit hyperactivity and shaker-waltzer behaviour. This type of behaviour in mice tends to correlate with poor parenting, with pregnancies being irregular and the majority of litters born into a cage with a homozygous parent being trampled or cannibalised, thereby reducing the chances of offspring surviving to adulthood. During general colony maintenance this problem can be bypassed by establishing breeding pairs consisting of a heterozygous female and homozygous mutant male, then removing the male from the cage once a pregnancy has been established. Since the generation of a large number of offspring is crucial to the success of a mapping project, this limits the usefulness of the backcross (see Figure 3.1) for three reasons. Firstly, the number of breeding pairs at the backcross stage is constrained by the availability of mutant males from the original colony which does not always breed efficiently, and also by the fact that only female F_1 animals can be used for subsequent breeding. Secondly, since homozygous mutant males do not breed very effectively the rate at which pups are born can be very irregular and lastly, the rate of production of F_2 offspring is further slowed by the removal of the male from the cage until each litter of pups has been weaned. By contrast, with an intercross strategy (see figure 4.1) the F_1 breeding pairs will both be heterozygous at the *bv* locus and hence manifest no phenotype.

This means that all of the F_1 animals can be used, that pregnancies can overlap with nursing of litters, that breeding will be more predictable and in addition, hybrid vigour might be expected to give larger and more frequent litters.

The second situation where an intercross may be most suitable is when the focus of the mapping has previously been narrowed to a small genomic interval of a few centimorgans or less. At this high level of resolution the data analysis will be much less complex, with only a small fraction of animals expected to show predominantly single recombination events within the region of interest. Under these circumstances, the increased probability of generating a mouse with an informative recombination within the small predefined interval outweighs the difficulties posed by analysis of the data, making an intercross mapping strategy suitable.

With just 1.83cM lying between the established flanking markers, this last set of criteria applies to the current status of the *bronx waltzer* mapping project. Taken in addition to the practical advantages conferred by the breeding strategy, it was decided that the generation of an intercross would be the most beneficial approach for the fine mapping of the *bv* mutation.

4.2 METHODS

Some of the methods employed in this chapter are described in Chapter 2. The following procedures are specific to this chapter.

4.2.1 Inbred strain DNA

Some of the inbred strains tested were already maintained as colonies within the lab and DNA from these was prepared as described in Section 2.2. The remainder of the inbred strain DNA was obtained from the Mouse DNA Resource maintained by the Jackson Laboratory (Bar Harbor, Maine). Table 4.1 shows the inbred strain DNAs analysed and lists their origin.

Mouse Strain	Genealogical Group	Source
101/H	Castle's	IHR Nottingham
129X1/SvJ	Castle's	Jackson Lab
A/J	Castle's	Jackson Lab
BXD-1/Ty	C57 x DBA	Jackson Lab
C58/J	Castle's	Jackson Lab
CE/J	Other	Jackson Lab
DA/HuSn	Swiss	Jackson Lab
DBA/2J	Castle's	Jackson Lab
DDY/Jc1	China/Japan	Jackson Lab
FL/1Re	Castle's	Jackson Lab
LP/J	Castle's	Jackson Lab
NON/LtJ	Swiss	Jackson Lab
RBG/Dn	C57 x DBA x AET	Jackson Lab
ST/bJ	Other	Jackson Lab
SWR/J	Swiss	Jackson Lab
C3HeB/FeJ	Castle's	IHR Nottingham
C57BL/6J	Castle's	IHR Nottingham
BALB/C	Castle's	IHR Nottingham
CBA/Ca	Castle's	IHR Nottingham

Table 4.1: Inbred strains making up the panel of DNAs to be tested for polymorphism with *bronx waltzer* within the critical region. Genealogical groups are taken from Beck *et al.* (2000).

The panel of DNA from a number of inbred strains was tested with markers from across the *bv* critical interval for polymorphism by PCR. Some strains were chosen because colonies of the mice were already maintained within the

lab and thus their employment in a new intercross would be greatly simplified. Others were selected to represent as broad as possible a cross section of the laboratory inbred strains in order to increase the chances of identifying a mouse with a high level of polymorphism with *bronx waltzer*, and also of discovering which strain the mutation may have arisen on. The selection of these strains was informed by the work of Beck and colleagues (2000) to determine the origins of the various laboratory inbred strains, and particularly by the accompanying lineage chart depicting their genealogies

4.2.2 Microsatellite markers

The markers used are listed in Table 4.2. Some of these have previously been mapped onto the *bv*/101 map, while others have been shown to map within the physical interval but do not exhibit polymorphisms on *bv* and 101/H backgrounds.

Marker	Position (Mb)	Forward primer	Reverse primer
D5Mit25	111.27	AACACACCTCCATACTGGTCG	GGCTAACTGAAATTGTTTTGTGC
D5Mit241	111.89	TGTTTATCAGGGTTGGTCTGC	CATATGGGTCATCAGATATCATGG
D5Mit158	112.37	AAAGACGCTGAGGAGTCACTG	CAGGAGACCTTGTAATAAAGGAAA
D5Mit318	112.68	ATATGGGCTTGGCTTTCATG	GACTACACACATCACTCTCTCTCTCA
D5Mit187	113.29	GGACCCACAAGATGGAAAGA	CCTCAGTGGATACATGTTTAAACTT
D5Mit209	114.06	TCTGAGCAAGGTCGTCCAC	CCCTGTCTCAAGATAAAAGCTAGG
D5Mit405	114.18	CAACAACAACAAAAAAAGAAAGATG	CACAGTCCCACATCCACCTA
D5Mit424	117.36	GACTCCTCCTCGCCTTTCTT	AAAATTACATTTGCATCTGGGG

Table 4.2: Markers from within and surrounding the *bv* critical region to be used in the analysis of polymorphisms between various inbred strains and the *bronx waltzer* genetic background. Positions given are taken from Ensembl Build 33.

4.2.3 Phenotyping F_2 intercross offspring

The intercross breeding strategy illustrated in Figure 4.1 was followed, with the resulting generation of F_2 offspring possessing genotypes of either +/+, +/*bv* or *bv*/*bv*. Mice were scored in a similar manner to that described in Section 3.1.1.4 for the generation of the *bv*/101 backcross, their behaviour being assessed and scored according to the presence or absence of a shaker-

waltzer phenotype indicative of vestibular dysfunction. In addition to this, a Preyer reflex test for auditory function was administered with the use of a click box. This was held 30cm directly above the mouse to be tested and a tone-burst of 20kHz and 90 dB SPL emitted while the mouse's response was observed. A positive result was recorded if the animal retracted its pinnae, a negative one if they failed to respond. Mice which exhibited shaker-waltzer behaviour and lacked a Preyer reflex were scored as *bv*/*bv*, with any particular remarks regarding their behaviour being recorded. Animals which behaved normally and exhibited a Preyer reflex were scored as +/?, since it is not possible to phenotypically discern heterozygote +/*bv* animals from wild type +/+ ones. All mice were given an identifier consisting of the letters BC followed by a consecutive number unique to each mouse. This code was used to associate notes taken about each animal with all the tissues later collected.

4.2.4 Tissue collection

At the time of the sacrifice, tissue was collected for DNA preparation as described in Section 2.2. In addition, the inner ears of each mouse were dissected and fixed in a manner suitable for their analysis by scanning electron microscopy. Following bisection of the head and removal of the brain, each half head was placed immediately into fixative (2.5% glutaraldehyde in 0.1M sodium cacodylate and 2mM $CaCl_2$). The inner ear was removed from the skull, the bulla detached and the oval window and the apex of the cochlea were opened up using a sharp needle and fix perfused gently through the resulting holes. The ears were transferred to fresh fixative and placed in rotating stirrers overnight at 4°C to ensure full fixation of the tissue. The samples were washed 6 times for 5 minutes in cocodylate buffer (0.1M sodium cacodylate; 2mM $CaCl_2$) and were then stored at 4°C until required for further analysis.

4.3 RESULTS

4.3.1 Strain selection

As discussed, the choice of inbred strain employed at the outcross step of the intercross breeding strategy is crucial to the success of the linkage mapping project. The strain must have polymorphisms making it distinguishable from the *bronx waltzer* background within the critical interval. As such, the following study was conducted in order to make an informed decision regarding which strain to use.

Each inbred strain genomic DNA sample was used as the template in PCR reactions with primers from markers in and around the *bv* critical region, and the size of the resulting product determined by agarose gel electrophoresis. The results for the markers flanking and surrounding the region are shown in Figure 4.2a and summarised in Table 4.3a. Those for the markers within the region are depicted in Figure 4.2b and summarised in Table 4.3b

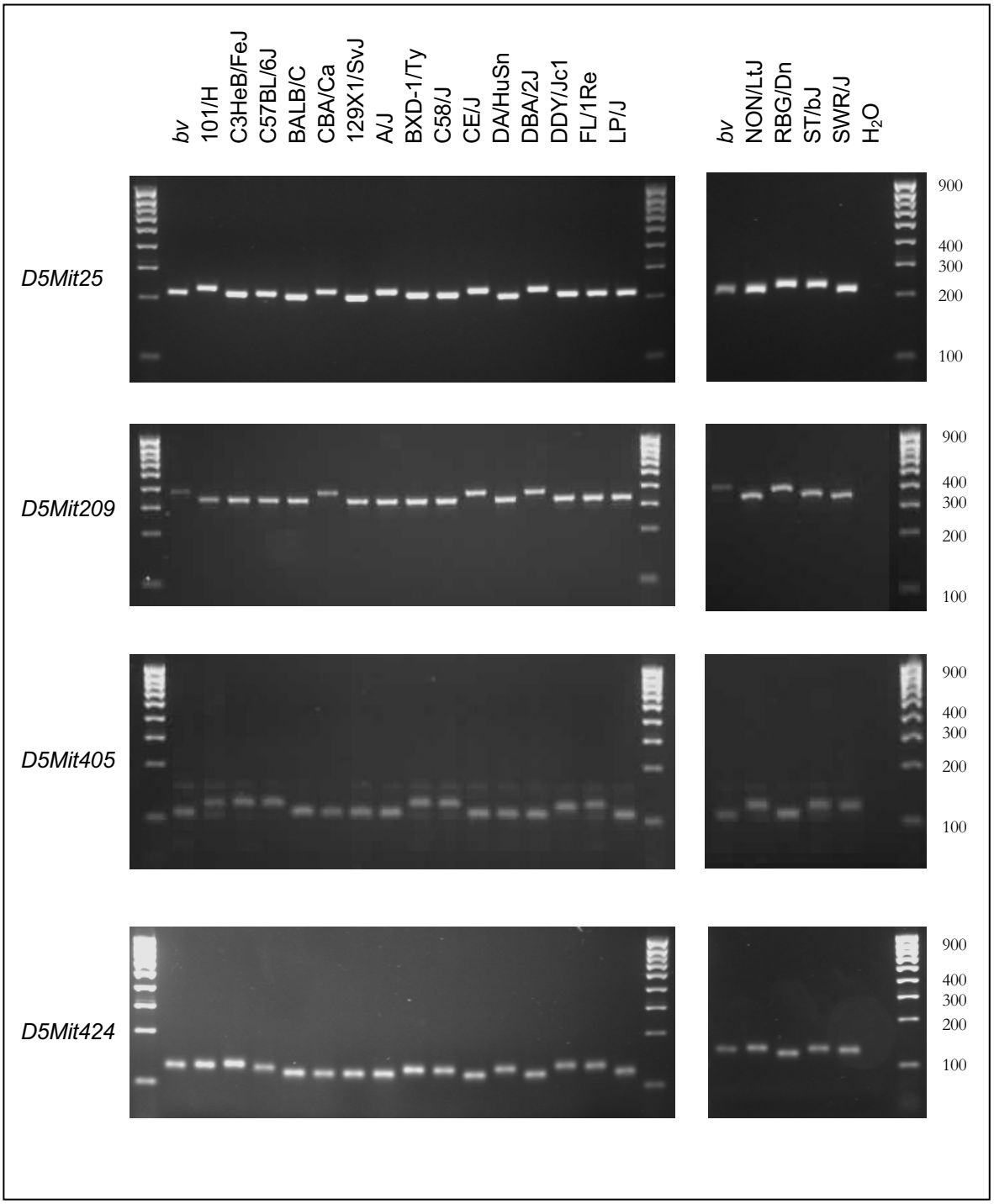

Figure 4.2a: Flanking marker polymorphisms
Agarose gel electrophoresis showing the sizes of fragment amplified when screening polymorphic genetic markers against a panel of DNA from a variety of inbred strains. These markers flank or lie outside the established candidate region.
The marker lane contains 1Kb ladder and the figures given are in base pairs.

Strain	*D5Mit25*	*bv*	*D5Mit209*	*D5Mit405*	*D5Mit424*
101/H	**Y**		**Y**	Y	N
C3H	N		**Y**	Y	N
C57BL/6J	**Y**		**Y**	Y	Y
BALB/C	N		**Y**	N	Y
CBA	**Y**		N	N	**Y**
129X1/SvJ	N		**Y**	N	Y
A/J	**Y**		**Y**	N	Y
BXD-1/Ty	N		**Y**	Y	Y
C58/J	N		**Y**	Y	Y
CE/J	**Y**		N	N	**Y**
DA/HuSn	N		**Y**	N	Y
DBA/2J	**Y**		N	N	**Y**
DDY/Jc1	N		**Y**	Y	N
FL/1Re	N		**Y**	Y	N
LP/J	N		**Y**	N	Y
NON/LtJ	N		**Y**	Y	N
RBG/Dn	**Y**		N	N	**Y**
ST/bJ	**Y**		**Y**	Y	N
SWR/J	N		**Y**	Y	N

Table 4.3a: Summary of flanking marker polymorphisms
Summary of the polymorphism screen of inbred strains for markers flanking the *bronx waltzer* region. A difference in product size when compared to *bv* DNA is indicated by the letter Y, a product size indiscernible from *bv* is indicated by the letter N.
For those strains possessing polymorphic flanking markers on either side of the region the closest markers are highlighted in **BLUE**. Those possessing only one polymorphic flanking marker are shown in **RED**.

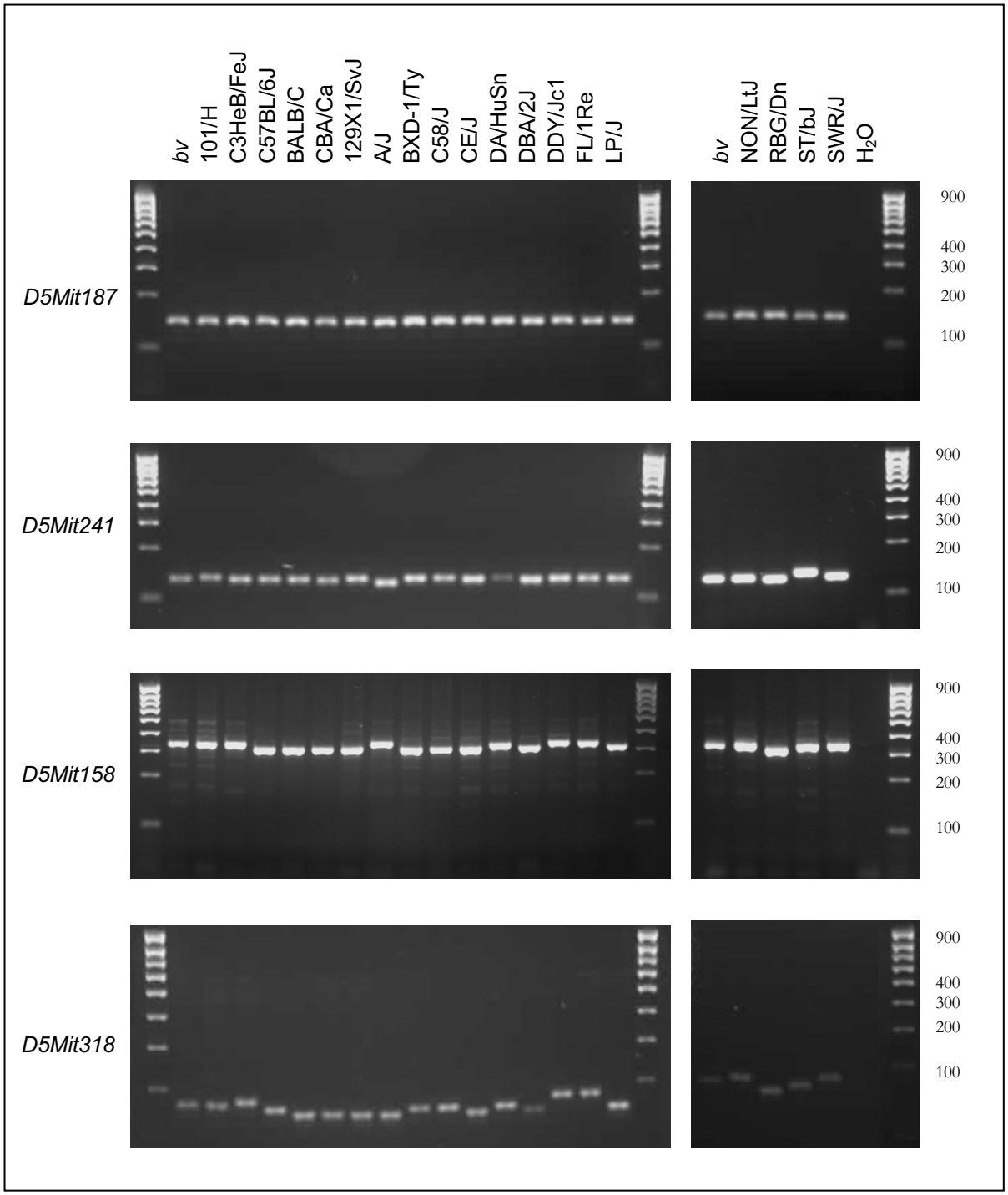

Figure 4.2b: Internal marker polymorphisms
Agarose gel electrophoresis showing the sizes of fragment amplified when screening polymorphic genetic markers against a panel of DNA from a variety of inbred strains.
These markers lie within the critical region, polymorphisms here could be used to narrow the region and therefore cut down the number of candidate genes being considered for *bronx waltzer*.
The marker lane contains 1Kb ladder and the figures given are in base pairs.

Strain	*D5Mit241*	*D5Mit158*	*D5Mit318*	*D5Mit187*	Total
101/H	N	N	N	N	0
C3H	N	N	**Y**	N	1
C57BL/6J	N	**Y**	N	N	1
BALB/C	N	**Y**	**Y**	N	2
CBA	N	**Y**	**Y**	N	2
129X1/SvJ	N	**Y**	**Y**	N	2
A/J	**Y**	N	**Y**	N	2
BXD-1/Ty	N	**Y**	N	N	1
C58/J	N	**Y**	N	N	1
CE/J	N	**Y**	**Y**	N	2
DA/HuSn	N	N	N	N	0
DBA/2J	N	**Y**	N	N	1
DDY/Jc1	N	N	**Y**	N	1
FL/1Re	N	N	**Y**	N	1
LP/J	N	**Y**	N	N	1
NON/LtJ	N	N	**Y**	N	1
RBG/Dn	N	**Y**	**Y**	N	2
ST/bJ	**Y**	N	N	N	1
SWR/J	**Y**	N	N	N	1

Table 4.3b: Summary of internal marker polymorphisms
Summary of the polymorphism screen of inbred strains for markers within the *bronx waltzer* region. A difference in product size when compared to *bv* DNA is indicated by the letter Y highlighted in **BLUE**, a product size indiscernible from *bv* is indicated by the letter N.
The total number of polymorphic markers within the *bv* region for each strain is given in the rightmost column.

4.3.2 An intraspecific intercross

Based on the results of the strain polymorphism assays, the strain CBA/Ca was chosen to be used in the outcross. It was shown to have polymorphisms with *bv* at two useful flanking markers as well as at two internal markers. Other strains gave similar results but as CBA/Ca was already maintained in the lab it was expedient to set up the outcross immediately. For a full discussion of the criteria considered for strain selection see Section 4.4.1.

An outcross was set up between a *bronx waltzer* male homozygous mutant and a CBA/Ca female as the first stage in the intercross breeding strategy (see Figure 4.1). Since the mutation is maintained on an unknown background a single male from the mutant strain was used in the matings to produce all F_1 hybrids, since this limits the number of potential alleles to be inherited by the offspring and makes analysis more straightforward (Silver 1995). These F_1 animals were then intercrossed, giving a total of 233 F_2 progeny, of which 47 were phenotyped as *bronx waltzer* homozygous mutants and the remaining 186 recorded as +/? since heterozygote and wild type animals are indistinguishable. Of the 47 mice recorded as mutants, three were noted as having slightly questionable phenotypes. The mouse identified as BC44 had some head-bobbing and no reaching response but appeared to exhibit a Preyer reflex. Mice BC74 and BC110 showed some head-bobbing but no circling. They lacked a reaching response and writhed on being picked up but had a weak Preyer reflex. On the balance of this evidence, all three mice were recorded as *bv/bv* by phenotype. A pedigree chart illustrating the lineage of the animals used in this mapping project is shown in Figure 4.3.

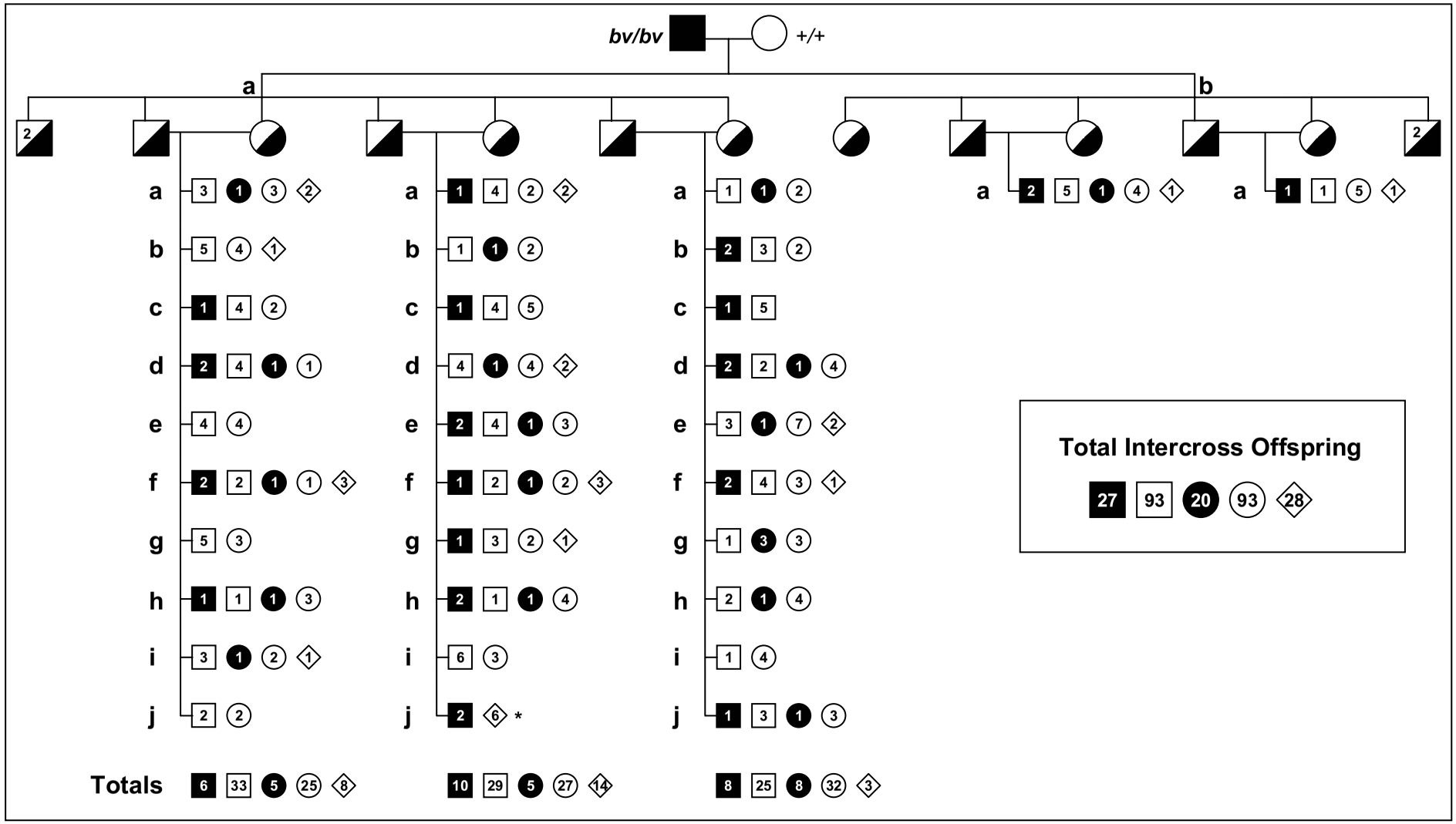

Figure 4.3: Pedigree chart illustrating the lineage of the mice used in the *bv*/CBA/Ca intercross mapping project. Males are represented by squares, females as circles and animals which died before being sexed or phenotyped are shown as diamonds. Animals with mutant phenotypes are shown as filled shapes, controls are unfilled. Known heterozygotes are shown half-filled. The litter marked * was sacrificed at age P12 and was only just beginning to show signs of shaker-waltzer behaviour, therefore only those animals which could be confidently typed as mutants were counted.

4.3.2.1 Statistical analysis

The number of males and females in the F_2 generation was 120 and 113 respectively, which when analysed using the G-test (likelihood ratio test) for goodness of fit (Sokal and Rohlf 1995) gives a value of 0.22 (see Table 4.4a), suggesting a close adherence to the expected ratio of 1:1 (d.f.=1; p=0.64). The same test was used to assess the ratio of control to mutant animals which according to Mendelian ratios is expected to equal 3:1 for this breeding strategy (see Figure 4.1). The observed figures of 186 control mice and 47 mutants give a G-value of 2.92 (see Table 4.4b), which indicates a slight but not significant deviation from the expected ratios (d.f.= 1; p=0.09).

Sex	**Observed frequencies**	**Observed proportions**	**Expected proportions**	**Expected frequencies**	**Ratio**	**G-value (ln L)**	**Adjusted G-value**
	f	$\frac{f}{n}$	$\hat{p}$ and $\hat{q}$	$\hat{f}$	$\frac{f}{\hat{f}}$	$f \ln\left(\frac{f}{\hat{f}}\right)$	2 ln L
Male (p)	120	0.515	0.5	116.5	1.03	3.55	7.1
Female (q)	113	0.485	0.5	116.5	0.97	-3.44	6.88
Sum (n)	233	1	1	233	-	0.11	**0.22**

Table 4.4a: G-test (likelihood ratio test) for goodness of fit applied to the proportion of males to female F_2 offspring obtained in the intercross of *bv* to CBA/Ca. The adjusted G-value allows a p-value to be obtained using chi-square tables.

Phenotype	**Observed frequencies**	**Observed proportions**	**Expected proportions**	**Expected frequencies**	**Ratio**	**G-value (ln L)**	**Adjusted G-value**
	f	$\frac{f}{n}$	$\hat{p}$ and $\hat{q}$	$\hat{f}$	$\frac{f}{\hat{f}}$	$f \ln\left(\frac{f}{\hat{f}}\right)$	2 ln L
Control (p)	186	0.798	0.75	174.75	1.064	11.539	23.078
Mutant (q)	47	0.202	0.25	58.25	0.807	-10.078	20.156
Sum (n)	233	1	1	233	-	1.461	**2.922**

Table 4.4b: G-test (likelihood ratio test) for goodness of fit applied to the proportion of mutant to control F_2 offspring obtained in the intercross of *bv* to CBA/Ca. The adjusted G-value allows a p-value to be obtained using chi-square tables.

4.3.2.2 Genotyping F_2 mice

Since wild type (+/+) and heterozygous (+/*bv*) mice cannot be distinguished from each other, only the homozygous mutant (*bv*/*bv*) F_2 offspring from this intercross can be included in linkage analysis. Genomic DNA was prepared

from tissue samples taken from each of the 47 mutant mice and screened using the flanking markers and markers from within the *bv* candidate region which had been shown to be polymorphic for *bv* and CBA/Ca (see Section 4.3.1). The results of this screen are shown in Figure 4.4. To genotype this cross *D5Mit25* and *D5Mit424* were used as flanking markers, while the markers within the region were *D5Mit158* and *D5Mit318*. As homozygous mutants, these mice will be expected to show a single band of the same size as the *bv* sample. Should any recombination have taken place within the critical region then we would expect to see two bands of different sizes, representing both *bv* and CBA/Ca.

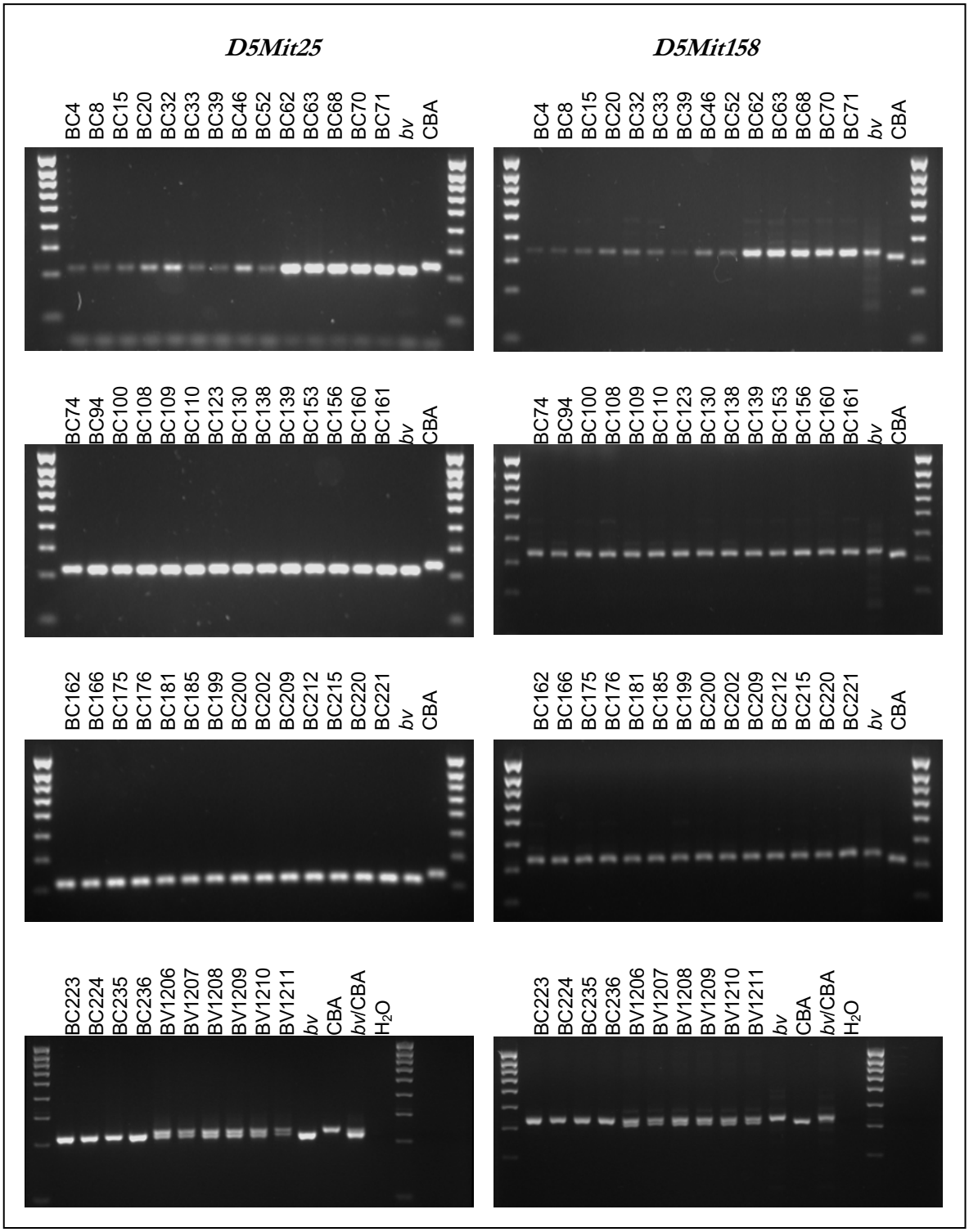

Figure 4.4a: Agarose gel electrophoresis showing PCR products obtained when amplifying polymorphic genetic markers from mutant mice in the F_2 generation of the intercross between *bv* and CBA/Ca. Mutant mice are designated by codes prefixed BC, controls showing the size of fragment expected from each parental strain are given on each row. The final row includes the F_1 parents as heterozygous controls; these are prefixed by the letters *BV*.

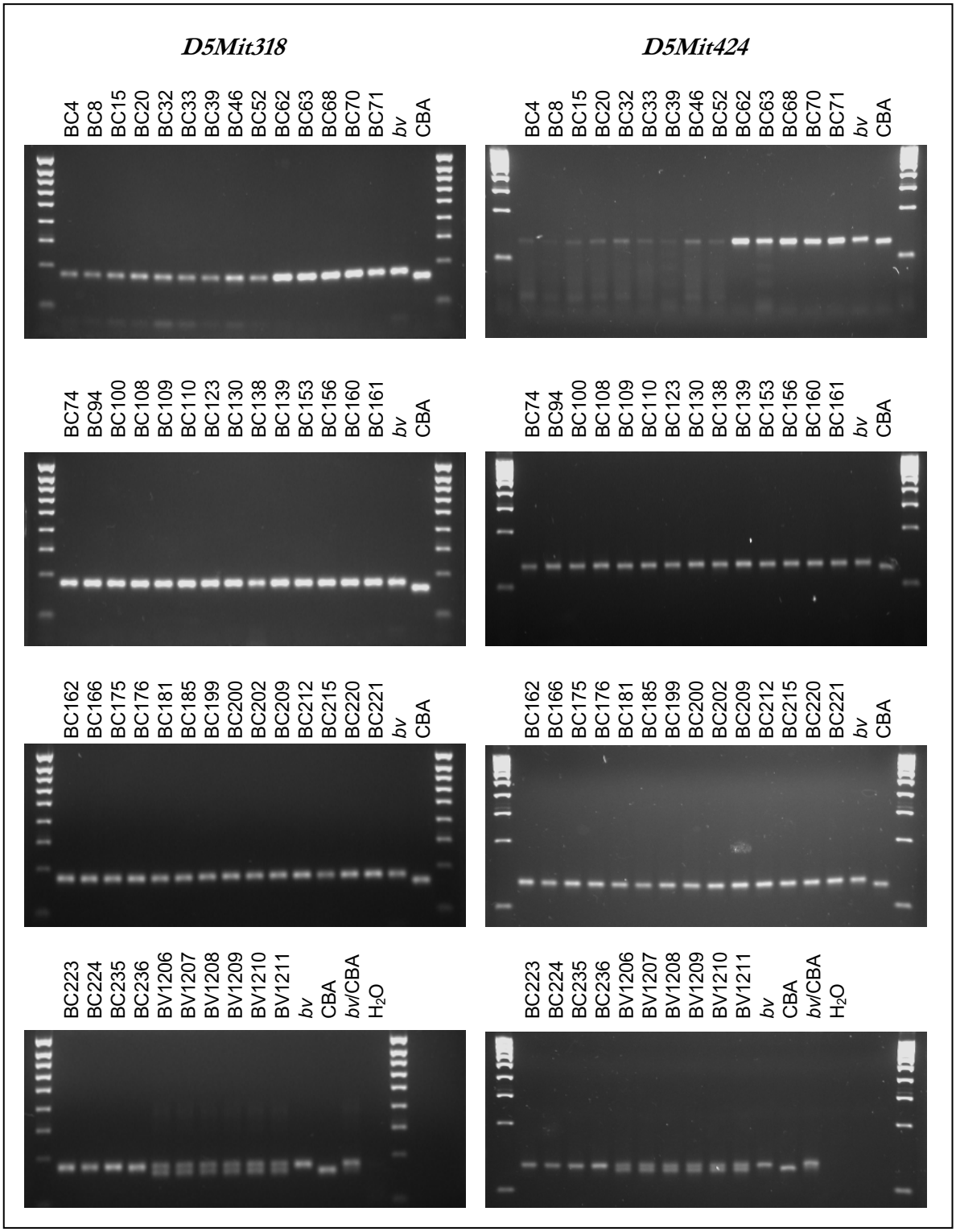

Figure 4.4b: Agarose gel electrophoresis showing PCR products obtained when amplifying polymorphic genetic markers from mutant mice in the F_2 generation of the intercross between *bv* and CBA/Ca. Mutant mice are designated by codes prefixed BC, controls showing the size of fragment expected from each parental strain are given on each row. The final row includes some of the F_1 parents as heterozygous controls; these are prefixed by the letters *BV*.

4.4 DISCUSSION

4.4.1 Strain selection

In order to select a suitable strain with which to outcross the *bronx waltzer* mice, a number of criteria were taken into account. Most importantly, the strain must exhibit polymorphisms within the region already defined by the *bv*/101 backcross map. Therefore strains which gave products distinguishable from those amplified from *bv* DNA with the markers *D5Mit241*, *D5Mit158*, *D5Mit318*, and *D5Mit187* were prioritised. Secondly, it must be possible to type the mice at points either side of the critical interval in order to establish a recombination rate between them, therefore the chosen strain must also possess polymorphisms close to or at the existing flanking markers. Finally, at the time the cross was to be established, it was known that the lab would be relocated in the near future and that any existing crosses could not be transferred. Since the final total of F_2 animals is critical to the probability of obtaining an informative recombination event, it was considered crucial that the breeding scheme began as quickly as possible. Hence priority was given to those strains which were already maintained as colonies within the lab (see Table 4.1).

Of the four markers which lie within the region, three gave polymorphisms with at least one strain, with *D5Mit187* giving the same product size in all the strains tested. Six strains – BALB/C, CBA/Ca, 129X1/SvJ, A/J, CE/J and RBG/Dn – gave polymorphisms with two of the remaining three markers. Eleven strains gave polymorphisms with one of the markers, and the remaining two – 101/H and DA/HuSn were not polymorphic for any of the selected markers. Of the six most polymorphic strains only A/J was also polymorphic with *bv* at the closest flanking markers *D5Mit25* and *D5Mit209*. However, CBA/Ca was an established colony within the lab and demonstrated polymorphisms at the proximal flanking marker *D5Mit25* and

at the more distal marker *D5Mit424*. It was decided that the increased simplicity and rapidity conferred by the use of an easily available strain outweighed the disadvantage of a more distant flanking marker, and hence the intercross was established using a CBA/Ca outcross parent.

4.4.2 The origins of the *bronx waltzer* genetic background

The *bronx waltzer* mutation arose spontaneously in a strain of laboratory mice kept at the Albert Einstein College of Medicine in New York and was first reported in 1979 (Deol and Gluecksohn-Waelsch 1979). The identity of this strain was unreported and the mutation has since been crossed to a variety of different inbred strains, leading to its current maintenance on a mixed genetic background. However, since the continuation of a mutant strain necessitates the selection of the original mutant allele, and since recombination frequencies are low within a small region, it is possible that the genetic material in close proximity to the *bv* locus is still that belonging to the strain on which the mutation arose. Hence an analysis of the polymorphism rates with various inbred strains within the *bv* candidate region may provide information regarding the identity of the original genetic background. This would be useful since it would facilitate the discovery of polymorphic markers.

Taking into account only those genetic markers which are located within the current candidate region and thus lie close to the *bv* allele (see Table 4.3b) we can see that two strains, 101/H and DA/HuSn, show no polymorphisms with the *bronx waltzer* genetic background. However, both of these strains show polymorphisms with *bronx waltzer* at the flanking marker *D5Mit209*, which according to the 101/H genetic map (see section 3.1.2) is located only 0.37cM from the *bv* allele. In addition, these two strains are in all likelihood unrelated or only distantly associated with each other, with 101/H stemming from the Castle's group and DA/HuSn from the Swiss mice (Beck *et al.* 2000). Therefore, since they are unrelated to each other, it is probable that

their apparent similarity to *bronx waltzer* is a consequence of a similar chance rather an indication of a shared genetic heritage. As previously mentioned, the mutation initially arose over 25 years ago and it is not known on which strain the mutation arose on or if the mutation was crossed to other strains in the early years before it was transferred to Nottingham. Over such a large number of generations it is possible that recombinations have occurred even within such a small region, meaning that only DNA extremely closely linked to the *bv* allele would still be that of the original strain. The discovery of markers which are non-recombinant with the mutation may make it possible to acquire more useful data informing the origins of the *bronx waltzer* mouse.

Interestingly, although CBA/Ca was found in this study to be one of the strains most polymorphic with *bv*, in the analysis carried out prior to the establishment of the backcross to 101/H (Bussoli 1996), CBA/Ca was found to be one of the least polymorphic strains with a 31% polymorphism rate in a panel of 32 genetic markers. By contrast, *Mus castaneus* gave an 86% polymorphism rate and 101/H gave 52%. The markers tested in this investigation were taken from a much more extensive region of mouse chromosome 5 since the mutation had yet to be localised at this stage. Therefore it is possible that this apparent discrepancy can be explained by the *bronx waltzer* chromosome 5 comprising some DNA from or closely related to CBA/Ca, but with genetic material from a different strain in close proximity to the locus.

The lack of clarity in these results and the failure to identify a single strain which correlates closely with *bronx waltzer* is probably a reflection and confirmation of its long and complicated breeding history.

4.4.3 Transmission ratio analysis

The transmission of the *bronx waltzer* gene is assumed to be inherited according to Mendelian genetics. As such, in the case of an intercross the F_2

generation would be expected to have a 3:1 ratio of control (either wild type or heterozygote) to mutant mice. The F_2 mice in the present intercross to CBA/Ca were found to deviate slightly but not significantly from this ratio when analysed using a G-test for goodness of fit (Sokal and Rohlf 1995). This adherence to the expected ratios suggests that the *bv* mutation is fully penetrant on the CBA/Ca genetic background, as well as providing some evidence that the *bv* allele is not lethal in its homozygous form. This is an interesting observation since in the previous cross to 101/H (Bussoli 1996; Cheong 2000) and also during the maintenance of the *bronx waltzer* stock on the original unknown background (unpublished observations), the transmission ratio of the *bv* allele has been found to be significantly lower than expected. It was postulated that some of the embryos homozygous for *bv* may be dying prenatally, but a discrepancy between the number of pups recorded at birth and the number still alive at the time of sacrifice led to the suggestion that a disproportionate proportion of *bv* homozygoyte pups were dying at an early age. These animals are often smaller, possibly as a result of their disorientation and lack of co-ordination making it difficult for them to feed properly. As a result, it is possible that the parents identify them as being less "fit" than their littermates and that they are preferentially subject to infanticide. As outlined in Section 4.1.2, the behaviour of *bv* mutants necessitates the removal of the male from the cage once a pregnancy has been established, a strategy which was followed for both the 101/H backcross and for maintenance of the *bronx waltzer* stock. In contrast, since both parents in the intercross breeding strategy are heterozygotes, they are left undisturbed and are both present when litters are born. In general this means that the parents are likely to be less stressed and are hence less likely to cannibalise their offspring (vom Saal and Howard 1982). In addition, levels of infanticide have been shown to vary greatly between strains (Svare *et al.* 1984; Perrigo *et al.* 1993), introducing the possibility that CBA/Ca mice are inherently more likely to keep their offspring after birth. Therefore, the adherence of the transmission ratio to expected frequencies in this case supports the suggestion

in previous studies that the reduction in the number of mutant animals was a result of their being preferentially chewed by the mother, rather than by a lethal effect of the *bronx waltzer* gene.

It is also possible that the *bronx waltzer* phenotype may be subject to a subtle reduction in penetrance or a modification of the phenotype on the CBA/Ca genetic background leading to some mice carrying two copies of the *bv* mutant allele failing to exhibit the behaviour typical of homozygous mutant mice and perhaps having a higher survival rate. However, when analysing the F_2 offspring of this cross, there were very few incidences of mice with indeterminate phenotypes. In the case of a modifier effect being present one might expect to find mice with some but not all of the characteristics of a mutant. For example, they may exhibit mild head-bobbing rather than circling and tail-chasing, or simply fail to show a detectable Preyer reflex. Of the 233 mice included in this cross, only 3 were noted as having slightly unclear phenotypes and all of these were confidently scored as *bv/bv*. Subsequent genotyping analysis showed these mice to be carrying *bronx waltzer* alleles at both flanking markers, thus confirming that their phenotypes were correctly recorded. Hence it is unlikely that the *bronx waltzer* allele is modified on the CBA/Ca genetic background.

4.4.4 Interpretation of intercross data

Of the 47 *bronx waltzer* homozygote F_2 offspring analysed in this study, none had undergone recombination within the critical region. All gave single bands corresponding to the size expected at a *bv* allele at the flanking markers and at each of the internal polymorphic markers. This outcome does not reduce the size of the candidate region for the *bronx waltzer* allele or allow the exclusion of any candidate genes. Recombination events are considered to be relatively random, although some regions recombine at a higher than average rate and are known as "hotspots", while others are less likely to undergo recombination (Steinmetz *et al.* 1987). In order to gauge the relative

recombination rates we might expect in the region surrounding the bv allele we can examine the findings of the previous genetic cross to 101/H (see Chapter 3). In this instance, the genetic distance between the flanking markers *D5Mit25* and *D5Mit209* was found to be 1.83cM. To determine the average recombination rate, we can compare the physical size of mouse chromosome 5 (150Mb, Ensembl Build 33) to its genetic size (92cM, Mouse Genome database) giving a conversion factor of 1cM:1.6Mb, thus the physical size of the region might be expected to be approximately 3.02Mb. The actual physical size is slightly smaller at 2.8Mb, implying that the recombination rate of the region is close to or slightly higher than average. In the panel of 1073 mice, 19 showed recombination within the critical region, equating to one in every 56 meioses. In the present intercross, 47 mutant mice represent 94 meioses since every mouse carries a recombined haplotype from each of its F_1 parents. Hence, should the recombination frequency be consistent with the previous cross, we might have expected to see at least one mouse carrying a recombination within the region. However, different strains exhibit different recombination rates over the same chromosomal region, and in addition the male recombination rate differs from that of females. The lack of recombinant mice arising from this cross is most probably a result of stochastic factors and it is probable that with a larger number of F_2 progeny a recombinant mouse or mice might be found. The scope of the present study was constrained by the imminent relocation of the lab, meaning that the production of litters was brought to a halt prematurely. In order to increase the numbers of F_2 offspring and hence the probability of obtaining recombinations within the region, a new outcross and F_1 intercross could be established. Although the parental animals would be different, the status of CBA/Ca as in inbred strain means that the new parents could be considered identical and while not inbred, *bronx waltzer* DNA in the proximity of the mutation is highly likely to be conserved. This means that data obtained from the F_2 animals generated could be added to those obtained in the present

study, thus increasing its statistical power, although a single recombination event may be all that is required to reduce the size of the region.

Chapter 5:

Assessment of genes located within the candidate region

CHAPTER 5

ASSESSMENT OF GENES LOCATED WITHIN THE CANDIDATE REGION

5.1 INTRODUCTION

The aim of this chapter is to investigate the relative probability of each gene within the critical region being responsible for the *bronx waltzer* phenotype. Each of the 52 genes which have been mapped to the 2.6Mb region between the flanking markers established in Chapter 3 is considered to be a candidate gene. Based on the approximation by the Mouse Sequencing Consortium of 30,000 genes in 2.5Gb euchromatic DNA, the average gene density of the mouse genome is estimated to be 12 per megabase (Waterston *et al.* 2002). The *bronx waltzer* candidate region with 20 genes per megabase is thus relatively very gene-rich and it would be unwieldy to carry out functional studies on each of these genes. Hence it was considered necessary to prioritise for further investigation those genes which were thought to have the highest likelihood of causing the balance and hearing defects observed in mice homozygous for the *bronx waltzer* mutation. This prioritisation was carried out by assessing each gene in a number of different ways, as described below.

5.1.1 What makes a good candidate gene?

Before analysing each potential candidate gene it is important to set out what we are looking for in such an analysis. The functioning of the mechanisms required for hearing has yet to be fully elucidated and it is therefore very difficult to completely rule out any gene since it may play an as yet undefined role in the ear. However, it is possible to pick out characteristics which may suggest a potential role in the ear and hence warrant further investigation. The

factors to be considered in making this decision are outlined in the following paragraphs.

5.1.1.1 A potential role in pathways known to be required for hearing

Through a combination of the cloning of genes responsible for various types of genetic deafness and tissue-specific gene discovery, some of the molecules and mechanisms required for hearing function have been characterised. Of those genes which have been implicated in sensorineural deafness like that seen in the *bronx waltzer* mutants, the roles which they play allow them to be grouped into a number of categories which are summarised in Table 5.1. With these groupings in mind, candidate genes can be assessed as to whether their known or predicted functions might be involved in similar processes. For example, given the importance of maintaining ion gradients in the inner ear for sound transduction to take place (see Section 1.1.2.2) and the discovery of a number of deafness genes involved in ion transport, a gene manifesting as an ion transporter or channel might make an interesting candidate. Similarly, with the knowledge that stereocilia require highly-organised actin bundles to maintain the shape so crucial to their function, any molecule exhibiting a potential role in cytoskeletal organisation or interaction would stand out as one warranting further investigation. The association of several genes shown to be involved in actin bundling, as well as a large number of unconventional myosins – molecular motors known to interact with actin – with forms of genetic deafness lends weight to this proposition.

However, *bronx waltzer* possesses a uniquely specific phenotype which makes it unlikely that such generic pathways should be seriously disrupted. In the organ of Corti only the inner hair cells are affected, and these begin to develop at E17.5 as expected but almost immediately degenerate and most are reabsorbed shortly after birth. A similar series of events can be observed in the maculae and cristae of the vestibular system, where hair cells begin to develop but fail to mature and are reabsorbed into the epithelium. This

suggests that the mutated gene lies downstream of the cell fate specification of hair cells into IHCs and OHCs, and since the outer hair cells appear normal, it must represent a factor necessary only for the correct differentiation or maintenance of inner hair cells and vestibular hair cells, rather than for general hair cell development or function. Even so, it is still possible that the phenotype may result from a mutation in a part of a more widely expressed gene which is transcribed only in the cell types affected, or indeed in a cell-type specific regulatory element associated with such a gene.

Table 5.1: Biological roles of identified genes for human nonsyndromic sensorineural hearing loss (Adapted from Friedman and Griffith 2003)
NSHL, nonsyndromic hearing loss
[a]Only one mutant allele of this gene has been reported in one family segregating NSHL. An inconsequential variant may be in disequilibrium with the actual mutant allele in a closely linked gene.
[b]In the absence of functional clues, proteins are categorised as having an unknown function

Biological role	**Gene product**	**Gene symbol**	**NSHL locus/location**	**Phenotypes of allelic mutations**	**Mouse model (gene symbol)**
Adhesion	cadherin 23 protocadherin 15	*CDH23* *PCDH15*	*DFNB12*/10q21-q22 *DFNB23*/10q21-q22	Usher syndrome 1D Usher syndrome 1F	waltzer (*v*) Ames waltzer (*av*)
Cytoskeleton	diaphanous 1 espin	*DIAPH1*[a] *ESPN*	*DFNA1*/5q31 *DFNB36*/1p36	- -	- jerker (*je*)
Enzyme	Transmembrane protease, serine 3	*TMPRSS3*	*DFNB8*, *B10*/21q22.3	-	-
Extracellular matrix	cochlin α2(XI) collagen otoanchorin α-tectorin	*COCH* *COL11A2* *OTOA* *TECTA*	*DFNA9*/14q12-q13 *DFNA13*/7q22.1 *DFNB22*/6p12.2 *DFNA8,A10,A12,B21*/ 11q22-q24	- Type 3 Stickler syndrome, OSMED - -	- *Col11a2*$^{-/-}$
Gap junction	connexin 26 connexin 30 connexin 31 connexin 43	*GJB2* *GJB6*[a] *GJB3* *GJA1*	*DFNB1,A3*/13q12 *DFNB1,A3*/13q12 *DFNA2*/1p34 n.a./6q21-q23.2	Keratodermia Clouston's syndrome - -	*Gjb2*$^{-/-}$ *Gjb6*$^{-/-}$ *Gjb3*$^{-/-}$ -
Ion channel, transporter	Potassium channel NQ4 pendrin	*KCNQ4* *SLC26A4*	*DFNA2*/1p34 *DFNB4*/7q31	- Pendred syndrome	- *Pds*$^{-/-}$
Integral membrane protein (predicted)	Transmembrane inner ear-expressed Transmembrane cochlear-expressed gene 1	*TMIE* *TMC1*	*DFNB6*/3p14-p21 *DFNB7*, B11, A36/ 9q13-q21	- -	spinner (*sr*) Beethoven (*Bth*), deafness (*dn*)

Biological role	**Gene product**	**Gene symbol**	**NSHL locus/location**	**Phenotypes of allelic mutations**	**Mouse model (gene symbol)**
Motor	myosin IA	*MYO1A*	*DFNA48*/12q13-q15	-	-
	myosin IIA	*MYH9a*	*DFNA17*/22q13	-	-
	myosin IIIA	*MYO3A*	*DFNB30*/10p12.1	-	-
	myosin VI	*MYO6*	*DFNA22,B37*/6q13	-	Snell's waltzer (*sv*)
	myosin VIIA	*MYO7A*	*DFNB2,A11*/11q12.3	Usher syndrome 1B	shaker 1 (*sh1*)
	myosin XVA	*MYO15A*	*DFNB3*/17p11.2	-	shaker 2 (*sh2*)
	prestin	*PRES*	n.a./7q22.1	-	*Pres*$^{-/-}$
	myosin heavy chain 14	*MYH14*	*DFNA4*/19q13.33	-	-
Macromolecular organiser	harmonin	*USH1C*	*DFNB18*/11p15.1	Usher syndrome 1C	-
Neuron/synapse	otoferlin	*OTOF*	*DFNB9*/2p22-p23	-	-
	whirlin	*WHRN*	DFNB31/9q32-q34	-	whirler (*wi*)
Tight junction	claudin 14	*CLDN14*	*DFNB29*/21q22	-	-
Translation	12S rRNA	-	mitochondrial gene	-	-
	tRNA-Ser(UNC)	-	mitochondrial gene	Myoclonic epilepsy, ataxia	-
Transcription regulator	Eyes absent 4	*EYA4*	*DFNA10*/6q22-q23	-	-
	Pou domain, class 4, factor 3	*POU4F3*	*DFNA15*/5q31	-	*Brn3c*$^{-/-}$, dreidel (*ddl*)
	Transcription factor, CP2-like 3	*TFCP2L3*[a]	*DFNA28*/8q22	-	-
	Pou domain, class 3, factor 4	*POU3F4*	*DFN3*/Xq21.1	-	*Pou3f4*$^{-/-}$, sex-linked fidget (*slf*)
Unknown function[b]	crystalline, mu	*CRYM*	n.a/16p13.11-p12.3	-	-
	DFNA5	*DFNA5*[a]	*DFNA5*/7q15	-	-
	stereocilin	*STRC*	*DFNB16*/15q21-22	-	-
	wolframin	*WFS1*	*DFNA6,A14,A38*/4p16	Wolfram syndrome (DIDMOAD)	-

5.1.1.2 Expression in the inner ear during development

Since the *bronx waltzer* phenotype is restricted to the sensory patches of the inner ear and is visible from E17.5, the point at which the hair cells begin to develop (see Section 1.2.3.6), it might be expected for the mutated gene to be expressed at this time point in the tissues affected. Specifically, one might anticipate expression of the gene in normal inner hair cells and vestibular hair cells at E17.5. However, it is also possible that the gene may be expressed not in these cells themselves but in cells nearby which have an inductive influence over them. For example, the supporting cells and pillar cells of the organ of Corti may secrete some factor necessary for the proper maintenance of inner hair cells, or conversely may produce an inhibitory signal which would normally be switched off.

Since the bronx waltzer phenotype so specifically affects IHCs which have abundant afferent innervation and not OHCs which are associated primarily with efferent nerve fibres, it is important to consider the possibility of the mutation affecting primarily neuronal tissue. However, although cochlear and vestibular neurons eventually degenerate in the absence of hair cells (Schuknecht 1974, pp 333), it has been shown that hair cells are able to survive even when the development of neurons is inhibited (Fritzsch *et al.* 2005) and that normal growth of nerve fibers can occur in the absence of hair cells (Fritzsch *et al.* 2005). Thus it is unlikely that the IHC degeneration seen in the *bronx waltzer* cochlea is a result of disruption to their innervation, unless the mutation manifests in a dominant negative manner, actively triggering the degeneration of IHCs.

It should also be considered that a gene may cause developmental defects in hearing in the absence of any detectable expression within the ear itself. An example of such a gene is the transcription factor *Hoxa1*. Murphy and Hill (1991) found it to be expressed in the neuroectoderm and mesoderm of the developing mouse hindbrain, adjacent to site of ear formation. No expression

was observed in the otic placode, the otic pit or the otocyst, and yet mice homozygous for a targeted deletion of the gene were found to have malformed inner ears, in addition to altered rhombomeres 4 and 5 of the hindbrain (Lufkin *et al.* 1991; Chisaka *et al.* 1992). This was thought to be due to the inductive influence of the neural tube on the morphogenesis of the ear (Gallagher *et al.* 1996; Noramly and Grainger 2002). However, this type of gross ear abnormality contrasts sharply with the highly tissue-specific nature of the *bronx waltzer* phenotype and it is unlikely that a remotely expressed gene could exert such fine control over different cell types. Thus it is relatively certain that the *bv* gene would not be expected to act in this manner, and will instead be found to be expressed within or in close proximity to the affected tissues of the organ of Corti and vestibular sensory patches.

5.1.1.2.1 Sources of expression data

For some previously characterised genes the expression patterns may have already been published, although it is important to verify that the experiment was carried out at an appropriate time point and that the authors looked for expression in the ear and at an appropriate time point since for many genes the expression may have only been characterised in a small selection of adult tissue types.

A second source of expression data exists in the form of searchable libraries or databases containing details of genes or ESTs which have been demonstrated to be expressed in a relevant tissue type. In this case, examples include the Washington University Inner Ear Protein Database (Thalmann and Thalmann) which lists proteins identified from the tissues and proteins of the guinea pig inner ear by 1D- and 2D-Polyacrylamide Gel Electrophoresis (PAGE), and the Morton human Fetal cochlear cDNA library (Robertson *et al.* 1994) which holds sequences of ESTs identified by a combination of subtractive hybridization and differential screening strategies. Other cDNA libraries of interest include the full-length mouse subtracted inner ear library

prepared by Beisel *et al.* (Beisel *et al.* 2004; Pompeia *et al.* 2004)) and the EST database resulting from the screening of the cDNA population from mouse Organ of Corti ranging from P5 to P13 to include the maturation of hair cells and onset of hearing (Pompeia *et al.* 2004). In addition, a number of microarray studies have identified genes or ESTs differentially expressed in the mouse inner ear (Chen and Corey 2002), mouse cochlea (Morris *et al.* 2005) or the rat vestibular epithelium (Cristobal *et al.* 2005).

The expression of individual genes, including those which have only been predicted, can also be investigated directly using techniques such as *in situ* hybridisation, Northern blotting and RT-PCR. For each of these techniques it is necessary only to have access to the sequence of the gene and a sample of the tissue to be tested.

5.1.1.3 The eye and the ear

Another indicator of a potential role in the ear may be when a gene has a known function or expression in the eye. Common features in their development have led to the suggestion that the eye and ear share a shared evolutionary origin, with the sensory receptors in both organs having evolved from a common ancestral ciliated cell (Popper and Fay 1997). This proposition is supported by evidence gathered in *Drosophila* by Jarman *et al.* (1994) who showed that *Atonal* (*Ato*) is responsible not only for the establishment of chordotonal precursors and controlling the differentiation of the modified chordotonal organs in the antenna which form Johnston's organ, the auditory organ of the fly, but is also the proneural gene for photoreceptors in the compound eye. Niwa *et al.* (2004) subsequently examined whether there exist any similarities in the conditions necessary for the formation of these different sensory organs. The development of all three organs was found to be initiated by the expression of *decapentaplegic* (*DPP*), with all of them failing to form when its signalling was blocked by overexpression of the inhibitor *Daughters Against DPP* (DAD). In addition, all

three organs form simultaneously and were each shown to rely on the presence of the hormonal factor ecdysone at an early third instar larval stage for proper development to take place, suggesting that ecdysone represents a temporal initiation signal common to the eye, Johnstone's organ and the chordotonal organ. This conservation of early developmental function in sensory organ formation suggests that there once existed a primitive sensory organ precursor which would differentiate according to the identity of its segment of origin.

A second reason to consider genes expressed in the eye as candidates for a deafness phenotype is the existence of single gene disorders which affect both the ear and the eye. The most widespread of these are the various forms of Usher Syndrome (Keats and Corey 1999) which are characterised by congenital sensorineural deafness and progressive retinitis pigmentosa. The syndromes are clinically variable and genetically heterogenous, with some but not all of the genes responsible having been identified. Many of these interact with each other to form the transmembrane complex which binds stereocilia bundles together (Ahmed *et al.* 2003) but for others the functions are unclear. The fact that a number of genes are necessary for proper development and maintenance of both the ear and the eye points to some overlapping of gene function. In addition, the mouse models for Usher Syndrome such as shaker-1 (*Myo7a*) and waltzer (*Cdh23*) exhibit hearing and vestibular defects show only minor abnormalities in the retina. Libby *et al.* (2003) showed that mice with mutations in *Cdh23* have abnormal retinal function when assessed by electroretinography but no anatomical abnormality could be detected, and mice with mutations in *Myo7a* have recently been shown to have abnormally distributed melanosomes in the retinal pigmented epithelium (Gibbs *et al.* 2004). Hence it is feasible that a gene affecting both the ear and the eye may initially manifest as solely a hearing phenotype when its function is disrupted in the mouse and retinal function is not specifically investigated as in the case of *bronx walter*. It has been suggested that the genes may play different roles in

the two species or that a level of functional redundancy may exist in the mouse. Other important differences include environmental factors such as light exposure since laboratory mice are generally kept in relatively dim light conditions, and also the lifespan of the mouse, which may not be long enough for the progressive degeneration of the retina to become measurable (Zheng *et al.* 2005). More significantly, the diversity in severity of phenotype in humans suffering from Usher Syndrome caused by the same mutation suggests a strong genetic or stochastic modifying effect (Petit 2001), thus one might expect variation to occur when the mutation manifests in a different species.

5.1.2 Assessing genes with known or predicted functions

Of the 52 genes annotated within the candidate region for *bronx waltzer*, 31 have been previously characterised. For these genes a certain amount of information is available making it possible to assess their candidacy to an extent based on the published literature. For some, a function may be fully elucidated and a mouse model may already exist. In these cases the possibility of their being responsible for the *bronx waltzer* phenotype can be investigated by enquiring as to whether the mouse model exhibits similar behaviour and establishing whether the function of the gene correlates with the phenotype of the *bv* mice. Other genes may have less information available and may have been identified only by homology of their protein domains to other, better characterised genes. These can be assessed and prioritised based on their possible function and on that of related family members but are harder to rule out since they may perform an as yet unreported function within the ear.

5.1.3 Assessing novel and predicted genes

The remaining 21 uncharacterised genes within the critical region have little or no published information associated with them. They may have been identified by gene-prediction programs based on conserved structures such as

splice sites and homology to known genes as well as the existence of ESTs which imply that the region is transcribed (Mathe *et al.* 2002; Brent and Guigo 2004). As a result there may be no information concerning their function, although some may have predicted protein domains based on their homology to known genes which may provide clues as to their function. In addition, since their sequence is known they can be compared to those inner ear derived cDNA libraries which have made EST sequences available for searching to establish whether or not they have been found to be expressed in the expected tissues.

5.2 METHODS

5.2.1 Data mining of inner ear expression databases

A number of studies have been carried out with the intention of identifying genes expressed in inner ear tissues. These have ranged from the characterisation of proteins isolated from tissues and fluids within the ear to the construction of cDNA libraries from specific inner ear tissue samples, and also the use of microarray technologies to identify differentially expressed genes. Some of these data are available in a searchable format, and these have been used to derive evidence for the expression of some of the *bronx waltzer* candidate genes in the tissue one might expect the causative agent for the mutation to be found. The databases examined, their origins, locations and the methods used to search them are summarised in Table 5.2

The Washington University Inner Ear Protein Database (Thalmann and Thalmann) and Inner Ear Gene Expression Database (Chen and Corey 2002) were designed to be searched using gene IDs and descriptions and thus novel genes could not be included. The Human Cochlea EST database (Robertson *et al.* 1994) was queried using translating BLAST (tBLASTn) in order to compensate for differences between the mouse and human gene sequences, while the mouse Organ of Corti EST database (Pompeia *et al.* 2004) was queried directly using cDNA sequences and BLASTn (Altschul *et al.* 1990).

Resource	Construction	Reference	Search procedure
Washington University Inner Ear Protein Database	Isolation and identification of proteins in guinea pig inner ear tissues and fluids by PAGE	http://oto.wustl.edu/thc/innerear2d.htm (Thalmann and Thalmann)	Online list searched for Gene IDs and descriptions. Unknown genes not included.
Inner Ear Gene Expression Database	Microarray screen of mouse cochleas at P2 and P32	http://www.mgh.harvard.edu/depts/coreylab (Chen and Corey 2002)	Database downloaded and searched locally with gene IDs and descriptions. Unknown genes not included.
Human Cochlea EST database	Human fetal cochlear cDNA library subtracted against total human fetal brain RNA	http://hearing.bwh.harvard.edu/estinfo.HTM (Robertson *et al.* 1994) Also at http://neibank.nei.nih.gov	Online list searched for Gene IDs and descriptions of orthologues. EST database queried using tBLASTn with protein sequences of all candidate genes to account for variation in human and mouse sequence
Organ of Corti EST database	cDNA library constructed from mice between P5 and P13	http://neibank.nei.nih.gov (Pompeia *et al.* 2004)	Online list searched for Gene IDs, RefSeq IDs and Accession numbers. EST database queried using BLASTn with cDNA sequences of all candidate genes.

Table 5.2: Origins, locations and methods of interrogation of publicly available resources describing genes showing expression in inner ear tissues

5.2.2 Expression studies using inner ear cDNA

As a means of ascertaining whether the genes lying within the critical region for *bronx waltzer* are expressed within the ear, studies were carried out using cDNA prepared from wild type inner ear tissue. Successful amplification of a fragment of the expected size from this material can be taken as an indication that the gene may be expressed in the tissue of interest.

5.2.2.1 Obtaining inner ear cDNA

The inner ear capsules were dissected out from a single litter of ten C3HeB/FeJ mice at age P0, with care being taken to remove as much extraneous tissue as possible. These were kept briefly in ice cold RNase-free Phosphate Buffered Saline (PBS) before being homogenised and incubated at room temperature for 5 minutes. RNA was prepared from this tissue as described in Section 2.6, including the optional DNase treatment to remove any genomic DNA contamination. Reverse transcription was then performed as described in Section 2.7.

5.2.2.2 Primers designed for amplification from cDNA

In order to make certain that any products amplified from the cDNA material were truly representative of an mRNA molecule isolated from inner ear tissue rather than from genomic DNA contamination, primers were designed in adjacent exons to span the intervening intron. In this manner, products resulting from cDNA and from genomic DNA can easily be distinguished by their differing sizes, with the genomic product being larger as a result of the inclusion of the intron which will have been spliced out in a cDNA template. This strategy is illustrated in Figure 5.1 and the primers designed for each of the genes within the *bv* region are given in Table 5.3. Two exceptions to this strategy were genes consisting of only one exon where the genomic and cDNA expected product lengths will be the same, and genes with no introns

small enough to be suitable for PCR amplification where no genomic band will be observed. These are indicated in Table 5.3.

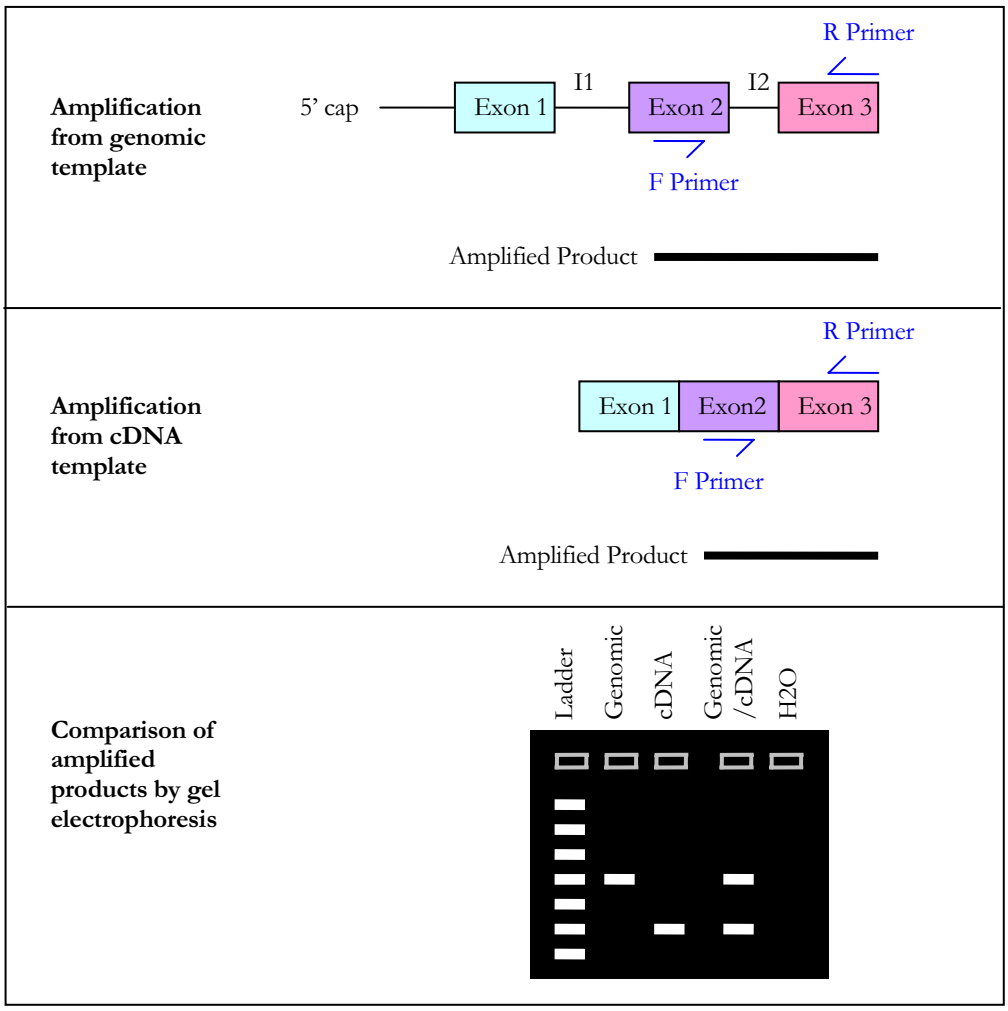

Figure 5.1: Diagram illustrating the strategy used in the design of primers to amplify fragments of candidate genes using cDNA obtained from P0 inner ears as the PCR template. The different sized products amplified from genomic DNA and cDNA as a result of the splicing out of Intron 2 allow the origin of the template to be confirmed by agarose gel electrophoresis.

Gene ID	Notes	Exons	Intron size	F primer	R primer	Expected Genomic size	Expected cDNA size
Acacb		4-5	144	GCTGATCATAGACATTGCCAAG	AAGTTTGGGGTTTTCCGAAG	226	82
Foxn4		4-5	89	TGAGCCCTATAGGCAACCAC	TGGGTAGCTGGGGAGTACAG	204	115
NM146163		3-4	139	GGGGAAGAAGGAAGGCTATG	CAAGCAGTTGGAGCACTTTG	237	98
Kctd10		4-5	546	CTTACGAGCCCTTCTGCAAG	CTGTTGTAGAGCAGCTTCACG	649	103
Ube3b		10-11	248	TGCGCAGTTCTCAGACAATC	CGAAGCATGTCATGGGACTC	377	129
Mmab		5-6	242	CCAGTGCATGCTACAGGAC	GGAGCTGGCTGGAGTACTTG	385	143
Mvk		4-5	284	CCTTGGAGCAACTGGAGAAG	GCCAGACACACAGAGTAGGC	495	211
E41930	2 exons, large intron	1-2	16366	GAGGACTCAGAACCCACCAG	TGGGGAAGATCTTGATGGAC	16545	179
Trpv4		8-9	229	GTAAGTTTGGGGCTGTGTCC	CTGTGAAGAGCGTGATGACC	400	171
Gltp	All introns too large	3-4	2060	GACCCAGCCAAGTTCAAGAC	GCCAGCCATGGTACTTCTTC	2301	241
NM029992		7-8	169	AACAGGAGAACCTGCTGAGG	CTGTTGAGCTGCGCGTTG	193	24
Git2		5-6	109	GAACAGGGAATCTTGAGACCTG	ATCTTGTGTGCCTGGGTCAG	276	167
NM175120	Only 1 exon	n/a	0	CGGGACACACAACAAACAAC	TTCTGACCAATCGTGGAAGG	238	238
Q9D1S6		2-3	611	TCGGACATTACTGCACCTTG	CCATGGACGTGTTGTGGTAG	802	191
NM181075		1-2	587	TTCAGTGATGCTGCGCTTAG	AAAGCCTCCAAGGGTCACTG	849	262
NM026263		6-7	453	GACACTTTGTCTATGGGACACG	GCTCTTGCTCTTCTGAGCTG	582	129
Q8C864	Only 1 exon	n/a	0	CTACAGCCCTCCACAAAAGC	TTCTCTGTTTCCTCCCTTGC	483	483
Oasl2	All introns too large	2-3	1209	AAGGTTCAGTCCCGGAAGAC	GGGCGAGTTTTCACAAAATG	1403	194
Oasl1	All introns too large	3-4	1516	CTCATCTTCACGATCCAGACC	AGTGTTTGACCAACCGAAGG	1745	229
NM028211		3-4	174	TTCGGACCACTCCTGAGTTC	GCTGCATCTTTGCCTTTTG	288	114
Tcf1		5-6	110	GCGGCCTTACACCAAGTATC	GGTAGCGAGGCCATGATAAG	298	188
E44804	Only 1 exon	n/a	0	ATGACGAAGGGAACGTCATC	TCCCGGTAGTGTTTCGTCTC	296	296
Usmg3		6-7	426	TCTCTGTGTTGCCATGATCG	GATTGTCAGCTGGCTGTGTG	590	164
Rpl37	Only 1 exon	n/a	0	ATGACGAAGGGAACGTCATC	TCCCGGTAGTGTTTCGTCTC	181	181
Acads		5-6	212	GCTTGGATCACCAACTCCTG	TCCTCAAAGATGAGGTTAGCTG	397	185
NM175352	All introns too large	1-2	3901	CTGGCAAGGAGGAGAAGAAG	GGCTTGGCAATCTCAAAGAG	4184	283
NM175403		3-4	81	GGACATCTTTGACCGTGTCG	GTGCACAGACTTTGGGATTG	245	164
Cabp1		5-6	208	ACTGATGGGCCCTAAACTCC	CACGTCTCGGATAATTTCCTC	398	190
Pop5		4-5	161	CAATGCCTACACTGGAGTCG	CTTCGTCAGTGCAATTCTGC	385	224

Gene ID	Notes	Exons	Intron size	F primer	R primer	Expected Genomic size	Expected cDNA size
Rnf10		5-6	74	CTGTGGACACATTTTCTGCTG	ATTCACCCACTTGGATTTGG	300	226
D5Ertd33e		6-7	87	CATTGGTGAGGTCATTGCAG	AGAGTGAATGGCCACAATCC	250	163
Dnclc1	All introns too large	2-3	1679	TGTCGGAAGAGATGCAACAG	AACAGAAGAATGGCCACCTG	1899	220
Sfrs9		3-4	286	CGTACAGAAGGACGGAATGG	GGCTTTGGTATGGCGAGTC	489	203
NM029645	All introns too large	1-2	5271	CGGTAATCGAGCATCTGGAG	GGGGCCACAAAGTATTCCTC	5521	250
Q8C4H9	Only 1 exon	n/a	0	TGTTTTTGACTCCTCCCTTTG	TAGTGGGTTCAGCGGGTAAG	250	250
15E1	2 exons, large intron	1-2	1257	GCGAGTACGACCAGTGCTTC	GAGTTTTCAGGCTTTTCTTTGC	1444	187
Cox6a1		1-2	131	CAGCGTCTCGGGTCTCTC	GGTCTCTCGTGCTCTTCGTG	324	193
Msi2h		4-5	99	GCGAATACTTCGGCCAGTTC	GATTGCGCCAGCACTTTATC	232	133
Q9D2I7	Only 1 exon	n/a	0	ATTCACATCCCACGAAGGAG	AAAGAGAGGTGGGTGTGGTG	177	177
Pla2g1b	All introns too large	2-3	1051	GTGGCAGTTCCGCAATATG	CCCGGAGCATGAGTAGGAG	1283	232
Sirt4		3-4	418	ACCGGACGTCGTTTTCTTTG	AAGGCAGCAACTCTCCACAG	663	245
NM133915		3-4	95	GGGCAGCAACCTCTCTGAAC	CGGAACTCTCCAGTTCATCC	364	269
Gcn1l1		3-4	219	AGTTGCTGCCTCGAGTGG	CAGCACGTCCACCTCCTC	383	164
NM198163		4-5	82	CCGAGTCCTTTGTCAACGTC	AGAGCTGGATCCCCATCTG	244	162
Q8R1D2	All introns too large	3-4	788	TGTCAGAGATCGAGCAGAGC	GCCTCTTGAGATCGTTGAGG	1028	240
Rpl29	Only 1 exon	n/a	0	AACCACGGTCGCAAAGATAC	TTAGGGTGAGCGATGAAAGC	235	235
Cit		8-9	270	TGAAGCTAGCCCTGGAAAAG	GAGTTGACGACTCCTTTCTGC	525	255
Prkab1		3-4	255	GGACCTGCCTGAAGGAGAG	TTCAAAGTCAGTTTTCTTCACTTG	391	136
NM177759		7-8	579	CAGGTGATCCAGAAGAAGTCG	TTCCTGAGGATTTCCATCTTG	728	149
Q9D4T7	2 exons, large intron	1-2	1389	GGCCTTCATATCCCACAATG	ACAGGTGGGAGCAGTTTCAC	1618	229
Hspb8	2 exons, large intron	2-3	5916	AGAGAAGCAGCAGGAAGGTG	CCTGGTTGTCTTGAGGAAGC	6113	197
NM026886		5-6	179	ATCTCGAAGCCGGAAGTCTC	CCCTGGCTGACAGGAAGC	424	245
Lnfrg	Positive control	3-4	103	CCACGTGGATGATGACAACTAC	CTGATGCAGAAGCCAGCTC	298	195
Actb	Positive control	5-6	125	ATCCATGAAACTACATTCAATTCCAT	ACCGATCCACACAGAGTACTTGCGC	332	207

Table 5.3: Primers used for the PCR amplification of fragments from genes which lie within the candidate region for *bronx waltzer*. Primers are located in adjacent exons and designed to amplify across the intervening intron, giving different sized products when genomic and cDNA templates are used. Exceptions to this strategy, such as genes with only one exon or introns too large for PCR amplification are indicated in the Notes column.

5.2.2.3 PCR from cDNA

Although the PCR method used here was very similar to the standard protocol described in Section 2.4.1, the PCR cycles used to amplify from genomic and cDNA templates differed in important ways. The cDNA PCR cycle (Table 5.4a) had a higher number of total cycles to account for the limited amount of template material available, while the genomic PCR cycle (Table 5.4b) included a longer extension time to take into account the large size of some of the included exons. The PCR programmes used are given in the tables below.

Step	PCR phase	Temperature	Time
1	Initial denaturation	95°C	2 minutes
2	Denaturation	95°C	30 seconds
3	Annealing	55°C (~2°C below T_M of primers)	30 seconds
4	Extension	72°C (ReddyMix™)	30 seconds
5	Thermocycling	Repeat steps 2-4, 39 times	–
6	Cooling	4°C	Indefinitely

A

Step	PCR phase	Temperature	Time
1	Initial denaturation	95°C	2 minutes
2	Denaturation	95°C	30 seconds
3	Annealing	55°C (~2°C below T_M of primers)	30 seconds
4	Extension	72°C (ReddyMix™)	60 seconds
5	Thermocycling	Repeat steps 2-4, 29 times	–
6	Cooling	4°C	Indefinitely

B

Table 5.4: PCR conditions used for amplification from cDNA (A) and genomic DNA (B). The differences between the two programmes are highlighted in red.

5.3 RESULTS

5.3.1 Assessment of previously characterised genes

A summary of the published information on each of the 31 characterised genes is presented in Table 5.5, including relevant expression data, known or predicted functions and any characterised models. Those genes marked by an asterisk have been selected as having a potential function or evidence which suggests they be involved in the *bv* phenotype and are discussed in greater detail in Section 5.4.

Table 5.5: Summary of published literature relating to previously characterised genes annotated within the described critical region for the *bronx waltzer* locus.
Gene locations were obtained from Mouse Ensembl Build 33 (http://www.ensembl.org/Mus_musculus/). Entrez Gene entries can be retrieved at http://www.ncbi.nlm.nih.gov/entrez/.
Genes marked with an asterisk were selected for further studies (see Section 5.4.3)

Mouse gene	Entrez Gene	Human orthologue	Entrez Gene	Expression information	Function or protein domains	Model	Phenotype	Key references
Acacb Acetyl-coenzyme A carboxylase beta	100705	ACACB/ ACC2	32	Heart and skeletal muscles. Localises to mitochondria.	Control of fatty acid oxidation in muscle tissue	Acacb$^{-/-}$ knockout mice	Higher fatty acid oxidation rate. Reduced storage of fat in adipose tissue.	(Oh *et al.* 2005)
Foxn4 * Forkhead box protein N4	116810	FOXN4	121643	Retina, ventral hindbrain, spinal cord, dorsalmidbrain	Transcription factor controlling retinal development by activation of Math3, NeuroD1, and Prox1	Foxn4$^{-/-}$ knockout mice	Retinal dysplasia	(Li *et al.* 2004) (Gouge *et al.* 2001)
Myo1h * Myosin 1h	231646	MYO1H	64004	Utricles (weaker than other myosins tested)	Myosin head (motor domain) Calmodulin-binding region ATP/GTP-binding site motif	-	-	(Dumont *et al.* 2002)
Kctd10 * potassium channel tetramerization domain-containing 10	330171	KCTD10	83892	-	Voltage-gated potassium channel activity	-	-	-
Ube3b * ubiquitin protein ligase E3B	117146	UBE3B	89910	Highly expressed in chick basilar papillar following noise exposure	Targeting of proteins for proteolytic degradation	-	-	(Gong *et al.* 2003) (Lomax *et al.* 2000)
Mmab Methylmalonic aciduria type B homolog	77697	MMAB	326625	Liver and skeletal muscle	Catalyses synthesis of the coenzyme adenosylcobalamin	Human methylmalonic aciduria	Deficient metabolism of some amino acids, resulting in a high level of acid in the blood	(Dobson *et al.* 2002)

Mouse gene	Entrez Gene	Human orthologue	Entrez Gene	Expression information	Function or protein domains	Model	Phenotype	Key references
Mvk Melavonate kinase	17855	MVK	4598	-	Conversion of mevalonic acid to 5-phosphomevalonic acid	Human mevalonic aciduria	Disorder of the cholesterol/isoprene biosynthetic pathway. Accumulation of mevalonic acid	(Schafer *et al.* 1992)
Trpv4 * transient receptor potential cation channel V4	63873	TRPV4	59341	Many tissues, including inner-ear hair cells, sensory neurons, and Merkel cells.	Osmotically activated cation-selective channel	Trpv4$^{-/-}$ knockout mice	Impaired pressure sensation and thermal responsiveness	(Suzuki *et al.* 2003) (Lee *et al.* 2005)
Gltp Glycolipid transfer protein	56356	GLTP	51228	Expressed in all tissues examined. Highest in cerebrum, lowest in liver and heart muscle.	Selectively accelerates intermembrane transfer of glycolipids	-	-	(Lin *et al.* 2000)
Git2 * G protein-coupled receptor kinase-interactor 2	26431	GIT2	9815		Regulation of golgi organisation, actin cytoskeletal organisation and paxillin localisation	-	-	(Mazaki *et al.* 2001)
Q9D1S6	-	ANKRD13 ankyrin repeat domain 13	88455	-	Leukotriene B4 type 2 receptor Ubiquitin interacting motif Ankyrin	-	-	-

Mouse gene	Entrez Gene	Human orthologue	Entrez Gene	Expression information	Function or protein domains	Model	Phenotype	Key references
Oasl2 2'-5'-oligoadenylate synthetase like protein 2	23962	OASL	8638	Most tissues, highest in primary blood leukocytes and other hematopoietic system tissues, colon, and stomach.	Involved in antiviral activity of interferons. Human orthologue found to interact with thyroid hormone receptors	-	-	(Eskildsen *et al.* 2003) (Lee *et al.* 1995)
Oasl1 2'-5' oligoadenylate synthetase-like 1	231655	OASL	8638	Most tissues, highest in primary blood leukocytes and other hematopoietic system tissues, colon, and stomach.	Not active in antiviral activity. Human orthologue found to interact with thyroid hormone receptors	-	-	(Eskildsen *et al.* 2003) (Lee *et al.* 1995)
Tcf1 Hepatocyte nuclear factor 1-alpha	21405	TCF1	6927	Predominantly in liver and kidney	Transcription factor for genes expressed exclusively in the liver	$Tcf1^{-/-}$ knockout mice Linked to MODY3 in humans	Defect in bile acid transport, increased bile acid and liver cholesterol synthesis, and impaired high-density lipoprotein metabolism.	(Shih *et al.* 2001)
Usmg3 Upregulated during skeletal muscle growth 3	83678	PSL4 Presenilin-like protein 4	121665	-	Membrane protein Peptidase activity	-	-	(Grigorenko *et al.* 2002)
Rpl37 60S ribosomal protein L37	67281	RPL37	6167	All tissues examined	Structural constituent of ribosome	-	-	(Su and Bird 1995)

Mouse gene	Entrez Gene	Human orthologue	Entrez Gene	Expression information	Function or protein domains	Model	Phenotype	Key references
Acads Acyl-CoA dehydrogenase, short-chain specific	11409	ACADS	35	Brain, particularly hippocampus	Fatty acid beta-oxidation. Regulation of theta oscillations during sleep	Acads mutant BALB/cByJ mice	Organic aciduria. Upregulation of Glo1 (involved in the detoxification of metabolic by-products)	(Tafti *et al.* 2003)
Cabp1 * Calcium-binding protein	29867	CABP1	9478	Brain, retina	Competitively inhibits calmodulin binding to CAMK2 May be involved in neuronal signal transduction	-	-	(Yamaguchi *et al.* 1999)
Pop5 Processing of precursor 5, ribonuclease P	117109	POP5	51367	-	Subunit of ribonucleaseP Required for 5'-end maturation of tRNAs	-	-	(Hartmann and Hartmann 2003)
Rnf10 Ring finger protein 10	50849	RNF10	9921	-	Ring finger motif, implies protein-protein interactions. Ubiquitin-protein ligase activity.	-	-	(Seki *et al.* 2000)
Dnclc1 * Dynein light chain 1, cytoplasmic	56455	DNCL1	8655	Wide variety of tissues Localizes to edge of postsynaptic differentiations, along cytoskeletal structures, and the edge of Golgi apparatus.	Inhibits the activity of neuronal NO synthase, implying regulatory role in numerous biologic processes	Drosophila dlc1 mutants	Pleiotropic morphogenetic defects in bristle and wing development and female sterility	(Dick *et al.* 1996) (Jaffrey and Snyder 1996)

Mouse gene	Entrez Gene	Human orthologue	Entrez Gene	Expression information	Function or protein domains	Model	Phenotype	Key references
Sfrs9 Splicing factor, arginine/serine rich 9	108014	SFRS9	8683	All tissues tested, highest expression in pancreas, followed by kidney, placenta, and heart.	Involved in mRNA formation Modulator of SMN exon 7 inclusion (causative agent for proximal spinal muscular atrophy)	-	-	(Stoss *et al.* 1999)
Cox6a1 Cytochrome c oxidase polypeptide VIa-liver	12861	COX6A1	1337	Brain, particularly cerebellum. Primary visual cortex	Subunit of COX, terminal enzyme of the respiratory chain. Probable housekeeping gene	-	-	(Wong-Riley *et al.* 2000)
Msi2h Musashi homolog 1	76626	MSI1	4440	Predominantly in brain	neural RNA-binding protein	-	-	(Good *et al.* 1998)
Pla2g1b Phospholipase A2 precursor	18778	PLA2G1B	5319	Many tissues, primarily secreted from pancreas	Catalyzes the release of fatty acids from glycero-3-phosphocholines Protection of membranes from oxidative injury is an important function	-	-	(Seilhamer *et al.* 1986) (van Kuijk and Dratz 1987)
Sirt4 NAD-dependent deacetylase sirtuin 4	75387	SIRT4	23409	Many tissues	Role in epigenetic gene silencing May function via mono-ADP-ribosylation of proteins	-	-	(Frye 1999)
Pxn * Paxillin alpha	19303	PXN	5829	All tissues tested, localises to focal adhesions	Scaffolding protein involved in actin organisation Role in fibronectin and integrin signalling	Paxillin$^{-/-}$ mice	Homozygous lethal	(Hagel *et al.* 2002)

Mouse gene	Entrez Gene	Human orthologue	Entrez Gene	Expression information	Function or protein domains	Model	Phenotype	Key references
Gcn1l1 General control of amino-acid synthesis 1-like 1	231659	GCN1L1	10985	Ubiquitous expression	S. cerevisiae GCN1 required for activation of protein kinase GCN2, leading to upregulation of aa synthesis during starvation	-	-	(Marton *et al.* 1997)
Rpl29 60S ribosomal protein L29	19944	RPL29	6159	Many tissues	Heparin/heparan sulfate-binding peptide. Possible pseudogene (human orthologue is on Chr3)	-	-	(Liu *et al.* 1996)
Cit * Citron protein (Rho-interacting, serine/threonine kinase)	12704	CIT	11113	Strongest in testis. Also keratinocytes, brain, spleen, lung, kidney.	Essential for cytokinesis in specific neuronal precursors	Citron-K$^{-/-}$ knockout mice	Grow slowly, severely ataxic, die prematurely from seizures. Development of CNS affected due to altered cytokinesis and massive apoptosis.	(Di Cunto *et al.* 2000)
Prkab1 5'-AMP-activated protein kinase, beta-1 subunit	19079	PRKAB1	5564	All tissues tested, strongest in liver	Plays a role in hormonal and nutrient-derived anorexigenic and orexigenic signals and in energy balance	-	-	(Minokoshi *et al.* 2004) (Thornton *et al.* 1998)
Hspb8 Heat-shock protein beta-8	80888	HSPB8	26353	Many tissues, most abundant in skeletal muscle, heart, and placenta. Not found in blood.	Neuromuscular function	Human motor neuropathy type II	Distal muscle atrophy	(Kappe *et al.* 2001)

5.3.2 Gene expression in the inner ear – published data

Of the four databases searched, three yielded data suggesting that clones contained within the collections represent transcripts of genes within the *bronx waltzer* region. These results are given in Table 5.6. The fourth database used – the Washington University Inner Ear Protein Database – was queried for all the known genes within the region but did not yield any positive results and is not included in the table.

Table 5.6: Results obtained from screening publicly available databases of inner ear ESTs.
The Inner Ear Gene Expression (IEGE) database is the result of a microarray study and the results represent clones which showed expression in the inner ear and match the candidate gene by sequence homology. Since the database is searched by gene description, only previously characterised genes could be screened and novel genes are therefore left blank.
The human fetal cochlea and mouse organ of Corti data sets are the result of cDNA library construction and sequencing. The results represent clones within the libraries which show strong sequence homology to the candidate gene. In each case the letter N indicates a negative result in querying the database. The human fetal cochlea library was screened by description and by tBLASTn, while the mouse organ of Corti library was screened by description and by BLASTn to allow inclusion of uncharacterised genes.
Genes which show homology to sequences within more than one database are highlighted in **red**, those which show homology to sequences in only one database are highlighted in **blue**, and those showing no homology are shown in **black**.

Gene ID	Alternate names	Inner Ear Gene Expression database (Chen & Corey)	Human fetal cochlea cDNA library (Morton)	Mouse organ of Corti cDNA library (Pompeia)
Acacb	Acc2, Accb	N	N	N
Foxn4		N	N	N
NM146163	Myo1h 4631401O15Rik	N	N	N
Kctd10		N	N	N
Ube3b		similar?	AW021415 BI492368	N
Mmab		N	N	N
Mvk		W50181, AA109721	N	gi98d12
E41930		N	N	N
Trpv4		N	N	gi119c11, gi215a11
Gltp		AA388875	BI495579 BI495580	gi62b04
NM029992	A930031F18Rik		N	gi147h04
Git2		N	N	N
NM175120			N	N

Gene ID	Alternate names	Inner Ear Gene Expression database (Chen & Corey)	Human fetal cochlea cDNA library (Morton)	Mouse organ of Corti cDNA library (Pompeia)
Q9D1S6	1100001D10Rik		BI494434, BI494435	gi212h02, gi14c04
NM181075			N	gi43g02, gi17h10, gi106f11, gi203c07
NM026263			N	N
Q8C864			N	N
Oasl2		N	N	N
Oasl1		N	N	N
NM028211			N	gi170c01, gi193e04
Tcf1		N	N	N
E44804			N	gi100d09, gi193e09, gi193e11, gi259b02
Usmg3		N	N	gi33c10, gi97c07, gi138f10
Rpl37		AA015377, AA013942, AA529915	N	gi180f07, gi159c04, gi159a04, gi76c07, gi10g11, gi51f12, gi149a05
Acads		N	N	gi178g07
NM175352			N	N
NM175403	2410014A08Rik		BI496418, BI496417	gi107f05, gi184g06, gi210g08
Cabp1		AA111277, W63874	AW023490, AW023596	N
Pop5			N	N
Rnf10		N	N	gi135c05, gi220e05
D5Ertd33e			N	gi172d11
Dnclc1		AA497776, AA184581, AA106442, AA260435, AA260435	AW020245, BI491303, BI491360, BI494005, BI494038, BI494999, N66476	gi140d06, gi185e09, gi186e09, gi251g06
Sfrs9		N	AW021515, AW022794, AW022564, BI492475, BI496917, H91554, N67420	gi131d02
NM029645			N	N
Q8C4H9			N	N

Gene ID	Alternate names	Inner Ear Gene Expression database (Chen & Corey)	Human fetal cochlea cDNA library (Morton)	Mouse organ of Corti cDNA library (Pompeia)
15E1_mouse			N	N
Cox6a1		L06465, AA529006, AA472081	BI495001, BI495002	gi101d12, gi133d04, gi136f09, gi199a01,gi199b11, gi204b08
Msi2h		D49654	AW022564, H88010	N
Q9D2I7			N	N
Pla2g1b		N	N	N
Sirt4		N	N	N
NM133915	Paxillin alpha	AA172749, W34244	AW023219	gi135e01
Gcn1l1		N	N	N
NM198163			BI494830, BI497452, H89152	gi06f02
Q8R1D2	2210403N09Rik		N	gi13f06
Rpl29		AA271049, X05021, AA073078, AA038751, AA182248, AA103915	N	gi169g01, gi164c07, gi75d07, gi121c02, gi189g07, gi219f12, gi12d07, gi255g10
Citron		U39904	BI492898, AW022177	N
Prkab1		AA098332, W71242, AA137821	N	gi105g11, gi130e06
NM177759			N	N
Q9D4T7	4930562A09Rik		N	N
Hspb8			N	N
NM026886	1500001A10Rik		N	N

5.3.3 Gene expression in the inner ear – RT-PCR data

Primers in adjacent exons of candidate genes were designed to amplify the intervening intron, giving different sized products when PCR was performed with genomic DNA and inner ear cDNA templates. Primers which gave the expected product sizes can be taken as an indication that the gene to which they are designed is represented as an mRNA transcript in the tissue obtained from P0 inner ears. Any which give a product of expected size with a genomic template but fail to produce a product from the inner ear cDNA library may indicate that the gene is not expressed in the ear at stage P0, making it less likely that they would be responsible for the *bv* phenotype.

For some genes, such as those with only one exon or large introns, it was not possible to design primers which would give differently sized products when amplified from genomic DNA and cDNA to provide confirmation that the cDNA product was genuine. However, none of the other cDNA amplifications gave products of the size expected from a genomic template, suggesting that the cDNA used was free of genomic DNA contamination. This should mean that any bands amplified from the cDNA are truly representative of an mRNA molecule extracted from inner ear tissue.

The agarose gel images resulting from this experiment are presented in Figures 5.2a-d and the sizes of the expected and observed products are given in the accompanying Tables 5.7a-d. The results for each gene are summarised in Table 5.8.

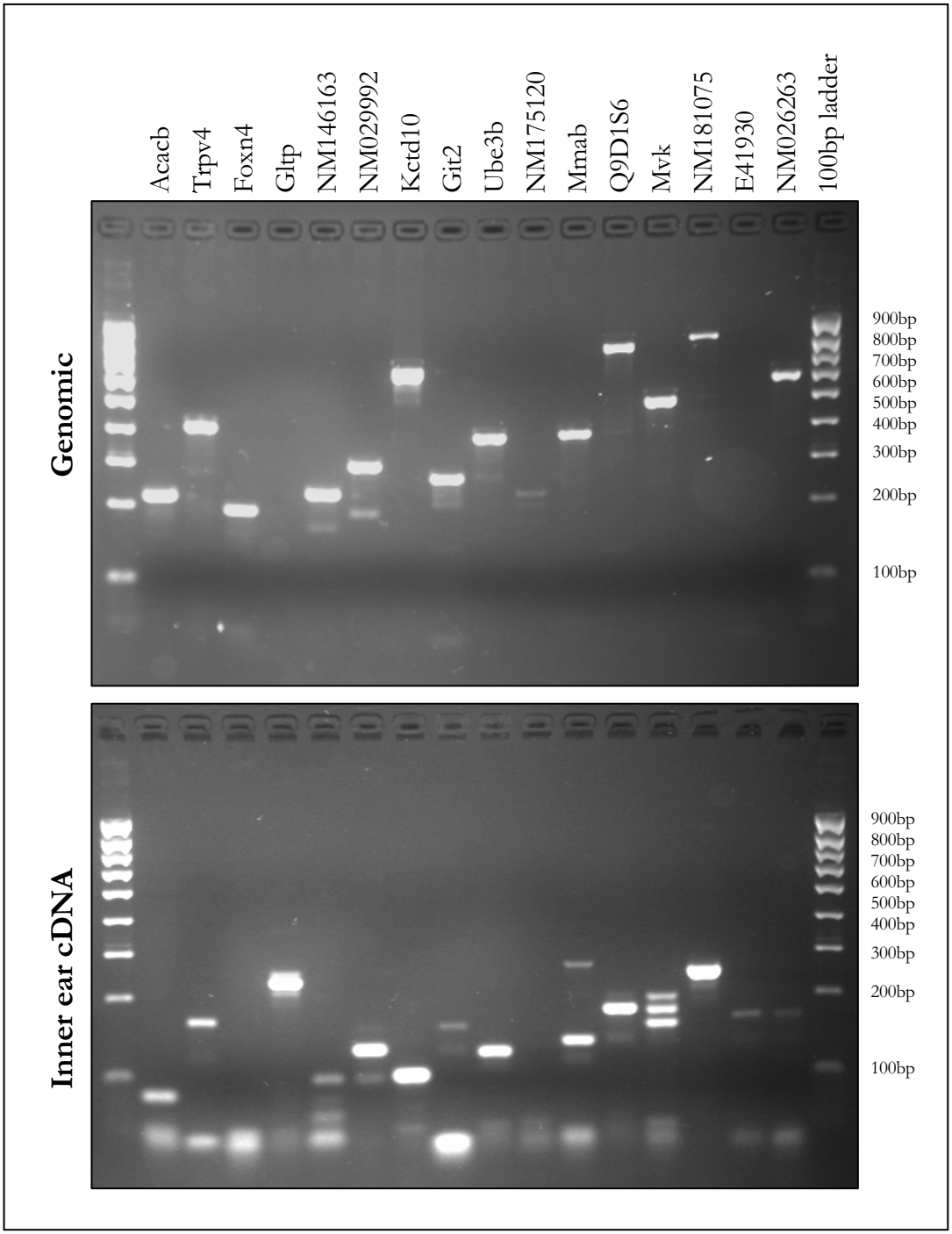

Figure 5.2a: Agarose gel electrophoresis showing the sizes of PCR products amplified from genomic DNA and inner ear cDNA templates using primers designed within adjacent exons of candidate genes. The differing sizes of genomic and cDNA products reflects the splicing out of introns in the cDNA material and serves as confirmation that a positive result represents a true transcript rather than genomic DNA contamination.

GENE	Expected genomic size (bp)	Observed genomic size (approx bp)	Expected cDNA size (bp)	Observed cDNA size (approx bp)
Acacb	226	220	82	80
Trpv4	400	400	171	170
Foxn4	204	190	115	Negative
Gltp	2301	Too large	241	240
NM146163	237	230	98	100
NM029992	193	290 (190)	24	130 (100)
Kctd10	649	650	103	100
Git2	276	270	167	170
Ube3b	377	380	129	130
NM175120	238	230	238	Negative
Mmab	385	380	143	140 (270)
Q9D1S6	802	800	191	180
Mvk	490	490	211	160 (200, 180)
NM181075	849	850	262	260
E41930	16545	Too large	179	180
NM026263	582	600	129	180

Table 5.7a: Comparison of expected and observed sizes of fragments obtained by PCR amplification using either genomic DNA or inner ear cDNA as template. The expected sizes are based on sequence data, while observed sizes are taken from the gel images shown in Figure 5.2a. Genomic fragments marked as "Too large" are beyond the scope of the PCR protocol used which will only amplify fragments up to approximately 1000bp. cDNA fragments marked as "Negative" gave no product on amplification. Observed sizes which differ significantly from expected sizes are highlighted in red.

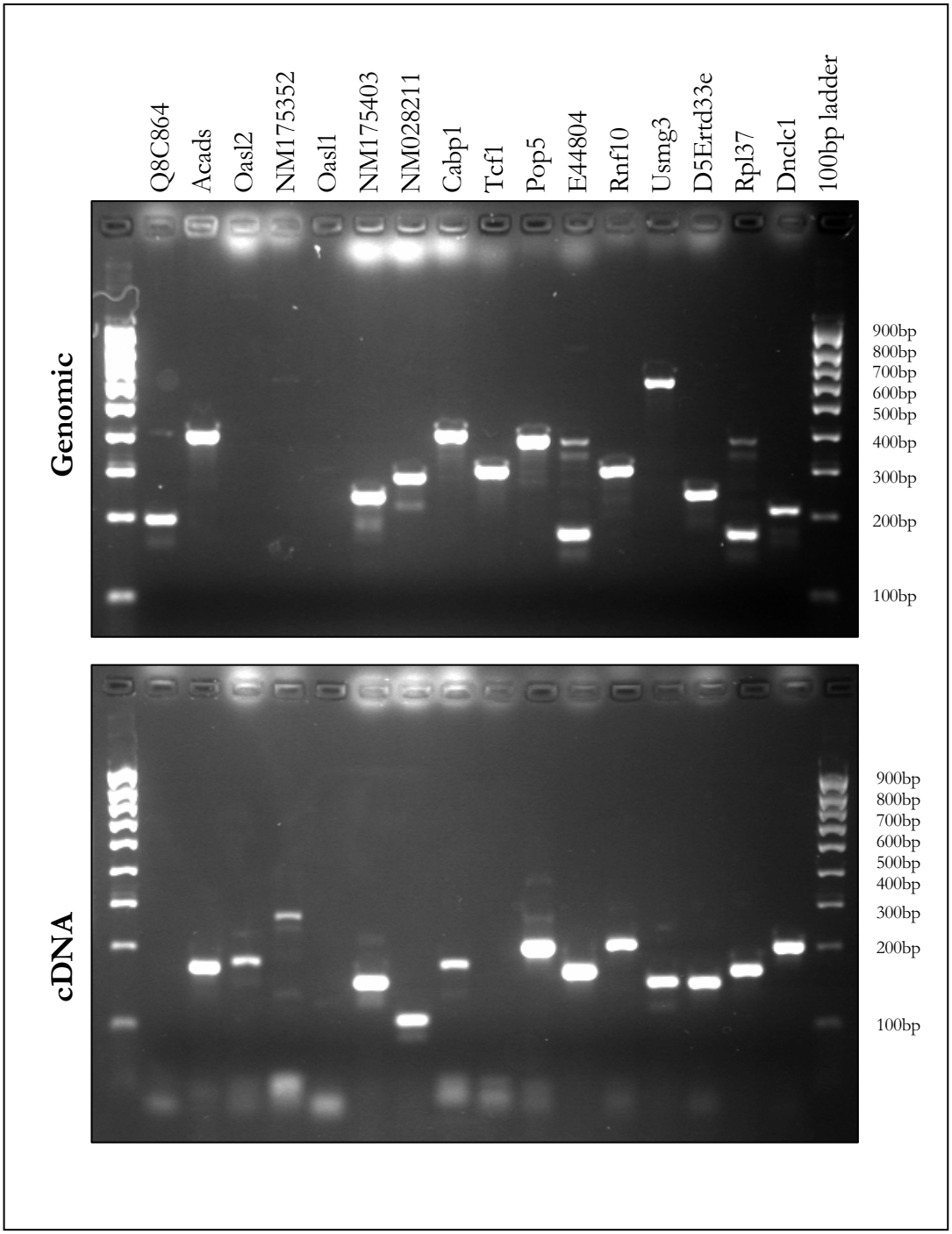

Figure 5.2b: Agarose gel electrophoresis showing the sizes of PCR products amplified from genomic DNA and inner ear cDNA templates using primers designed within adjacent exons of candidate genes. The differing sizes of genomic and cDNA products reflects the splicing out of introns in the cDNA material and serves as confirmation that a positive result represents a true transcript rather than genomic DNA contamination.

GENE	Expected genomic size (bp)	Observed genomic size (approx bp)	Expected cDNA size (bp)	Observed cDNA size (approx bp)
Q8C864	483	190	483	Negative
Acads	397	400	185	190
Oasl2	1403	Too large	194	200
NM175352	4184	Too large	283	300
Oasl1	1745	Too large	229	Negative
NM175403	245	230	164	160
NM028211	288	280	114	120
Cabp1	398	400	190	190
Tcf1	298	300	188	Negative
Pop5	385	380	224	220
E44804	181 (400)	180	181	180
Rnf10	300	300	226	230
Usmg3	590	600	164	170
D5Ertd33e	250	250	163	160
Rpl37	181 (400)	180	181	180
Dnclc1	1899	210	220	220

Table 5.7b: Comparison of expected and observed sizes of fragments obtained by PCR amplification using either genomic DNA or inner ear cDNA as template. The expected sizes are based on sequence data, while observed sizes are taken from the gel images shown in Figure 5.2b. Genomic fragments marked as "Too large" are beyond the scope of the PCR protocol used which will only amplify fragments up to approximately 1000bp. cDNA fragments marked as "Negative" gave no product on amplification. Observed sizes which differ significantly from expected sizes are highlighted in red.

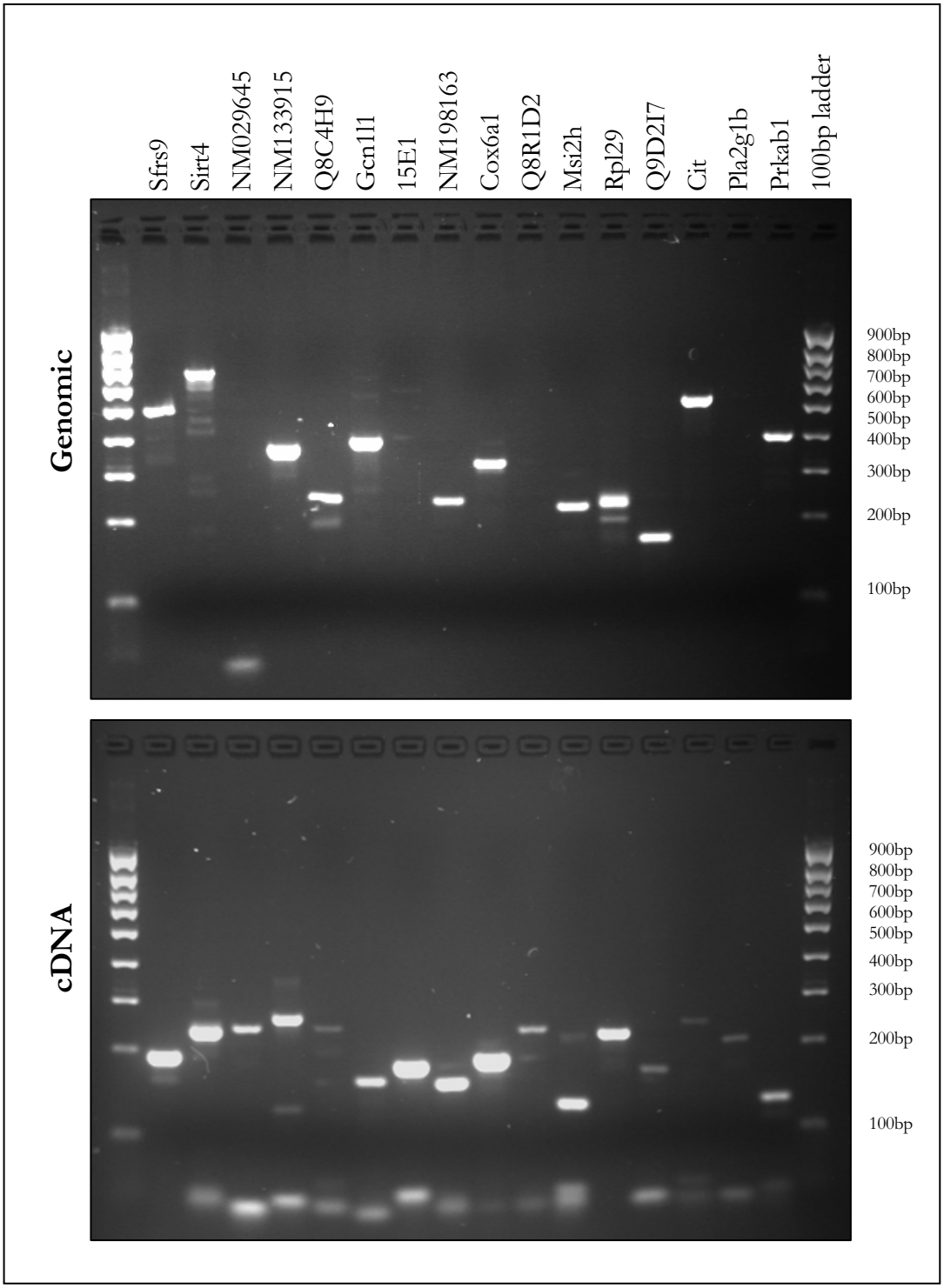

Figure 5.2c: Agarose gel electrophoresis showing the sizes of PCR products amplified from genomic DNA and inner ear cDNA templates using primers designed within adjacent exons of candidate genes. The differing sizes of genomic and cDNA products reflects the splicing out of introns in the cDNA material and serves as confirmation that a positive result represents a true transcript rather than genomic DNA contamination.

GENE	Expected genomic size (bp)	Observed genomic size (approx bp)	Expected cDNA size (bp)	Observed cDNA size (approx bp)
Sfrs9	489	500	203	190
Sirt4	663	700	245	240
NM029645	5521	Too large	250	250
NM133915	364	350	269	270
Q8C4H9	250	250	250	250
Gcn1l1	383	380	164	160
15E1	1444	Too large	187	180
NM198163	244	240	162	160
Cox6a1	324	330	193	190
Q8R1D2	1028	Too large	240	250
Msi2h	232	230	133	130
Rpl29	235	240	235	240
Q9D2I7	177	180	177	180
Cit	525	530	255	250
Pla2g1b	1283	Too large	232	230
Prkab1	391	400	136	140

Table 5.7c: Comparison of expected and observed sizes of fragments obtained by PCR amplification using either genomic DNA or inner ear cDNA as template. The expected sizes are based on sequence data, while observed sizes are taken from the gel images shown in Figure 5.2c. Genomic fragments marked as "Too large" are beyond the scope of the PCR protocol used which will only amplify fragments up to approximately 1000bp. cDNA fragments marked as "Negative" gave no product on amplification. Observed sizes which differ significantly from expected sizes are highlighted in red.

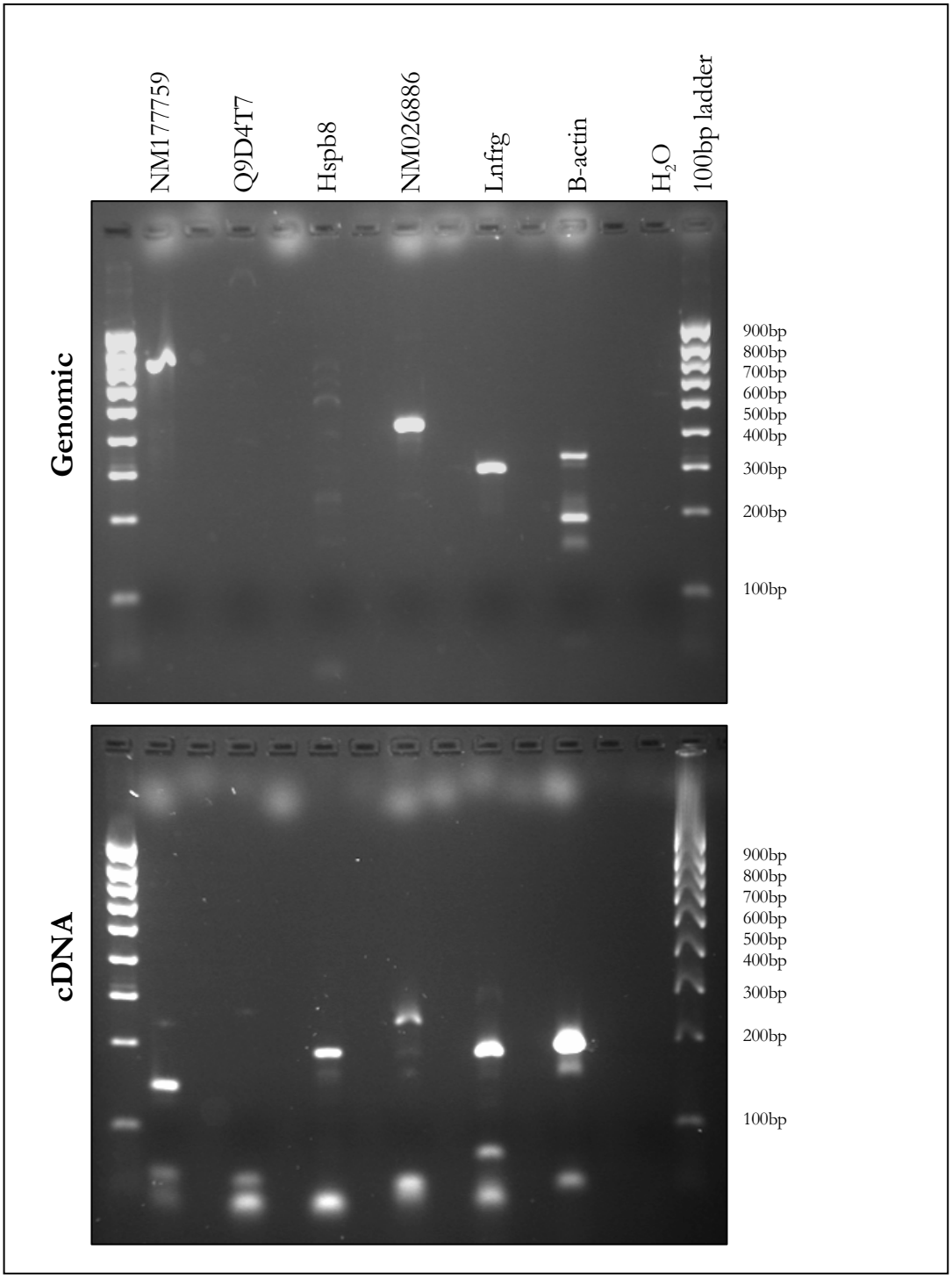

Figure 5.2d: Agarose gel electrophoresis showing the sizes of PCR products amplified from genomic DNA and inner ear cDNA templates using primers designed within adjacent exons of candidate genes. The differing sizes of genomic and cDNA products reflects the splicing out of introns in the cDNA material and serves as confirmation that a positive result represents a true transcript rather than genomic DNA contamination.

GENE	Expected genomic size (bp)	Observed genomic size (approx bp)	Expected cDNA size (bp)	Observed cDNA size (approx bp)
NM177759	728	750	149	150
Q9D4T7	1618	Too large	229	Negative
Hspb8	6113	Too large	197	190
NM026886	424	430	245	250
Lnfrg	298	310	195	190
B-actin	332	330 (180)	207	200

Table 5.7d: Comparison of expected and observed sizes of fragments obtained by PCR amplification using either genomic DNA or inner ear cDNA as template. The expected sizes are based on sequence data, while observed sizes are taken from the gel images shown in Figure 5.2d. Genomic fragments marked as "Too large" are beyond the scope of the PCR protocol used which will only amplify fragments up to approximately 1000bp. cDNA fragments marked as "Negative" gave no product on amplification. Observed sizes which differ significantly from expected sizes are highlighted in red.

GENE	Notes	Genomic result	cDNA result	Outcome
Acacb		✓	✓	**Positive**
Foxn4		✓	No band	**Negative**
NM146163		✓	✓	**Positive**
Kctd10		✓	✓	**Positive**
Ube3b		✓	✓	**Positive**
Mmab		✓	(✓)	**Positive**
Mvk		✓	(✓)	**Positive**
E41930	Large intron	No band	✓	**Positive**
Trpv4		✓	✓	**Positive**
Gltp	Large intron	No band	✓	**Positive**
NM029992		(✓)	✗	**Inconclusive**
Git2		✓	✓	**Positive**
NM175120	Only 1 exon	✓	No band	**Negative**
Q9D1S6		✓	✓	**Positive**
NM181075		✓	✓	**Positive**
NM026263		✓	✗	**Inconclusive**
Q8C864	Only 1 exon	✗	No band	**Inconclusive**
Oasl2	Large intron	No band	✓	**Positive**
Oasl1	Large intron	No band	No band	**Inconclusive**
NM028211		✓	✓	**Positive**
Tcf1		✓	No band	**Negative**
E44804	Only 1 exon	✓	✓	**Positive**
Usmg3		✓	✓	**Positive**
Rpl37	Only 1 exon	✓	✓	**Positive**
Acads		✓	✓	**Positive**
NM175352	Large intron	No band	✓	**Positive**
NM175403		✓	✓	**Positive**
Cabp1		✓	✓	**Positive**
Pop5		✓	✓	**Positive**
Rnf10		✓	✓	**Positive**

GENE	Notes	Genomic result	cDNA result	Outcome
D5Ertd33e		✓	✓	**Positive**
Dnclc1	Large intron	(✓)	✓	**Positive**
Sfrs9		✓	✓	**Positive**
NM029645	Large intron	No band	✓	**Positive**
Q8C4H9	Only 1 exon	✓	✓	**Positive**
15E1	Large intron	No band	✓	**Positive**
Cox6a1		✓	✓	**Positive**
Msi2h		✓	✓	**Positive**
Q9D2I7	Only 1 exon	✓	✓	**Positive**
Pla2g1b	Large intron	No band	✓	**Positive**
Sirt4		✓	✓	**Positive**
NM133915		✓	✓	**Positive**
Gcn1l1		✓	✓	**Positive**
NM198163		✓	✓	**Positive**
Q8R1D2	Large intron	No band	✓	**Positive**
Rpl29	Only 1 exon	✓	✓	**Positive**
Cit		✓	✓	**Positive**
Prkab1		No band	✓	**Positive**
NM177759		✓	✓	**Positive**
Q9D4T7	Large intron	No band	No band	**Inconclusive**
Hspb8	Large intron	No band	✓	**Positive**
NM026886		✓	✓	**Positive**
Lnfrg	Positive control	✓	✓	**Positive**
Actb	Positive control	(✓)	✓	**Positive**

Table 5.8: Summary of the data resulting from amplification of fragments of candidate genes from genomic DNA and inner ear cDNA templates. In the Genomic result and cDNA result columns a green tick (✓) indicates the obtained band was of the expected size, a bracketed tick indicates that bands of other sizes were also obtained and a red cross (✗) indicates that the band obtained was not of the expected size.
Where no band was obtained in the genomic sample, this is often explained by the large size of the intervening intron which prevented amplification by PCR.
Where no band was obtained in the cDNA sample but amplification in the genomic sample was successful, this is interpreted as a negative outcome and highlighted in **red**. Where a genomic band was also absent or where the cDNA product was not of the expected size, this is interpreted as an inconclusive outcome and highlighted in **blue**.

5.4 DISCUSSION

5.4.1 Analysis of inner ear expression data

5.4.1.1 Inner ear expression databases

The searching of four inner ear gene expression databases gave positive results in three, with none of the *bronx waltzer* candidate genes matching those described in the Washington University Inner Ear Protein Database (Thalmann and Thalmann). This is a relatively small database comprising 52 genes compiled by PAGE purification of fluids and tissues from the guinea pig inner ear, with identification of proteins carried out by amino acid sequencing, mass spectrometry and immunohistochemistry. This method is not especially sensitive and it might be expected that genes expressed at low levels could be missed, thus it is not remarkable that none of the 52 genes investigated here were found to be included.

The Inner Ear Gene Expression Database (Chen and Corey 2002) resulted from a microarray study where cochlear mRNA was extracted from mice at ages P2 and P32 and hybridised to Genechip oligonucleotide arrays. The effects of the *bronx waltzer* mutation can be observed from the beginning of hair cell development at E16.5 and hair cells can be seen to be degenerating until P1, after which point the observations are of disorganisation and missing hair cells. It is therefore possible, though not certain, that the gene responsible for the *bronx waltzer* phenotype may be down-regulated or even turned off by P2 and thus would not be present within this database. The microarrayed samples were associated with known genes and ESTs by sequence homology and it is these descriptions and gene IDs which are searchable in the database. However, since the data dates from 2001, many new transcripts have been reported and some gene IDs have altered, making effective querying of the database difficult. Therefore a negative result when screening this database may be less informative and the total number of genes found to be positive

might be expected to be lower than for the databases queried on the basis of sequence homology.

The Mouse organ of Corti EST database (Pompeia *et al.* 2004) and the Morton Human Fetal Cochlea EST database (Robertson *et al.* 1994) both take the form of cDNA library sequences which have been matched to published gene sequences using BLAST (Basic Local Alignment Search Tool). These matches can be searched by gene description, but it is also possible to directly screen the EST sequences by BLAST. This second approach greatly augments the sensitivity of the screen, since it allows the inclusion of novel genes which cannot be identified by description and bypasses the problem of fluidity in gene IDs. The limitations incurred are those found when using any sequence homology approach, namely that conserved regions and gene families may lead to false matches. This is particularly problematic when BLASTing against ESTs because the sequences are by nature relatively short and thus the differences between similar sequences which may emerge in longer sequence reads are not apparent. When searching the Mouse organ of Corti EST database this problem could be avoided by using a high cut-off value since the query sequence and database sequences originate from the same organism and might be expected to show a high level of homology in the case of a true match. When querying the Human Fetal Cochlea EST database, divergence between the two organisms necessitates the use of lower cut-off in order to detect orthologues. This carries the risk of identifying a different member of the same gene family, although one could argue that the expression of a close family member within the inner ear should contribute towards the potential candidacy of a gene. One solution to this problem would be to query the EST database not with the mouse protein sequences but instead with their human orthologues. However, very few orthologues have been directly confirmed by means other than sequence similarity, thus introducing the same uncertainty as regards conservation of function. In addition, this approach would not allow the inclusion of novel genes since few of these possess verified

orthologues. Once again, in the case of these EST libraries the age of the analysed tissue must be taken into account. The Mouse Organ of Corti ESTs were derived from tissue of mice between P5 and P13, once again introducing the possibility that the *bv* gene may have been turned off or down-regulated in the samples studied if it required only for the maintenance of hair cells. The tissue used in the preparation of the Human Fetal Cochlea Library was obtained from foetuses between the ages of 16 and 22 weeks. Although the maturation of the hearing process has not been widely studied in humans, it is thought that cochlear anatomy is grossly mature by 22-26 foetal weeks but that hair cells may continue to mature beyond this stage (Larsen 1997). Thus the mRNA molecules represented in this library are likely to represent those present in the developing ear at the appropriate stage.

Given the advantages and drawbacks of the different databases as outlined above, it was considered when evaluating these data that greater significance should be given to those genes which are represented in more than one of the databases screened.

5.4.1.2 RT-PCR data

Of the 52 candidate genes tested for expression in P0 inner ear tissue by PCR amplification, 42 gave a positive result where bands of the expected size were observed in both the genomic and cDNA amplifications. Two – *Mmab* and *Mvk* – were probably positive, with additional bands other than that of the expected size being observed. This may be a reflection of other gene family members, repeat regions or alternative transcripts. However, since the question being addressed here is the presence or absence of a specific band, its presence even in the company of other bands can be interpreted as a positive result. Five genes gave an inconclusive result, with two of these – *Oasl1* and Q9D4T7 – being primers which gave no product with either genomic or cDNA templates where the genomic product was too large for amplification. It is thus possible that these represent a negative result, but may

also be the result of primer failure. The remaining three inconclusive results were those where the bands obtained in either the genomic or cDNA assay were not of the expected size. This may represent non-specific amplification, but since each of these genes – NM029992, NM026263 and Q8C864 – are novel predictions, it is also possible that their coding regions have not been correctly annotated and that the observed sizes are representative of the actual gene product. Only three genes were found to be negative, giving a genomic product of the expected size but no product when amplified from the cDNA sample. These genes – *Foxn4*, NM175120 and *Tcf1* - represent the most interesting data from this study. Given that the great majority of genes tested were found to be present in the cDNA sample, the apparent absence of these genes can be interpreted as significant evidence that they are not expressed in the P0 inner ear.

The 42 genes which were found to be positive in the course of this simple expression screen compare to the total of 26 genes which were identified as being positive in at least one of the published gene expression databases (see Table 5.5). This discrepancy is most likely to be a reflection of the comparative impurity of the starting material. Although care was taken when dissecting out the inner ears for RNA extraction to remove as much extraneous tissue as possible, it is likely that a small amount of brain and muscle tissue was processed with it. This would result in mRNA populations from these tissues being represented at low levels in the cDNA sample which was later screened with gene-specific primers, thus increasing the likelihood of a positive result. Since the amplification from cDNA was not quantitative, it is not possible to infer whether a positive band suggests that a gene is either strongly or weakly represented in the sample. In any case, this would not be informative since a gene required only in a very specific cell type would appear to exhibit low level expression but could still play an important role in ear development, while a ubiquitously expressed muscle gene might show a

high level expression despite the relatively low number of muscle cells in the total tissue.

In order to rectify the issue of contamination with other tissue, more of the inner ear could be dissected away before processing. Since it is expected the *bv* gene should be detectable in inner hair cells during development, it might seem sensible to generate cDNA purely from the organ of Corti. However, this procedure is not a simple one. The mouse organ of Corti is extremely small at P0, making it very difficult to dissect and also necessitating the collection of tissue from a large number of mice in order to obtain sufficient RNA to carry out the study. By way of an example, in the construction of the mouse organ of Corti library, Pompeia *et al.* (2004) finely microdissected OCs from mice aged P5 to P13 and even with the larger size of the ear at this age, four hundred ears were required to obtain sufficient tissue. Another solution would be to carefully dissect the organ of Corti from a small number of ears and use an RNA amplification technique such as T7-based linear amplification (Van Gelder *et al.* 1990; Baugh *et al.* 2001) in order to generate sufficient material. This was the approach used by (Morris *et al.* 2005) in their study of genes differentially expressed in the lateral wall, organ of Corti and spiral ganglion. If sufficient time and expertise were available, this method would have been employed and the PCR screen repeated using the same sets of primers with the new material as template.

5.4.2 Assessment of candidacy based on the evidence gathered

The various sources of information described in this chapter are intended to allow the prioritisation of candidate genes for further investigation. To this end, the data available for each gene are summarised in Table 5.11 in order to simplify the process of comparison. In addition, a scoring system has been developed to allow a relatively objective method of selecting those genes with the most evidence in their favour for inclusion in further studies. The criteria for scoring are described in Table 5.9. The allocation of points was weighted, with stronger evidence contributing +1 or -1 point depending on whether it strengthened or weakened the case for the gene in question, while less strong evidence contributed +0.5 or -0.5 points. For example, when assessing the published literature available for a given gene, information concerning a mouse model was weighted more strongly than that arising from a human disorder or other model organism since disruption of the gene in the mouse might be expected to give a phenotype more closely resembling that of *bronx waltzer*. In the case of the inner ear cDNA screen, negative results were rare and positive ones may have been the result of contamination with other tissue as discussed in Section 5.4.1.2. Therefore negative results were considered to have more significance and were weighted +1, while a positive result contributed +0.5 points.

Data source	Criteria	Points
Published literature	Expression described in the ear or retina	+1
	Involvement in pathways known to be important in hearing	+1
	Gene function extensively studied and no evidence reported of involvement in hearing	-1
	Knockout mouse model lacking a hearing or vestibular phenotype	-1
	Human condition or other model organism not showing a hearing or vestibular abnormality	-0.5
Inner ear gene expression databases	Represented in no queried database	0
	Represented in one queried database	+0.5
	Represented in more than one queried database	+1
Inner ear cDNA PCR screen	Inconclusive result	0
	Positive result	+0.5
	Negative result	-1

Table 5.9: System used for the allocation of points to candidate genes from the *bronx waltzer* region in order to quantify the evidence for and against their being responsible for the phenotype.

These scores were then used to establish a candidacy rating ranging from "Very low" to "Very high" using the cut-off values shown in Table 5.10. The points awarded to each candidate gene along with their total scores and assigned level of candidacy are given in Table 5.11.

Total points	Candidacy rating
≥ 2.5	Very high
1.5 – 2	High
1	Medium
0 – 0.5	Low
≤ -0.5	Very low

Table 5.10: Cut-off values used in the assignment of candidacy ratings to genes from the *bronx waltzer* region

Table 5.11: Summary of functional and expression data available for genes situated within the *bronx waltzer* candidate region. Genes assigned a candidacy rating of either "Very high" or "High" are highlighted in red. For a full explanation of the weighted scoring system employed see Section 5.4.2

Gene	Description	Summary of relevant published data	Representation in inner ear expression databases	Inner ear cDNA PCR screen	Total points	Candidacy rating
Acacb	Acetyl-coenzyme A carboxylase beta	Involved in control of fatty acid oxidation in muscle tissue (-1) Knockout mice do not have a hearing or vestibular phenotype (-1)	-	Positive (+0.5)	-1.5	Very low
Foxn4	Forkhead box protein N4	Expressed in the retina and brain (+1) Transcription factor involved in activation of Math3 (+1) Knockout mice do not have a hearing or vestibular phenotype (-1)	-	Negative (-1)	0	Low
NM146163 (*Myosin 1h*)	Myosin 1h	Expressed in utricles (+1) Many other non-conventional myosins have roles in the inner ear (+1)	-	Positive (+0.5)	2.5	Very high
Kctd10	potassium channel tetramerization domain-containing 10	Voltage-gated potassium channel activity (+1)	-	Positive (+0.5)	1.5	High
Ube3b	ubiquitin protein ligase E3B	Highly expressed in chick basilar papillar following noise exposure (+1) Targets proteins for degradation.	Chen & Corey (+1) Morton	Positive (+0.5)	2.5	Very high
Mmab	Methylmalonic aciduria type B homolog	Involved in amino acid metabolism (-1) Human disorder results in high level of acid in the blood (-0.5)	-	Probably positive (+0.5)	-1	Very low
Mvk	Melavonate kinase	Involved in cholesterol metabolism (-1) Human disorder results in accumulation of mevalonic acid (-0.5)	Chen & Corey (+1) Pompeia	Probably positive (+0.5)	0	Low
E41930	Ensembl predicted gene	n/a	-	Positive (+0.5)	0.5	Low
Trpv4	transient receptor potential cation channel V4	Expressed in many tissues, including inner ear hair cells (+1) Osmotically activated cation-selective channel (+1) Knockout mice do not have a hearing or vestibular phenotype (-1)	Pompeia (+0.5)	Positive (+0.5)	2	High

Gene	Description	Summary of relevant published data	Representation in inner ear expression databases	Inner ear cDNA PCR screen	Total points	Candidacy rating
Gltp	Glycolipid transfer protein	Widespread expression. Selectively accelerates intermembrane transfer of glycolipids (-1)	Chen & Corey (+1) Morton Pompeia	Positive (+0.5)	0.5	Low
NM029992	Novel gene	n/a	Pompeia (+0.5)	Inconclusive (0)	0.5	Low
Git2	G protein-coupled receptor kinase-interactor 2	Involved in regulation of golgi organisation, actin cytoskeletal organisation and paxillin localisation (+1)	-	Positive (+0.5)	1.5	High
NM175120	Novel gene	n/a	-	Negative (-1)	-1	Very low
Q9D1S6	Novel gene	Predicted protein domains include Leukotriene B4 type 2 receptor, Ubiquitin interacting motif, Ankyrin	Morton (+1) Pompeia	Positive (+0.5)	1.5	High
NM181075	Novel gene	n/a	Pompeia (+0.5)	Positive (+0.5)	1	Medium
NM026263	Novel gene	n/a	-	Inconclusive (0)	0	Low
Q8C864	Novel gene	n/a	-	Inconclusive (0)	0	Low
Oasl2	2'-5'-oligoadenylate synthetase like protein 2	Important in anti-viral activity of interferons (-1) Human orthologue found to interact with thyroid hormone receptors	-	Positive (+0.5)	-0.5	Very low
Oasl1	2'-5' oligoadenylate synthetase-like 1	Inactive in 2'-5' oligoadenylate synthesis, but function not yet described Human orthologue found to interact with thyroid hormone receptors	-	Negative (-1)	-1	Very low
NM028211	Novel gene	n/a	Pompeia (+0.5)	Positive (+0.5)	1	Medium
Tcf1	Hepatocyte nuclear factor 1-alpha	Transcription factor, found abundantly in liver Knockout mice do not have a hearing or vestibular phenotype (-1)	-	Negative (-1)	-2	Very low
E44804	Ensembl predicted gene	n/a	Pompeia (+0.5)	Positive (+0.5)	1	Medium

Gene	Description	Summary of relevant published data	Representation in inner ear expression databases	Inner ear cDNA PCR screen	Total points	Candidacy rating
Usmg3	Upregulated during skeletal muscle growth 3	Membrane protein with peptidase activity	Pompeia (+0.5)	Positive (+0.5)	1	Medium
Rpl37	60S ribosomal protein L37	Structural constituent of ribosome (-1)	Chen & Corey (+1) Pompeia	Positive (+0.5)	0.5	Medium
Acads	Acyl-CoA dehydrogenase, short-chain specific	Involved in fatty acid beta-oxidation (-1) Knockout mice do not have a hearing or vestibular phenotype (-1)	Pompeia (+0.5)	Positive (+0.5)	-1	Very low
NM175352	Novel gene	n/a	-	Positive (+0.5)	0.5	Low
NM175403	Novel gene	n/a	Morton (+1) Pompeia	Positive (+0.5)	1.5	High
Cabp1	Calcium-binding protein	Expressed in brain and retina (+1) May be involved in neuronal signal transduction	Chen & Corey (+1) Morton	Positive (+0.5)	2.5	Very high
Pop5	Processing of precursor 5, ribonuclease P	Subunit of ribonucleaseP, required for 5'-end maturation of tRNAs (-1)	-	Positive (+0.5)	-0.5	Very low
Rnf10	Ring finger protein 10	Ring finger motif, implies protein-protein interactions. Ubiquitin-protein ligase activity	Pompeia (+0.5)	Positive (+0.5)	1	Medium
D5Ertd33e	Novel gene	n/a	Pompeia (+0.5)	Positive (+0.5)	1	Medium
Dnclc1	Dynein light chain 1, cytoplasmic	Inhibits the activity of neuronal NO synthase, implying regulatory role in numerous biologic processes Drosophila mutants have pleiotropic morphogenetic defects.	Chen & Corey (+1) Morton Pompeia	Positive (+0.5)	1.5	High
Sfrs9	Splicing factor, arginine/serine rich 9	Involved in mRNA formation (-1)	Morton (+1) Pompeia	Positive (+0.5)	0.5	Low

Gene	Description	Summary of relevant published data	Representation in inner ear expression databases	Inner ear cDNA PCR screen	Total points	Candidacy rating
NM029645	Novel gene	n/a	-	Positive (+0.5)	0.5	Low
Q8C4H9	Novel gene	n/a	-	Positive (+0.5)	0.5	Low
15E1	Novel gene	n/a	-	Positive (+0.5)	0.5	Low
Cox6a1	Cytochrome c oxidase polypeptide VIa-liver	Subunit of COX, terminal enzyme of the respiratory chain. Probable housekeeping gene (-1)	Chen & Corey (+1) Morton Pompeia	Positive (+0.5)	0.5	Low
Msi2h	Musashi homolog 1	neural RNA-binding protein (-1)	Chen & Corey (+1) Morton	Positive (+0.5)	0.5	Low
Q9D2I7	Novel gene	n/a	-	Positive (+0.5)	0.5	Low
Pla2g1b	Phospholipase A2 precursor	Involved in protection of membranes from oxidative injury	-	Positive (+0.5)	0.5	Low
Sirt4	NAD-dependent deacetylase sirtuin 4	Role in epigenetic gene silencing	-	Positive (+0.5)	0.5	Low
NM133915 (*Paxillin*)	Paxillin alpha	Required at focal adhesions for actin organisation (+1) Knockout mice do not have a vestibular or hearing phenotype (-1)	Chen & Corey (+1) Morton Pompeia	Positive (+0.5)	1.5	High
Gcn1l1	General control of amino-acid synthesis 1-like 1	Required for activation of protein kinase GCN2, leading to upregulation of aa synthesis during starvation (-1)	-	Positive (+0.5)	-0.5	Very low
NM198163	Novel gene	n/a	Morton (+1) Pompeia	Positive (+0.5)	1.5	High

Gene	Description	Summary of relevant published data	Representation in inner ear expression databases	Inner ear cDNA PCR screen	Total points	Candidacy rating
Q8R1D2	Novel gene	n/a	Pompeia (+0.5)	Positive (+0.5)	1	Medium
Rpl29	60S ribosomal protein L29	Ribosomal subunit (-1)	Chen & Corey (+1) Pompeia	Positive (+0.5)	0.5	Low
Cit	Citron protein (Rho-interacting, serine/threonine kinase)	Involved in Rho/Rac signalling (+1) Knockout mice do not have a hearing or vestibular phenotype (-1)	Chen & Corey (+1) Morton	Positive (+0.5)	1.5	High
Prkab1	5'-AMP-activated protein kinase, beta-1 subunit	Plays a role in hormonal and nutrient-derived anorexigenic and orexigenic signals and in energy balance (-1)	Chen & Corey (+1) Pompeia	Positive (+0.5)	0.5	Low
NM177759	Novel gene	n/a	-	Positive (+0.5)	0.5	Low
Q9D4T7	Novel gene	n/a	-	Inconclusive (0)	0	Low
Hspb8	Heat-shock protein beta-8	Neuromuscular function (-1)	-	Positive (+0.5)	-0.5	Very low
NM026886	Novel gene	n/a	-	Positive (+0.5)	0.5	Low

5.4.3 Selection of candidate genes for further analysis

Of the 54 genes examined, twelve scored greater than 1.5 points using the weighted scale and obtained a candidacy rating of either "High" or "Very high". Of these twelve, three were the novel genes Q9D1S6, NM175403 and NM198163 which each scored 1.5 points. Their points were accrued via expression data which was not dissimilar from that of many of the known genes, with the difference being that the lack of specific literature meant that no negative points were assigned to them. Therefore these genes were not initially prioritised but may be investigated at a later date. The remaining nine genes in the "High" or "Very high" candidacy categories were *Myo1h, Kctd10, Ube3b, Trpv4, Git2, Cabp1, Dnclc1, Paxillin* and *Citron*. These genes were all selected for further analysis. One other gene, *Foxn4*, was included in later studies. At the time the assessment was carried out this gene appeared to represent an interesting candidate but in September 2004, data regarding the phenotype of a knockout mouse (Li *et al.*, 2004) was published and personal communication confirmed that the mouse did not exhibit any hearing or vestibular phenotype.

Taken together, these ten genes represent a manageable subset of genes from within the *bronx waltzer* candidate region for which further investigation is justified on the merit of the evidence considered. All ten of them have been previously described to some degree, with none of the novel genes having been selected. It is very possible that the *bronx waltzer* gene could be as yet undescribed, however it is very difficult to select which of the 23 uncharacterised genes to investigate when there is so little information to go on. It would be beneficial in this case to carry out more detailed expression studies using sections or whole mount in situ hybridisations to determine whether they are expressed in the expected tissues of the inner ear. This work

was beyond the scope of the current project, but should be considered in further pursuance of the *bv* gene.

Chapter 6:

Gene knockdown in zebrafish as an assessment of candidate gene function

CHAPTER 6

GENE KNOCKDOWN IN ZEBRAFISH AS AN ASSESSMENT OF CANDIDATE GENE FUNCTION

6.1 INTRODUCTION

One means of assessing the role of a gene is to somehow prevent it from performing its normal function and observe the outcome. In the mouse this can be a slow and expensive process since knockouts require several generations before a phenotype can be assessed. The zebrafish (*Danio rerio*) offers several advantages in this respect. The fish have a much shorter life cycle and produce large numbers of offspring (about 200 eggs per lay), making them amenable to large-scale screening. Zebrafish eggs are fertilised externally and the embryos are transparent, allowing for continuous study of embryonic stages, impossible in the mouse where development takes place *in utero*. In addition to these practical advantages, the techniques available for causing specific gene knockdown or knockouts in zebrafish are much simpler and faster than those which have been demonstrated as effective in the mouse. Use of antisense technology allows for the screening of a phenotype in the treated individuals without the need for further breeding and the relatively large zebrafish oocytes are well suited for the injection of antisense agents.

Hence the zebrafish represents a rapid and cost efficient model for the assessment of function in a relatively large number of genes, though the success and validity of such an approach is dependent on two factors. The first of these is the capacity to identify homologous genes within the zebrafish genome which show enough similarity to the mouse genes under scrutiny to allow their functions to be assumed to be similar. This question is complicated by the duplication event which the teleost genome underwent

following its divergence from the mammalian lineage (Postlethwait *et al.* 1998; Postlethwait *et al.* 1999). This means that the zebrafish often carries two or more paralogous copies of a particular gene, each of which is homologous to a mammalian counterpart. It is thought that the duplicated genes have been maintained as a result of a division of function between the two copies, with each taking on a more specialised role (Force *et al.* 1999). Despite this, paralogous pairs of genes often retain some shared functions, meaning that zebrafish phenotypes resulting from a single gene defect may be appear to be less severe than in the mammalian ortholog. The implication of this when selecting genes to target in the zebrafish is that when more than one presents as being a possible ortholog, both should be considered suitable candidates and the effects of knocking down both observed. It may also be prudent to knock down both concurrently in order to assess the phenotype in the absence of either function.

The second factor is the ability to recognise a phenotype analogous to the hearing loss and vestibular dysfunction shown by *bronx waltzer* mouse mutants in the fish, a premise which assumes a conservation of function in the ear of the two organisms and demands that fish with a hearing or vestibular defect are discernable from unaffected littermates. These considerations are discussed in the following paragraphs.

6.1.1 The zebrafish ear

Zebrafish possess an inner ear which is roughly analogous to the vestibular systems of other vertebrates. While it does not include a specialised structure for acoustic sound detection, the otic placode contains maculae for the detection of gravity and semicircular canals for detecting dynamic rotation. In addition, zebrafish are members of the Otophysi, a group of ostariophysan fish that possess Weberian ossicles, four small bones which link the swim bladder to the inner ear (Bang *et al.* 2001). These enhance the fish's ability to hear by transferring vibrations to the ear in a similar manner to the ossicles in

mice and humans. Indeed, the otophysans are sometimes known as "hearing specialists" and may be sensitive to a frequency range between 100 and 5000Hz (Fay and Simmons 1999). The sensory patches of the zebrafish ear are remarkably similar to those of humans and mice, with cristae located within each semicircular canal and maculae beneath each of the otoliths (see Figure 6.1d). Each of these sensory patches possesses highly organised stereociliary bundles which detect movement in their surroundings and produce an electrical transduction in response. This conservation of function, alongside the other advantages offered by the zebrafish as a model organism, make it a very attractive system for the study of hearing dysfunction.

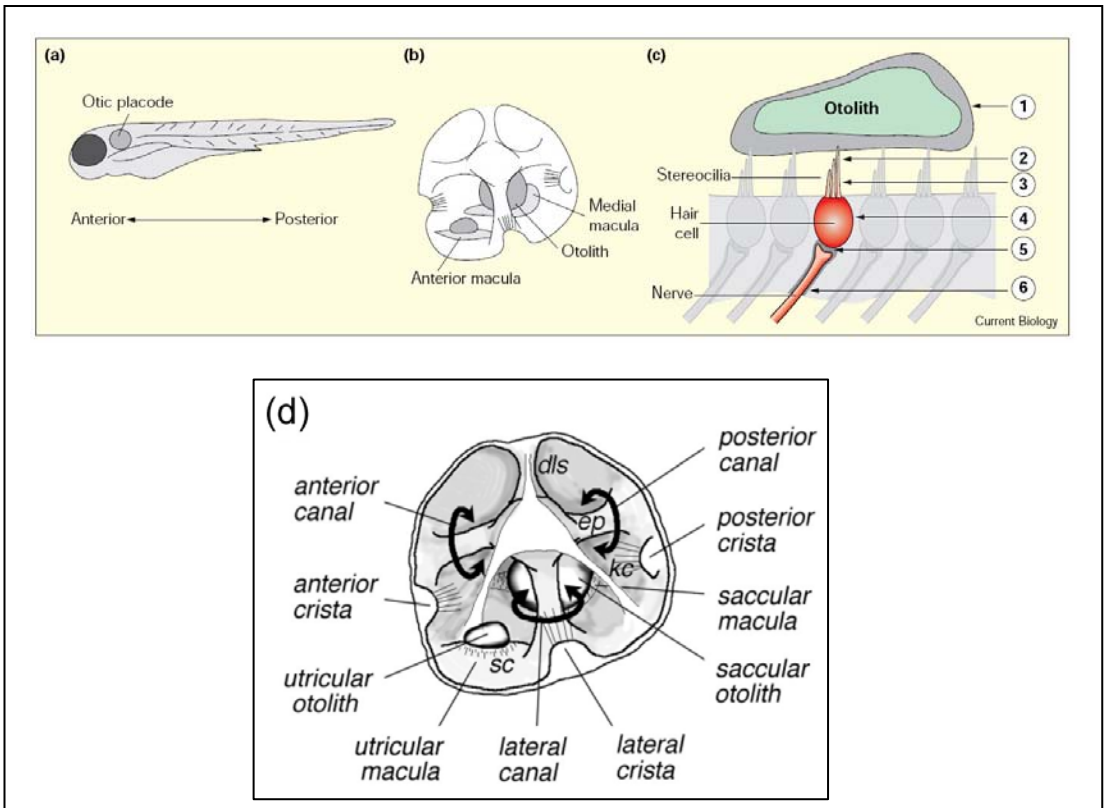

Figure 6.1:
(a) The zebrafish ear. At five days, the embryo is about 3 mm long, with an evident otic placode.
(b) The otic placode, behind the eye, measures about 150 mm across at this stage; it contains hair cell epithelia as maculae and in the semicircular canals.
(c) Sensing by hair cells requires integrity at multiple sites: 1, otoliths; 2, transducer complex in stereocilia; 3, stereocilia; 4, hair cell development; 5, synapse; and 6, auditory pathway (Ashmore 1998)
(d) Detailed representation of the zebrafish ear at 4 days post fertilisation: ep, epithelial pillars; dls, dorsolateral septum; sc, stereociliary bundles; kc, kinocilia of cristae hair cells. (Whitfield *et al.* 2002)

6.1.2 Hearing and vestibular phenotypes in zebrafish

In order to successfully use the zebrafish as a model in the search for the *bronx waltzer* gene, it must be possible to measure hearing and vestibular function in the fish to determine whether the knocked down gene has caused a phenotype similar to that observed in the mouse. The two measures used to assess the phenotype in mice are the Preyer reflex test for auditory function and the observation of circling and head-bobbing behaviour as an indication of vestibular abnormality (see Section 3.1.1.4) and equivalent assessments of both features are possible when working with the zebrafish. In response to a sharp sound such as the tapping of a metal implement on the side of the dish, wild type zebrafish perform a startle response similar to the Preyer reflex which takes the form of a rapid tail flick. This can normally be observed as a brisk darting movement and its absence is immediately apparent, an illustration of this response is shown in Figure 6.2. Behavioural observations of zebrafish with vestibular dysfunction demonstrate striking similarities to those made with deafness and balance mouse mutants. The fish are seen to rest on their sides or upside-down and may swim in circles or loops. Some of these mutants may be unviable beyond approximately 5 days post fertilisation (dpf) since their lack of spatial orientation inhibits them from inflating their swim bladder and engaging in normal feeding behaviour.

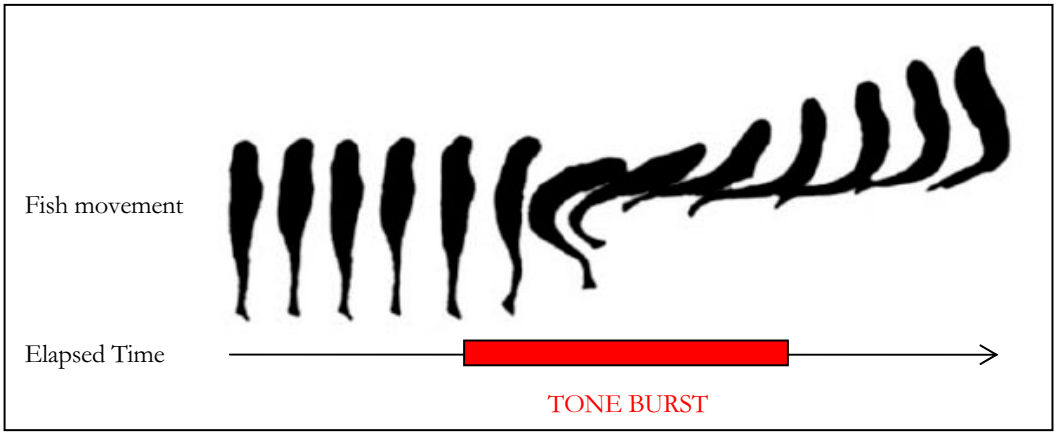

Figure 6.2: An illustration of the startle response in zebrafish adapted from (Bang *et al.* 2002) The drawings show the movement made by a fish when exposed to a short tone burst, with images from left to right showing the position as time elapses. The fish responds to the noise by a sharp flick of the tail which results in a rapid forwards darting movement.

6.1.3 Conservation of function in the mouse and the zebrafish

As described in Section 6.1.1, the zebrafish ear can be considered to be roughly analogous to the vestibular system in the mouse. Since the *bronx walter* mutation affects both the auditory and vestibular systems, it might be expected that a defect in the zebrafish orthologue would give a comparable phenotype, although this expectation is based on the assumption that the functioning of the ear is somewhat conserved between the two species. In considering the validity of such a supposition it is pertinent to examine the group of zebrafish mutants identified in a recent screen which exhibited defective balance yet appeared to possess structurally normal inner ears. It was thus thought that their phenotype may be a result of a disruption to the mechanotransduction apparatus in the ear (Granato *et al.* 1996). Analysis of these circler mutants (Nicolson *et al.* 1998) demonstrated that they fell into 8 discrete linkage groups and showed that the phenotype included hair cell degeneration or bundle defects in three of the mutants, *skylab*, *sputnik* and *mariner*. These mutants are of particular interest here since the *bronx walter* mutation causes degeneration of hair cells in both the cochlea and the

vestibular system and we wish to determine whether the development and functioning of this system is conserved between the mouse and the zebrafish. The cloning of the *mariner* gene by a candidate gene approach (Ernest *et al.* 2000) demonstrated that the five alleles of the mutation, which cause affected fish to circle, all possessed mutations in *Myo7a*. This gene is also responsible for the *shaker1* mutation in mice (Gibson *et al.* 1995) and for Usher syndrome type 1B as well as autosomal dominant and recessive forms of non-syndromic hearing loss in humans (Weil *et al.* 1995; Liu *et al.* 1997; Liu *et al.* 1997; Weil *et al.* 1997). The phenotype of *shaker1* mice includes circling and deafness as a result of stereocilia disorganisation and bundling defects of the hair cells, indicating that the *Myo7a* gene may play a similar role in both organisms. More recently, the defects in *sputnik* fish which show splayed stereocilia and reduced acoustic sensitivity (Nicolson *et al.* 1998) have been demonstrated to be the result of mutations in *cadherin 23* (Söllner *et al.* 2004). Mutations in *cadherin 23* are also responsible for the phenotype of *waltzer* mice (Di Palma *et al.* 2001; Wilson *et al.* 2001) and for Usher syndrome type 1D in humans (Bolz *et al.* 2001; Bork *et al.* 2001). *Waltzer* mice are deaf, exhibit circling behaviour and manifest disorganised stereocilia, suggesting that the function of *cadherin 23* in the inner ear may also be conserved in mice and zebrafish. Whilst the causative agent for the third circler mutant with normal gross ear morphology, *skylab,* has yet to be identified, a number of other genes and pathways have been demonstrated to be important in the development of sensory epithelia in both model organisms. These include members of the Delta-Notch signalling pathway such as *deltaA* (Riley *et al.* 1999) and mind bomb (Itoh *et al.* 2003) in the zebrafish, and *Jagged1* (Kiernan *et al.* 2001; Tsai *et al.* 2001) and *Delta1* (Morrison *et al.* 1999) in the mouse. This pathway is known to be crucial in determining the fate of cells in sensory epithelia, with alterations in the expression of the different ligands being strongly associated with the development and patterning of hair cells and supporting cells, and evidence to support this model is strong in both the mouse (Zine *et al.* 2001) and the zebrafish (Haddon *et al.* 1998). Although many genes involved in

inner ear development are yet to be identified and whilst some have only been characterised in one organism or the other, with such an extensive degree of overlap between those so far described it is possible to imagine that there exists a significant level of conservation of function between the mouse and zebrafish ears, and between the genes encoding them.

6.1.4 Disrupting gene function in zebrafish

Since the publication of much of the sequence of the human genome (Lander *et al.* 2001), as well as the progress made with the sequencing of the genomes of model organisms such as mouse (Waterston *et al.* 2002) and the as yet unfinished zebrafish, much research has focussed on the elucidation of the roles played by genes for which the sequence but not the function is now known. To accomplish this, a variety of forward and reverse genetic approaches have been developed to disrupt individual genes and allow the effects to be observed within a model system.

Both forward and reverse genetic approaches have been successfully demonstrated in the zebrafish. Forward genetic approaches have included large scale mutagenesis screens using ENU (Haffter *et al.* 1996) or insertional mutagenesis (Amsterdam *et al.* 1999) followed by selection for phenotypes of interest and identification of the causative mutation. Meanwhile reverse genetic strategies have included TILLING (Targeting Induced Local Lesions IN Genomes) (Henikoff *et al.* 2004) as well as the extensive use of antisense technologies such as morpholinos (Ekker 2000). Reverse genetics offers the advantage that the identity of the disrupted gene is known and can be specifically targeted, and when carried out using antisense it can also give rapid results since a phenotype is seen in the experimental subject with no requirement for further breeding before the effects of the disruption can be assessed.

6.1.5 Morpholinos

Morpholino oligonucleotides (MO) are non-ionic DNA analogs which possess altered backbone linkages compared with DNA and RNA. In place of a deoxyribose or ribose sugar they possess a morpholine ring and individual subunits are joined by non-ionic phosphorodiamidate linkages. Figure 6.3 illustrates the structure of a morpholino oligo in comparison to a DNA molecule of the same length. They were devised by James Summerton in 1985 and were designed to address the problems encountered with other antisense agents such as sequence specificity and varying activity levels (Summerton and Weller 1997).

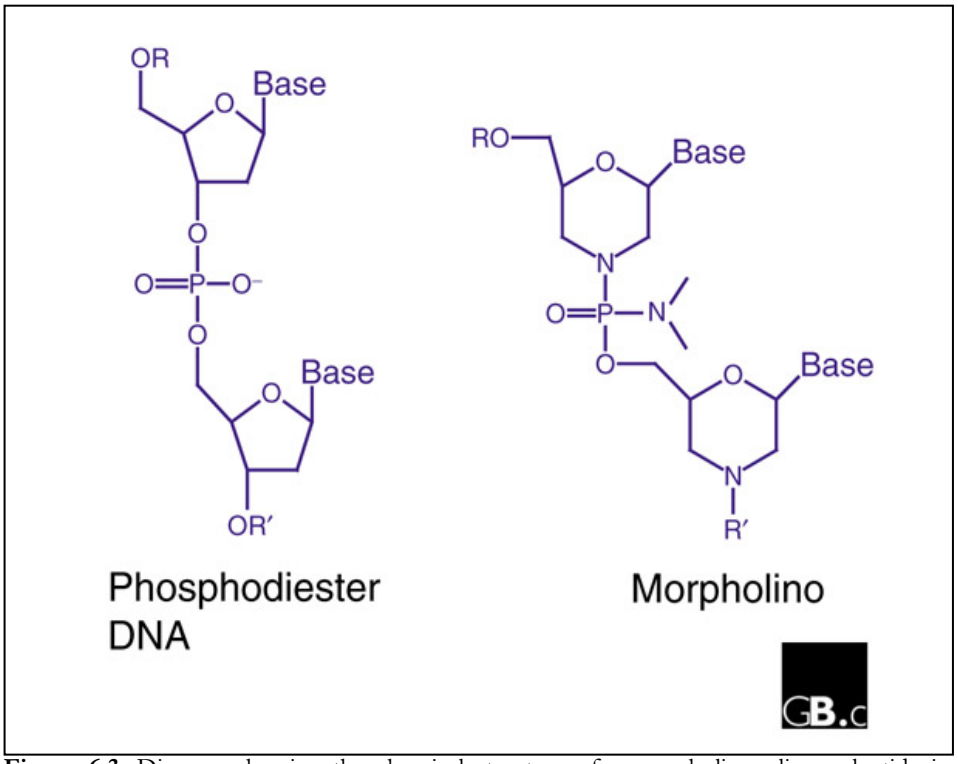

Figure 6.3: Diagram showing the chemical structure of a morpholino oligonucleotide in comparison to DNA. In each example two nucleotide units are joined by an intersubunit bond. R and R' denote continuation of the oligomer chain in the 5' and 3' direction, respectively (from Corey and Abrams, 2001).

Morpholinos bind to complementary nucleic acid sequences via Watson-Crick hydrogen bonding with a similar affinity as for DNA and RNA oligomers and

operate by steric blocking. When designed to block translation they inhibit the binding of the ribosome to an mRNA molecule, but can also be used to target nuclear processing events when designed to bind to splice junctions. The mechanisms involved and factors to be considered when designing morpholinos are discussed in subsequent sections.

6.1.5.1 Advantages of morpholinos

Ideally, a gene targeting technique should be highly specific, straightforward to perform, competent for action in all cell types, efficient at depleting the selected protein, amenable to the targeting of many genes, have little or no non-specific effects, and be reproducible. Most antisense agents fit some of these criteria, with all of them being simpler to administer and more amenable to the targeting of many genes than mutagenesis schemes. Morpholinos have recently become widely used as a result of their many advantages over other antisense technologies. One of the most important of these is that the alteration of the backbone makes them resistant to degradation by nucleases. Most other antisense molecules are targeted for degradation but the morpholine backbone is not recognised by the nucleases and can thus remain present for much longer in the cell (Hudziak *et al.* 1996). This allows the effects of the targeted knockdown to be observed over a much longer time period, thus greatly expanding the possibilities of their application. Another advantage of their altered structure is that the phosphorodiamate linkage which joins individual subunits has no charge and promotes efficient base-stacking, thus minimising any non-specific cellular activity while maintaining good solubility properties (Summerton and Weller 1997).

Morpholinos also offer higher specificity at lower concentration than RNase H-mediated systems such as DNA and S-DNA oligos. Since DNA/RNA and S-DNA/RNA duplexes of only 5 base pairs in length can be cleaved by RNase H (Crouch and Dirksen 1982), there is a high probability that non-target mRNAs will be cleaved, resulting in unpredictable disruption of normal

cellular processes. In addition, the cleavage process releases the antisense oligo in its original form, allowing a single molecule to trigger many non-specific cleavage events. By contrast, the steric blocking mechanism employed by morpholinos requires very close sequence homology in order to be effective, since the oligo will be displaced by the ribosome if it is improperly bound to the target as a result of basepair mis-matches (Hudziak *et al.* 2000). In addition, since morpholinos are effective only when targeted to specific regions of the mRNA molecule (see sections 6.1.4.2 and 6.1.4.3), their potential for causing non-specific effects is greatly reduced. A morpholino need only distinguish its target from the 2%-5% of cellular RNA sequences comprising these targetable regions, as opposed to the full complement of RNA sequence which can be bound to and marked for degradation in an RNase H-mediated approach. An additional advantageous property of morpholinos is their ability to successfully invade and bind to the stable secondary structures sometimes found within leader sequences which can reduce the binding efficiency of other antisense molecules. This point is illustrated in Figure 6.5

While morpholinos have effectively superseded the majority of other antisense approaches, the use of RNA interference (RNAi) has recently become widespread in many organisms (reviewed in Campbell and Choy, 2005). However, Zhao and colleagues (Zhao *et al.* 2001) showed that RNAi was not suitable for use in zebrafish embryos. Using dsRNA designed to block the maternal gene *pouII-1*, the transgene GFP, and an intron of the zebrafish gene *terra*, they showed by *in situ* hybridisation that degradation of both co-injected and endogenous mRNA occurred without sequence specificity. All three targeted sequences gave extensive non-specific effects, while transgenic embryos injected with dsRNA targeted to GFP did not show reduced GFP expression. As a result of this and the other advantages previously discussed, morpholinos have become the antisense tool of choice when studying the zebrafish.

6.1.5.2 Blocking translation (targeting start sites)

Morpholinos designed to block translation operate by displacing the ribosomal complex, preventing it from processing the targeted mRNA. This principal is illustrated in Figure 6.4.

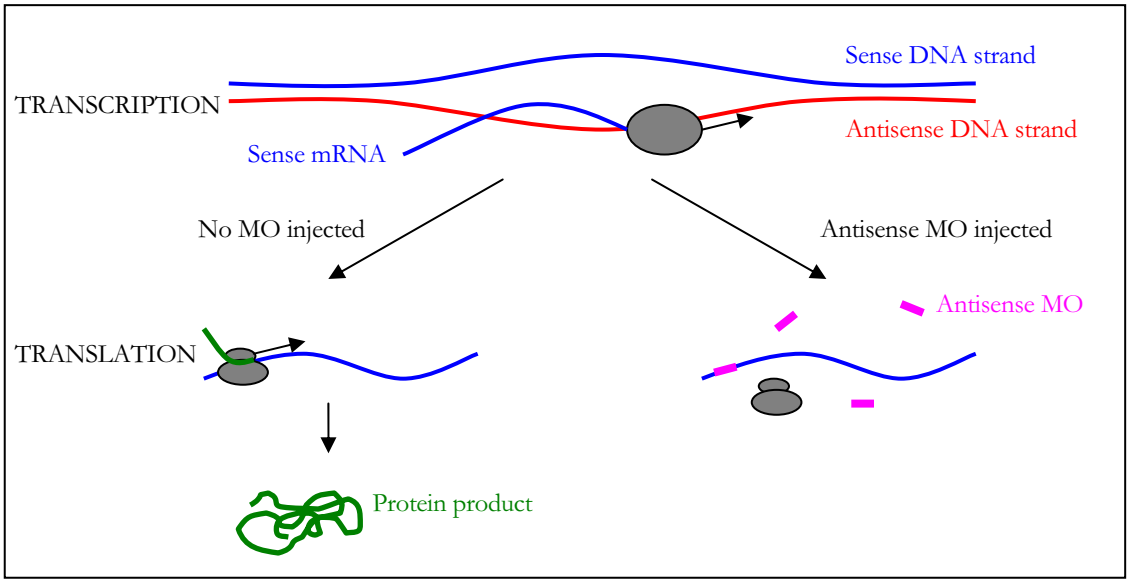

Figure 6.4: Diagram showing the mechanism by which a morpholino (MO) targeted to the start site of a specific mRNA molecule blocks its translation. The complementary binding of the MO to the translational start site inhibits the ribosomal complex from adhering, thus preventing the formation of a protein product.

The most effective translation-blocking morpholinos are those designed at or immediately preceding the AUG translational start site which prevent the initial formation of the ribosomal complex. Those targeted at sequence further downstream show a large reduction in inhibition efficiency which is thought to be a result of the powerful unwindase activity associated with ribosomes following their full assembly at the AUG start site (Nishikura 1992). Figure 6.5 shows the relative inhibition efficiencies of MOs complementary to a series of sections of the leader sequence of Hepatitis B mRNA and illustrates the importance of targeting a morpholino to the correct section of sequence. It also demonstrates the ability of MOs to effectively invade stable secondary structures in mRNA molecules.

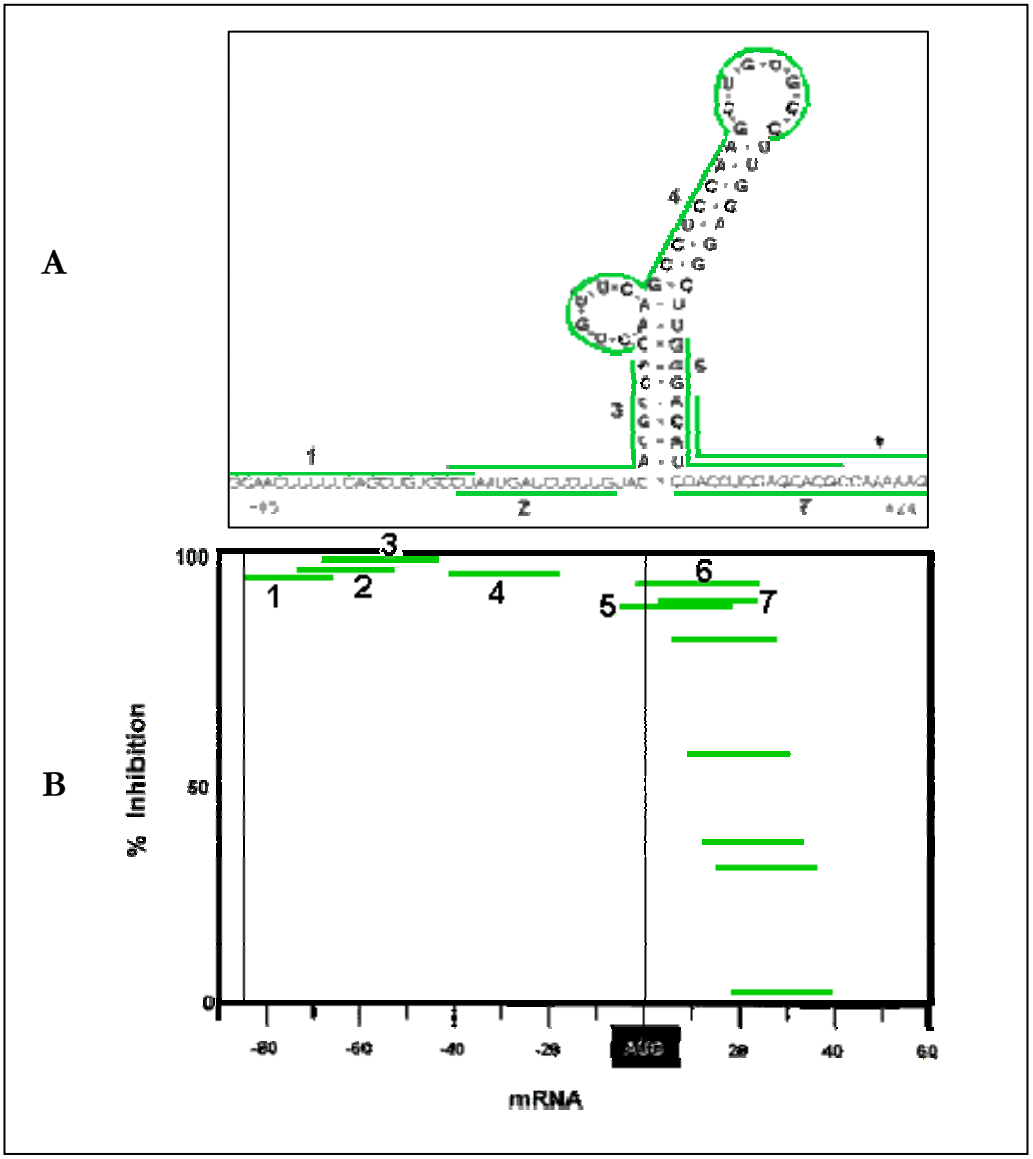

Figure 6.5: Diagram summarising the results of a study to determine the most effective target sites for morpholinos designed to block translation.
The leader sequence of Hepatitis B mRNA is shown in **A**, with the locations of the seven MOs to be tested shown by numbered green lines. In **B**, the inhibition efficiencies of each MO are shown by their position on the y-axis, with the x-axis representing their position on the mRNA molecule relative to the AUG start site. The data demonstrate that MOs are most effective when targeted to sequence either upstream of or immediately subsequent to the AUG start site, with a steep drop in efficiency occurring when the target site is further downstream. This is illustrated by the unnumbered MOs in **B**, which show much lower % inhibition despite being only a few base pairs 3' of MO7. This is thought to be a consequence of the unwindase activity associated with ribosome complex after full assembly at the translational start site. In addition, this experiment illustrates the ability of MOs to bind to mRNA molecules even in the presence of stable secondary structures. (Data and diagrams from Gene Tools – http://www.gene-tools.com)

6.1.5.3 Blocking nuclear processing (targeting splice junctions)

Morpholinos which target mRNA start sites and block their translation can be expected, if achieving efficient inhibition, to cause an almost total absence of the targeted protein product in the developing organism or cell. Many mutations do not have such a dramatic effect since the affected protein may still be partially functional, and thus one may see a different phenotype in an organism carrying a mutation and one which has been injected with a MO targeting the start site of the same gene. A second approach to using morpholinos is to instead target them to splice junctions with the intention of blocking nuclear processing and resulting in a modified but not completely non-functional protein product. Since the purpose of this study is to replicate the *bronx waltzer* phenotype in the zebrafish, and since the nature of the *bv* mutation is unknown, it was thought prudent to also follow this alternative method of gene knockdown using morpholinos.

Morpholinos targeted to splice junctions operate by blocking the progress of the nuclear splicing apparatus and typically cause either the exclusion of a single exon or the activation of a cryptic splice site (AG or GT sites within adjacent exons or introns) which results in the inclusion of a part of the exon or an intron. This principal is illustrated in Figure 6.6

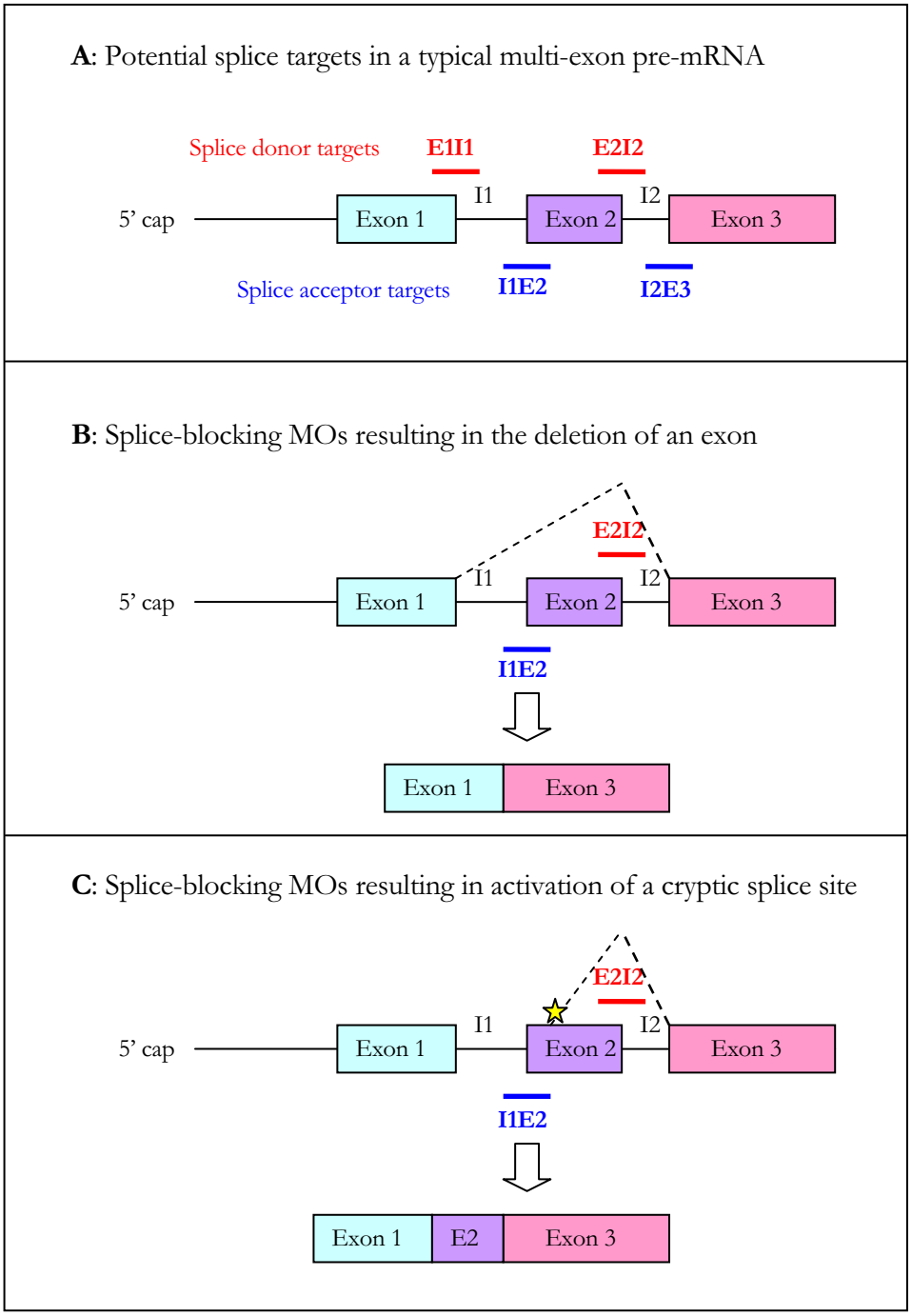

Figure 6.6: Diagrams illustrating the effects of targeting morpholinos to splice donor and acceptor sites on nuclear processing. Figure **A** shows the locations of possible target sites, while **B** and **C** illustrate the potential outcomes of using the most predictive of these sites, the acceptor and donor sites of the exon to be targeted. In **C** the cryptic splice site within exon 2 is represented by a yellow star.

A further property of morpholinos targeted to splice junctions is that they will exert their inhibitory effects only on mRNAs produced by the embryo, since any maternally inherited mRNAs will have already undergone nuclear processing. This can make it possible to observe the more subtle effects of a gene which may result in lethality if its presence is required during early development.

6.2 METHODS

6.2.1 Selection of target genes

The *bronx waltzer* candidate region comprises a total of 53 annotated genes of which 31 have been previously characterised. Even for a relatively rapid method such as the generation of morphants by injection of morpholinos this would represent a significantly larger allocation of time and resources than was available for this project. Therefore it was decided that a subsection of the genes which seemed most promising as candidates for the *bv* causative agent would be investigated using this approach. The criteria used for selecting the most interesting of the candidate genes are described in Chapter 5: Candidate gene assessment. The genes initially chosen for investigation by knockdown using morpholinos targeted to start sites in zebrafish orthologues were *Foxn4, Tcf1, Citron, Ube3b, Myo1h, Cabp1, Paxillin* and *Trpv4*. Later, when designing morpholinos to splice junctions, new published data warranted the additional inclusion of *Git2* and *Kctd10*.

6.2.2 Identification of orthologous genes

The first part of this study, comprising the targeting of morpholinos to the start sites of candidate genes, was carried out several months prior to the second part, the targeting of splice donor sites within the genes. During this time, progress was made in the quality of zebrafish sequence available and also in the accessibility of large-scale computational data relating to predicted orthologs. As such, the approaches followed when selecting zebrafish genes to target were different in each case. In addition, during the interim period a number of new genes emerged as interesting candidates and so were included in the splice donor MO analysis but not in the start site MO study.

6.2.2.1 Morpholinos targeted to start sites

At the time that this study was begun, the sequence data available for the zebrafish consisted mainly of un-annotated public domain sequence reads. Therefore the strategy employed to identify zebrafish genes showing good homology to the mouse genes of interest made use of the sequence alignment and comparison program BLAST (Basic Local Alignment Search Tool).

Peptide sequences of the mouse genes were obtained in FASTA format and used to query the continually updated database of zebrafish ESTs using the WU-BLAST program tblastn (Gish, 1996-2003; http://blast.wustl.edu). This program enables a peptide sequence to be searched against a nucleotide database by first converting it into all the possible nucleotide sequences which might encode it, thus allowing degeneracy in the genetic code to be ignored. Those ESTs which were returned with a score of 90% or greater in respect of similarity to the original sequences were then themselves obtained as FASTA files. These were imported into the genome assembly programme Gap4 (Bonfield *et al.* 1995) and aligned into contigs in order to obtain as large as possible a portion of the expressed sequence and to identify location of the start site. If the start site was not immediately located in this manner then the contiguated sequence was used to search the EST database once again, this time using blastn to identify overlapping sequences and build on the contig until the start site was found. At this stage, the sequence was used to query the full genomic sequence database in order to find the upstream sequence and allow the design of a morpholino to block the start site.

6.2.2.2 Morpholinos targeted to splice junctions

When morpholinos were being designed to target splice junctions, a significant amount of new data regarding the zebrafish genome had recently become available. Within the Ensembl Zebrafish database (http://www.ensembl.org/danio_rerio) many genes had been analysed for

similarity to genes within other genomes and were assigned a score depending on the confidence of the ortholog prediction. In addition, many genes had been annotated with predicted exon and protein structures, making it possible to identify protein domains to disrupt and splice junctions to target.

6.2.3 Morpholino design

6.2.3.1 Designing morpholinos to start sites

In order to achieve optimum efficiency, a morpholino intended to block translation of a particular mRNA should be targeted as closely as possible to the AUG translational start site (see section 6.1.4.2). With this in mind, when designing morpholinos to start sites the first 25 bases of coding sequence (including the start codon) was analysed and then the 25-base window was slid upstream until a 25-base target was found that satisfied the requirements. An optimal MO should have 40-60% GC content and no significant self-complementarity to avoid dimerisation. In addition, it should not contain stretches of 4 or more contiguous G residues which can cause problems with solubility. If no suitable 25-mer was found, the size of the window was reduced until a stretch of sequence was found to satisfy the criteria. Once an appropriate target site was found, its reverse complement was determined and this sequence used as the template for MO synthesis. The sequences of the translation-blocking morpholinos used in this study are given in Table 6.1

Gene	MO sequence
Foxn4	GCAGCGCGAGCCGTGATGAGAGGAG
Myo1h	TCCATAGAAATTCCCCGATTCTTTC
Ube3b	CATCGAGCAGAGATCAATGTAAGTA
Trpv4	GAAGAGCACCTCGTGCCGAAT
Cabp 1	CGATTTAACACAGTTTCCCATAGTA
Cabp 5	GTCTACGTCTCTTCTTTAAGCTGGA
Citron A	TTCTCTCCGCTCCTAGCGACATTTT
Citron B	TTAACTTCCACTCGACCTCAAACTG
Paxillin A	TAAATCGTCCATGTTTCGCGGTCGT
Paxillin B	TCGTCCATGTTTCGCGGTCGTTCTG
Tcf1	CTCTCCTCCGTCCATCCTCCTAGAT
Cdh23	CTCCCGAACCTTCACACCACGACAT

Table 6.1: Sequences of morpholino oligonucleotides designed to block translation of *bronx waltzer* candidate gene orthologs in zebrafish.

6.2.3.2 Designing morpholinos to splice junctions

In designing morpholinos to interfere with nuclear processing, it was first necessary to identify a suitable exon to target. This was achieved by studying

the known or predicted protein domains of each gene and selecting an exon which would disrupt a domain essential for normal protein function. Sequence was then obtained from the splice donor site to include the last 25 bases of the exon and the first 25 of the following intron and this was analysed in a similar manner to that described in Section 6.2.2.1. In this case, targets were selected to span the GT splice donor site rather than the AUG start site but other aspects of MO design remained the same. The sequences of the morpholinos used in this study to target mRNA splicing are given in Table 6.2

Gene	**Protein domain targeted**	**MO position**	**MO sequence**
Foxn4	TF; Forkhead	E2I2	CCCTTACTTCAAGGTGAGGAATTTG
Myo1h	Myosin head	E3I3	TTGGACCAACCTCTAACACAGGGT
Ube3b	HECT domain	E19I19	ATTATTACTGACCTTAATGGAGGTG
Trpv4	Cation channel; TrpL	E11I11	CTTATTGGAATACCTGAAGCATAAC
Cabp1	Calflagin; EF hand	E2I2	CAGACACTGAAACTTACAGTTCATA
Git2	ATP_GTP_A	E6I6	CATCTCCCTCACCTGGCGTAGTCAA
Paxillin A	Paxillin	E4I4	GTCTCTGTGTTTACCTGTAGTGGAG
Paxillin B	Zn-binding LIM	E2I2	GTGTAACGCTTACGTCCAGAATGGG
Citron	Pleckstrin homology	E8I8	GAGTGATGGTGTACCTTCAGTGGGC
Kctd10	K+ channel tetramerisation	E2I2	GTGTGTACTTTACCTGCAATGCTGC
Tcf1	Homeobox; HNF1b_C	E4I4	GTGAATGTATCAGTACCTTGCATCT
Cdh23	Cadherin	E4I4	TGTTTGAGACACTCACCCACTGGTG

Table 6.2: Sequences of morpholino oligonucleotides designed to block splicing of *bronx waltzer* candidate gene orthologs in zebrafish. Cdh23 has not been fully characterised in the zebrafish, the sequence of the splice MO used here was taken from the work of Söllner et *al.*, 2004.

6.2.4 Administration of morpholinos

6.2.4.1 Morpholino preparation

Morpholinos were obtained as 300 nanoMolar aliquots of freeze-dried, lyophilized oligonucleotides from Gene Tools, LLC (Philomath, OR, USA) and on arrival were resuspended in 60µl RNase-free water. Of this stock solution 1µl was diluted in 800µl HCl and its optical density read at λ 265nm. This figure was used to calculate the concentration of the stock using the equation below. The molecular weight and molar absorbance are calculated

from the nucleotide composition of the morpholino and are supplied with the oligonucleotides.

$$\text{Morpholino Concentration} = OD_{\lambda 265} \times \frac{\text{Molecular Weight}}{\text{Molar Absorbance}}$$

The volume of stock solution required for a single dose at the required concentration was calculated using the following equation:

$$\text{Volume of stock solution} = \frac{\text{Required Dose}}{\text{Concentration of stock} \times \text{Dosage volume} \times \text{Total volume required}}$$

The remaining volume was made up with Morpholino Buffer and was calculated thus:

$$\text{Volume of buffer} = \text{Total volume} - \text{Volume of MO stock}$$

Morpholino buffer was composed of one part 25mg/ml phenol red stock and four parts 5mM HEPES (pH7.2) and 200nM KCl. Buffer was filter sterilised before being added to the morpholino stocks. Initially, 7µl of injection aliquots were made up at a dilution of 8ng/1.4nl, with 1.4nl being the calibrated single dosage. These were then serially diluted with 3.5µl being taken and added to a further 3.5µl of Morpholino buffer to give aliquots which would deliver 4ng, 2ng, 1ng and 0.5ng in a 1.4nl dose. Morpholino stocks and injection aliquots were both stored at -20°C.

6.2.4.2 Morpholino injection

Injection needles were prepared from filamented borosilicate capillary tubes (World Precision Instruments, Sarasota, USA) using a Model 720 needle puller (Kopf, Tujunga, USA) with the solenoid set to 3 and heater set to 15. The needle was then opened up using a razor blade to remove the fused tip. This was carried out under a Leica MZ 95 light microscope and needles were cut at an angle in order to provide a sharp point. Prior to being used, morpholino injection aliquots were denatured at 65°C for 5 minutes and immediately cooled on ice. A 1.5µl aliquot was then taken and transferred to an injection needle using a GELoader tip (Eppendorf) and this placed into the pen attachment of a PV820 Pneumatic Picopump (World Precision Instruments, Sarasota, USA). The pen attachment was mounted on a micromanipulator (Narishge, Tokyo) held on a magnetic base (Kanetec, Tokyo) close to the light microscope. To account for the varying size of the needle aperture, a calibration step was performed. The needle was positioned under a light microscope in a small Petri dish filled with mineral oil. Beneath the Petri dish was placed a graticule (Graticules Ltd, Tonbridge, UK). Following a single expulsion to expel any air in the needle, 10 expulsions of morpholino solution were made into the oil and the size of the resulting bubble measured against the graticule. Adjustments were made using the Picopump to control the power of each expulsion and the calibration repeated until the bubble size equalled seven graticules. This had been calculated to be the equivalent of 14nl, hence a single expulsion should give 1.4nl, the required dosage volume.

Zebrafish oocytes were transferred using a glass Pasteur pipette to a glass Petri dish containing a glass slide. The edge of the slide was used to line up the oocytes in a single row, and excess egg water was removed to minimise movement of the eggs. This was placed under the light microscope and the needle positioned against the first in the row. The holding pressure was adjusted using the PicoPump until a small amount of MO leaked out when

the needle came into contact with the surface of an oocyte. This ensures that the contents of the yolk are not drawn up into the needle following injection. The micromanipulator was used to push the needle through the chorion and into the yolk of an oocyte. Injections were made into the streaming part of the yolk using a single depression of the foot pedal and the needle was immediately removed. The presence of phenol red in the buffer made it possible to visualise the location of the injected fluid within the egg, and any where the morpholino had not successfully been delivered into the yolk were discarded. For each morpholino at each dilution 50 oocytes were injected, before being transferred to a labelled Petri dish containing egg water (180mg/L Red Sea Salt; 2mg/L Methylene Blue) and placed in an incubator at 28°C.

6.2.5 Negative and positive controls

As a negative control for the injection process, Morpholino buffer was injected into oocytes in the same manner as described in section 6.2.3.2 and their development monitored. In addition, to control for variability between batches of oocytes from different parental pairs, 50 from each were removed and allowed to develop without intervention.

The positive controls used in this study were morpholinos designed to block the gene *Cadherin23* which is the causative agent for Usher syndrome type 1D in humans and is also mutated in the *waltzer* mice which have a behavioural phenotype similar to *bronx waltzer*. The sequences for these morpholinos were kindly supplied by Christian Söllner and had already been demonstrated to cause disruption to ear function in injected zebrafish larvae (Söllner *et al.* 2004).

6.2.6 Zebrafish

The zebrafish used in this study are maintained in the laboratory of Dr Derek Stemple at the Wellcome Trust Sanger Institute, Hinxton, Cambridge.

General maintenance, collection, and staging of zebrafish were carried out according to the Zebrafish Book (Westerfield 2000); http://zfin.org/zf_info/zfbook/cont.html). The approximate stages are given in hours postfertilization (hpf) or days postfertilisation (dpf) at 28°C.

6.2.6.1 Zebrafish oocytes

One day prior to injections, mating pairs of zebrafish were placed into individual tanks with mesh dividing them from the bottom of the tank to prevent the eggs from being cannibalised. On the day of injections, the fish would begin spawning as soon as their daylight cycle began and oocytes could be collected from the bottom compartment of the tank. These were placed into Petri dishes containing egg water (180mg/L Red Sea Salt; 2mg/L Methylene Blue) and the eggs arising from each mating pair used separately. Injections were carried out using oocytes between the 1-cell and 4-cell stages (Kimmel *et al.* 1995).

6.2.7 Assessment of phenotype

6.2.7.1 Observing development

Approximately five hours after injection when they were between 50% epiboly and shield stages (Kimmel *et al.* 1995), the oocytes were examined under the light microscope. At this stage it was possible to pick out any which were unfertilised and hence failing to divide. In addition, the dye present in the morpholino buffer made it possible to identify those oocytes which had successfully taken up the injected fluid since the cells of these appeared pink and any which did not could be removed. Over the next five days, the developing larvae were observed daily. Notes were made regarding their development and any dead or arrested larvae were counted and removed.

6.2.7.2 Assessing hearing and vestibular defects

Hearing ability was assessed by the administration of a tap test. The Petri dish containing five day old larvae was placed on a hard surface and the edge tapped sharply with the handle of a mounted needle. Those fish which are able to detect the sound and vibration caused by such an action make a sudden and pronounced darting movement, while those which cannot will remain still.

Vestibular function was assessed by observation of behaviour. Fish with vestibular defects are unable to locate the surface in order to inflate their swim bladders so tend to be restricted to the base of the dish. Additionally, when they swim they can be seen to move in circular patterns.

6.2.7.3 Tissue collection

Following assessment of phenotype on the fifth day following injection, zebrafish larvae were culled by overdose of Tricaine anaesthetic (3-aminobenzoic acid ethyl ester). Ten from each sample group were then placed into fix (4% paraformaldehyde in phosphate buffered saline) for use in staining of actin bundles and ten were placed into TRIzol (Invitrogen) for extraction of RNA. These were stored at 4°C until required for further use.

6.2.7.4 Phalloidin staining of actin bundles

Following fixation at five days old, larvae were rinsed and permeabilised by four washes of 30 minutes each in 2% Triton X-100. Staining was carried out with 2.5μg/ml FITC phalloidin (Sigma) in PBS overnight in the dark to prevent leaching of the stain. Samples were then washed with four changes of PBS before being bisected and mounted onto glass slides. Microscopy was carried out using a Biorad Radiance 2100 confocal head attached to a Nikon Eclipse E800 microscope. Images were obtained using a 40X objective lens with a 0.75 numerical aperture.

6.3 RESULTS

6.3.1 Orthologous genes

6.3.1.1 Morpholinos targeted to start sites

In the absence of complete zebrafish genomic sequence or available data regarding orthologues at the time that design of morpholinos targeted to start sites was carried out, transcripts showing significant sequence similarity were identified using the tBLASTn tool to compare mouse peptide sequence to zebrafish EST sequences. Where more than one incomplete coding sequence was identified using this approach, the sequences were assembled and the composite sequence used to query the EST database again until the start site was located. Where more than one distinct zebrafish sequence showed good homology to the mouse peptide, morpholinos were designed to both possible targets as in the cases of *Citron* and *Paxillin* and these were designated A and B. The mouse gene *Cabp1* gave good matches to two zebrafish genes, *Cabp1* and *Cabp5*, both of which were included. The sequences identified in this manner which were used for the design of morpholinos to block transcriptional start sites are shown in Table 6.3

Gene	Mouse Transcript	ESTs	Zebrafish sequence	Description
Foxn4	ENSMUST00000044790	CK236593 AF424786	NP_571174	forkhead box N4; winged helix nude
Myo1h	ENSMUST00000076152	AW422534 AW233228 BM529907	n/a	cDNA clones only
Ube3b	ENSMUST00000072473	BC055184 CD593989	n/a	cDNA clones only
Trpv4	ENSMUST00000071968	BI476124	n/a	cDNA clone only
Cabp1	ENSMUST00000031519	BE015950 BE015751 BG884283	n/a	cDNA clones only
Cabp5	ENSMUST00000031519	CK354975 AL918992	n/a	cDNA clones only
Citron A	ENSMUST00000051704	AF295804	NP_777288	rho-associated, coiled-coil containing protein kinase 2
Citron B	ENSMUST00000051704	BC044428	n/a	cDNA clone only
Paxillin A	ENSMUST00000067268	AW419523	n/a	cDNA clone only
Paxillin B	ENSMUST00000067268	BI673753	n/a	cDNA clone only
Tcf1	ENSMUST00000031535	AF244934	NP_739570	transcription factor 1; hepatocyte nuclear factor 1-alpha

Table 6.3: Zebrafish ESTs identified by BLAST using mouse protein sequences as template sequence. Where multiple ESTs are given, these were aligned into a single sequence fragment using Gap4. Where a single EST is given, this was already a complete coding sequence or contained an identifiable start site to which a morpholino could be designed. Where a single mouse gene matched more than one distinct zebrafish sequence which could not be aligned together, morpholinos were designed to both alternative sequences.

6.3.1.2 Morpholinos targeted to splice junctions

For the design of morpholinos to splice junctions, use was made of the newly available sequence homology-based orthologue predictions in the Zebrafish Ensembl database which also provides predicted exon structures and protein domains, allowing MOs to be targeted to disrupt particular regions of the gene. The orthologues identified by this method, as well as the protein domains and exons to be targeted are given in Table 6.4 Sequence similarity was confirmed using the multiple sequence alignment tool ClustalW (Chenna *et al.* 2003). As an example of the alignment between mouse and zebrafish genes, the Clustal sequence alignment for the mouse gene *Kctd10* and the novel zebrafish gene it shows similarity to is presented in Figure 6.7 The remaining sequence alignments are given in Appendix B.

Mouse Gene	Mouse Ensembl IDs (Gene/Transcript)	Zebrafish Gene	Zebrafish Ensembl IDs (Gene/Transcript)	Alignment score	Target exon	Target protein domain
Foxn4	ENSMUSG00000042002 ENSMUST00000044790	foxn4	ENSDARG00000010591 ENSDART00000008994	1639	2	TF; Forkhead
Myo1h	ENSMUSG00000041972 ENSMUST00000076152	Novel prediction	ENSDARG00000020924 ENSDART00000022921	3270	3	Myosin head
Ube3b	ENSMUSG00000029577 ENSMUST00000072473	Novel prediction	ENSDARG00000020271 ENSDART00000002815	5107	19	HECT domain
Trpv4	ENSMUSG00000014158 ENSMUST00000071968	Novel prediction	ENSDARG00000018242 ENSDART00000021356	3231	11	Cation channel TrpL
Cabp1	ENSMUSG00000029544 ENSMUST00000031519	Novel prediction	ENSDARG00000033411 ENSDART00000041500	854	2	Calflagin; EF hand
Git2	ENSMUSG00000041890 ENSMUST00000019497	Novel prediction	ENSDARG00000016679 ENSDART00000009913	2999	6	ATP_GTP_A
Paxillin (A)	ENSMUSG00000029528 ENSMUST00000067268	Novel prediction	ENSDARG00000017302 ENSDART00000017712	750	4	Paxillin
Paxillin (B)	ENSMUSG00000029528 ENSMUST00000067268	paxillin	ENSDARG00000030659 ENSDART00000040494	1781	2	Zn-binding LIM
Citron	ENSMUSG00000029516 ENSMUST00000051704	Novel prediction	ENSDARG00000011867 ENSDART00000011989	1569	8	Pleckstrin homology
Kctd10	ENSMUSG00000001098 ENSMUST00000001125	Novel prediction	ENSDARG00000017115 ENSDART00000011596	1804	2	K+ channel tetramerisation
Tcf1	ENSMUSG00000029556 ENSMUST00000031535	tcf2	ENSDARG00000006615 ENSDART00000006883	1695	4	Homeobox; HNF1b_C
Cdh23	ENSMUSG00000012819	Not annotated	n/a	n/a	4	n/a

Table 6.4: Mouse genes were matched with predicted zebrafish homologues via large-scale alignment of the two genomes (http://www.ensembl.org). These were verified and an alignment score obtained using ClustalW (http://www.ebi.ac.uk/clustalw/). The structure of the identified ortholog was then examined and a functionally important protein domain selected for disruption. Splice donor site morpholinos were designed to disrupt the processing of an exon within the target region. Where more than one zebrafish gene presented with good homology to the mouse gene, MOs were designed to both candidates as in the case of *Paxillin*.

```
CLUSTAL W (1.82) multiple sequence alignment


ENSMUST00000001125      MSGDSVVSSAVPAAATRTTSFKGASPSSKYVKLNVGGALYYTTMQTLTKQDTMLKAMFSG 60
ENSDART00000011596      MSGESVVSSAVPAATTRTTSFKGSSPSSKYVKLNVGGALYYTTMQTLTKQDTMLKAMFSG 60
                        ***:**********:********:************************************

ENSMUST00000001125      RMEVLTDSEGWILIDRCGKHFGTILNYLRDGGVPLPESRREIEELLAEAKYYLVQGLLEE 120
ENSDART00000011596      RMEVLTDSEGWILIDRCGKHFGTILNYLRDGVVPLPESRRETEELLAEAKYYLVQGLVDE 120
                        ****************************** ********* ***************::*

ENSMUST00000001125      CQAALQNKDTYEPFCKVPVITSSKEEQRLIATSNKPAVKLLYNRSNNKYSYTSNSDDNML 180
ENSDART00000011596      CQAALQNKDAYEPFCKVPLVTSSKEEQRLIATANKPTVKLLYNRSNNKYSYTSNSDDNML 180
                        *********:********::************:***:**********************

ENSMUST00000001125      KNIELFDKLSLRFNGRVLFIKDVIGDEICCWSFYGQGRKIAEVCCTSIVYATEKKQTKVE 240
ENSDART00000011596      KNIELFDKLSLRFNGRVLFIKDVIGDEICCWSFYGQGRKIAEVCCTSIVYATEKKQTKVE 240
                        ************************************************************

ENSMUST00000001125      FPEARIYEETLNILLYEAQDGRGPDNALLEATGGAAGRSHHLDEDEERERERIERVRRIH 300
ENSDART00000011596      FPEARIYEETLNILLYESQDGRGPDNALLEATGGAAGRSHHIDEDEERER--HDRVRRIH 298
                        *****************:************************:********   :******

ENSMUST00000001125      IKRPDDRAHLHQ 312
ENSDART00000011596      IKRPDDRTHHHQ 310
                        *******:* **
```

Figure 6.7: Multiple sequence alignment of the mouse gene *Kctd10* (ENSMUST00000001125) and its predicted zebrafish orthologue (ENSDART00000011596) obtained using the software Clustal W (Chenna *et al.* 2003). Residues which match exactly are marked "*", those which are different but have a strong similarity of function are marked ":". Amino acids with weak similarity are shown as "." and those which are functionally dissimilar are indicated by a space.

6.3.2 Morpholino injections

Following injection, the development of the zebrafish larvae was monitored daily. The number of dead or arrested embryos was recorded and these results are shown as survival curves in Figures 6.9 and 6.10 for start site and splice donor MOs respectively. In addition, notes were made regarding their developmental progression and appearance, and on Day 5 following injection their hearing and vestibular phenotype was assessed. In each case, the highest dosage which did not give rise to widespread lethality was used for the assessment of phenotype. For MOs which caused lethality at all concentrations, the results given are for the lowest dosage. These data are presented in Tables 6.5 and 6.6 The data obtained from the negative control experiment where MO buffer only was injected is given in Figure 6.8 and Table 6.5

6.3.2.1 Morpholinos targeted to start sites

By and large, the larvae which were injected with morpholinos targeted to the start sites of candidate genes showed wide-ranging, non-specific developmental defects which made it difficult to identify a phenotype resulting from the disruption of the specific gene. Only those larvae injected with the morpholino targeted to the zebrafish *Cabp1* orthologue developed consistently at a rate comparable to the un-injected wild type controls and appeared phenotypically normal at 5dpf. These fish did not exhibit circling behaviour and gave a positive reaction to the tap test, indicating that their ear function was probably normal. Ooctyes injected with MOs targeted to the start sites of *Citron, Ube3b, Myo1h, Cabp5, Paxillin* and *Trpv4* all gave rise to larvae which were stunted in growth and showed a variety of non-specific defects such as bent tails, poor circulation, pulmonary oedema and fused otoliths. However, none of the fish which were well developed enough at 5dpf to be capable of movement showed either circling behaviour or non-

responsiveness to tapping. It should be noted that some fish with bent tails may appear to circle but this is a direct result of their malformation rather than a vestibular defect. The fish injected with morpholinos directed at the start sites of *Foxn4* and *Tcf1* suffered very retarded development leading ultimately to a widespread failure to hatch.

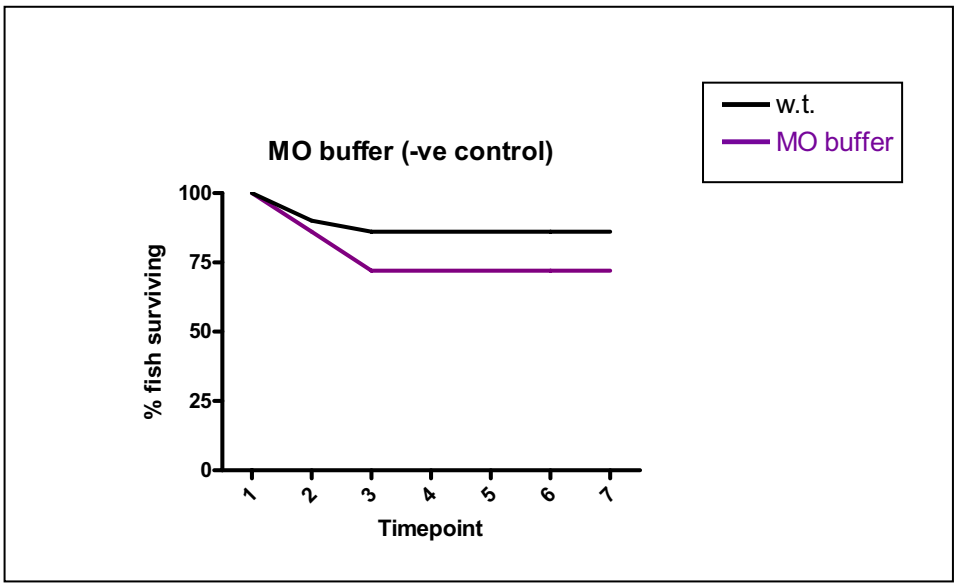

Figure 6.8: Survival curve illustrating the fate of zebrafish embryos injected with MO buffer containing no morpholino oligonucleotide. To control for variability between oocytes from different mating pairs, a wild type group of uninjected embryos was also monitored and is shown by a black line. In both cases the total number of injected oocytes was 50.

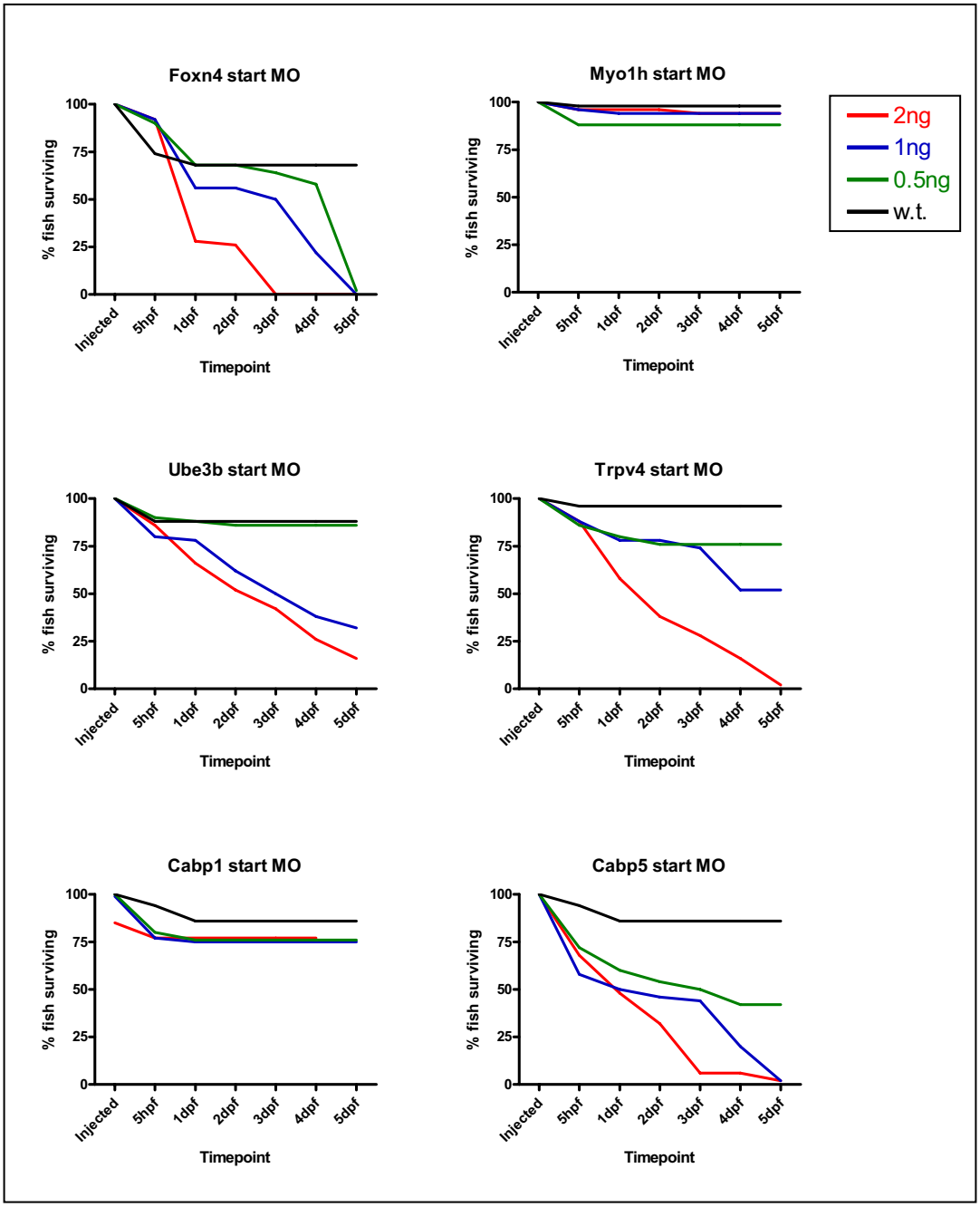

Figure 6.9a: Survival curves illustrating the fate of zebrafish embryos injected with morpholino oligonucleotides designed to block the start sites of *bronx waltzer* candidate genes. Each MO was injected at three different dosages, represented by differently coloured lines. To control for variability between oocytes from different mating pairs, a wild type group of uninjected embryos was also monitored and is shown by a black line. In all cases the total number of injected oocytes was 50.

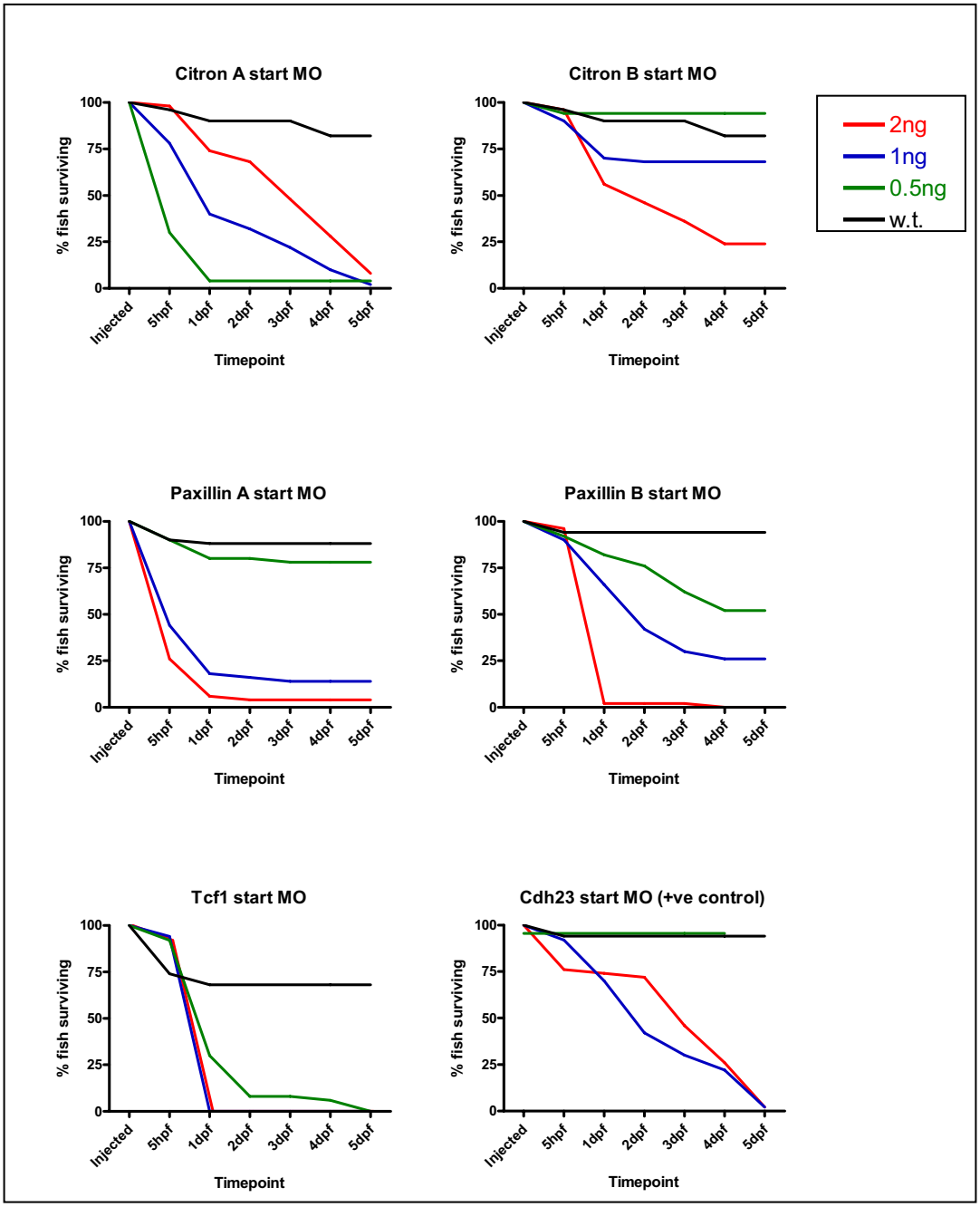

Figure 6.9b: Survival curves illustrating the fate of zebrafish embryos injected with morpholino oligonucleotides designed to block the start sites of *bronx waltzer* candidate genes. Each MO was injected at three different dosages, represented by differently coloured lines. To control for variability between oocytes from different mating pairs, a wild type group of uninjected embryos was also monitored and is shown by a black line. In all cases the total number of injected oocytes was 50

.

Gene	MO	Dose	Development notes	5 dpf phenotype	Tap test result
Foxn4	Foxn4	0.5ng	Very retarded development and stunted growth	Only one fish hatched	Positive
Myo1h	Myo1h	2ng	Stunted growth but relatively normal	Small , no circulation. Many have pulmonary oedema	Positive
Ube3b	Ube3b	0.5ng	Stunted growth, many with bent tails	Very small and stunted, many have no circulation	Positive for mobile fish
Trpv4	Trpv4	0.5ng	Variable development rate, some similar to wild type, others small and stunted	Varied – some appear normal, others very small with twisted tails	Positive for mobile fish
Cabp 1	Cabp 1	2ng	Development rate very similar to wild type	Normal in appearance and behaviour	Positive
Cabp 5	Cabp 5	0.5ng	Stunted growth, many with bent tails	Small fish, twisted tails	Positive
Citron	Citron A	0.5ng	Stunted growth, many with bent tails	Small fish, twisted tails, fused otoliths	Fish not moving
Citron	Citron B	0.5ng	Variable development rate, some similar to wild type, others small and stunted	Similar to wild type, a few stunted, fused otoliths	Positive for mobile fish
Paxillin	Paxillin A	0.5ng	Development similar to wild type until 4 dpf, then many fail to fill swim bladders	Many have not filled swim bladders. Circulation appears slow	Positive for mobile fish
Paxillin	Paxillin A	0.5ng	Variable development rate, some similar to wild type, others small and stunted	Varied – some appear normal, others are stunted. Some otoliths fused	Positive for mobile fish
Tcf1	Tcf1	0.5ng	Very retarded development and stunted growth	No fish hatched	n/a
Cdh23	Cdh23	0.5ng	Development retarded, many not hatched by 5 dpf	Hatched fish swim a little and exhibit circling	Negative for most fish
MOBuffer	MOBuffer	n/a	Development rate very similar to wild type	Normal in appearance and behaviour	Positive

Table 6.5: Summary of recorded observations regarding the appearance and behaviour of zebrafish larvae following injection with morpholino oligonucleotides (MO) designed to block the start site of the targeted gene. In each case the observations given are for the lowest dosage which did not result in widespread lethality. Where all doses resulted in lethality, the results are given for the lowest dosage administered. At 5 dpf the fish were examined for circling behaviour which can be a sign of vestibular dysfunction. Their response to the tap test (see Section 6.2.6.2) was also assessed as a measure of their ability to detect and respond to vibration. . A positive result is a sign of normal function in fish which are mobile, whilst a negative one is suggestive of an ear defect.

6.3.2.2 Morpholinos targeted to splice junctions

Of the 12 MOs designed to bind to splice donor sites in order to interfere with nuclear processing, eight consistently resulted in well-developed 5 day old larvae which were sufficiently mobile to allow reliable assessment of their phenotype. This is a significant improvement on the one morpholino targeted to the start site of *Cabp1* which gave useful data in the previous part of this experiment. Since two different sequences were used to target *Paxillin*, the 12 MOs represent 11 genes, of which eight can now be associated with knockdown data in the zebrafish. Only *Citron*, *Tcf1* and *Kctd10* still gave extensive fatalities or non-specific phenotypes at the lowest administered dosage of 0.5ng/cell. The fish injected with morpholino designed to bind at a splice junction within *cadherin23* demonstrated a very clearly abnormal hearing and vestibular phenotype. They rested on their sides, failed to respond to the tap test and swam in tight circling motions. This behaviour is illustrated in Figure 6.11.

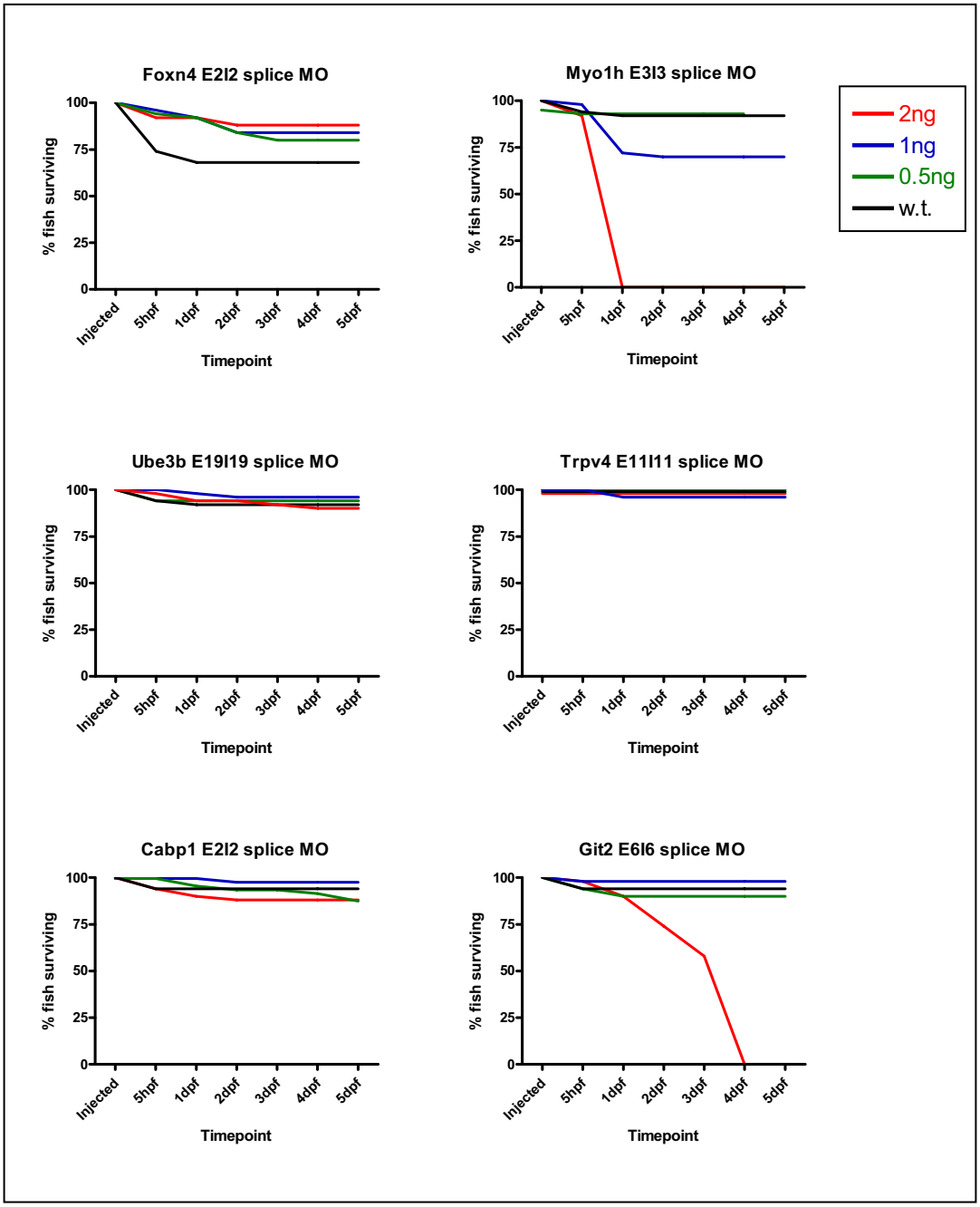

Figure 6.10a: Survival curves illustrating the fate of zebrafish embryos injected with morpholino oligonucleotides designed to block splice donor sites within *bronx waltzer* candidate genes. Each MO was injected at three different dosages, represented by differently coloured lines. To control for variability between oocytes from different mating pairs, a wild type group of uninjected embryos was also monitored and is shown by a black line. In all cases the total number of injected oocytes was 50.

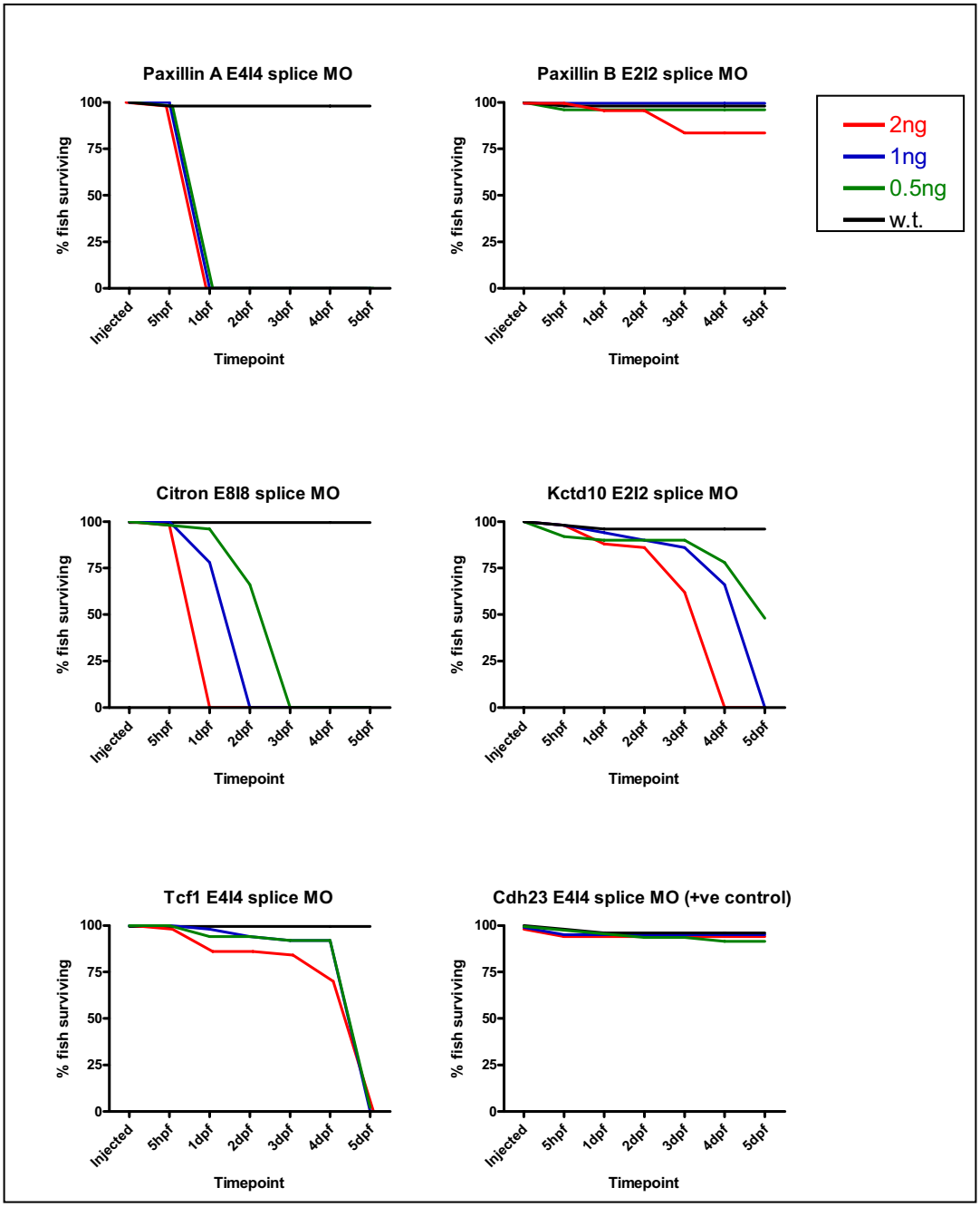

Figure 6.10b: Survival curves illustrating the fate of zebrafish embryos injected with morpholino oligonucleotides designed to block splice donor sites within *bronx waltzer* candidate genes. Each MO was injected at three different dosages, represented by differently coloured lines. To control for variability between oocytes from different mating pairs, a wild type group of uninjected embryos was also monitored and is shown by a black line. In all cases the total number of injected oocytes was 50.

Gene	MO	Dose	Development notes	5dpf phenotype	Tap test result
Foxn4	Foxn4 E2I2	1ng	Development rate mostly similar to wild type	Mostly normal, a few fish are small with bent tails	Positive
Myo1h	Myo1h E3I3	0.5ng	Development rate mostly similar to wild type	Mostly normal, a few fish are small with bent tails	Positive
Ube3b	Ube3b E19I19	2ng	Variable, some similar to wild type, others small and stunted	Varied – some appear normal, others very small with twisted tails	Positive for mobile fish
Trpv4	Trpv4 E11I11	2ng	Development rate very similar to wild type	Normal appearance and behaviour	Positive
Cabp1	Cabp1 E2I2	2ng	Development rate very similar to wild type	Normal appearance and behaviour	Positive
Git2	Git2 E6I6	1ng	Development somewhat retarded	Varied, some appear normal, some have bent tails and pulmonary oedema	Positive for mobile fish
Paxillin	PaxillinA E4I4	0.5ng	Development severely retarded	All fish dead by 1 dpf	n/a
Paxillin	PaxillinB E2I2	1ng	Development rate very similar to wild type	Normal appearance and behaviour	Positive
Citron	Citron E8I8	0.5ng	Development severely retarded	All fish dead by 3 dpf	n/a
Kctd10	Kctd10 E2I2	0.5ng	Very retarded development and stunted growth	All very small and stunted	Fish not mobile
Tcf1	Tcf1 E4I4	0.5ng	Development appears normal until 3 dpf when all fail to hatch	None hatched, all arrested	Fish not mobile
Cdh23	Cdh23 E4I4	2ng	Development rate very similar to wild type	Pronounced circling behaviour, many have unfilled swim bladders	Negative for most fish

Table 6.6: Summary of recorded observations regarding the appearance and behaviour of zebrafish larvae following injection with morpholino oligonucleotides (MO) designed to block a specific splice donor site within the targeted gene. In each case the observations given are for the lowest dosage which did not result in widespread lethality. Where all doses resulted in lethality, the results are given for the lowest dosage administered. At 5 dpf the fish were examined for circling behaviour which can be a sign of vestibular dysfunction. Their response to the tap test (see Section 6.2.6.2) was also assessed as a measure of their ability to detect and respond to vibration. A positive result is a sign of normal function in fish which are mobile, whilst a negative one is suggestive of an ear defect. The negative control for these results was the injection of MO buffer only, the results of which are shown in Table 6.5.

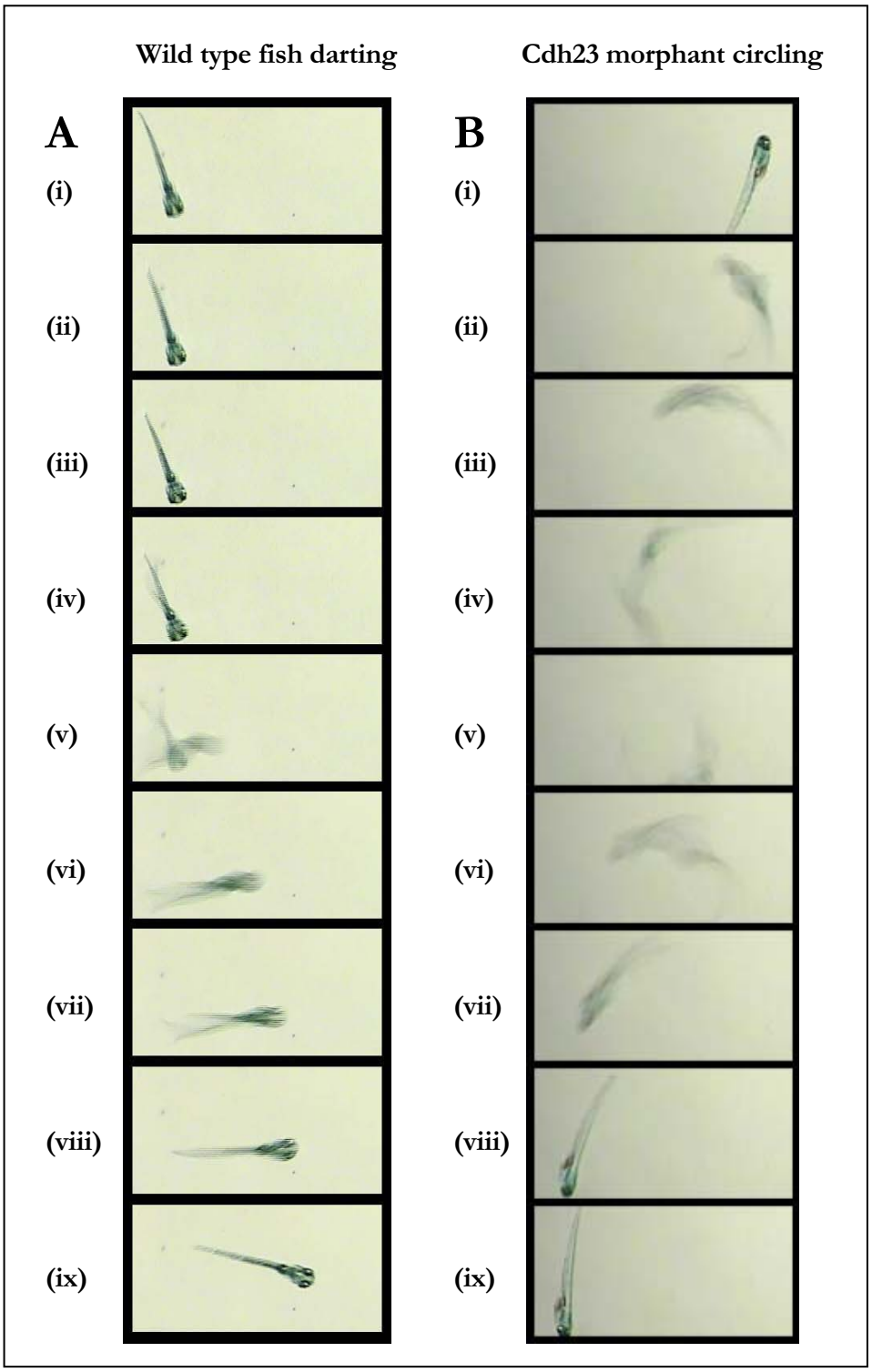

Figure 6.11: Frame-by-frame video stills showing typical fish behaviour observed after 5 days development in **A**) wild type un-injected controls and **B**) larvae injected with 0.5ng of *cdh23* E4I4 morpholino designed to block a splice donor site within the known deafness gene *cadherin 23*. The wild type fish move with a characteristic darting motion which begins with a tail flick as seen in A(iv). By contrast the morphants' movement is much less controlled and often manifests as circling patterns. In addition, their inability to orient themselves or to fill swim bladders results in their resting on their sides at the bottom of the dish (B(i) and (ix)) compared to the normal upright positioning of the controls (A(i) and (ix)).
Both movements take place in less than one second.

6.3.2.3 Phalloidin staining of actin bundles

Initially, samples were processed from wild type control fish and from those injected with 0.5ng of *Cdh23* E4I4 morpholino. These morphants had demonstrated a pronounced circling phenotype and failed to react when the tap test was administered but appeared otherwise normal. Following staining, the hair bundles of these fish were examined using confocal microscopy and examples of the resulting images are shown in Figure 6.12. Splayed stereocilia were observed in all the sensory patches of both the wild type and morphant samples. It should be noted that the varying sizes of the sensory patches in the images is a result of their being from different locations within the ear, rather than being an effect of the MO injection.

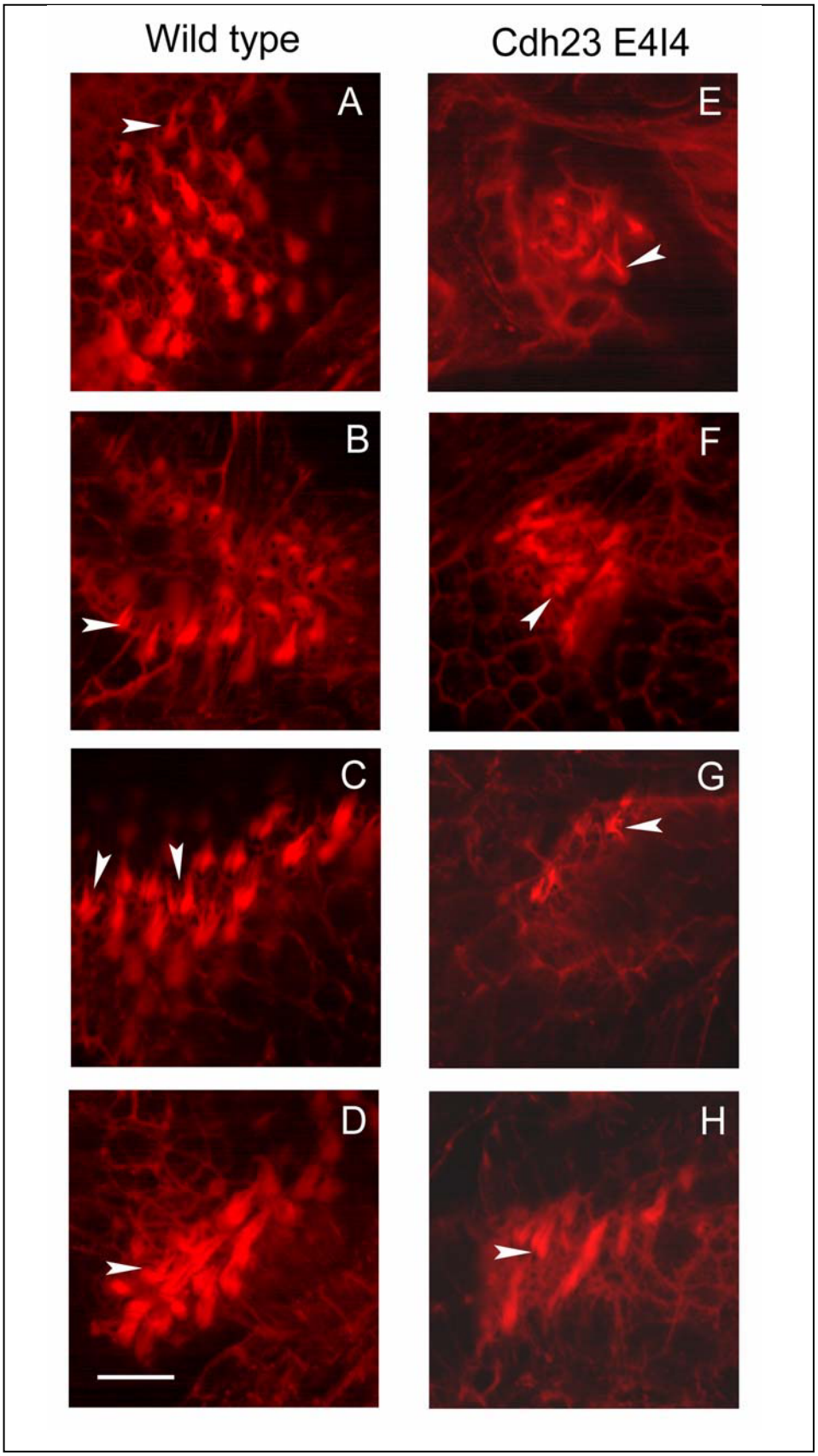

Figure 6.12: Confocal microscope images showing typical inner ear hair cell bundles in wild type un-injected control larvae (A-D) and larvae injected with 0.5ng of *cdh23* E4I4 morpholino designed to block a splice donor site within the known deafness gene *cadherin 23* (E-H). Splayed stereocilia were observed in all the samples examined, some of the bundles showing notable splaying are marked by white arrows. Scale bar = 10μm.

6.4 DISCUSSION

6.4.1 Analysis of negative and positive controls

In order that any interpretation of the results obtained from blocking the *bronx waltzer* candidate genes using morpholinos may be considered valid, it is important that both the negative and positive controls were observed to give the expected results.

6.4.1.1 Negative control: injection of MO buffer

In the course of this experiment, the negative control was to inject zebrafish oocytes with MO buffer containing no morpholino oligonucleotide. This controls for any effects of the manipulation process and the introduction of the dye and other buffer components into the cell. As shown in Figure 6.8 and Table 6.5, the injection of buffer into cells gave rise to a mortality rate slightly higher than that observed in wild type oocytes after the first 24hrs but resulted in no further hindrance to development. After five days the larvae appeared behaviourally normal and responded to tapping with the tail flick characteristic of wild type fish. The fatalities seen after the first day are likely to be due to the invasiveness of the procedure and may be the result of damage caused by the injection process. If the needle is not removed quickly enough from the yolk or if the pressure within it is slightly negative then the injection can cause a small amount of the yolk to leak out of the chorion. This then becomes a target for fungal infection, making it more likely that the oocyte will not survive. However, the normal progression of the buffer-injected eggs supports the premise that any developmental defects or subsequent abnormalities in MO-injected larvae are caused by the presence of the morpholino within the cells.

A more rigorous control would be to inject eggs with a morpholino differing by only one base pair from the target sequence in order to control for the

presence of the oligonucleotide as well as to prove the specificity of the individual morpholino. However, since a large number of morpholinos were already being used in this process, it was decided that this control would not be carried out routinely in order to control the overall cost of the procedure. In the case of any of the morpholinos giving an interesting phenotype, a specific control morpholino would be designed and its effects ascertained.

6.4.1.2 Positive control: injection of cadherin 23 morpholinos

Cadherin 23 (*cdh23*) is a gene whose function within the ear has been well described and has been the subject of previous morpholino studies in the zebrafish. Morpholinos were targeted to both start and splice sites within the gene and both gave rise to larvae exhibiting the circling behaviour and non-responsiveness to sound indicative of an ear abnormality (Söllner *et al.* 2004). In this study the published MO sequences were synthesised and injected in the same manner as those targeted to *bronx waltzer* candidate genes in order to ensure that the methods being employed were capable of detecting an ear abnormality in the fish.

The results of injecting oocytes with the MO targeted to the start site of *cdh23* are shown in Figure 6.9b and Table 6.5. At 0.5ng, the lowest dosage administered, the larvae were relatively retarded in development but those which hatched exhibited circling behaviour and failed to respond with a tail flick when subjected to the tap test. This observation differs from the published data which used dosages of up to 50ng without causing widespread lethality, but the phenotype obtained in those larvae which developed sufficiently correlates with the original findings. This dramatic difference in the response of the fish to higher dosages of the same morpholino is difficult to explain but may result from a difference in experimental design such as the composition of the MO buffer, the particular strain of zebrafish used or the injection procedure.

The injection of oocytes with MO targeted to the splice donor site of *cdh23* exon 4 gave rise to larvae with a pronounced vestibular and balance defect. The data for these experiments are presented in Figure 6.10b and Table 6.6, whilst images depicting their behaviour are shown in Figure 6.11. At all the dosages injected, fish developed relatively normally but showed clear circling behaviour and were observed to rest on their sides rather than remaining upright. They also failed to respond when subjected to the tap test, suggesting a hearing impairment. This confirmation of the phenotype caused by the disruption of *cdh23* carried out under the conditions employed in the present study provides reassurance that should the disruption of one of the candidate genes give rise to an ear abnormality, its presence should be detected using the methods described.

6.4.2 Phalloidin staining of actin filaments

Phalloidin staining of the larvae injected with *Cdh23* E4I4 morpholino which had demonstrated significant vestibular abnormality and circling behaviour seemed to show splaying of stereocilia consistent with the results of the authors who first used this MO sequence (Söllner *et al.* 2004). However, splaying was also observed in the ears of wild type larvae. This suggests that it may be an artefact due to slow fixation, especially as the fix must diffuse through several layers of tissue before reaching hair bundles within the ear. Previous studies of both mice and zebrafish with defective copies of *cadherin23* have given rise to conflicting information regarding the effect of its disruption on stereociliar organisation. It was initially shown to localise to the tip links which connect the stereocilia within a bundle in both mice (Siemens *et al.* 2004) and fish (Söllner *et al.* 2004), leading to the suggestion that its absence may lead to their becoming disorganised and thus prevents normal transduction from occurring. A more recent study by Michel and colleagues (Michel *et al.* 2005) showed *Cdh23* to be a component of lateral links but only during bundle development and also found it to be present in the cuticular plate of adult animals. Meanwhile a similar study by Lagziel *et al.* (Lagziel *et al.*

2005) found *Cdh23* to be present not only in the interstereocilial links but also along the length of sterociliar bundles in vestibular hair cells, the kinocilium and kinocilia/stereocilia links and in the Reisner membrane. Söllner *et al.* (2004) used transmission electron microscopy (TEM) to show that tip links were absent from hair cells in zebrafish carrying mutations in *cadherin 23*. However, since the nature of TEM is such that samples must be looked at in very thin sections, it is possible that the notoriously difficult to visualise tip links were not present in those sections examined. More recent data obtained using field emission scanning electron microscopy (A. Rzadzinska, *pers.comm.*) has shown that not only are tip links present in the stereocilia bundles of *waltzer* mice which carry a *Cdh23* mutation, but that the stereocilia show signs of fusing, rather than of splaying.

Given this uncertainty over the cause of splaying in the hair cell bundles and the evidence of a similar appearance in un-injected control zebrafish larvae, it was considered that phalloidin staining of the larvae injected with morpholinos would not provide informative data concerning the effects on the fine structure of the zebrafish ear of blocking the start or splice sites of candidate genes. Ideally, the hair bundles would be examined using SEM, but this was beyond the scope of the present study.

6.4.3 Comparison of start site and splice site morpholinos

The identification of orthologous genes was carried out in a different manner during the design of morpholinos to start and splice sites. However, in most cases the zebrafish transcripts identified were the same. The use of the additional data available in Ensembl when choosing sequence to target using splice donor MOs allowed the identification of the single best orthologue for both *Citron* and *Cabp1* which previously had two possible candidate transcripts. *Paxillin* still showed a high level of homology to two different zebrafish transcripts, although these matched to different regions of the

mouse gene (see Appendix B), suggesting a division of subunits or possibly a divergence of function.

Many of the oocytes injected with morpholinos directed at the start sites of the candidate genes gave rise to larvae which either arrested early in development or suffered from wide-ranging non-specific defects. For some genes this may be an indication that they play an important role during early developmental stages, with their disruption giving rise to early arrest. However, it is unlikely that so many of the genes investigated in the present study would perform such a function. Non-specific abnormalities are often associated with high dosages but in this experiment even the very low dosages of 0.5ng resulted in very sick fish, while in the literature reports of 10ng doses resulting in specific effects are not unusual (Draper *et al.* 2001; Söllner *et al.* 2004). The normal development of the fish injected with *Cabp1* morpholino at all doses administered makes it unlikely that the experimental method or reagents were at fault since all the fish were subject to the same treatment. It is interesting to note that the fish injected with the control *Cdh23* MO also showed more non-specific abnormalities than reported in the literature from which the sequence was obtained (Söllner *et al.* 2004). This may indicate that the conditions used here varied, although it is not clear how.

In order to address the issues of early arrest and non-specific effects caused by the morpholinos targeted to translational start sites, it was decided to employ splice donor site blocking morpholinos. Since these take effect during nuclear processing of mRNA rather than at the point of translation, the maternal mRNA molecules which are present in eggs when they are laid are unaffected. This allows the embryo to progress through the vital early stages of development before any alterations caused by the MO take effect. Since the *bronx waltzer* phenotype is a subtle one and is not visible in the mouse embryo until E16.5, it is unlikely that such an approach should result in the causative gene being missed. In addition, MOs targeting nuclear processing will tend to cause disruptions to genes such as exon skipping or premature

truncation rather than the effectively total blocking achieved by the use of MOs targeted to start sites. In this way, splice blocking MOs are similar to mutational alterations whereas start blocking MOs mimic the effects of a deletion in the target gene. Of the 11 morpholinos targeted against splice sites of *bv* candidate genes, eight resulted in larvae at 5dpf which were well developed enough to have their hearing and balance phenotype assessed. In contrast, most start site MO produced underdeveloped or grossly abnormal fish are frequently unable or reluctant to move and therefore their swimming behaviour and reactions to the tap test cannot be ascertained. Therefore the splice site MOs offer a clear advantage when searching for an equivalent to subtle phenotypes such as *bv* in the zebrafish.

6.4.4 Confirmation of splice-blocking MOs

An advantage of using splice-blocking MOs is that the products of MO-targeted mRNA processing events can be characterised using RT-PCR. With primers designed within the exons flanking that to be targeted it is possible to establish from the size of product obtained whether the exon has been excised or altered and hence to confirm that the MO has acted effectively. This principle is illustrated in Figure 6.13.

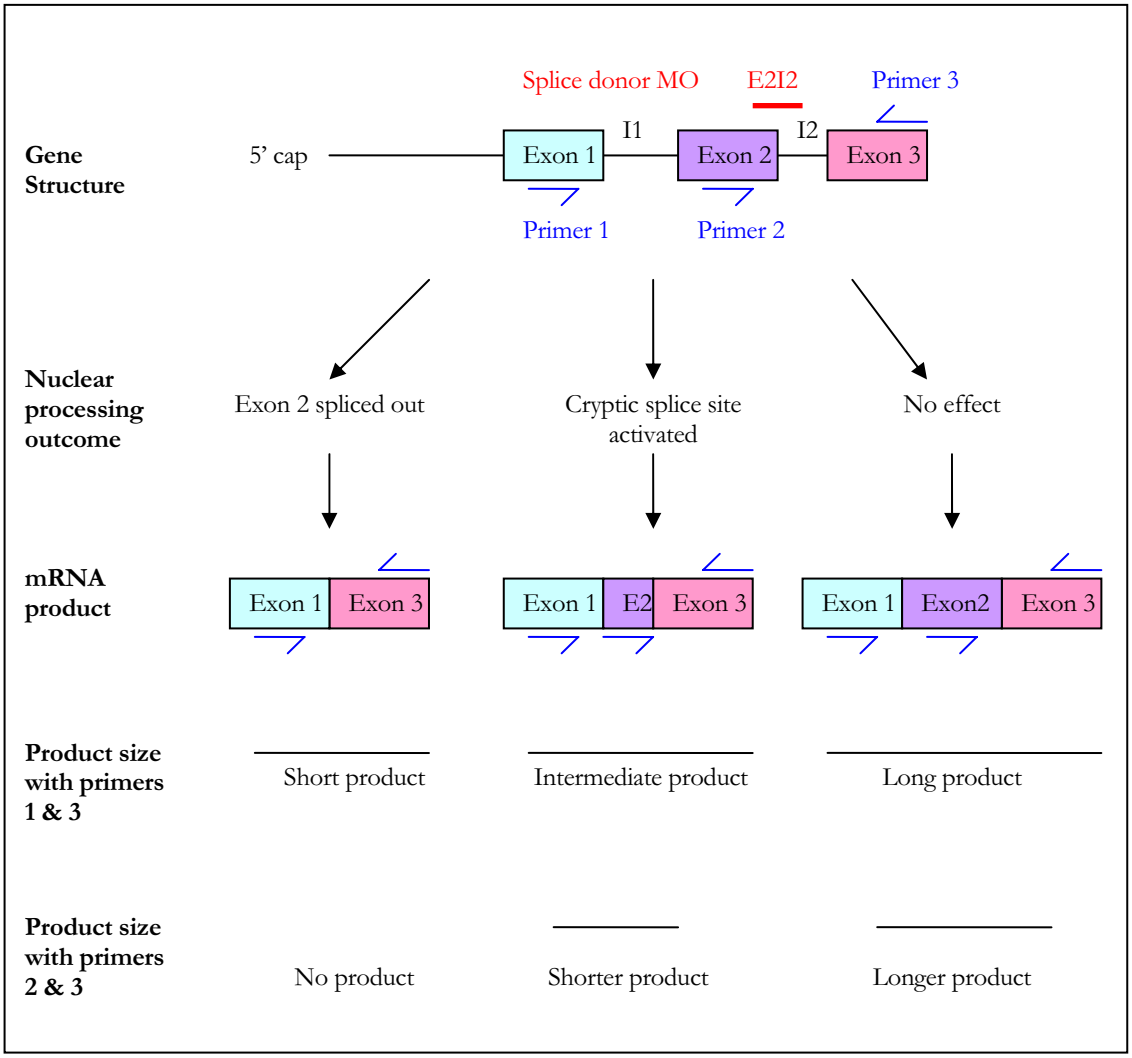

Figure 6.13: Diagram illustrating the strategy for confirmation of the efficacy of morpholino oligos designed to block nuclear processing by binding to splice donor sites. The splice donor MO E2I2 (**red**) is expected to cause the excision of exon 2, or possibly the activation of a cryptic splice site between exons 2 and 3. In order to determine what effect the MO has had on nuclear processing, PCR primers (**blue**) are used to amplify from cDNA samples obtained from injected embryos. The size of the PCR product obtained can be used to infer the structure of the targeted mRNA.

6.4.5 Conclusions

None of the novel morpholinos used in this study gave rise to zebrafish larvae displaying signs of a hearing or balance defect. Most of the start site MOs and four of the splice site MOs caused widespread lethality or non-specific phenotypes, leaving one start MO and eight splice MOs which gave rise to larvae that could be reliably phenotyped. If it is possible to be certain that the MOs caused an effective disruption to the target gene, and that the orthologues identified perform the same function in the zebrafish as they do in the mouse, then these data could represent strong evidence that the included genes do not represent the *bronx waltzer* gene. In the case of the splice MOs, their efficacy at disrupting the target gene should be confirmed by RT-PCR as described in Section 6.4.4, leaving only the question of whether the genes they target represent true functional orthologues of the mouse genes from within the *bv* region. In order to establish this, it would be necessary to carry out further functional analysis. Should any of the genes have given a positive result then this avenue would have been pursued in order to strengthen the case for it representing an orthologue of *bronx waltzer*. In the absence of a good candidate however, further analysis was not considered a priority and it is therefore possible that the genes knocked down in the zebrafish do not represent true orthologues of the mouse genes which map to the critical region. This means that the 11 candidate genes used in this zebrafish study, whilst not being ruled out are less likely to be responsible for the *bv* phenotype.

Although this approach has not yet been of substantial assistance in the search for the *bronx waltzer* gene, it does still hold the potential to contribute to the project. Firstly, a larger selection of candidate genes could be targeted using MOs designed to block splice sites since these proved to be the most successful in producing viable larvae. All of the genes tested here were previously characterized or showed homology to other proteins since their selection relied on a certain level of information being available. However, it is

perfectly possible that the *bv* mutation actually resides within one of the 22 novel genes currently annotated between the flanking markers. Given unlimited time and funds it would be possible to design and inject morpholinos targeted to these, provided that good homology to zebrafish transcripts can be determined, and hopefully one would give fish at 5dpf manifesting behaviour typical of a hearing or vestibular dysfunction like that seen in the larvae injected with *cadherin 23* morpholinos. Secondly, and more realistically, in the event of the discovery of the *bronx waltzer* gene by another means, this method could be use as a verification tool. Since *bv* exists as a single allele, any mutation identified would need to be demonstrated to be causative rather than simply a polymorphism. This approach was taken by Liu and colleagues (Liu *et al.* 2002) who used morpholinos designed to block *Nek8* in order to demonstrate that it was responsible for the cystic kidney disease they had characterised in a single allele mouse model. In these circumstances it would also be possible to generate a mouse knockout but as shown here, knockdowns in the zebrafish are fast, relatively inexpensive and can give recognisable phenotypes when orthologous genes are disrupted. Additionally, the generation of a zebrafish phenocopy would facilitate investigation into the developmental consequences of the mutation, since fish larvae mature externally and can be monitored continuously throughout development.

Chapter 7:

Exon resequencing of genes within the bronx waltzer *candidate region*

CHAPTER 7

EXON RESEQUENCING OF GENES WITHIN THE *BRONX WALTZER* CANDIDATE REGION

7.1 INTRODUCTION

Following extensive mapping studies (see Chapters 3 and 4), the candidate region for *bronx waltzer* has proved difficult to refine and currently stands as a 2.6Mb region of chromosome 5 comprising 52 annotated genes. Since none of these have emerged as a clear causative agent for the phenotype, they must all be considered as potential candidates. This chapter describes the strategy utilised to carry out large-scale mutation screening in an effort to identify which of these genes is responsible for *bronx waltzer*, or alternatively to narrow down the list of candidates by demonstrating that they do not harbour any mutations in the *bronx waltzer* mutant genome.

7.1.1 Large scale mutation detection

Many strategies for large scale mutation detection rely on the differing properties of the two strands when a DNA sample is heterozygous. Differences in the secondary structure adopted by single-stranded molecules (Single Strand Conformation Polymorphism - SSCP) can be detected by their differing electrophoretic mobilities which allow samples differing by a single base pair to be separated by electrophoresis. Other methods rely on the differing properties of the heteroduplexes and homoduplexes that are formed during hybridisation of heterozygous molecules, with a heteroduplex generally having reduced electrophoretic mobility and a lower melting temperature. This latter means that samples can be analysed to high resolution using a specialized form of HPLC (High Performance Liquid Chromatography), and in the guise of WAVE analysis this has become a common method of

detecting mutations in large numbers of samples in the fields of both research (Rossetti *et al.* 2002) and clinical diagnostics (Marsh *et al.* 2001; Ou-Yang *et al.* 2004).

7.1.1.1 WAVE analysis

The WAVE system developed by Transgenomic (Omaha, Nebraska, USA) operates by resolving heteroduplexes and homoduplexes and is based on the principle that heteroduplexes are less stable and therefore will be denatured at a lower temperature. Following PCR amplification the samples are denatured and then hybridised at gradually decreasing temperatures before being loaded onto a WAVE machine for the performance of HPLC. When performed at denaturing temperatures, this analysis results in a unique trace pattern which will differ depending on whether the sample contains only homoduplexes or a mixture of homoduplexes and heteroduplexes. Thus, where a mutation or polymorphism is present, the trace obtained for that sample will differ from the control homozygous trace, highlighting the amplicon for further analysis. An example of such data is shown in Figure 7.1. In the case of the *bronx waltzer* mutation, heterozygous samples would need to be compared to wild type or mutant samples in order to identify any differences. This can be easily achieved since in a normal maintenance mutant (*bv*/*bv*) by heterogygote (+/*bv*) mating, any animals which do not exhibit the bronx waltzer phenotype must have the genotype +/*bv*.

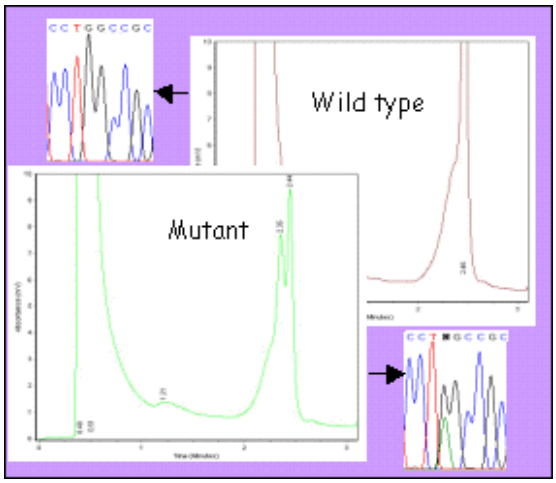

Figure 7.1: An example of the data obtained from WAVE analysis used for the detection of mutations. The mutant sample carries a shoulder on the second peak which is not present in the wild type, suggesting a variation in the two samples which was later confirmed by sequencing. Figure and data from the MRC Mammalian Genetics Unit, Harwell. (http://www.mgu.har.mrc.ac.uk/facilities/gems/mutdetect.html)

7.1.1.2 High-throughput exon resequencing

A straightforward method of determining whether a gene harbours a mutation in a given DNA sample is to obtain sequence reads for each of the exons and compare these to those obtained from a wild type control. This has the advantage that any differences are immediately identified without any further analysis required, and is also the most sensitive method of detecting mutations since it displays directly the alteration to the nucleotide sequence, rather than relying on any secondary effects of such a change which may vary in their intensity and thus in their chances of detection. In the light of this, and given the recent advances which make high-throughput sequencing a relatively routine procedure, it was decided that the genes in the *bronx waltzer* candidate region would be screened by exon resequencing.

Like other methods though, the success of this approach is limited by the regions of sequence that can be covered, which may be restricted by a number of factors. Firstly, exons can only be sequenced if they can first be amplified successfully by PCR, and even then they may prove difficult to sequence as a

result of repeat regions, high GC content or a secondary structure which inhibits the progress of the DNA polymerase. Second, the resequencing of exons assumes that the causative mutation lies within a coding region or splice junction of a gene. While this is true in the majority of cases, it is possible that it may instead be located within a promoter or regulatory element, the exact position and features of which are not easily defined, and thus it would be difficult to include these in the screen. Finally, exons can only be resequenced if their location is known, and thus the coverage obtained is limited by the quality of published sequence and gene annotation within the candidate region. This point is discussed in the following section.

7.1.2 The mouse genome sequence

The published sequence for the mouse is derived from the strain C57BL/6J and was compiled by composite assembly of whole genome shotgun (WGS) and High Throughput Genome Sequence (HTGS) sequence data (Waterston *et al.* 2002). End sequencing and fingerprinting of BAC libraries allowed the creation of a tiling path for each chromosome (Gregory *et al.* 2002) around which the sequence reads were arranged to give the NCBI Mouse Builds 30-33. The currently available Build 33 comprises HTGS sequence from clones which are either finished or in the advanced stages of sequencing, with WGS sequence being used to bridge any gaps and give an overall relatively high degree of sequence coverage. However, this stage of the project is currently underway, meaning that different regions of the mouse genome presently have varying levels of sequence quality, as illustrated in Figure 7.2.

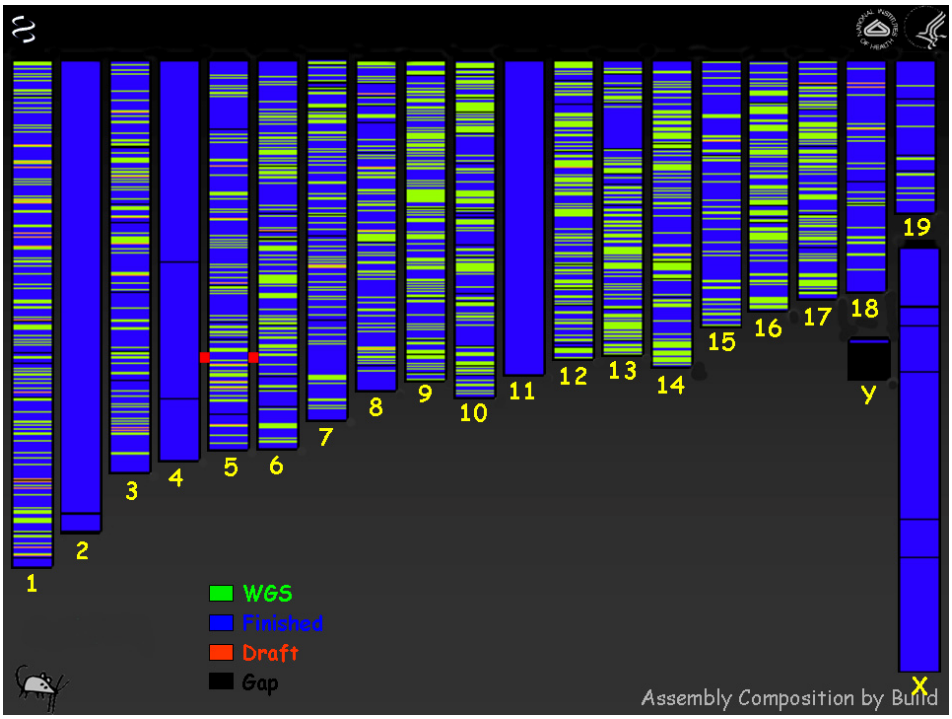

Figure 7.2: Graphical representation of the sequencing status across the mouse genome. The location of the *bronx waltzer* candidate region is highlighted by red bars. Diagram adapted from NCBI (http://www.ncbi.nlm.nih.gov/genome/seq/NCBIContigInfo.html).

7.1.2.1 Sequence quality in the *bv* candidate region

The *bronx waltzer* candidate region spans from 111609074 to 114063755bp of chromosome 5 in Ensembl Build33, with the whole region being contained within the single mapping contig 5015b (see Figure 7.3). This contiguous mapping coverage allows it to be said with reasonable certainty that the size and ordering of the region as a whole has been well established. Fifteen BACs from this map have been selected for HTGS sequencing with four of these being finished and all the others having some sequence available (See Table 7.1). Two gaps exist in the BAC sequence tiling path at present (see Figure 7.3), which are partially covered by WGS sequence. In sequencing terms, the region is currently spanned with a total of five sequence gaps, with three of these coinciding with one of the tiling path gaps. This is not a region where BAC sequencing has been prioritised as yet, although discussions are underway in order to facilitate this.

Accession Number	Clone	Sequencing Centre	Sequence Status
AC122282	RP23-240B12	WUGSC	finish_start
AC127255	RP24-291I7	WUGSC	submitted
AC132102	RP24-360K9	WUGSC	submitted
AC124228	RP23-345O14	WIBR	working draft sequence
AC087330	RP23-3M10	HPGC	complete sequence
AC116500	RP24-297N9	WIBR	sequencing in progress
AC117799	RP24-556H22	WIBR	working draft sequence
AC119205	RP24-188M1	WIBR	working draft sequence
AC145070	RP23-41I11	WIBR	complete sequence
AC117735	RP24-132L16	WIBR	working draft sequence
GAP			
AC139562	RP24-180G11	WIBR	sequencing in progress
AC113200	RP23-265I19	WIBR	working draft sequence
AC115795	RP23-400O10	WIBR	working draft sequence
AC119977	RP24-486F14	WIBR	sequencing in progress
GAP			
AC115972	RP24-79A6	WIBR	sequencing in progress

Table 7.1: Sequence status of BACs selected for High Throughput Genome Sequencing (HTGS) across the *bronx waltzer* candidate region.
Those clones with a status of "finish_start", "complete sequence" or "submitted" are in the more advanced stages of sequencing and generally have 5-10 fold coverage along their length. Those with a status of "working draft sequence" or "sequencing in progress" are in the earlier stages of sequencing and generally have 3-6 fold coverage.

Abbreviations of sequencing centres:
WUGSC – Washington University genome Sequencing Center
WIBR – Whitehead Institute for Biomedical Research (BROAD Institute)
HPGC – Harvard Partners Genome Center

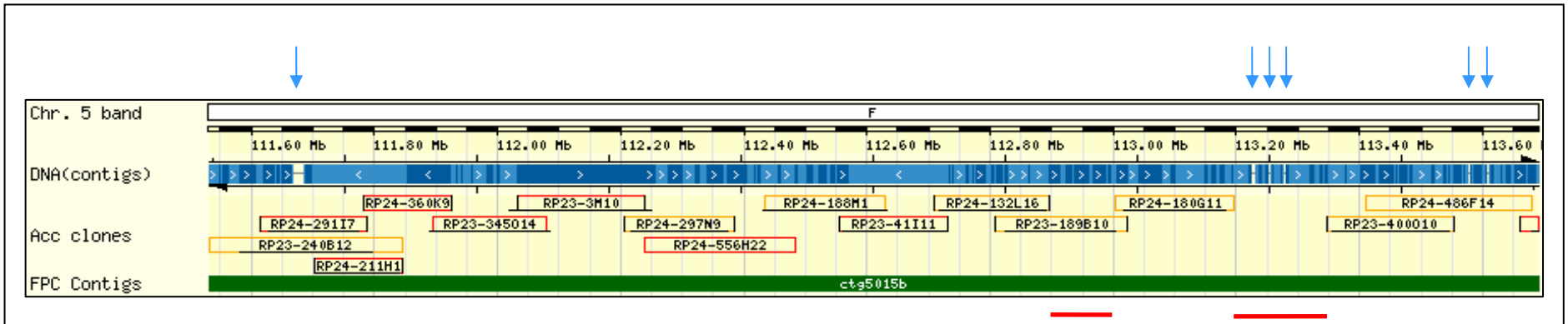

Figure 7.3: Map showing sequence and BAC coverage across the *bronx waltzer* candidate region, taken from Ensembl CytoView (http://www.ensembl.org).
Gaps in the DNA (contigs) represent areas where no sequence is available and are highlighted by **blue arrows**.
Accessioned clones are shown as red and yellow boxes, and gaps in the tiling path are highlighted by **red bars**. The clone RP23-189B10 has been "abandoned", and therefore does not represent part of the tiling path.
The region is contained within one single mapping contig – ctg5015b – suggesting that the gross structure and order of the interval has been well established.

7.1.2.2 Gene annotation

Gene annotation of the mouse genome has been based on a number of sources of information. Some genes were already well characterised as a result of earlier studies and could thus be immediately annotated. In other cases, the homology to EST and cDNA sequences or genes in other species can provide strong evidence for the annotation of a gene, although genes which are expressed at low levels or in very specific tissues or periods of development may be underrepresented when such an approach is used. A powerful tool in the annotation of genomes has been the development of gene prediction algorithms based on hidden Markov models (HMMs) and related models such as Genscan (Burge and Karlin 1997), GeneMark (Borodovsky and McIninch 1993) and FGENE (Solovyev *et al.* 1995). While none of these is foolproof, taken together they can provide analysis of potential splice sites, 5'-coding, internal exon, and 3'-coding regions, as well as taking into account GC content, CpG islands, promoter sites and open reading frames, amongst other indicators. This can provide additional evidence in the case of existing EST sequence, or can act as a hypothesis in a directed search for corroborating experimental evidence via systematic RT-PCR and sequencing. Historically, this type of analysis has lead to the over-prediction of genes as a result of the presence of pseudogenes within genomes. The development of dual-genome *de novo* predictors such as SLAM (Alexandersson *et al.* 2003) and TWINSCAN (Korf *et al.* 2001; Flicek *et al.* 2003) has helped to eliminate many such false positives (Brent and Guigo 2004)

7.2 METHODS

7.2.1 Template DNA samples

Exons were amplified using template DNA from a *bronx waltzer* mutant mouse (*bv*/*bv*) and a wild type control (+/+) mouse, both from the original *bronx waltzer* colony. Since the background on which *bv* is maintained is unknown, it was important to compare the mutant sequence to equivalent sequence from a wild type mouse on the same background rather than simply comparing it to the published sequence in order to eliminate the confusion caused by SNPs and other non-pathogenic variations between strains.

Since *bronx waltzer* is recessive, heterozygote (+/*bv*) and wild type (+/+) mice in the *bronx waltzer* stock are phenotypically indistinguishable. Therefore, as no genotyping tool exists for this mutation, test matings were established in order to identify a mouse carrying two unaffected *bv* alleles. In the first stage, two heterozygote mice were paired in order to give offspring which could be typed as either *bv*/*bv* if they manifested the *bronx waltzer* phenotype or as +/? if they did not. Second, +/? mice were paired with a male homozygous *bv*/*bv* mouse in a test mating to verify their genotype. If any of the offspring showed a *bronx waltzer* phenotype then they must have inherited a mutated allele from each parent, thus confirming that the uinknown genotype must be +/*bv*. Should all the offspring appear normal then they must all be inheriting a wild type allele from the unknown parent. After 21 classifiable births (offspring which survive and can be phenotyped) which all show no signs of the *bronx waltzer* phenotype, the genotype can be confirmed as +/+. This strategy is illustrated in Figure 7.4.

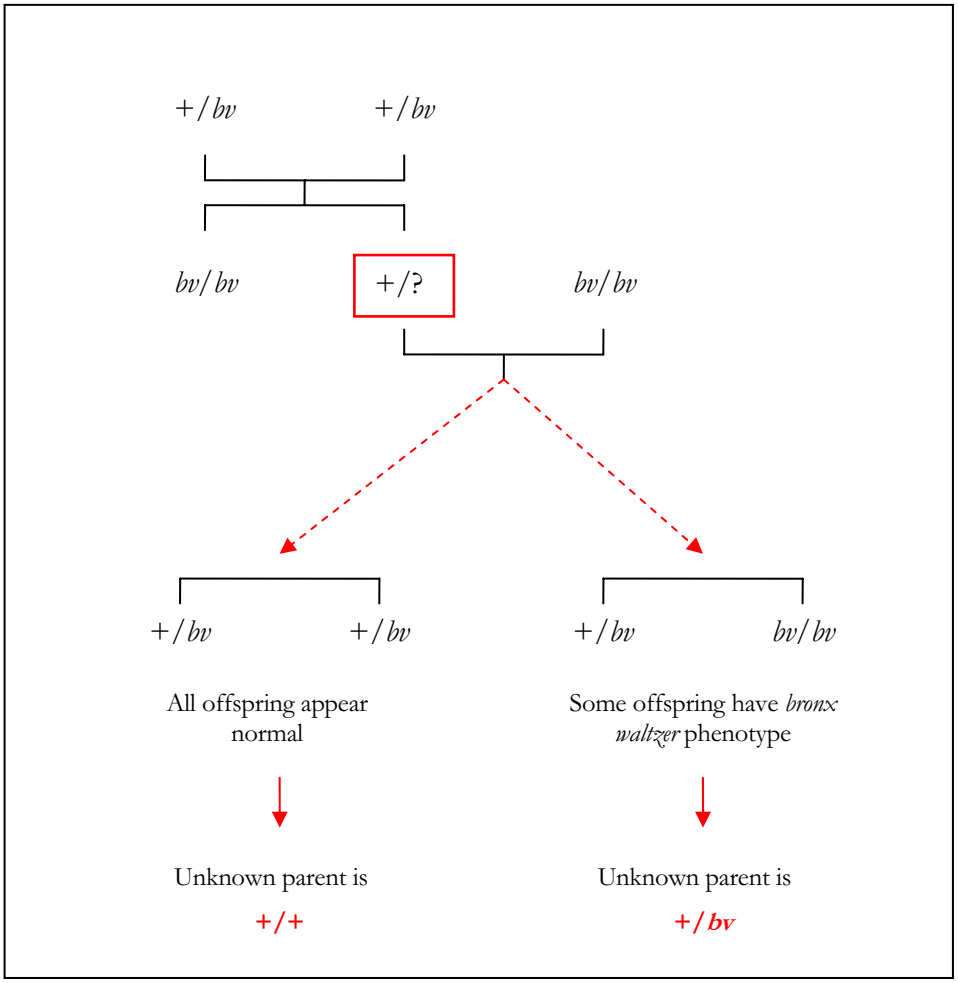

Figure 7.4: Mating strategy employed in the identification of a mouse from the *bronx waltzer* colony which could be confirmed as carrying two wild type copies of the *bv* allele.
Mice from a mating of two known *bronx waltzer* heterozygotes (+/*bv*) which do not manifest a phenotype may be either +/+ or +/*bv* and are designated +/? (red box). In order to determine their genotype, they can be mated with a *bronx waltzer* homozygous mutant, with the phenotype of their offspring revealing whether or not they carry a mutant *bv* allele.

In the case of *bronx waltzer*, three +/? females were paired with *bv/bv* males in order that the male could be removed from the cage before birth to avoid the problem of offspring being cannibalised by a hyperactive parent. Of these three females, two gave birth to offspring which were typed as *bronx waltzer* and thus their genotypes were confirmed as +/*bv*. One female gave birth to 24 offspring, of which 19 were classifiable (the remainder dying prior to being old enough to determine their phenotype) and all of which were normal in behaviour. Although this was two short of the 21 classifiable births required in order to definitively designate the mouse as +/+, the mating pair had stopped producing offspring and so tissue was taken for DNA extraction in the relative certainty that the genotype was +/+.

7.2.2 Large-scale primer design

The large number of amplicons required to obtain sequence for every gene in the *bronx waltzer* candidate region necessitated the employment of a semi-automated system for primer design. This was achieved using the primer design pipeline established at the Sanger Institute, which uses Ensembl Gene IDs to retrieve the flanking sequences of annotated exons. These are then processed in a similar manner to that employed by Primer3 (Rozen and Skaletsky 2000) with potential primers being screened for similarity to repeat sequences and for self-complementarity. All the primers used correspond to intron sequence such that coding sequence and intron/exon boundaries were examined for mutations.See Appendix C for primer sequences.

7.2.3 Nested PCR amplification

Those exons for which good quality sequence was not obtained in the first pass of amplification were then amplified using nested PCR. This method employs two rounds of PCR, with the second set of PCR primers lying within the fragment amplified by the first. Since these will only amplify from the desired sequence and not from any non-specific products generated in the

first round, the result is a higher quantity of a more specific product which in turn can be used as template DNA to give higher quality sequence traces with reduced background. This strategy is illustrated in Figure 7.5

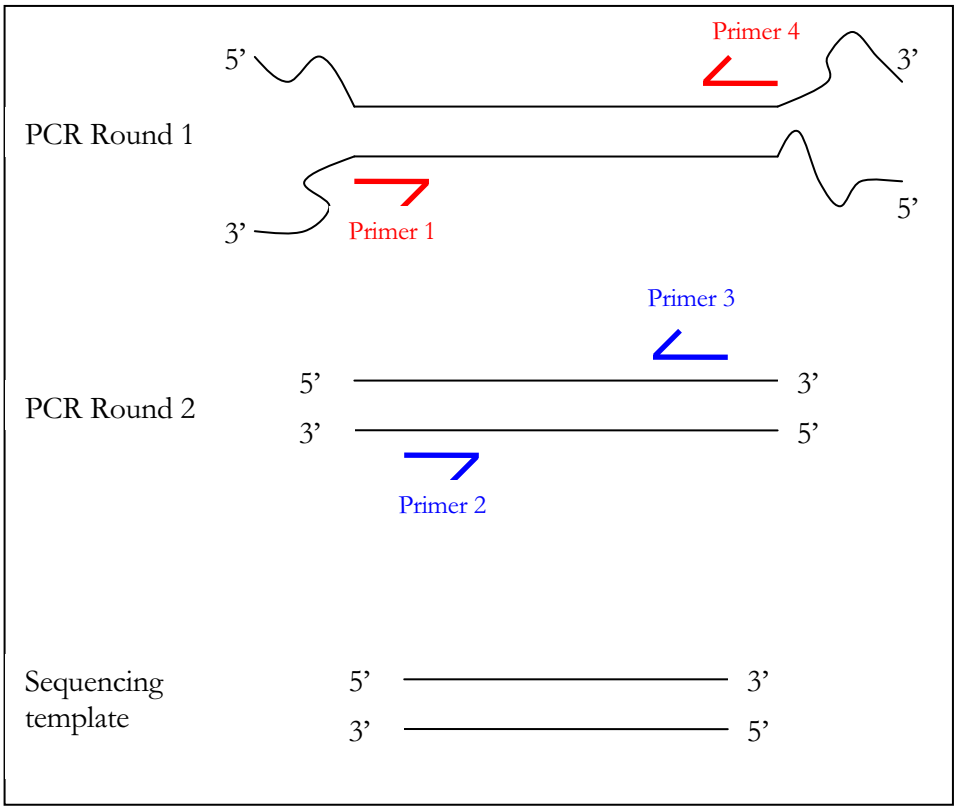

Figure 7.5: Nested PCR allows the elimination of non-specific products sometimes generated in single stage PCR which can give rise to poor quality sequence reads. The second round of PCR uses the product from the first round as template DNA, and the primers are designed to bind to sequence within the desired amplicon.

The design of nested PCR primers was carried out using LIMSTILL (LIMS for Identification of Mutations by Sequencing and TILLING; http://limstill.niob.knaw.nl/), an open-source software developed by the Hubrecht Laboratory (Netherlands). This allows querying of the Ensembl database for the selection of exons for amplification, followed by primer design using a Perl/CGI interface. Primer sequences are given in Appendix C.

The first round of PCR was carried out using the standard PCR protocol described in Section 2.4. In the second round of PCR, the concentration of primers was limited in order to generate final products of roughly equal concentrations, allowing the subsequent sequencing reactions to be performed at optimal concentration and thus giving higher quality sequence. In this study, primers were diluted to a concentration of between 100 – 130nM to give an approximate amplicon concentration of 115nM.

7.2.4 Sequence analysis

DNA sequencing was carried out as described in Section 2.8 and the sequence reads analysed using the software package Gap4 (Bonfield *et al.* 1998). Analysis consisted of the creation of a database containing all the sequence reads for a given gene alongside a reference flat file exported from Ensembl which included the annotated positions of exons. These sequences were then assembled into contigs and examined for differences between those originating from a *bv* mutant template and those amplified from the wild type control. A list of every exon within the candidate region was created and annotated with details of the sequence coverage obtained. Coverage of each exon in both DNA samples was preferred, but where a region was not covered by wild type sequence and the mutant sequence matched that of the published strain, the exon was considered to be covered. Where partial sequence of an exon was obtained, the distance remaining was recorded and the percentage of base pairs covered for each gene was calculated.

7.3 RESULTS

7.3.1 Sequence coverage

A list was compiled of all the annotated exons within the *bv* candidate region. This spans the distance between the flanking markers DASNP3 and D5Mit209 and extends from 111609074bp to 114063755bp of chromosome 5 in Mouse Ensembl Build33. Where more than one alternative transcript was given for a particular gene, each unique exon was only included once with the largest being selected where they differed in size. Coding sizes of each exon were obtained, with untranslated exons assigned a value of zero, and these were used to calculate the figure for the total number of coding base pairs within the region. At the time of writing, the region contains 534 exons which constitute 52 genes and include 72523 base pairs of coding sequence.

Following the first round of primer design and sequencing, approximately 72% of the coding exons had good sequence coverage, but only four genes were fully sequenced. It was thus necessary to carry out a second round using the modifications describe in section 7.2.3 to improve the quality of the data. Following this step, 91% of coding exons had good coverage and 22 genes were fully sequenced. The total number of base pairs covered using both sets of data was 65608bp, representing 90.5% of the total coding sequence within the region. Examples of the sequence obtained by both approaches are given in Figure 7.6, and the sequence coverage obtained for each gene within the candidate region is represented in Figure 7.7.

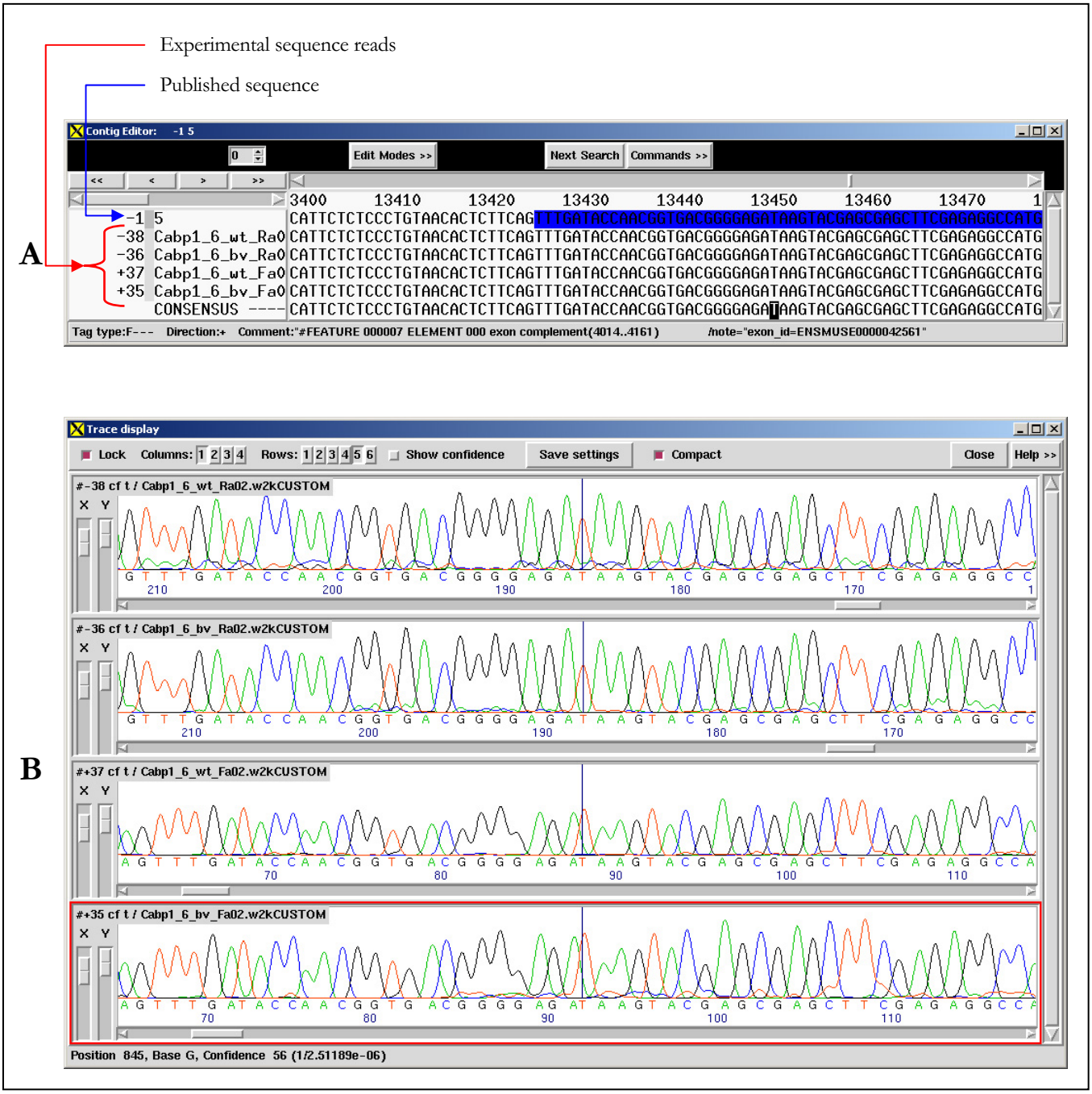

Figure 7.6: Screenshots from the software package gap4, illustrating the manner in which sequence reads were analysed.
In the Contig Editor (A), the forward and reverse sequence reads obtained from wild type and mutant templates are aligned to each other and to the published sequence for comparison. Exons annotated onto the published sequence are highlighted in blue and the exon identifier is shown in the data bar at the bottom of the screen, making assessment of exon coverage relatively simple. Any discrepancies between the sequence reads are also automatically highlighted any which occur can be examined by visualising the sequence reads in the Trace Display window (B).

Figure 7.7: (Overleaf)
Sequence coverage obtained for genes within the *bronx waltzer* candidate region.
Exons are represented as coloured boxes, with those for which *bv* mutant sequence has been obtained and analysed shown in **DARK RED** (for known genes) or **BLACK** (for predicted genes). Exons for which partial sequence is available are shown in **GREEN**, and those which are unsequenced are represented in **BLUE**.
The diagrams and figures represent coding sequence only. Sequencing of untranslated regions (**YELLOW**) was attempted but the data is not shown.
The direction of transcription is shown by a black arrow, with those reading left to right being annotated on the plus strand and those reading left to right on the minus strand.
Genes are given in the order in which they are annotated along chromosome 5, from the centromeric to the telomeric end of the region. Graphical representations of the genes are taken from Ensembl Build33.
Genes marked by an asterisk were not annotated at the time of primer design, and therefore no sequencing of these has been attempted.

Gene name and structure	Coding sequence (bp)	Sequence covered (bp)	% coverage
Acetyl-coenzyme A carboxylase beta 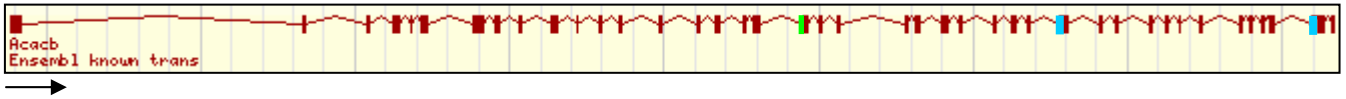	7373	7136	96.8%
Forkhead box protein N4 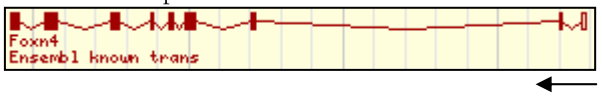	1557	1557	100%
Myosin 1h 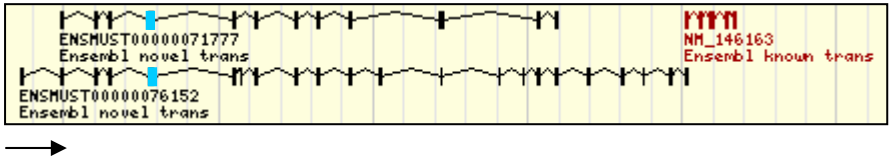	2846	2766	97.2%
Potassium channel tetramerization domain-containing 10 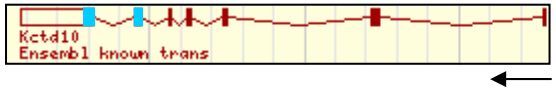	933	623	66.8%
Ubiquitin protein ligase E3B 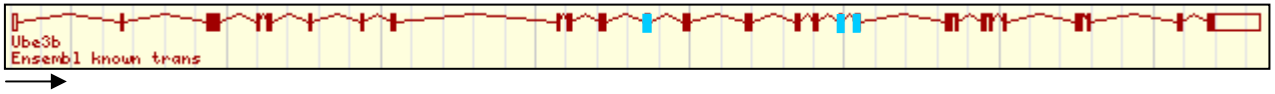	3187	2797	87.8%
Methylmalonic aciduria type B homolog 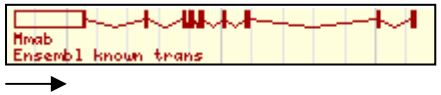	735	735	100%
Melavonate kinase 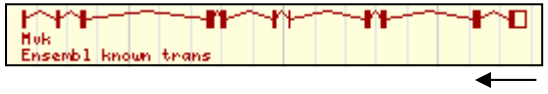	1178	1178	100%

Gene name and structure	Coding sequence (bp)	Sequence covered (bp)	% coverage
ENSMUSG00000041930 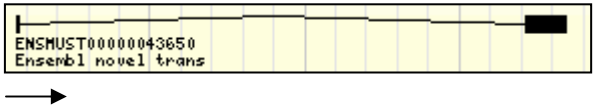	1362	1362	100%
Transient receptor potential cation channel V4 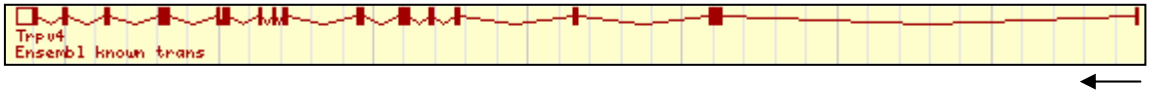	2601	2601	100%
Glycolipid transfer protein 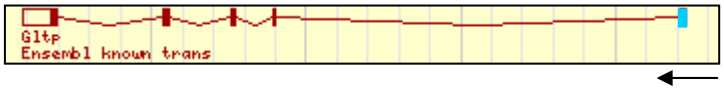	625	523	83.7%
NM_029992 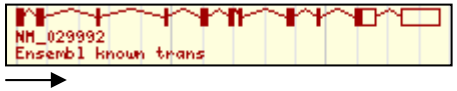	1379	1379	100%
G protein-coupled receptor kinase-interactor 2 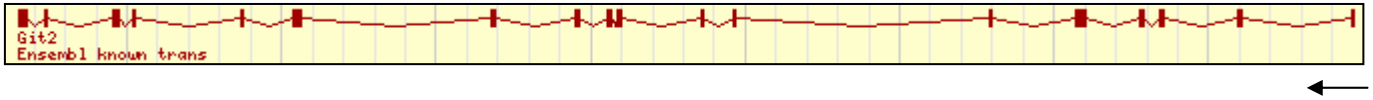	2126	2126	100%
NM_175120 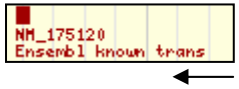	374	374	100%
Q9D1S6 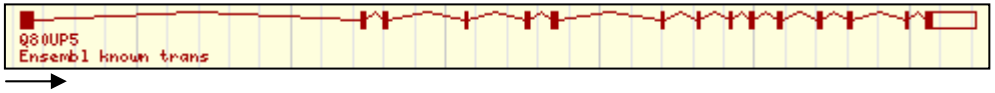	2031	2031	100%

Gene name and structure	Coding sequence (bp)	Sequence covered (bp)	% coverage
NM_181075 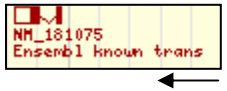	418	418	100%
NM_026263 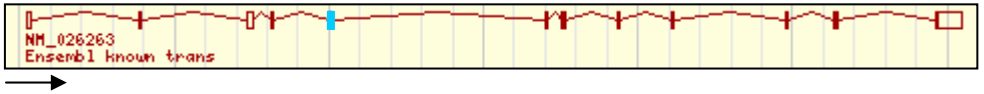	547	463	84.6%
Q8C864 * 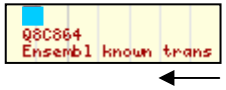	482	0	0%
2'-5'-oligoadenylate synthetase like protein 2 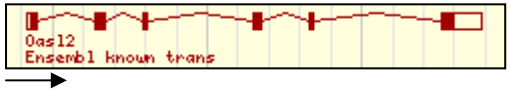	1398	1398	100%
2'-5' oligoadenylate synthetase-like 1 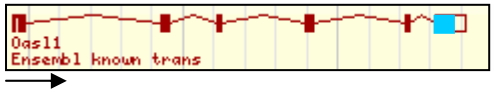	1530	1030	67.3%
NM_028211	765	765	100%
Hepatocyte nuclear factor 1-alpha 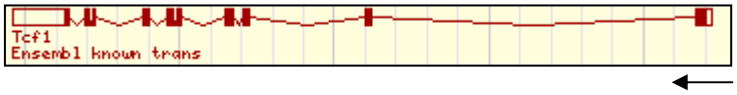	1877	1877	100%

Gene name and structure	Coding sequence (bp)	Sequence covered (bp)	% coverage
ENSMUSG00000044804 * 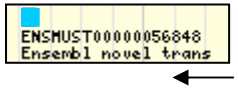	378	0	0%
Upregulated during skeletal muscle growth 3 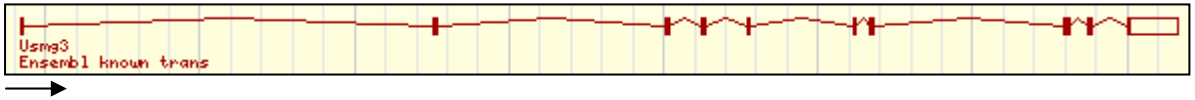	1345	1345	100%
60S ribosomal protein L37 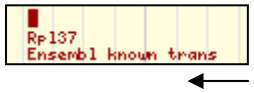	293	293	100%
Acyl-CoA dehydrogenase, short-chain specific 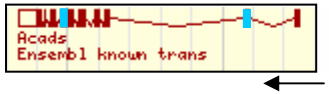	1229	929	75.6%
NM_175352 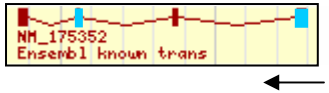	712	362	50.8%
NM_175403 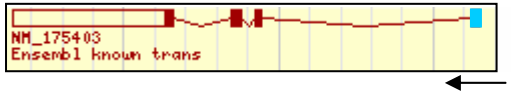	871	640	73.5%
Calcium-binding protein 1 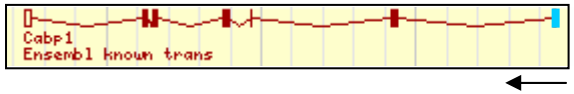	680	636	93.5%

Gene name and structure	Coding sequence (bp)	Sequence covered (bp)	% coverage
Processing of precursor 5, ribonuclease P 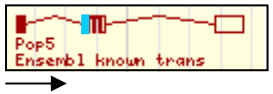	516	379	73.4%
Ring finger protein 10 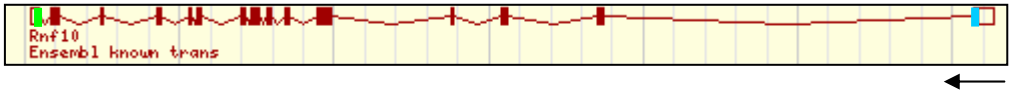	2398	2255	94%
D5Ertd33e 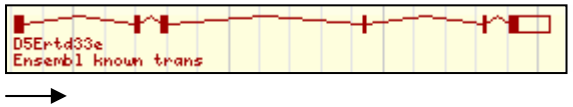	977	977	100%
Dynein light chain 1, cytoplasmic 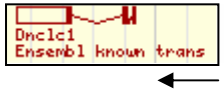	268	268	100%
Splicing factor, arginine/serine rich 9	665	475	71.4%
NM_029645	465	465	100%
Q8C4H9 * 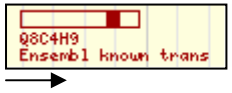	341	341	0%

Gene name and structure	Coding sequence (bp)	Sequence covered (bp)	% coverage
15E1_MOUSE 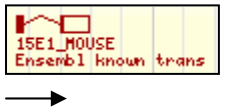	229	229	100%
Cytochrome c oxidase polypeptide VIa-liver 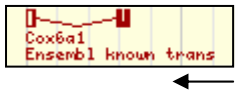	336	336	100%
Musashi homolog 1 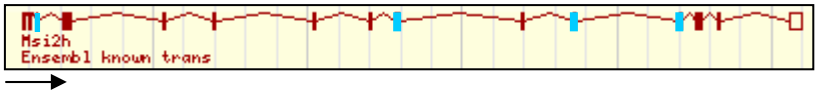	1016	736	72.4%
Q9D2I7 * 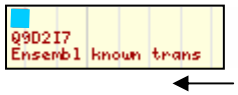	464	0	0%
Phospholipase A2 precursor 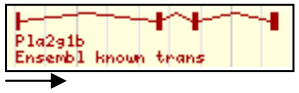	437	437	100%
NAD-dependent deacetylase sirtuin 4 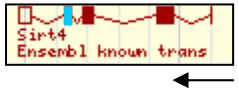	990	781	78.9%
Paxillin alpha 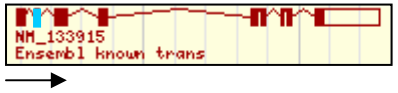	1787	1672	93.6%

Gene name and structure	Coding sequence (bp)	Sequence covered (bp)	% coverage
General control of amino-acid synthesis 1-like 1 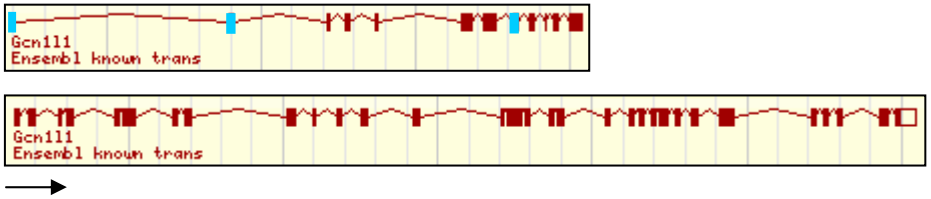	6752	6614	98%
NM_198163 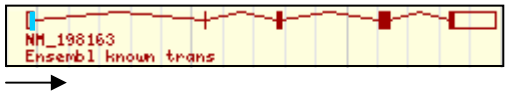	600	549	91.5%
Q8R1D2 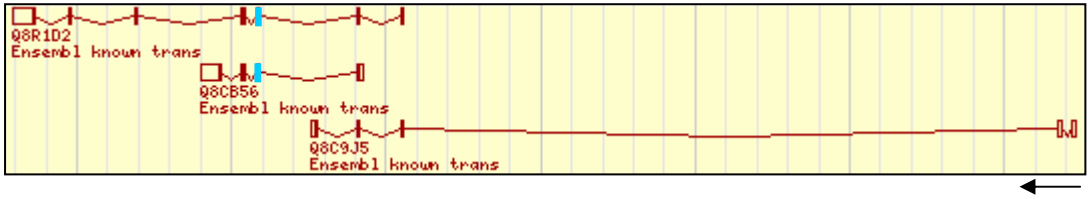	2239	2109	94.2%
60S ribosomal protein L29 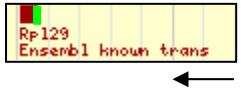	482	392	81.3%
Citron protein 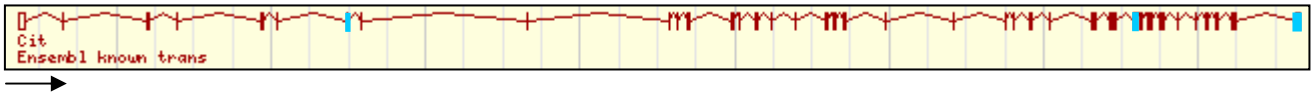	6220	5859	94.2%

Gene name and structure	Coding sequence (bp)	Sequence covered (bp)	% coverage
5'-AMP-activated protein kinase, beta-1 subunit 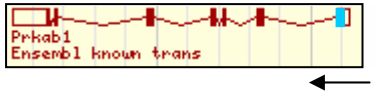	808	648	80.4%
NM_177759 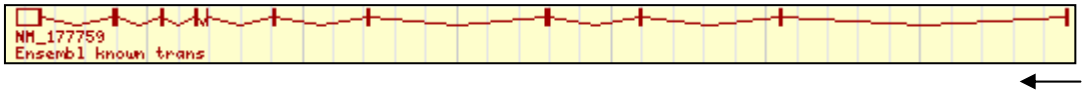	1432	1432	100%
Q9D4T7 * 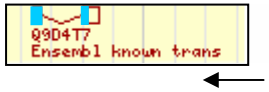	340	0	0%
Heat-shock protein beta-8 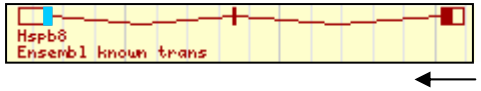	588	429	72.9%
NM_026886 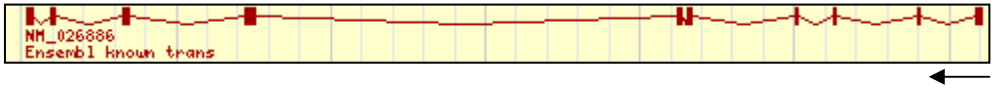	1343	1343	100%

7.3.2 Sequence polymorphisms

During the analysis of sequence data, several polymorphisms were identified. In several locations, polymorphisms were found where the *bronx waltzer* mutant and wild type sequences matched each other but differed from the published sequence. These variations included coding and non-coding SNPs, as well as a number of tandem repeat copy number variations, examples of these are shown in Figure 7.8.

In addition, in a localised portion of the candidate region centred on the gene Citron, a number of polymorphisms were identified where the *bronx waltzer* and wild type sequences differed from each other. These are described and illustrated in Table 7.2. All of these coding nucleotide substitutions were silent, resulting in no change to the peptide sequence.

A – Tandem repeat copy number variation

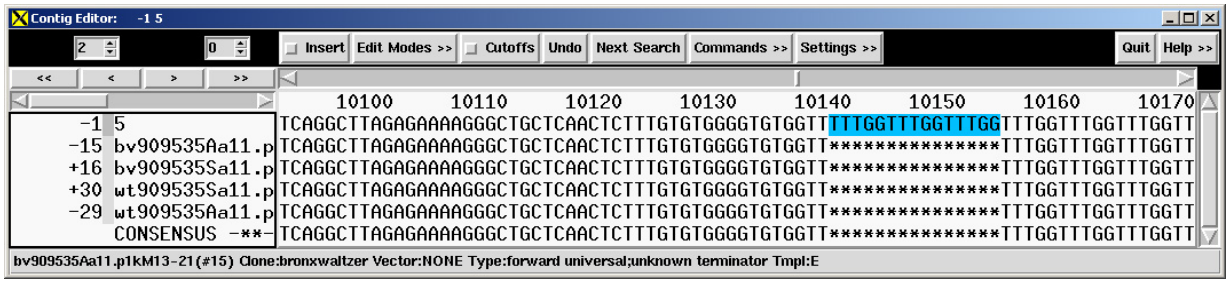

B – Coding SNP

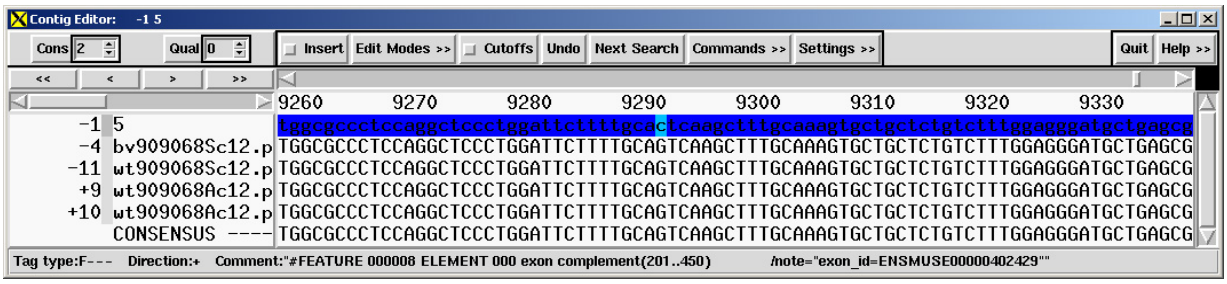

C – Non-coding SNP

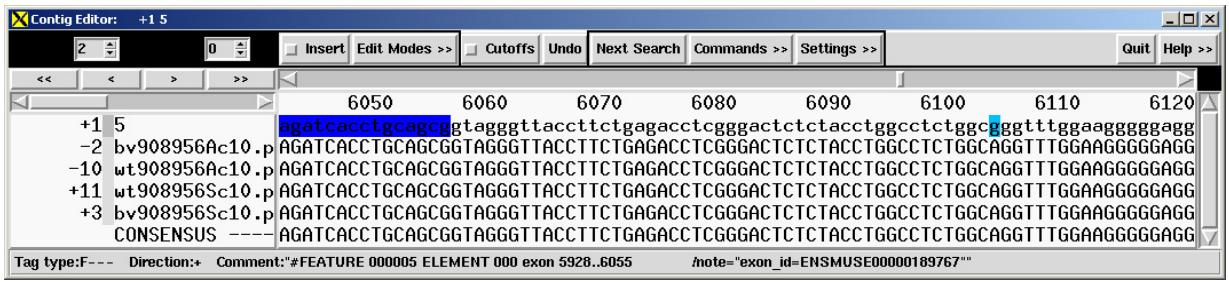

Figure 7.8: Examples of polymorphisms identified between the *bv* genetic background and the published sequence. In each case the published sequence is shown as the top line and assigned the identifier "5". Exonic sequence is highlighted in **ROYAL BLUE**, while discrepancies between the sequences are highlighted in **SKY BLUE**.

Polymorphism	1	2	3	4	5	6
Exon	ENSMUSE00000464783	ENSMUSE00000462386	ENSMUSE00000265597	ENSMUSE00000265591	ENSMUSE00000499740	ENSMUSE00000265576
Chromosomal location	113364973	113367988	113388242	113395210	113396084	113398326
Location relative to exon	Downstream	Coding	Coding	Downstream	Coding	Upstream
bv allele	T	A	A	C	C	G
wt allele	C	G	C	T	T	T
Sequence traces *bv* wt	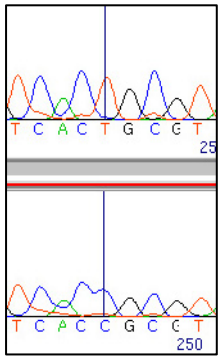	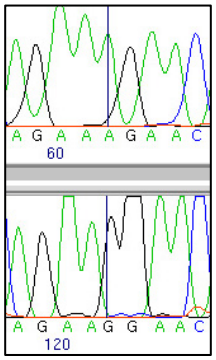	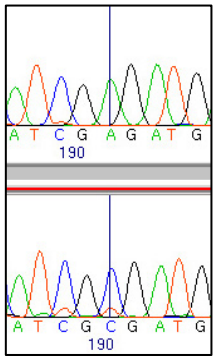	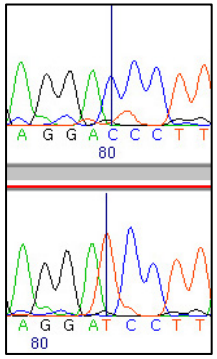	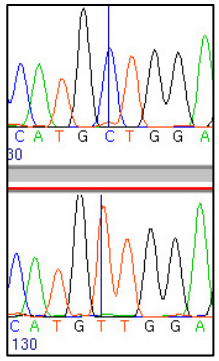	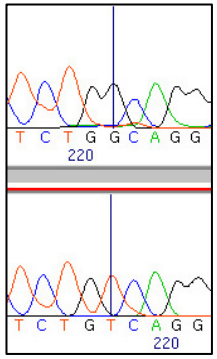
Codon change	-	AAA → AAG	CGA → CGC	-	CTG → TTG	-
Amino acid change	-	K → K	R → R	-	L → L	-
Consequence	-	Silent	Silent	-	Silent	-

Table 7.2: Locations, alleles and effects of SNPs identified between the bv/bv sequence and +/+ sequence from the same genetic background (continued overleaf). All of these polymorphisms are located within either introns or exons of the gene Citron.

Polymorphism	**7**	**8**	**9**	**10**	**11**	**12**
Exon	ENSMUSE00000265562	ENSMUSE00000265546	ENSMUSE00000265528	ENSMUSE00000264882	ENSMUSE00000264868	ENSMUSE00000264854
Chromosomal location	113406661	113409285	113412602	113421086	113422608	113424716
Location relative to exon	Upstream	Downstream	Downstream	Coding	Downstream	Coding
***bv* allele**	A	A	G	C	T	C
wt allele	C	G	A	T	A	T
Sequence traces ***bv*** **wt**	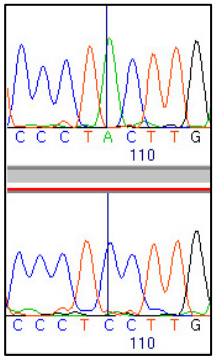	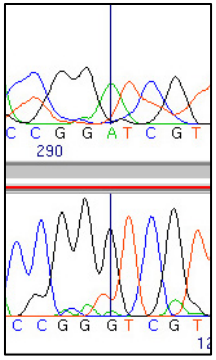	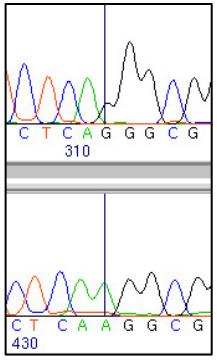	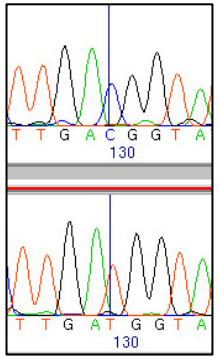	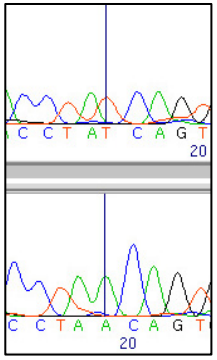	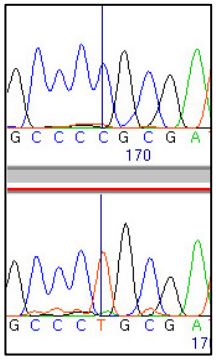
Codon change	-	-	-	GAC → GAT	-	CCC → CCT
Amino acid change	-	-	-	D → D	-	P → P
Consequence	-	-	-	Silent	-	Silent

7.4 DISCUSSION

7.4.1 Sequence coverage

Following two rounds of primer design and sequencing, a total of 65729 base pairs of coding sequence, representing 90.63% of that lying within the *bv* candidate region have been successfully sequenced in the *bronx waltzer* mutant mouse genome. The use of nested PCR primers in the second round allowed a significant improvement in the level of sequence coverage, since the resulting sequence reads were longer and more consistent. In order to achieve full sequence coverage a number of further steps could be taken. Initially, the PCR conditions for the existing primer sets could be altered in an attempt to amplify a product of high enough concentration and specificity for sequencing. Initial adjustments could include alteration of the annealing temperature and magnesium concentration. In the case of fragments in regions with high GC content or secondary structure, modifications such as increasing the denaturation temperature, the addition of DMSO and betaine, or linearisation of the template can help to prevent polymerase slippage. There are many GC-rich PCR kits available which perform these functions, as well as including a proofreading enzyme to maximise the chances of obtaining a specific PCR product. Exons which still fail primer design or amplification from genomic DNA could then be amplified instead from a cDNA template using primers designed in adjacent exons. This would circumvent any problematic intronic repeat regions which cause difficulties in amplification and sequencing, or regions where no sequence is available and therefore primers cannot be designed. Finally, exons for which a PCR product can be obtained but which prove difficult to sequence may be subcloned into a vector in order to minimize the amount of high GC template and reduce the opportunity for stable secondary structures to form. In addition, T7 and SP6 primers can then be used in the sequencing reactions, thus eliminating any issues with the suitability of the PCR primers for use in sequencing.

7.4.2 Candidacy of genes following re-sequencing

No mutations have so far been discovered in the *bv* candidate region, and thus the gene responsible for the mutation has not been identified, although the coding regions of 23 genes have been fully sequenced in the mutant genome, although it is not possible to completely rule out the involvement of these genes since a pathogenic mutation may lie in a regulatory element (see Section 7.1.1.2). Indeed, given the highly specific nature of the *bronx waltzer* phenotype, it is plausible that the mutation may lie in a regulatory element controlling expression of the gene in the cell types affected – that is the inner hair cells of the organ of Corti and the hair cells of the vestibular system. The implications of this are discussed further in Section 9.1.3. Even so, the successful resequencing of the complete coding region of a gene can be said to significantly reduce the probability of its being the causative agent for the *bronx waltzer* phenotype. Those genes for which full coding sequence has been obtained are listed below in Table 7.3.

Gene symbol	Description
Foxn4	Forkhead box protein N4
Mmab	Methylmalonic aciduria type B homolog
Mvk	Melavonate kinase
ENSMUSG00000041930	n/a
Trpv4	Transient receptor potential cation channel V4
NM_029992	n/a
Git2	G protein-coupled receptor kinase-interactor 2
NM_175120	n/a
Q9D1S6	n/a
NM_181075	n/a
Oasl2	2'-5'-oligoadenylate synthetase like protein 2
NM_028211	n/a
Tcf1	Hepatocyte nuclear factor 1-alpha
Usmg3	Upregulated during skeletal muscle growth 3
Rpl37	60S ribosomal protein L37
D5Ertd33e	n/a
Dnclc1	Dynein light chain 1, cytoplasmic
NM_029645	n/a
15E1_MOUSE	n/a
Cox6a1	Cytochrome c oxidase polypeptide VIa-liver
Pla2g1b	Phospholipase A2 precursor
NM_177759	n/a
NM_026886	n/a

Table 7.3: Genes within the *bv* candidate region for which full coding sequence has been obtained and no mutations have been identified. Those highlighted in **RED** were previously assessed as being good candidates for *bronx waltzer* (see Chapter 5).

Of the remaining 29 candidate genes, 24 are partially sequenced and 5 have no sequence available. These 5 consist of small, generally single-exon transcripts which were annotated subsequent to the second round of primer design and thus no attempt has been made to sequence them. As such, the next round of sequencing is likely to result in sequence coverage for these predicted transcripts. However, analysis of the evidence supporting their annotation (Table 7.4) suggests that most of them are unlikely candidates. Four out of the five are supported by only one cDNA clone, do not share similarities with ESTs from other species and do not match any protein domains in the protein families database Pfam (http://www.sanger.ac.uk/Software/Pfam/). This suggests that they may be the result of genomic contamination in the cDNA library, and therefore do

not represent true transcripts. They are therefore very unlikely to be involved in the causation of the *bronx waltzer* phenotype. The exclusion of these four genes leaves 25 genes with partial sequence coverage which may harbour a mutation within their coding regions.

Predicted Gene	Supporting evidence	Analysis
Q8C864	1 mouse cDNA clone No hits in other species No Pfam domains predicted	Possible false transcript
ENSMUSG00000044804	9 mouse cDNA clones Hits in other species Pfam predicts ribosomal protein S12	Good supporting evidence, probably genuine transcript
Q8C4H9	1 mouse cDNA clone No hits in other species No Pfam domains predicted	Possible false transcript
Q9D2I7	1 mouse cDNA clone Weak hit to rat cDNA No Pfam domains predicted	Possible false transcript
Q9D4T7	1 mouse cDNA clones Weak hit to rat EST No Pfam domains predicted	Possible false transcript

Table 7.4: Summary of evidence in support of newly annotated, unsequenced transcripts. Data is collated from Ensembl entries, BLAST searches against the EST database and from Pfam.

7.4.3 Sequence polymorphisms

During the analysis of sequence data, a number of differences were identified between the *bronx waltzer* genetic background and the published mouse sequence derived from the strain C57Bl/6J, which either represent errors in the sequence reads or genuine polymorphisms between the two strains. These observations reinforce the importance of carrying out sequencing not only in the mutant *bv* mouse but also in the wild type congenic genome in order to eliminate the possibility of mistaking a polymorphism for a mutation. Future studies should utilise these data by carrying out sequencing of the putative polymorphism sites in 101/H, the strain used for the mapping backcross (see Chapter 3), in the hope that some may prove useful as markers in reducing the size of the critical region.

The second class of polymorphisms identified, those which differed between the *bv* mutant and wild type congenic genomes, represent an interesting finding. These 12 sites were extremely localised, with all of them occurring within sequence reads designed to amplify exons from the gene *Citron*. In every case, the *bv* allele matched that reported in the published mouse sequence derived from the strain C57Bl/6J (Waterston *et al.* 2002). Five of them were located within coding sequence and for each of these, the wild type allele matched the accessioned sequence for the gene (NM_007708), which was derived from the strain CD-1 (Holzman *et al.* 1994; Di Cunto *et al.* 2000).

Firstly, the identification of homozygous differences between the *bronx waltzer* mutant and congenic wild type DNA samples supports the assumption that the wild type sample is truly homozygous for the wild type allele, which is useful since the mouse from which the sample was taken did not quite reach the number of certifiable births required in order to be confidently pronounced +/+ (see Section 7.2.1).

More interesting is the possibility that the cluster of polymorphisms represents a localised region of non-recombination where the otherwise seemingly homogenous *bronx waltzer* genetic background has maintained some of the sequence variation introduced throughout successive generations of breeding. The *bv* mutation arose spontaneously on an unknown background in 1979 and has since been crossed to various other unrecorded strains. The colony used in this study has been maintained within a closed colony for 25 years, and although it is not "inbred" since brother-sister matings are not always possible, is likely to have become relatively homogenous, especially since several "bottle-necks" where few mice of breeding age were available have meant a reduction in genetic variation. This is supported by the evidence of this exon re-sequencing project, during which no other polymorphisms were identified between the two samples. Evidently, throughout the breeding process the original *bv* allele has been maintained and selected for over each generation, presenting the possibility that the localised region of

polymorphisms identified around *Citron* may represent a portion of the *bronx waltzer* genome which has remained intact because it lies very close to the mutation and has thus been preserved in its original state, while the wild type alleles represent a strain to which the mutant mouse was crossed at some point in its history. In this scenario, the polymorphisms could be described as being in linkage disequilibrium with the mutation, that is, they co-segregate more frequently than might be expected if they were un-associated with it. In order to test this hypothesis, the simplest approach would be to carry out a screen of archived DNA samples from the *bronx waltzer* colony which have been collected over the years and establish whether the polymorphisms do indeed segregate with the mutation, effectively exploiting the background sequence variation to employ the breeding colony as a mapping cross.

It is also possible that the recombination events which gave rise to this localised region of sequence variation occurred before the mutation arose, and that the whole region has been conserved. However, the existence of 15 mice with recombinations within the candidate region defined by the *bv*/101 mapping cross, and the correlation of 1.77cM to 2.45Mb of physical distance (a ratio of 1:1.4, compared to the average 1:6 across mouse chromosome 5) suggests that this region generally undergoes recombination at relatively normal rates. This would imply that the localised region which has maintained these polymorphisms has done so independently of the rest of the candidate region, and its uniqueness is suggestive of an association with the *bv* locus.

It may seem beneficial to screen the inbred strain 101/H for these polymorphisms in the hope that the alleles may differ, making them useful as markers in the mapping cross to help narrow down the critical region. However, this would only be possible if it is found that the polymorphisms co-segregate with the mutation since any variability in the homozygous *bv*/*bv* mutant background would make it impossible to differentiate between that and the inbred strain. In this situation, where the polymorphisms prove to be co-segregating or even non-recombinant with the mutation throughout the

breeding colony, the likelihood is that the markers would also be non-recombinant in the mapping cross and would thus add no new informative data. Nonetheless, in the absence of any other useful markers within the region, the nature of these should be fully investigated.

In order that this study can be more brought to completion more comprehensively, it is imperative that the quality of genome sequence and gene annotation within the region is improved. This would allow fully sequenced genes to be excluded more confidently since their full structure would be known, and may also bring to light novel genes which are as yet un-annotated and as such have not yet been sequenced. To this end, negotiations are underway to prioritise the finishing of the clones in the tile path already selected for HTGS, and to select and sequence new clones to fill the two tiling path gaps. Once this has been achieved, manual annotation of the region will be carried out and higher quality sequence coverage of the region will be made possible.

Chapter 8:

Modifiers of the

bronx waltzer *mutation*

CHAPTER 8

MODIFIERS OF THE *BRONX WALTZER* MUTATION

8.1 INTRODUCTION

8.1.1 Variability in the *bronx waltzer* phenotype

Although the phenotype of *bronx waltzer* mice has been well described (see Section 1.4), studies over the years have pointed to a level of variability in the severity of the mutation when manifested on different genetic backgrounds. In particular, the number of surviving inner hair cells in the organ of Corti in *bv/bv* mutants has been observed to range from as low as 5% (Keithley and Feldman 1983) to as high as 30% (Schrott *et al.* 1989). In addition, variability has been observed in the occurrence and frequency of atypical hair cells, these being hair cells with the appearance of outer hair cells but which are located in the inner hair cell row.

During the initial mapping of *bv*, a backcross to *Mus castaneus* gave rise to *bv/bv* homozygotes with variable and often significantly reduced behavioural phenotypes (Bussoli and Steel, unpublished observations). While this rendered the backcross inappropriate for genetic mapping purposes owing to the difficulty in determining the genotype of the mice at the *bv* locus by behavioural observation, it suggests that the *Mus castaneus* genome may contain one or more dominant modifiers of the *bronx waltzer* phenotype. This is an interesting proposition, since the identity of the *bv* gene is unknown and thus so are the pathways within which it operates. The identification of molecules which exert a modifying effect on the manifestation of the *bronx waltzer* phenotype may well provide clues to the function of the gene itself.

8.1.2 A backcross to *Mus castaneus*

In a previous study, Nogueira (2000) generated a backcross [(*bv*/*bv* x *Mus castaneus*) F1 x *bv*/*bv*] of 241 mice and performed behavioural tests to assess the severity of the phenotype in the mice as compared to a control panel consisting of 14 F1 (+/*bv*) mice, 15 *bronx waltzer* (*bv*/*bv*) mice and 14 *Mus castaneus* (+/+) mice. The tests were carried out on mice aged six to seven weeks and were based on the standard battery developed by Hardisty *et al.* (1997) to provide a quantitative measure of vestibular abnormalities. They included behavioural observation in an open field arena, contact righting response, reaching response and a test for swimming ability, with each mouse being assigned a score of 1 for behaviour similar to that expected from wild type mice and a score of 0 if their behaviour matched that of *bv*/*bv* mice. In addition the Preyer reflex was tested using a click-box as an assessment of hearing ability, with a strong reflex being scored as 2, a weak one as 1 and an absent one as 0. As an example of the variability in phenotype, Figure 8.1 shows some of the results from the open field test. The number of squares traversed is used as a measure of the hyperactive behaviour which is often exhibited by mice with vestibular dysfunction. Wild type mice tend to investigate cautiously, traversing a relatively small number of the marked squares and keeping to the outside of the space. This can be seen in Figure 8.1 where very few of the F1, *Mus castaneus* or heterozygote mice from the backcross traversed more than 299 squares. The heterozygous backcross mice showed a very restricted distribution to between 0 and 199 squares, while the homozygous mutant backcross mice showed a broad variation. Some of them traversed more than 1000 squares whilst others entered fewer than 100, overlapping with the number of squares traversed by heterozygous mice. The swimming, contact righting and reaching response tests each showed clear evidence of variation within the group of homozygous backcross mutants (data not shown).

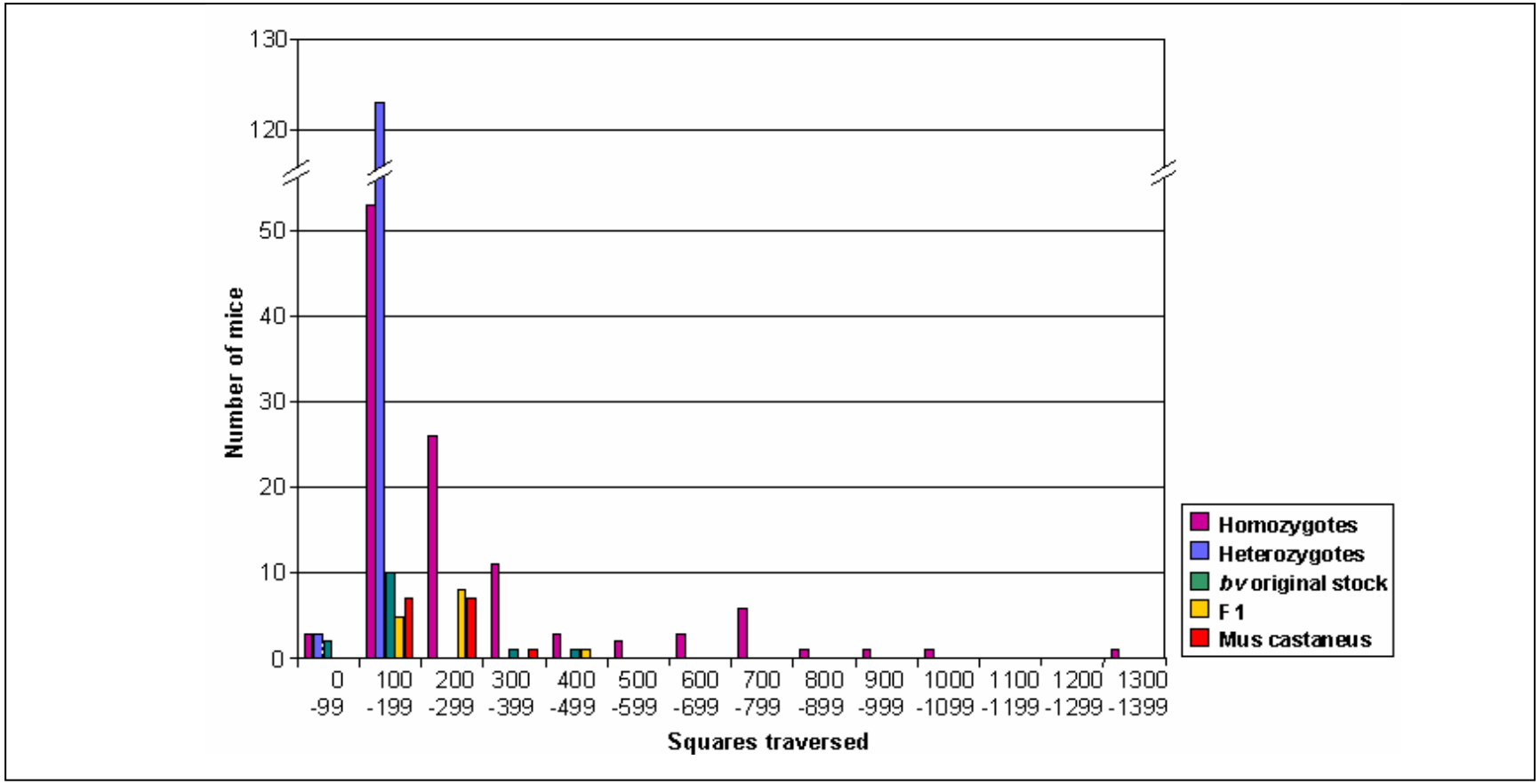

Figure 8.1: Bar chart illustrating the number of squares traversed by mice originating from the *bronx waltzer/Mus castaneus* backcross as compared to control mice in an open field arena. Homozygous mutants from the *bv/cast* backcross show a very wide distribution for this trait, several behaving similarly to control mice while others traverse many more squares than mice from the original *bv* stock. Data from Nogueira (2000).

8.1.3 Linkage analysis of behavioural trait modifiers

The behavioural testing was carried out blind to genotype, with typing later carried out on DNA samples from each mouse using the flanking markers from the *bv*/101 backcross, *D5Mit25* and *D5Mit209*. Linkage analysis was initially performed on the 30 homozygous backcross mice with the highest and lowest total scores in the hearing and balance tests. This approach was adopted because selection of individuals with extreme phenotypes as opposed to genotyping all the individuals significantly increases power over random sampling to detect linkage with modifiers (Lander and Botstein 1989; Darvasi *et al.* 1993; Darvasi and Soller 1994; Darvasi 1997). A genome scan using 76 simple sequence repeat length polymorphic markers was carried out on these 30 mice in order to determine linkage to modifiers, and the markers *D4Mit27*, *D5Mit101*, *D5Mit408*, *D12Mit274* and *D12Mit64* exhibited a significant, low P-value (below 0.05) while *D4Mit125*, *D9Mit224* and *D17Mit49* exhibited a slightly higher P-value (between 0.05 and 0.1) using the χ^2 test.

In the second stage of modifier analysis, markers exhibiting nominal significance ($p<0.1$) in the initial genome scan (chromosomes 4, 5, 9, 12 and 17), together with further polymorphic markers in these regions, were typed in the total set of 113 homozygous backcross *bv*/*bv* mice. Mapmaker QTL (Lander *et al.* 1987) analysis for each of the traits was carried out at this stage rather than the χ^2 test. In this analysis of linkage, a probability (P) $\leq 1.0 \times 10^{-4}$ (LOD 3.3) was considered as significant linkage and a $P \leq 3.4 \times 10^{-3}$ (LOD 1.9) as suggestive linkage (Lander and Schork 1994; Lander and Kruglyak 1995). Of the nine traits analyzed over the five chromosomes, ten combinations showed suggestive or significant linkage indicating the possible location of modifier loci. LOD score plots representing these loci are presented in Figure 8.2. Only LOD scores at a distance of 0cM from each marker used are plotted, because Mapmaker QTL otherwise maximizes predicted LOD scores between markers. The percentage of the variance of

the trait explained by the genotype at each marker is given at the top of each plot.

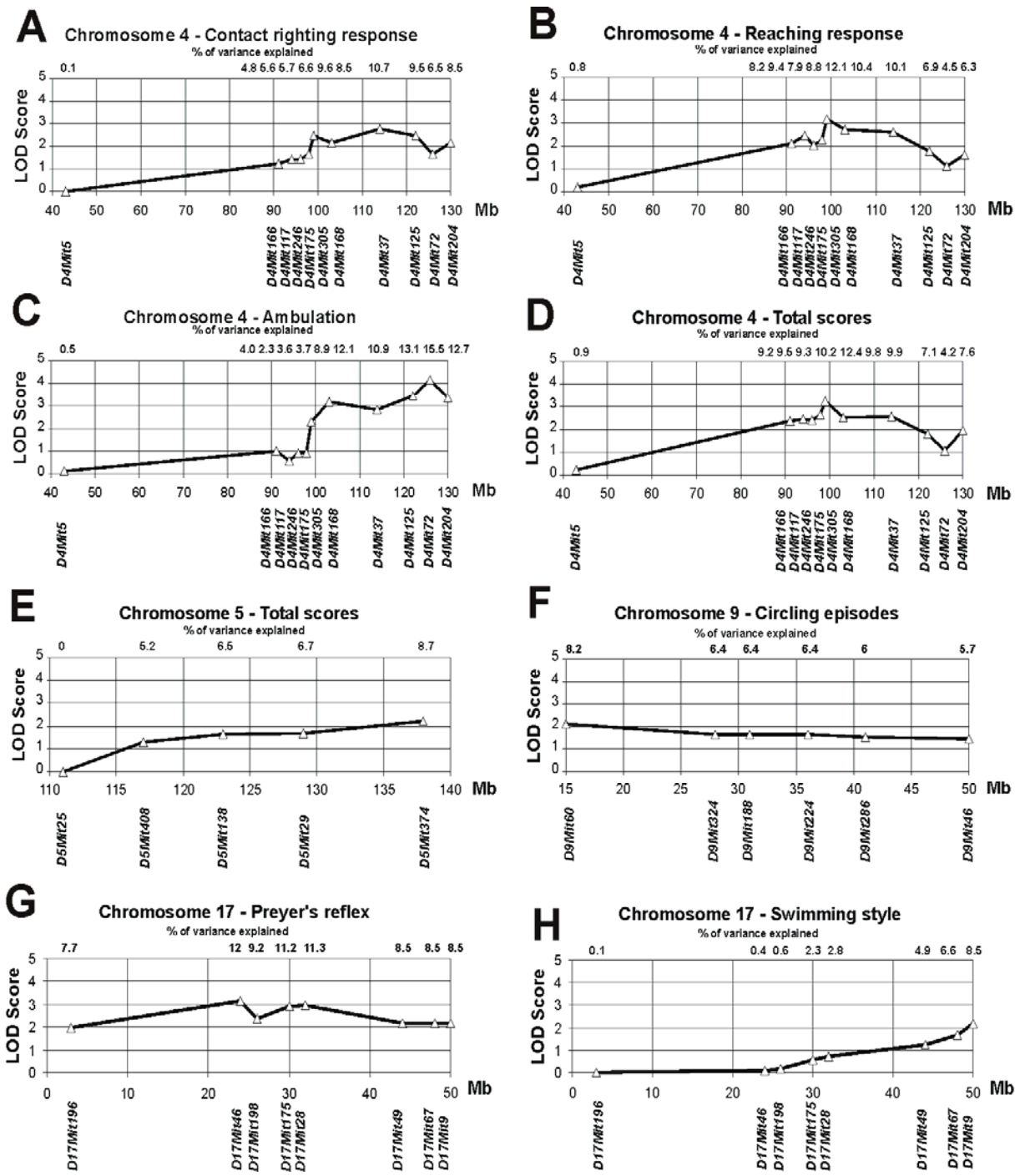

Figure 8.2: LOD score plots showing the possible locations of modifier loci identified in a backcross of *bronx waltzer* to *Mus castaneus* (Nogueira 2000). A significant modifier was found to map to chromosome 4 near *D4Mit72* affecting ambulation in the open field tests (C). The remaining graphs show loci which were found to be suggestive modifiers (LOD score >1.9) for the traits tested.

Five traits showed linkage to chromosome 4. A broad region associated with ambulation was detected with the peak near *D4Mit72* (LOD 4.14, accounting for 15.1% of the variance in phenotype; Fig. 8.2C). The large interval with raised LOD scores may suggest the presence of more than one modifier in distal chromosome 4. A suggestive modifier (LOD 3.26 accounting for 12.4% of the variance) associated with variation in total scores of all traits mapped to central chromosome 4, near *D4Mit305* (Fig. 8.2D). Two other traits showed a suggestive linkage to the same region near *D4Mit305*: the reaching response (LOD 3.16 accounting for 12.1% of the variance; Fig. 8.2B) and total balance scores (LOD 3.18 accounting for 12.1% of the variance; data not shown). The fifth trait mapping to chromosome 4 was the contact righting response, with a peak at *D4Mit37* (LOD 2.77 explaining 10.7% of the variance; Fig. 2A). On chromosome 5, *D5Mit374* showed suggestive linkage with a peak LOD score of 2.2 explaining 8.7% of the variance for the total scores as well as for the total balance scores (Fig. 8.2E). On chromosome 9, only circling episodes showed linkage, with a suggestive modifier near *D9Mit60* (LOD=2.1 explaining 8.2% of the variance; Fig. 2F). No traits showed any evidence of linkage to chromosome 12, with the highest LOD score reaching only 0.61. Finally, on chromosome 17, two traits showed suggestive linkage: the Preyer reflex, with a broad region with LOD scores above 2 and a peak at *D17Mit46/D17Mit80* (LOD 3.13 explaining 12.0% of the variance; Fig. 8.2G), and swimming style with a peak LOD score of 2.19 at *D17Mit9* explaining 8.5% of the variance (Fig. 2H). The only remaining trait, swimming vigour, showed no evidence of modifier loci.

8.1.4 Hair cells in backcross mutants

The analysis so far carried out on the mice arising from the *bronx waltzer/Mus castaneus* backcross has been entirely behavioural in nature, and whilst this is often a good indicator of vestibular abnormality and the standard battery of tests allow it to be somewhat quantifiable, there remain further measures of the severity of the *bv* phenotype which have yet to be explored. The most

obvious of these is the number of surviving inner hair cells within the organ of Corti, since this has previously been observed to vary when the mutation is hosted on different genetic backgrounds, and since the loss of inner hair cells is one of the most defining features of *bronx waltzer* mutant mice. In addition, the data obtained up to this point are mainly concerned with the measurement of vestibular function, with only the Preyer reflex being used as a measure of hearing ability. This test is relatively crude and will only detect a profound hearing impairment, since a mouse with a mild hearing deficit is still able to respond to sound.

Thus, in the present study, the survival of IHCs and the frequency of atypical hair cells in a sample of *bv*/*bv* mutants from the *bv*/cast cross at the extremes of observed behaviour (normal and severely affected) will be examined using scanning electron microscopy of the organ of Corti. These will be used as further measures of the penetrance of the phenotype on the *Mus castaneus* background, and the data subjected to QTL analysis in order to determine whether linkage can be described between these measures and any of the existing or any new modifier loci.

8.2 METHODS

8.2.1 Phenotypic extremes

This analysis was carried out on the 30 homozygous backcross mice with the highest and lowest total scores in the hearing and balance tests, referred to as the mice at the phenotypic extremes. The balance tests were carried out by assigning homozygous mice that performed in a similar way to heterozygous mice a score of 1, and homozygous mice that displayed a behavior outside the normal range of the heterozygous mice a score of 0. Thus high scoring mice are those which behave most like wild type mice, while low scoring mice exhibited the behaviour most typical of mutant mice. The traits analyzed to detect any modifier effect were contact righting response, swimming vigour, swimming style, reaching response, ambulation and number of circling episodes (Noguiera, 2000). In addition, the Preyer reflex was analyzed using an extended scoring system, giving mice with a good reflex a score of 2, mice with a reduced reflex a score of 1, and mice with no response a score of 0.

8.2.2 Cochlear dissection

At the time the backcross animals were sacrificed in order to obtain material for the genome scan, the inner ears of each mouse were removed from the skull and fixed as described in section 4.2.4. They were then stored for a period of years in cocodylate buffer (0.1M sodium cacodylate; 2mM $CaCl_2$) at 4°C and during this time some of the samples became fragile or were colonised with fungal matter, making them unsuitable for further analysis. For the remaining samples which were in good condition, dissection of the outer cochlear shell and tectorial membrane was performed in order to allow the apical surface of the organ of Corti to be viewed using scanning electron microscopy.

8.2.3 Preparation of samples for scanning electron microscopy

Fixed cochleas were processed for SEM using the osmium tetroxide-thiocarbohydrazide (OTOTO) method (Hunter-Duvar 1978; Self *et al.* 1998). They were first washed in 1% osmium tetroxide in cocodylate buffer (0.1M sodium cacodylate; 2mM $CaCl_2$) for one hour before being washed in ddH_2O 6 times for 5 minutes each. There followed a wash in freshly dissolved, saturated thiocarbahydrazide in water for 20 minutes, followed by a further 6 washes in ddH_2O for 5 minutes each. A wash in 1% osmium tetroxide in water for 1 hour was followed by another series of 6 washes in ddH_2O for 5 minutes, and this was followed by a second 20 minute wash in thocarbohydrazide, with 6 washes in ddH_2O for 5 minutes. Finally a third wash for one hour in osmium tetroxide in water was performed, with the excess rinsed away in a series of 6 washes in ddH_2O for 5 minutes each.

Having been fixed and coated, the samples were next dehydrated in a dilution series of acetone washes, each of 15 minutes. Washes were performed at 70%, 80%, 90% and three washes were carried out in 100% acetone. Once fully dehydrated, the samples were dried in a critical point drier (Polaron) and were mounted on aluminium SEM stubs (TAAB) using silver conductive paint (Agar Scientific, Stansted, Essex). These were then coated with a fine layer of gold using a sputter coater (Polaron) prior to being visualised using a Phillips XL30 scanning electron microscope. Specimens were routinely examined at a working distance of 10mm, at an accelerating voltage of 10kV, and with a spot size of 3nm.

8.2.4 Hair cell counts

SEM images were obtained from between 30-50% (mid-basal turn) and 70-90% (apical turn) of the total length of the cochlear duct from the base to the apex. These regions were determined by measuring and dividing the visible portion of the cochlea into nine equal parts corresponding to between 10% and 100% of the length, with the first 10% being made up by the hook which is not visible when the cochlea is viewed from above. These images were then used to construct montages covering approximately 300μm of the length of the organ of Corti, and from these the number of inner hair cells and atypical hair cells per 100μm was calculated.

8.3 RESULTS

8.3.1 Hair cells in backcross mutants

Control mice showed a full complement of IHCs (14-15 IHCs/100μm) and no sign of atypical hair cells (data not shown). Amongst the mutants, there was a large variation observed in the numbers of remaining IHCs and the numbers of atypical hair cells (hair cells within the inner hair cell row but with a hair bundle like that of outer hair cells) as shown in Figure 8.3. Inner hair cells and atypical hair cells were counted at two locations along the length of the cochlear duct, mid-basal (30-50% of distance from base) and apical (70-90% of distance from base) turns, the distributions of counts are shown in Figure 8.4. Mutants with the lowest balance scores showed fewer IHCs and more atypical hair cells than mutants with the highest balance scores (Table 8.1). The balance score was calculated by the summation of all the phenotypic test scores except for the Preyer reflex (see Section 8.2.1).

Cells per 100μm	Lowest balance scores	Highest balance scores	p-value
IHCs in base	1.373 +/- 0.4577 (Range 0.26 – 3.76) (n=10)	11.344 +/- 2.0617 (Range 3.44 – 15.26) (n=7)	0.0029
IHCs in apex	1.93 +/- 0.3315 (Range 0.89 – 3.22) (n=8)	11.951 +/- 1.9185 (Range 5.55 – 15.01) (n=6)	0.001
Atypical hair cells in base	4.253 +/- 0.806 (Range 1.79 – 9.00) (n=10)	0.396 +/- 0.287 (Range 0 – 1.06) (n=7)	0.0006
Atypical hair cells in apex	1.651 +/- 0.488 (Range 0 – 3.74) (n=8)	0.106 +/- 0.0747 (Range 0 – 0.37) (n=6)	0.0081

Table 8.1: Comparison of hair cell counts between mutants from the two phenotypic extremes.

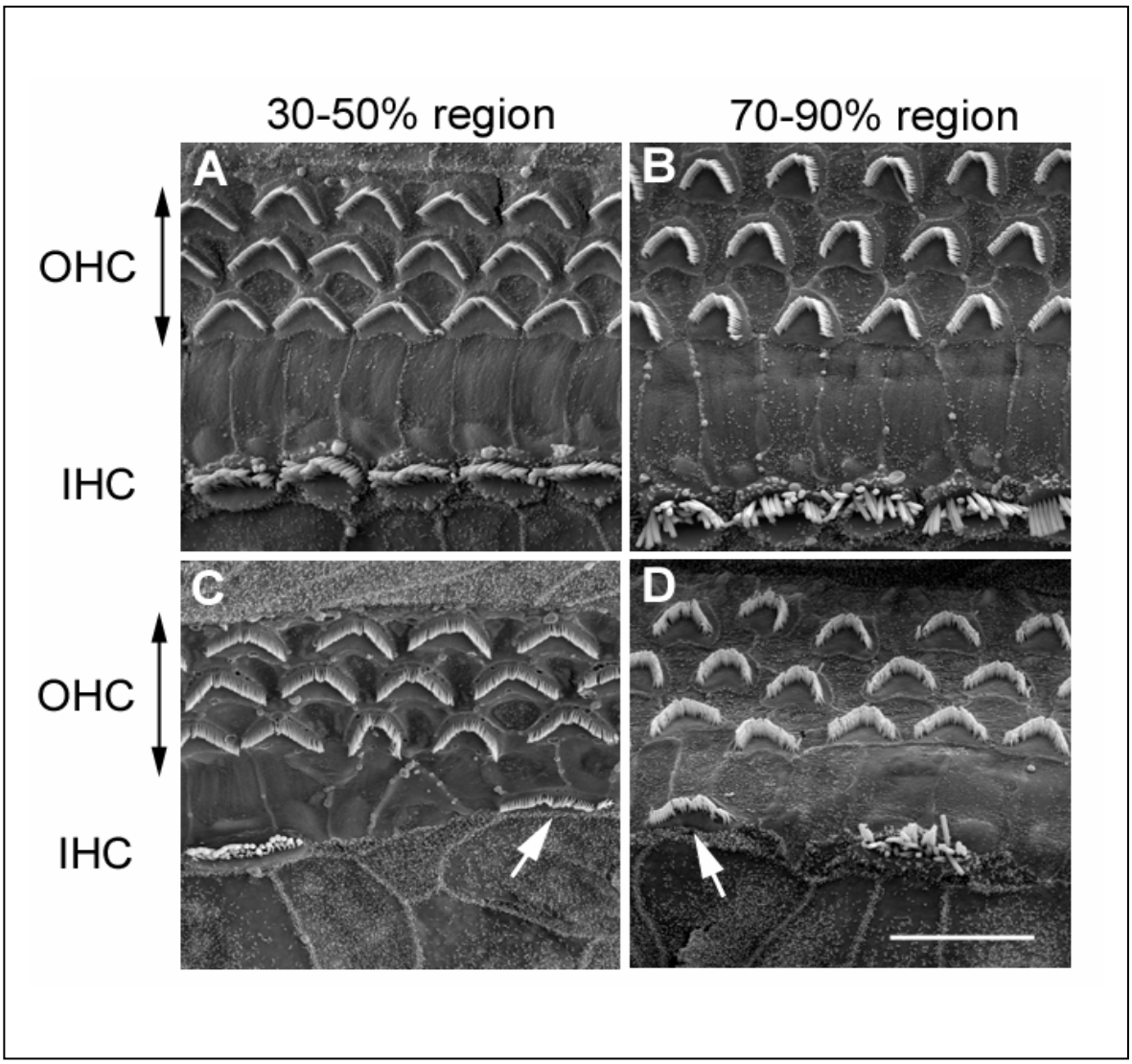

Figure 8.3: Scanning electron micrographs showing apical surfaces of cells in the organ of Corti reveal variation between mutants at the extremes of observed phenotype.
A,B high scoring mutants, C,D low scoring mutants.
Most homozygous mutants which scored highly in the behavioral tests showed an arrangement of hair cells similar to that seen in control mice. Both in the mid-basal 30-50% region (A) and the apical 70-90% region (B) there are three rows of outer hair cells (OHC) and a single row of inner hair cells (IHC). In mutants having low scores in the behavioral tests many IHCs are missing, causing some disruption of the surrounding support cells and OHCs. Atypical hair cells are also observed (indicated by arrows) in the mid-basal 30-50% region (C) and the apical 70-90% region (D) of low scoring mutants. These are cells which have the appearance of OHCs but are present in the row where IHCs are expected to be situated.
Scale bar = 10μm

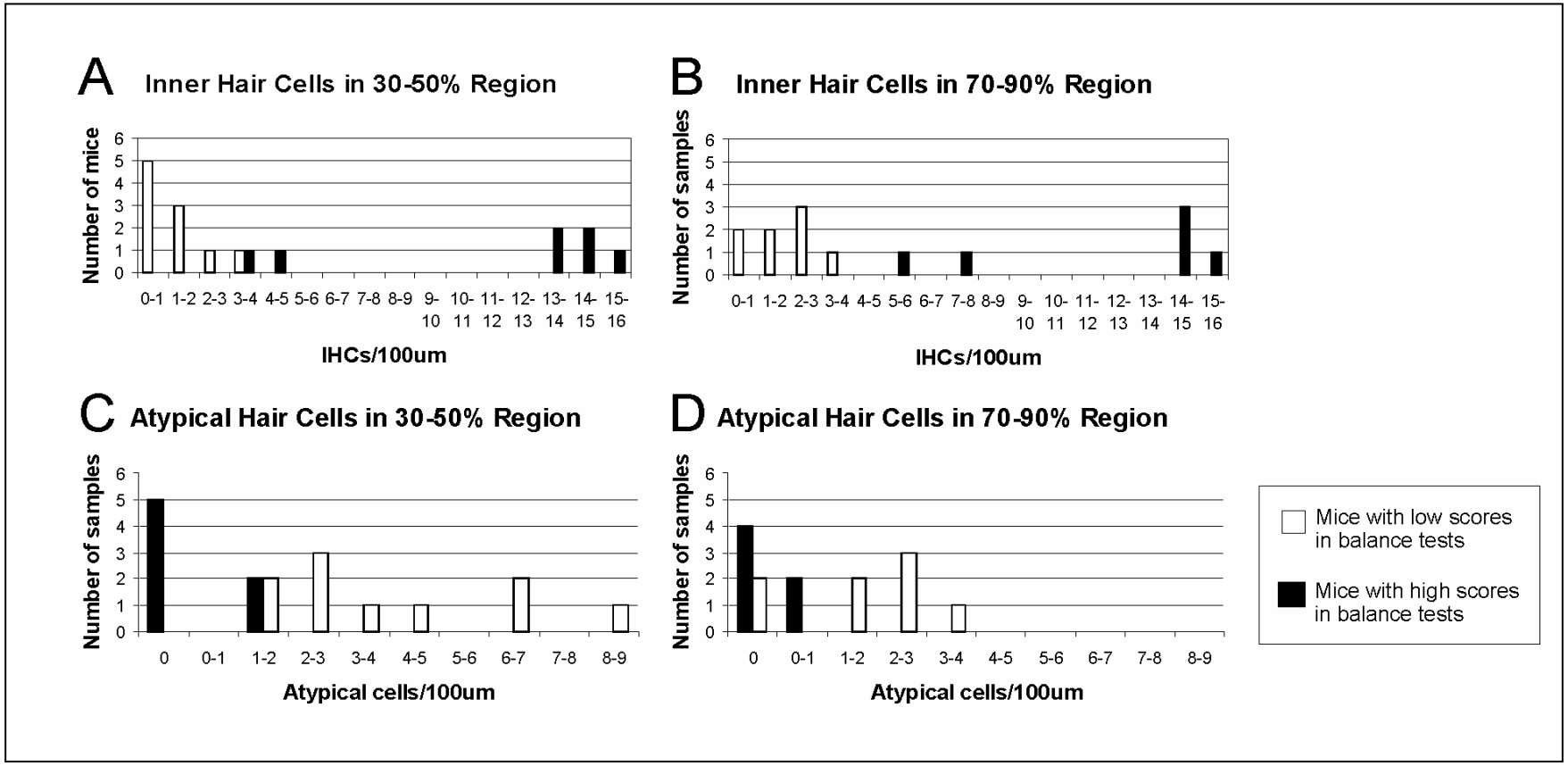

Figure 8.4: Distributions of inner hair cell and atypical hair cell counts
Numbers of inner hair cells and atypical hair cells in the cochleae of mice from the phenotypic extremes. The two groups show clear segregation both in relation to the number of inner hair cells (A and B) and the number of atypical hair cells (C and D) present.

Statistical analysis was carried out using t-tests to compare counts for both cell types at the two cochlear locations investigated revealed significant differences between the two phenotypic extremes (see Table 8.1). Furthermore, among the ten mutants examined by scanning electron microscopy with the lowest balance scores, 5 had a Preyer reflex and 5 showed no reflex, and there was a significant difference in IHCs numbers between these two groups, with those with no Preyer reflex showing fewer IHCs (see Table 8.2).

	With Preyer reflex	**No Preyer reflex**	**p-value**
IHCs in base	2.078 +/- 0.472 (n=5)	0.669 +/- 0.188 (n=5)	0.025
IHCs in apex	2.456 +/- 0.286 (n=5)	1.070 +/- 0.146 (n=3)	0.0043
Atypical hair cells in base	2.889 +/- 0.552 (n=5)	5.616 +/- 1.182 (n=5)	0.075
Atypical hair cells in apex	1.130 +/- 0.518 (n=5)	2.519 +/- 0.670 (n=3)	0.19

Table 8.2: Comparison of hair cell counts between mutants with and without a Preyer reflex among the group with the lowest balance scores

.

8.3.2 Linkage analysis of hair cell modifiers

The IHC and atypical hair cell counts at the two cochlear locations were used as four further traits to study by χ^2 analysis and by MapmakerQTL, to detect linkage of modifiers of these traits. For atypical hair cells, mice with none were given a score of 1 and mice with some a score of 0 in the analysis. For IHC counts, the actual numbers of IHCs/100 μm were used for the χ^2 analysis, and for MapmakerQTL analysis an additional score of 1 for 3.0 or more IHCs/100 μm and 0 for fewer than 3.0 IHCs/100 μm was assigned. By χ^2 analysis, markers on chromosomes 4, 5, 9, 10, 11, 12, 15, 17 and 19 all showed p values below 0.05 for at least one of the four traits (Table 8.3). IHCs in the base showed the largest number of potential modifier loci. By MapmakerQTL analysis, only one of these loci reached the criterion for suggestive linkage to a modifier, *D15Mit63* for IHCs in the base, with a LOD score of 2.05 explaining 42.6% of the variance. Several other markers reached LOD scores over 1.2 (Table 8.4), corresponding broadly to the χ^2 probabilities. The relatively small numbers of samples available probably contributed to the lack of significant LOD scores.

Marker	IHCs base	Atypicals base	IHCs apex	Atypicals apex
D4Mit27	0.0295			
D5Mit80	0.0269	0.0031		
D5Mit155	0.0153			0.0241
D5Mit101	0.0429			
D9Mit60		0.0358		
D9Mit46	0.0269			
D10Mit43				0.0308
D10Mit237		0.0493		0.0157
D11Mit358				0.0308
D12Mit64	0.0153			
D12Mit274	0.0269			
D15Mit49	0.0295			
D15Mit63	0.0071			
D17Mit9	0.0295	0.0358	0.0308	

Table 8.3: P values from χ^2 analysis of markers associated with hair cell traits ($p<0.05$ only included)

Trait	LOD	Variance explained	Marker
Preyer reflex	1.887	40%	*D4Mit305*
IHCs in base	1.326	30.20%	*D4Mit305/168/37*
IHCs in base	1.254	28.80%	*D9Mit46*
Atypicals in apex	1.233	33.40%	*D10Mit43*
Preyer reflex	1.255	28.80%	*D15Mit63*
IHCs in base	2.050*	42.60%	*D15Mit63*
IHCs in base	1.568	34.60%	*D19Mit45/48*
Atypicals in base	1.359	30.80%	*D19Mit45/48*

Table 8.4: Peak LOD scores for Preyer reflex and hair cell traits among the mutants from the phenotypic extremes (LOD >1.2 only included). An asterisk indicates that the locus meets the criterion for suggestive linkage to a modifier

8.4 DISCUSSION

This study identified a large amount of variation in the hair cell counts from mutants of the two phenotypic extreme group. As the phenotypic extreme groups were determined on the basis of their balance scores reflecting vestibular function and hair cell counts reflected the effects upon the cochlea, the difference between the phenotypic extremes in hair cell counts suggested that the two systems (auditory and vestibular) are subject to some extent to similar influences of modifiers (Table 8.1). As both systems depend upon inner ear hair cell function, this is not too surprising. The observation of more IHCs and fewer atypical hair cells in mice with a Preyer reflex compared with those without amongst the group of mutants with the lowest balance scores (Table 8.2) suggests that the Preyer reflex can reflect hair cell status in this situation, although the number of mice studied is low. It was interesting that the chi-squared analysis and LOD scores using hair cell counts as traits indicated some new potential modifier loci (albeit at low likelihoods) that were not detected by the behavioral trait analysis (Tables 8.3 and 8.4). In particular, the only marker that reached the criterion for suggestive linkage with a LOD score of 2.05 (for IHCs in the base) was on chromosome 15 at *D15Mit63*, a chromosome that was not picked out by the behavioral test results. A number of these potential modifier loci may be spurious results, resulting from the relatively low numbers of samples available to study hair cells, so these putative loci should be regarded with some caution.

In the initial study, all of the putative modifier loci demonstrated a broad distribution of LOD scores along the respective chromosomes (Figure 8.2). This is probably due to the relatively small number of mice used (113) leading to limited opportunity for informative recombinations to accrue and define the locus more precisely. Furthermore, each modifier is likely to exert an effect that is less than fully penetrant upon the phenotype, and this will interact with the variance inevitably associated with any behavioral measurements to reduce the precision of the mapping. It is also possible that

there is more than one putative modifier located in each chromosomal region, and several of the LOD score plots show secondary peaks.

The number of putative modifiers detected in this work is very likely to be an underestimate of the total number, for several reasons. Only can detect modifiers that happen to segregate in the two parental strains used will be detected, and two modifiers that are closely linked will be difficult to segregate as mentioned above. Modifiers may have positive or negative effects upon the phenotype, and may show different patterns of inheritance and only dominant modifiers can be detected using the existing backcross. This may complicate interpretation and reduces the chances of detecting some modifiers. Finally, there may be many loci each with a small effect upon the phenotype, which will make detection of any of them difficult. The calculations of relatively small proportions of the phenotypic variance explained by the putative modifiers in this study (e.g. 15.5% of the variance for our most significant locus, *D4Mit72*) supports a model including several modifiers with additive effects. However, it is not uncommon to find values of less than 10% of the variance explained by individual modifiers, and a value of 20% may be considered a locus of major effect (Tanksley 1993).

Further work on the putative modifier loci will be needed to verify the loci and ultimately to identify the genomic polymorphisms underlying the modifier effects. Several approaches can be used, including refining the mapping of the loci by increasing the number of mice studied, developing congenic lines to further define the modifier locations, and using transgenic rescue techniques or large scale sequencing when candidate regions are narrowed down to a handful of genes. These approaches have been successful in identifying other modifiers (e.g. Johnson *et al.* 2001; Ikeda *et al.* 2002). However, these will all be difficult approaches to adopt when it is clear that there is not a single modifier of major effect in the case of the *bronx waltzer* phenotype. It may be sensible to adopt another approach in this case: to await reports of good candidates from the large-scale mouse mutagenesis

programmes and microarray expression studies that are identifying many new genes involved in hearing and deafness, and to specifically test these new candidate genes by typing intragenic polymorphisms provided by SNP consortia efforts.

Chapter 9:

General Discussion

CHAPTER 9

GENERAL DISCUSSION

9.1 SUMMARY OF RESULTS

9.1.1 Mapping and sequencing progress

Through the discovery of new polymorphisms between the *bv* genetic background and the inbred strain 101/H which was used in the mapping backcross, the critical interval for *bronx waltzer* has been reduced by 0.09cM to 1.77cM and by 334Kb to 2.45Mb with the exclusion of seven candidate genes (Figure 3.30). This leaves 52 genes which have been mapped to the 2.6Mb region delineated by the flanking markers DASNP3 and *D5Mit209*, each of which are considered to be candidate genes for the *bronx waltzer* phenotype (Figure 3.32).

Following two rounds of primer design and sequencing, a total of 65729 base pairs of coding sequence, representing 90.63% of that lying within the *bv* candidate region have been successfully sequenced in the *bronx waltzer* mutant mouse genome and no mutations have been identified (Figure 7.7). Of the 52 genes mapped to the critical region full sequence has been obtained for 23 (Table 7.3), making these significantly less likely as candidates for the mutation.

9.1.2 Critical evaluation of candidate genes

The candidacy of each gene within the *bronx waltzer* region was assessed in Chapter 5, with consideration given to existing published literature and expression study data as well as to the results of an experiment to screen inner ear cDNA for the presence of candidate gene exons (Table 5.11). This led to the prioritisation of a subset of genes for further characterisation. The background literature and new data obtained for these genes is described in following paragraphs, and summarised below in Table 9.1.

Gene	Background Literature	Expression data	Zebrafish splice knockdown	Sequence coverage
Foxn4	Transcription factor controlling retinal development by activation of Math3, NeuroD1, and Prox1. Knockout has no hearing phenotype.	Expressed in retina and brain Not represented in expression databases Negative result in cDNA screen	Relatively normal development Positive tap test	100%
Myo1h	Myosin superfamily implicated in many inner ear abnormalities, including members of the myosin I class.	Not represented in expression databases Positive result in cDNA screen	Relatively normal development Positive tap test	97.2%
Kctd10	Voltage-gated potassium channel activity, potentially important in maintainiong ion gradients	Not represented in expression databases Positive result in cDNA screen	Development very stunted Fish not mobile	66.8%
Ube3b	Targets proteins for proteolytic degradation	Highly expressed following noise exposure Represented in 2 expression databases Positive result in cDNA screen	Variable rates of development Positive tap test	87.8%
Trpv4	Osmotically activated cation-selective channel. Drosophila orthologues involved in hearing. Knockout mice have progressive deafness.	Expressed in many tissues, including hair cells Represented in 1 expression database Positive result in cDNA screen	Normal development Positive tap test	100%
Git2	Regulation of golgi organisation, actin cytoskeletal organisation and paxillin localisation	Not represented in expression databases Positive result in cDNA screen	Variable rates of development Positive tap test	100%
Cabp1	Competitively inhibits calmodulin binding to CAMK2, possible role in Ca^{2+} regulation. May be involved in neuronal signal transduction	Represented in 2 expression databases Positive result in cDNA screen	Normal development Positive tap test	93.5%
Dnclc1	Inhibits the activity of neuronal NO synthase, implying regulatory role in numerous biologic processes	Represented in 3 expression databases Positive result in cDNA screen	Not tested	100%
Paxillin	Scaffolding protein involved in actin organisation Role in fibronectin and integrin signalling Knockout embryonic lethal, mesodermally derived structures affected	Represented in 3 expression databases Positive result in cDNA screen	Normal development Positive tap test	93.6%
Citron	Cit-K essential for cytokinesis in neuronal precursors Cit-N acts as Rho-modulator for actin-dependent organelle organisation	Represented in 2 expression databases Positive result in cDNA screen	Development stunted All fish dead by 3dpf	94.2%

Table 9.1: Summary of published and novel data regarding genes from within the *bronx waltzer* critical region identified as strong potential candidates

9.1.2.1 Forkhead box protein N4 (*Foxn4*)

Foxn4 is a member of the winged helix/forkhead family of transcription factors which is involved in many aspects of development (Gajiwala and Burley 2000). Expression of the gene has been noted during development in the retina and parts of the brain and spinal cord (Gouge *et al.* 2001) and subsequent studies showed that it is involved in the activation of *Math3*, *NeuroD1* and *Prox1* (Li *et al.* 2004).

Given the close evolutionary and developmental relationship between the ear and the eye as discussed in section 5.1.1.3, *Foxn4* presents itself as an interesting candidate. In addition, other winged helix/forkhead family members are known to be important in the development of the ear such as *Foxi1* (previously known as *Fkh10*). Mice with a targeted disruption of the *Foxi1* locus exhibit circling behaviour, poor swimming ability and abnormal reaching response as well as failing to elicit a Preyer reflex in response to a suprathreshold auditory stimulation (Hulander *et al.* 1998), a phenotype very similar to that displayed by the *bronx waltzer* mice.

The recent generation of *Foxn4* knockout mice by Li *et al.* (2004) showed that disruption of the gene affects retinal development but no hearing or balance defect was detected in the mice (M. Xiang, *pers. comm*). This makes it unlikely that *Foxn4* represents the causative agent for *bronx waltzer*, although these data were not available when candidates were selected for further investigation. In addition, during the course of this study, full sequence of *Foxn4* in *bv* mutant mice has been obtained and no were mutations identified.

9.1.2.2 Myosin 1H (*Myo1h*)

Given that some of the most crucial tissues of the inner ear are rich in actin and rely heavily for proper functioning on a correctly formed cytoskeleton (see Section 1.1.2.1), it comes as no surprise that several different myosin family members have been implicated in deafness since these molecular

motors are commonly known to interact with actin. Of the unconventional myosin isoforms, *myosin Ia, myosin IIIa, myosin VI, myosin VIIa* and *myosin XV* have all been shown to be associated with human genetic deafness loci (Libby and Steel 2000; Walsh *et al.* 2002). In addition, mutations in two members of the conventional nonmuscle myosin II family, *MYH9* and *MYH14* have also been demonstrated to give rise to hearing deficiencies, with *MYH9* being associated with Fechtner syndrome and DFNA17 (Seri *et al.* 2000) and *MYH14* being the gene responsible for the DFNA4 locus (Donaudy *et al.* 2004).

The myosin I class consists of the eight isozymes *Myo1a – Myo1h*, which have been implicated in various motile processes including organelle translocation, ion-channel gating and cytoskeleton reorganisation. All of these molecules were shown by Dumont *et al.* (2002) to be expressed in the mouse utricle by RT-PCR analysis with *Myo1b*, *Myo1c* and *Myo1e* exhibiting the highest expression levels. Myo1h was only sometimes amplified in the course of these experiments suggesting a lower and perhaps variable level of expression. However, this was also the case for *Myo1a* which has subsequently been linked with the DFNA48 locus (Donaudy *et al.* 2003), demonstrating that a lower expression level does not preclude an important role for *Myo1h* within the ear. *Myo1c* is considered to be the vertebrate orthologue of the bullfrog *myosin Iβ* and is thought to be involved in the gating of the mechanotransduction channel of sensory hair cells. Garcia *et al.* (1998) showed that *myosin Iβ* is localised near to the ends of the tip links in frog saccular cells as would be expected since these are the sites of adaptation. Further studies on *Myo1c* by Batters *et al.* (2004) demonstrated that the protein it encodes possesses a strain-sensing ADP release mechanism, allowing it to adapt to mechanical load and making it a good candidate for the mediator of slow adaptation of mechanoelectrical transduction.

Although relatively little is known about the functioning of *Myo1h* itself, its membership of the myosin superfamily which has been implicated in so many

and varied forms of inner ear abnormality makes it an interesting candidate gene. During the course of this work, 97.2% of the coding sequence has been sequenced in the *bronx waltzer* genome, with only one exon remaining to be sequenced and no mutations have been identified. The knockdown of the zebrafish ortholog using a splice blocking morpholino gave rise to larvae which developed normally and responded positively to the tap test, indicating that they had normal auditory function. These data make Myo1h less likely as a candidate for the *bv* mutation.

9.1.2.3 Potassium channel tetramerization domain-containing 10 (*Kctd10*)

Little is known about *Kctd10*, with no specific literature being currently available. However, its predicted potassium channel tetramerization protein domain and homology to other genes involved in potassium channel formation make it a potentially interesting candidate. The N-terminal, cytoplasmic tetramerization domain (T1) of voltage-gated K+ channels encodes molecular determinants for subfamily-specific assembly of alpha-subunits into functional tetrameric channels and is highly conserved in eukaryotes (Liu *et al.* 2005). As discussed in section 1.1.2.2, the maintenance of a potassium gradient is crucial for the proper functioning of the inner ear. In addition, other proteins associated with potassium transport have been shown to result in a deafness phenotype, including *KCNQ4*, a member of the voltage-gated potassium gene family which has been associated with the deafness locus DFNA2 (Kubisch *et al.* 1999). Meanwhile Jervell & Lange-Nielsen Syndrome has been demonstrated to be the result of mutations in the *KCNQ1* and *KCNE1* genes coding for the delayed rectifier potassium channel responsible for controlling endolymph homeostasis (Neyroud *et al.* 1997; Tyson *et al.* 1997) and mice with targeted disruptions in the *Kcnq1* gene displayed deafness and shaker-waltzer behaviour (Casimiro *et al.* 2001). Hence a novel protein with predicted involvement in potassium ion motility mechanisms presents as a good candidate for the *bronx waltzer* locus.

The sequence coverage achieved for this gene was 66.8%, and zebrafish larvae injected with a morpholino designed to block splicing in the ortholog showed very stunted development. These data are insufficient to rule out *Kctd10*, and thus it should still be considered a good candidate for *bronx waltzer*.

9.1.2.4 Ubiquitin protein ligase E3B (*Ube3b*)

Ube3b was initially identified in a screen examining differential gene expression following noise trauma in the chick basilar papilla. Lomax *et al.* (2000) found *Ube3b* to be highly expressed immediately after noise in the lesion, but not in the undamaged ends of the chick basilar papilla, suggesting that it may play a role in the regeneration of the specialised cells located there. Ubiquitination is a common process allowing molecules to be targeted for degradation by the 26S proteosome and requires the sequential action of three enzymes (Pickart 2000). An activating enzyme (E1), a conjugating enzyme (E2) and a ligase (E3) each act in turn to form polyubiquitin chains on the substrate protein. Vertebrates have a single E1 but may have several different E2s and E3s, allowing for a high degree of specificity in the targeting of proteins for degradation (Kumar *et al.* 1997). Lomax *et al.* (2000) found UBE3B to be expressed strongly in the pituitary gland and the heart, and at lower levels in all tissues examined, indicating that it may play a role under normal conditions as well as under stress and making it unlikely that its functionality should be confined to the ear. Gong *et al.* (2003) noted that the *C.elegans* homologue *Oxi-1* was identified in a screen for oxidative stress (Yanase and Ishi 1999), suggesting that *UBE3B* may play a role in the stress response triggered by oxidative damage following noise trauma. These findings, whilst not pointing to an obvious developmental function for *Ube3b* in the ear, do suggest that it plays a role in the ear and make it a possible candidate for *bronx waltzer*.

The sequence coverage achieved for this gene was 87.8%, and zebrafish larvae injected with a morpholino designed to block splicing in the ortholog showed

variable rates of development but reacted positively to the tap test, suggesting normal auditory function. These data make *Ube3b* less likely as a candidate for *bronx waltzer*, but do not rule it out.

9.1.2.5 Transient receptor potential cation channel V4 (*Trpv4*)

The transient potential cation channel superfamily V is made up of non-specific cation ion channel receptors gated by heat, protons, low extracellular osmolarity and arachidonic acid derivatives. *Trpv4* has been shown to be osmotically activated, described by Liedtke *et al.* (2000) as a cation-selective channel gated by exposure to hypotonicity. The maintenance of osmotic gradients is crucial for the proper functioning of the inner ear as discussed in Section 1.1.2.2, making this molecule an interesting candidate for the *bv* mutation, especially since Liedtke *et al.* reported expression of *Trpv4* in the hair cells of the inner ear amongst other tissues. Furthermore, the related ion channel Nanchung (*Nan*) in Drosophila was demonstrated to be necessary for hearing by Kim *et al.* (2003). They found that *Nan* mediates hypo-osmotically activated calcium influx and cation currents in cultured cells. In vivo it was shown to be expressed exclusively in chordotonal neurons and localised to the sensory cilia. Mutants lacking *Nan* showed absent sound-evoked potentials, suggesting a key role for the protein in the chordotonal mechanotransducer.

They hypothesised that *Nan* may be the Drosophila orthologue for *Trpv4* based on the expression of both molecules in mechanosensory cells and their activation by cellular hypotonic stress. By sequence homology though, it was found to be equally similar to *TRPV1*, suggesting that it belongs to the same family but does not necessarily represent a direct orthologue. Indeed, the generation of *Trpv4* knockout mice by Mizuno *et al.* (2003) suggests that *Trpv4* plays a role distinct from that of the proposed Drosophila orthologue. Mice lacking *Trpv4* were observed to have impaired osmotic sensation (Mizuno *et al.* 2003), impaired pressure sensation (Suzuki *et al.* 2003) and altered thermal

selection behaviour (Lee *et al.* 2005). They were later observed to develop a hearing deficit, with mice at 8 weeks having normal hearing but those at 24 weeks displaying significantly higher thresholds by auditory brainstem response (ABR). They were also found to be more susceptible to acoustic injury than wild type controls, showing a significantly larger auditory threshold shift one week after exposure (Tabuchi *et al.* 2005). The cause of this hearing loss is as yet unknown, and it would be interesting to examine the sensory epithlia of *Trpv4* knockout mice in order to establish this. These data have only recently come to light, and although they confirm that *Trpv4* plays a role in inner ear function and thus was a good candidate for *bronx waltzer,* the described phenotype differs significantly from that of *bv* mutant mice. In *bronx waltzer* mice the inner hair cells fail to mature at all, suggesting a disruption in their development rather than in their maintenance as is suggested by a phenotype of late-onset deafness and vulnerability to acoustic injury. In addition, the *Trpv4* knockout mice do not display any of the behaviour typical of those with vestibular abnormality (see Section 3.1.1.4) which might be expected if the gene were the same in both cases.

Zebrafish larvae injected with a morpholino designed to block splicing in the ortholog showed variable rates of development but reacted positively to the tap test, suggesting normal auditory function. In addition, the full coding sequence of *Trpv4* has been examined in the *bronx waltzer* mutant genome and no mutations have been identified, making *Trpv4* a much less attractive candidate as the causative agent for *bv*.

9.1.2.6 G protein-coupled receptor kinase- interactor 2 (*Git2*)

Git2 is an ADP-ribosylation factor GTPase-activating protein (ARFGAP) which has been shown to interact with *paxillin* (Mazaki *et al.* 2001), a protein important in actin organisation and intracellular signalling (see section 9.2.1.9). The authors found that overexpression of the short isoform of *Git2* caused the redistribution of Golgi protein β-COP and reduced the numbers of

paxillin-containing focal adhesions and actin stress fibres. In particular, the role of *Git2* in the regulation of actin cytoskeletal organisation could indicate a function for it in relation to the stereocilia on the apical surfaces of sensory hair cells within the inner ear whose structure depends on the arrangement of actin filaments and without which hearing and vestibular function are greatly compromised. In addition, Premont *et al.* (2000) found that the human homologue *GIT2* undergoes extensive alternative splicing and exists in at least 10 and potentially as many as 33 distinct forms, thus opening up the possibility that a mutation in a particular exon may cause a very specific phenotype, despite expression being detected in all tissues examined. During the course of this study the full annotated sequence of *Git2* has been analysed in *bv* mutant DNA and no mutations identified. Knockdown of the zebrafish ortholog gave rise to larvae which developed abnormally but which responded positively to the tap test, suggesting normal auditory function. It is therefore unlikely that *Git2* represents the causative agent for *bronx waltzer*, but since this gene shows a great deal of variability in its manifestation in different tissues, it is plausible that another exon as yet unidentified is necessary for the proper functioning of *Git2* in the ear, and therefore it should not be fully ruled out.

9.1.2.7 Calcium-binding protein 1 (*Cabp1*)

CABP1 was first identified as a human brain cDNA clone showing similarity to the calmodulin family of calcium binding proteins (Yamaguchi *et al.* 1999) and was later demonstrated by Haeseleer *et al.* (2000) to be capable of substituting functionally for calmodulin (*CaM*), a protein whose functions include roles in growth and the cell cycle as well as in signal transduction and the synthesis and release of neurotransmitters. This suggested a role for *CABP1* in the central nervous system where it may augment or substitute for CaM. Subsequently, Lee *et al.* (2002) used co-immunoprecipitation assays to demonstrate modulation of a rat P/Q-type voltage-dependent Ca^{2+} channel by *CABP1* through interaction with the alpha-1 subunit. They postulate that

this interaction between Ca^{2+} channels and *CaBP1* may regulate Ca^{2+}-dependent forms of synaptic plasticity by inhibiting Ca^{2+} influx into neurons. In order for hair cells in the inner ear to function correctly they are surrounded by fluid containing calcium at concentrations that must be maintained by active transport, hence a protein involved in the regulation of calcium channels may potentially have a role in the ear. Some examples which demonstrate the importance of controlling calcium in the inner ear include the deaf, ataxic mouse deafwaddler mice with mutations in the *Atp2b2* gene encoding plasma membrane calcium ATPase type 2 (*PMCA2*) which have been shown to result in reduced Ca^{2+} concentration in the endolymph (Wood *et al.* 2004), and mice deficient for the alpha1D Ca^{2+} channel which have impaired hearing but no vestibular defect (Dou *et al.* 2004).

Cabp1 is thought to be neuron specific and is expressed strongly in the retina (Sokal *et al.* 2000). As previously discussed (see Section 5.1.1.3) expression of a gene in the eye can sometimes indicate a role for it in the ear, and the expression of *Cabp1* in the ear has not been investigated. This suggestion, along with a potential role in Ca^{2+} regulation makes this a possible candidate gene. During the course of this work, 93.5% of the coding sequence has been sequenced in the *bronx waltzer* genome, with only one exon remaining to be sequenced and no mutations have been identified. The knockdown of the zebrafish ortholog using a splice blocking morpholino gave rise to larvae which developed normally and responded positively to the tap test, indicating that they had normal auditory function. These data make *Cabp1* less likely as a candidate for the *bv* mutation.

9.1.2.8 Dynein light chain 1, cytoplasmic (*Dnclc1*)

Cytoplasmic dyneins are large, multi-subunit ATPases involved in the transport of particles and organelles along microtubules and in the transport of condensed chromosomes during mitosis. These molecular motors function by interacting with microtubules to generate force and are encoded by a

number of separate genes. Of these, the best characterised are the cytoplasmic heavy chains which share extensive sequence similarity and are conserved throughout species. More recently, several genes encoding intermediate and light chains have been identified and have been found to encode a remarkable diversity of products, which also seem to be highly conserved between species, although they fall into several complex groups (Milisav 1998). Light chains are thought to play roles in cargo-binding as well as in regulatory control of the dynein motor (King 2000).

DLC1, the human form of *Dnclc1*, was shown by Dick *et al.* (1996) to be ubiquitously expressed and localised to the cytoplasm. The authors also demonstrated that mutations in the Drosophila orthologue ddlc1 resulted in pleiotropic morphogenetic defects in bristle and wing development, as well as in oogenesis. Meanwhile, Jaffrey and Snyder (1996) found that human *DLC1* inhibits the activity of neuronal nitric oxide, a major messenger molecule in the cardiovascular, immune, and nervous systems, suggesting that *DLC1* may play a regulatory role in numerous biological processes.

The full sequence of *Dnclc1* has been obtained during the course of this study and no mutations identified in the sequence from *bv* mutants, making it unlikely that this gene represents the causative agent for *bronx waltzer*.

9.1.2.9 Paxillin (*Pxn*)

Paxillin localises to focal adhesions (FAs), specialised sites where cells adhere to the extracellular matrix (ECM) (Turner *et al.* 1990). This process is mediated by integrin receptors which connect intracellular actin to the ECM, and it is thought that FAs are required for the maintenance of actin organisation within the cell (Jockusch *et al.* 1995; Burridge and Chrzanowska-Wodnicka 1996) as well as mediating tyrosine kinase signalling relating to growth control (Aplin *et al.* 1998). These data suggest roles for FAs in the regulation of cell morphology, migratory properties, growth and

differentiation (Burridge and Chrzanowska-Wodnicka 1996). In keeping with this broad functionality, *paxillin* knockout mice were embryonic lethal with defects as early as E7.5 and resorbed by E9-9.5. (Hagel *et al.* 2002). *Paxillin* was found to be involved in the development of mesodermally derived structures such as heart and somites, while cultured *paxillin*$^{-/-}$ fibroblasts displayed abnormal FAs, reduced cell migration and a reduction in the levels of other FA-related proteins, as well as showing defects in the cortical cytoskeleton and cell spreading on fibronectin. Since the mice do not develop beyond E9.5, no studies of the inner ear have been possible.

With respect to the *bronx waltzer* phenotype, the role of paxillin in actin organisation marks it out as a potentially interesting candidate gene. The stereocilia of the sensory hair cells which are affected by the *bv* mutation are packed with actin filaments which maintain their structure and are constantly renewed by means of a molecular treadmill (Rzadzinska *et al.* 2004). The shape of these structures is crucial to their operation (see Section 1.1.2.1), and thus any disruption to the organisation of actin in the cell may well cause the cell to cease functioning, leading to downstream apoptotic events. Apoptosis may also result from a loss of paxillin-mediated signalling, or by the loss of cell adhesion normally provided by FAs.

Paxillin is a multi-domain protein which has been shown to bind to with several structural and signalling proteins within FAs (Turner and Miller 1994; Hildebrand *et al.* 1995; Brown *et al.* 1996). This property may provide one possible explanation for how a mutation in such a ubiquitously important gene could give a phenotype as specific as that seen in *bronx waltzer* mice. A mutation in a single binding domain could potentially cause the protein to malfunction only when it is required to interact with a specific molecule, or even a particular combination of molecules whose purpose once conjugated is specific to inner hair cells. Alternatively, the tissue specificity may result from an alternative splice form or promoter site which results in a slightly different configuration of the protein, as discussed in Section 9.1.3.

During the course of this study, 93.6% coverage of the coding sequence for *paxillin* has been analysed in the *bronx waltzer* background and no mutations identified, with only one exon remaining to be sequenced. The knockdown of the zebrafish ortholog using a splice blocking morpholino gave rise to larvae which developed normally and responded positively to the tap test, indicating that they had normal auditory function. These data make *paxillin* less likely as a candidate for the *bv* mutation, but do not rule it out.

9.1.2.10 Citron (*Cit*)

The *Citron* transcription unit gives rise to two isoforms – Citron-K and Citron-N – produced via alternative transcriptional initiation (Di Cunto *et al.* 2000). Citron-K is the longer of the two variants since it comprises an additional amino-terminal serine/threonine kinase domain (Di Cunto *et al.* 1998). Citron-K shares a high degree of homology with the Rho-kinases (ROCKs) (Leung *et al.* 1996) with its activity stimulated by activated Rho-A (Di Cunto *et al.* 1998) and evidence suggests it is involved in the control of cytokinesis downstream of Rho (Madaule *et al.* 1998). Citron-K knockout mice were found to suffer developmental abnormalities in the central nervous system as a result of altered cytokinesis and massive apoptosis (Di Cunto *et al.* 2000). Although the ears of these mice have not been fully examined, they show no behaviour indicative of deafness or vestibular abnormality and the vestibulo-cochlear receptors of these mice appeared superficially normal (Di Cunto, *pers. comm.*). In addition, other mutations generated in the same gene gave rise to very similar phenotypes, making it unlikely that a mutation in the Citron-K transcription unit would result in isolated deafness (Di Cunto, *pers. comm.*).

The functions of Citron-N are less well characterised, although it was first identified for its ability to interact with the GTP-bound (active) forms of Rho and Rac (Madaule *et al.* 1995; Fujisawa *et al.* 1998) and has been proposed as a link between the Rho signalling cascades and NMDA receptor complexes

(Zhang *et al.* 1999). Rho is an important molecule in focal adhesions (see section 9.1.2.9), being the trigger for their formation and for the assembly of actin filaments (Ridley and Hall 1992), while Rac has been shown to be involved in the polymerisation of actin filaments in lamellipodia (Nobes and Hall 1995; Nobes and Hall 1995). Camera *et al.* (2003) carried out analysis of hippocampal neurons in culture which indicated that Citron-N controls actin in the Golgi apparatus by assembling the Rho effector ROCK-II and the actin-binding, neuron-specific protein Profilin-IIa. They postulated that Citron-N acts as an organelle-specific Rho-modulator for actin-dependent organelle organisation and dynamics. This is an interesting proposition, since as has been previously discussed the proper organisation of actin filaments is vital to the functioning of inner ear hair cells. While the current literature suggests that Citron-N is brain specific, expression in the ear has not been explicitly examined. In addition the fact that *Citron* demonstrates alternate mechanisms of transcription raises the possibility that another isoform may exist which could be specific to the hair cells of the inner ear, and is required for actin organisation within them. Some methods for testing this hypothesis are outlined in Section 9.2.3.

During the course of this study, 94.2% of the coding sequence of *Citron* has been analysed in the *bronx waltzer* mutant genome and no mutations have been found. Three exons from a total of 51 remain to be sequenced, with two of these lying within the region of the gene which is common to Citron-N and Citron-K. Zebrafish larvae injected with a morpholino designed to block splicing in the ortholog showed very stunted development. These data are insufficient to rule out *Citron*, and thus it should still be considered a good candidate for *bronx waltzer*.

9.1.3 Tissue specific expression

Many of the candidate genes examined in the paragraphs above, whilst having functions suggestive of a role in the ear also show widespread expression or involvement in many other important pathways. This seems to be in conflict with the very restricted nature of the *bronx waltzer* phenotype, which affects only the sensory hair cells of the inner ear. Even more specifically, in the cochlea only the inner hair cells are affected with the outer hair cells appearing normal, suggesting a very precise role for the mutated gene. In these cases, the possibility of tissue-specific modification of gene expression must be considered. Most commonly, distinct isoforms of a gene are produced by alternative splicing in individual cells or tissues, with a varying combination of exons being retained in the processed mRNA and thus a different protein produced following translation (reviewed in Smith *et al.* 1989). Another possible mechanism is that of alternative transcriptional regulation. Here, cell-specific expression is achieved by the activation of different control elements such as promoters or termination sequences, resulting in a pre-mRNA of differing composition. For example, the activation of different promoters associated with the α and γ clusters of neural protocadherin (*Pcdh*) genes causes the incorporation of a variable first exon which is then spliced to the remainder of the gene following transcription (Wu and Maniatis 2000; Tasic *et al.* 2002). A detailed study of the mouse *UGT1* cluster showed that its genomic organisation is very similar to that of the *Pcdh* clusters, and that the various isoforms are expressed in a tissue-specific manner (Zhang *et al.* 2004). Analysis of mammalian Genbank databases (Zhang *et al.* 2004) and *Arabidopsis* full-length gene transcripts (Haas *et al.* 2002) has indicated that multiple transcription initiation sites are widespread within eukaryotic genomes and are much more common than was previously thought, making this an important mechanism in regard to cell- and tissue-specific, as well as developmentally regulated gene expression.

In addition to providing a possible explanation for the specificity of the *bronx waltzer* phenotype, this mechanism also suggests a potential reason for the failure to detect a mutation within the coding regions of the candidate genes despite achieving over 90% coverage in the mutant genome. If the mutation were to lie within a promoter or other regulatory element then exon-resequencing would not reveal it. An example of such a mutation is the dinucleotide deletion in the promoter region of the gene *ankyrin* which causes hereditary spherocytosis as a result of abnormal gene expression (Gallagher *et al.* 2005).

Furthermore, although the splice junctions at either end of each exon were examined during this study, mutations within an intron may occasionally cause a phenotype if they disrupt the normal function of transcription or of mRNA processing. For example, a cryptic splice donor site may be activated, as in the case of mutations in intron 2 of *CDKN2A* which have been associated with six English melanoma pedigrees (Harland *et al.* 2001). Alternatively, the splice machinery may be disrupted by a mutation in a lariat branchpoint consensus sequence, such as the point mutation located in intron 4 of *lecithin:cholesterol acyltransferase* (*LCAT*) which gives rise to fish-eye disease (Kuivenhoven *et al.* 1996), or by the expansion of an unstable polymorphic repeat such as that found in intron 1 of the gene FRDA which results in the autosomal recessive disease Friedreich's Ataxia (Campuzano *et al.* 1996).

The expression studies described in Section 9.2.3 should allow these possibilities to be fully investigated.

9.2 FURTHER WORK

Through limitations imposed by time, not all of the avenues opened up by the present work have been fully explored. Suggestions for extensions to the described work, as well as for novel areas of investigation are outlined in the paragraphs below.

9.2.1 Further mapping

Sequence traces obtained from the resequencing of exons within the *bronx waltzer* candidate region (see Chapter 7) brought to light new data regarding polymorphisms which could potentially be exploited for mapping purposes. The majority of these were SNPs or length polymorphisms between the *bv* genetic background and the publicly sequenced strain C57Bl/6J. In order to establish whether these could be used to aid in the mapping of *bronx waltzer*, they should be sequenced in the backcross strain 101/H and that sequence compared to the *bv* sequence. Where polymorphisms between these two strains exist, they can then be tested against the panel of recombinant mice and placed as new markers on the *bv*/101 genetic map (see Chapter 3).

The second type of polymorphisms identified during exon resequencing were those where SNPs existed between the *bronx waltzer* mutant (*bv*/*bv*) sequence and the wild type (+/+) sequence derived from the *bronx waltzer* genetic background. In each case the allele from the mutant sample matched that of the published sequence, suggesting that the base substitutions were not pathogenic. Interestingly, all the SNPs of this type were clustered around the gene *Citron*, indicating a possible linkage disequilibrium effect. In order to test this hypothesis, archived samples from the *bronx waltzer* colony could be tested for the markers to establish whether they do indeed segregate with the mutation. If so then further sequencing and characterisation efforts should be concentrated on this region.

9.2.2 Further sequencing

Coding sequence coverage of 90.63% in the mutant genome has been achieved, and yet no mutation has been identified. It is possible that the mutation lies within the remaining 9.37% of the annotated coding sequence. It may also be the case that it lies within a coding region which has not yet been annotated, or even in a non-coding region as discussed in Section 9.1.3.

The quality of published sequence and gene annotation in the *bronx waltzer* region is currently not high. Few of the selected tiling path clones have had their sequence fully finished, and there exist two gaps in the tiling path which are bridged by lower quality whole genome shotgun data. Proper annotation of coding regions is dependent on a high quality of sequence, and thus the finishing of the tiling path clones is imperative for a confident analysis and characterisation of the candidate region. Negotiations are underway to ensure the prioritisation of this work.

Following two rounds of sequencing, 90.63% of the annotated coding regions of genes within the *bv* candidate region have been analysed in the mutant genome and no mutations have been identified. Of the 52 genes annotated, full sequence has been obtained from the mutant genome for 23, with the majority of the remaining 29 having partial sequence available. Many of these genes lack sequence for only one or two exons, making the prospects for a third sequencing pass very favourable. The successful sequencing of a relatively small number of exons in the mutant genome could allow the coding sequence of a significant number of genes to be completed, thus reducing the list of those to be considered as likely candidates for the mutation. Detailed suggestions for the implementation of this third round of sequencing can be found in Section 7.4.1.

9.2.3 Further expression studies

In assessing candidacy, the expression data considered for each gene was obtained from a variety of sources – published literature, cDNA databases and the screening of cDNA obtained from P0 ears using gene-specific primers. This last data source was a relatively simple experiment, with much scope for refinement. Since the gene-specific primers have already been obtained and optimised, the process of screening a new, more specific cDNA sample would be relatively simple. Suggestions for the procurement of RNA

which better represents the mRNA population of the ear and has a lower level of contamination from other tissues are detailed in Section 5.4.1.2.

An alternative approach to this study which would provide more detailed data regarding the level and location of expression would be to carry out high throughput *in situ* hybridisation. Probes designed to hybridise to the mRNA product of each candidate gene would be incubated with inner ear tissue from a developmental stage at which the bronx waltzer gene is expected to be expressed, such as at E17.5 – E19.5 when the hair cells are maturing and when the phenotype becomes apparent. In order to facilitate the screening of a large number of genes and also to provide more detailed information regarding the cell types in which a gene is expressed, it would be advantageous to carry out hybridisation to sections of ear tissue rather than to whole ears (Wilkinson 1992).

In order to investigate the possibility of the mutation lying in a non-coding regulatory element it would be useful to carry out a number of Northern blot experiments. The first of the proteins expressed in the inner ear versus other tissues in order to establish whether an ear-specific isoform exists, and the second of mutant versus control samples to identify whether the transcription or splicing of a gene differs between the two. In both cases probes should be designed to a region of the gene likely to be included in all isoforms, such as one containing a domain necessary for its functioning, while at the same time being specific to the gene rather than a gene family. If any anomalies were identified, these could be investigated using 5' and 3' RACE (Rapid Amplification of cDNA Ends) to recover any differences in the incorporation of exons at the beginning or the end of a gene. Localised sequencing of the non-coding regions could then be carried out in order to identify the mutation.

9.2.4 Gene knockdowns and knockouts

Although none of the gene knockdowns using morpholinos in zebrafish (see Chapter 6) gave rise to larvae exhibiting a hearing or balance phenotype, the success of the negative and positive controls indicates that this is a strand of investigation worth continuing. Firstly, it is important that the efficacy of the morpholinos is confirmed using the RT-PCR experiment described in Section 6.4 to ascertain what effect the splice MOs have had on their corresponding gene products. Once this technique has been validated, the potential for the zebrafish to be used as a second confirmatory allele could be quickly and easily exploited in the event of the identification of a mutation in the *bv* genome. The additional advantage of a zebrafish phenocopy allowing a fuller investigation into the developmental effects of the mutation as a result of the transparent and externally maturing larvae lends further support to the pursuance of this approach.

A second means of investigating gene function by targeted disruption is the generation of mouse knockouts. This can be a relatively slow process since it requires the breeding of several generations of mice before the phenotype can be assessed, however the current establishment of a large scale programme at the Sanger Institute to generate and characterise around 250 such mouse mutants per year could provide the opportunity to focus on this approach. These will be generated using a combination of gene-trapping and homologous recombination recombineering techniques, both of which support a forward genetics approach i.e. the identity of the disrupted gene is known before mice are produced. Gene-traps function by randomly targeting genes in embryonic stem (ES) cell lines (Skarnes *et al.* 2004), while recombineering techniques allow the targeted inactivation of genes which are not amenable to trapping in ES cells (Liu *et al.* 2003). Depending on available capacity, a larger or smaller subset of the candidate genes for *bronx waltzer* could be prioritised in this study to allow investigation of the effects of their disruption. In addition, this could prove a highly useful resource when the *bv*

mutation is identified, as a means of proving that it is indeed the causative agent for the phenotype.

9.3 *BRONX WALTZER* AS A MODEL OF HEREDITARY DEAFNESS

As well as holding insights into the development and function of the inner ear sensory epithelia, and particularly into the molecular differences between inner and outer hair cells, *bronx waltzer* mice serve as a potential model for human hereditary deafness. The human homologs of the genes from within the *bv* candidate region on mouse chromosome 5 are localised to a region of human chromosome 12 which spans from 12q24.11 to 12q24.31. This region forms part of the mapped interval for the deafness locus DFNA25 which has been localised to 12q22-24 (Greene *et al.* 2001; Petek *et al.* 2003). It has been hypothesised that this form of human congenital deafness is the human ortholog of *bronx waltzer* (Greene *et al.* 2001), and some of the same candidate genes have been examined. One of these was *VR-OAC*, now renamed *TRPV4*, which as discussed in Section 9.1.2.5 has given rise to a progressive deafness phenotype when knocked out in the mouse, although the cell types affected by the deficiency have not been established. Since DFNA25 also manifests as delayed-onset sensorineural hearing loss, it seems that *TRPV4* is a good candidate for this dominant hereditary hearing impairment locus. However, it is difficult to reconcile these clinical and laboratory observations with the *bronx waltzer* phenotype, where inner hair cells and vestibular hair cells fail to develop to maturity, and affected mice are deaf from birth. Congenital neuroepithelial progressive hearing impairment tends to be the result of mutations in genes required for the maintenance and function of the sensory patches, rather than for their proper development (reviewed in Gratton and Vazquez 2003). In addition, when degeneration of the organ of Corti is observed, the order of hair cell loss is generally from base to apex, with OHCs degenerating first, later followed by IHCs. This pattern is markedly different from that reported in *bronx waltzer* mutants, where only

IHCs are seen to degenerate and OHCs appear normal even as the mice grow old. Furthermore, during the course of this study the full coding sequence of *Trpv4* has been examined in the *bv* genome and no mutations identified. Thus it is likely that *bronx waltzer* still represents a novel locus which when mutated causes disruption to the normal development of the auditory system, and holds the potential for new discoveries concerning the development of the ear.

References

References

Adams, D. J., P. J. Biggs, T. Cox, R. Davies, L. van der Weyden, J. Jonkers, J. Smith, B. Plumb, R. Taylor, I. Nishijima, Y. Yu, J. Rogers and A. Bradley (2004). "Mutagenic insertion and chromosome engineering resource (MICER)." Nat Genet **36**: 867-71.

Ahmed, Z. M., S. Riazuddin, S. Riazuddin and E. R. Wilcox (2003). "The molecular genetics of Usher syndrome." Clin Genet **63**: 431-44.

Alexandersson, M., S. Cawley and L. Pachter (2003). "SLAM: cross-species gene finding and alignment with a generalized pair hidden Markov model." Genome Res **13**: 496-502.

Altschul, S. F., W. Gish, W. Miller, E. W. Myers and D. J. Lipman (1990). "Basic local alignment search tool." J Mol Biol **215**: 403-10.

Amsterdam, A., S. Burgess, G. Golling, W. Chen, Z. Sun, K. Townsend, S. Farrington, M. Haldi and N. Hopkins (1999). "A large-scale insertional mutagenesis screen in zebrafish." Genes Dev **13**: 2713-2724.

Aplin, A. E., A. Howe, S. K. Alahari and R. L. Juliano (1998). "Signal transduction and signal modulation by cell adhesion receptors: the role of integrins, cadherins, immunoglobulin-cell adhesion molecules, and selectins." Pharmacol Rev **50**: 197-263.

Ashmore, J. (1998). "Mechanosensation: Swimming round in circles." Curr Biol **8**.

Bang, P. I., W. F. Sewell and J. J. Malicki (2001). "Morphology and cell type heterogeneities of the inner ear epithelia in adult and juvenile zebrafish (Danio rerio)." J Comp Neurol **438**: 173-190.

Bang, P. I., W. F. Sewell, J. J. Malicki, P. C. Yelick and P. I. Bang (2002). "High-throughput behavioral screening method for detecting auditory response defects in zebrafish." J Neurosci Methods **118**: 177-187.

Batters, C., C. P. Arthur, A. Lin, J. Porter, M. A. Geeves, R. A. Milligan, J. E. Molloy and L. M. Coluccio (2004). "Myo1c is designed for the adaptation response in the inner ear." Embo J **23**: 1433-40.

Baugh, L. R., A. A. Hill, E. L. Brown and C. P. Hunter (2001). "Quantitative analysis of mRNA amplification by in vitro transcription." Nucleic Acids Res **29**: E29.

Beck, J. A., S. Lloyd, M. Hafezparast, M. Lennon-Pierce, J. T. Eppig, M. F. Festing and E. M. Fisher (2000). "Genealogies of mouse inbred strains." Nat Genet **24**: 23-5.

Beisel, K. W., T. Shiraki, K. A. Morris, C. Pompeia, B. Kachar, T. Arakawa, H. Bono, J. Kawai, Y. Hayashizaki and P. Carninci (2004). "Identification of unique transcripts from a mouse full-length, subtracted inner ear cDNA library." Genomics **83**: 1012-23.

Benson, G. (1999). "Tandem repeats finder: a program to analyze DNA sequences." Nucleic Acids Res **27**: 573-580.

Bergstrom, D. E., L. H. Gagnon and E. M. Eicher (1999). "Genetic and physical mapping of the dreher locus on mouse chromosome 1." Genomics **59**: 291-9.

Bermingham, N. A., B. A. Hassan, S. D. Price, M. A. Vollrath, N. Ben-Arie, R. A. Eatock, H. J. Bellen, A. Lysakowski and H. Y. Zoghbi (1999). "Math1: an essential gene for the generation of inner ear hair cells." Science **284**: 1837-41.

Bock, G. R., G. K. Yates and M. S. Deol (1982). "Cochlear Potentials in the Bronx Waltzer Mutant Mouse." Neurosci Lett **34**: 19-25.

Bolz, H., B. Von Brederlow, A. Ramirez, E. C. Bryda, K. Kutsche, H. G. Nothwang, M. Seeliger, M. D. C.-S. Cabrera, M. C. Vila, O. P. Molina, A. Gal and C. Kubisch (2001). "Mutation of CDH23, encoding a new member of the cadherin gene family, causes Usher syndrome type 1D." Nat Genet **27**: 108-112.

Bonfield, J. K., C. Rada and R. Staden (1998). "Automated detection of point mutations using fluorescent sequence trace subtraction." Nucleic Acids Res **26**: 3404-9.

Bonfield, J. K., K. F. Smith and R. Staden (1995). "A new DNA sequence assembly program." Nucleic Acids Res **23**: 4992-4999.

Bork, J. M., L. M. Peters, S. Riazuddin, S. L. Bernstein, Z. M. Ahmed, S. L. Ness, R. Polomeno, A. Ramesh, M. Schloss, C. R. S. Srisailpathy, S. Wayne, S. Bellman, D. Desmukh, Z. Ahmed, S. N. Khan *et al.* (2001). "Usher syndrome 1D and nonsyndromic autosomal recessive deafness DFNB12 are caused by allelic mutations of the novel cadherin-like gene CDH23." Am J Hum Genet **68**: 26-37.

Borodovsky, M. and J. McIninch (1993). "Recognition of genes in DNA sequence with ambiguities." Biosystems **30**: 161-71.

Bosman, E. A., A. C. Penn, J. C. Ambrose, R. Kettleborough, D. L. Stemple and K. P. Steel (2005). "Multiple mutations in mouse Chd7 provide models for CHARGE syndrome." Hum Mol Genet **14**: 3463-76.

Breen, M., L. Deakin, B. Macdonald, S. Miller, R. Sibson, E. Tarttelin, P. Avner, F. Bourgade, J. Guenet, X. Montagutelli, C. Poirier, D. Simon, D. Tailor, M. Bishop, M. Kelly *et al.* (1994). "Towards High-Resolution Maps Of The Mouse And Human Genomes - A Facility For Ordering Markers To 0.1 Cm Resolution." Hum Mol Genet **3**: 621-627.

Brent, M. R. and R. Guigo (2004). "Recent advances in gene structure prediction." Curr Opin Struct Biol **14**: 264-72.

Brown, M. C., J. A. Perrotta and C. E. Turner (1996). "Identification of LIM3 as the principal determinant of paxillin focal adhesion localization and characterization of a novel motif on paxillin directing vinculin and focal adhesion kinase binding." J Cell Biol **135**: 1109-23.

Burge, C. and S. Karlin (1997). "Prediction of complete gene structures in human genomic DNA." J Mol Biol **268**: 78-94.

Burridge, K. and M. Chrzanowska-Wodnicka (1996). "Focal adhesions, contractility, and signaling." Annu Rev Cell Dev Biol **12**: 463-518.

Bussoli, T. (1996). Localisation of the bronx waltzer gene (bv) and its effect on organ of Corti development. MRC Institute of Hearing Research. Nottingham, University of Nottingham. **Ph.D. Thesis:** 326.

Bussoli, T., A. Kelly and K. P. Steel (1997). "Localization of the bronx waltzer mouse mutation and its effect on organ of Corti development." Br J Audiol **31**: 83-83.

Bussoli, T. J., A. Kelly and K. P. Steel (1997). "Localization of the bronx waltzer (bv) deafness gene to mouse Chromosome 5." Mamm Genome **8**: 714-717.

Camera, P., J. S. da Silva, G. Griffiths, M. G. Giuffrida, L. Ferrara, V. Schubert, S. Imarisio, L. Silengo, C. G. Dotti and F. Di Cunto (2003). "Citron-N is a neuronal Rho-associated protein involved in Golgi organization through actin cytoskeleton regulation." Nat Cell Biol **5**: 1071-8.

Campuzano, V., L. Montermini, M. D. Molto, L. Pianese, M. Cossee, F. Cavalcanti, E. Monros, F. Rodius, F. Duclos, A. Monticelli, F. Zara, J.

Canizares, H. Koutnikova, S. I. Bidichandani, C. Gellera *et al.* (1996). "Friedreich's ataxia: autosomal recessive disease caused by an intronic GAA triplet repeat expansion." Science **271**: 1423-7.

Casimiro, M. C., B. C. Knollmann, S. N. Ebert, J. C. Vary, Jr., A. E. Greene, M. R. Franz, A. Grinberg, S. P. Huang and K. Pfeifer (2001). "Targeted disruption of the Kcnq1 gene produces a mouse model of Jervell and Lange-Nielsen Syndrome." Proc Natl Acad Sci U S A **98**: 2526-31.

Chen, P., J. E. Johnson, H. Y. Zoghbi and N. Segil (2002). "The role of Math1 in inner ear development: Uncoupling the establishment of the sensory primordium from hair cell fate determination." Development **129**: 2495-505.

Chen, P. and N. Segil (1999). "p27(Kip1) links cell proliferation to morphogenesis in the developing organ of Corti." Development **126**: 1581-90.

Chen, Z. Y. and D. P. Corey (2002). "An inner ear gene expression database." J Assoc Res Otolaryngol **3**: 140-8.

Chenna, R., H. Sugawara, T. Koike, R. Lopez, T. J. Gibson, D. G. Higgins and J. D. Thompson (2003). "Multiple sequence alignment with the Clustal series of programs." Nucleic Acids Res **31**: 3497-500.

Cheong, M. A. (2000). Genetic and physical mapping of the mouse deafness gene bronx waltzer (bv) and its effect on the vestibular system. MRC Institute of Hearing Research. Nottingham, University of Nottingham. **Ph.D. Thesis:** 397.

Cheong, M. A. and K. P. Steel (2002). "Early development and degeneration of vestibular hair cells in bronx waltzer mutant mice." Hear Res **164**: 179-89.

Chisaka, O., T. S. Musci and M. R. Capecchi (1992). "Developmental defects of the ear, cranial nerves and hindbrain resulting from targeted disruption of the mouse homeobox gene Hox-1.6." Nature **355**: 516-20.

Cristobal, R., P. A. Wackym, J. A. Cioffi, C. B. Erbe, J. P. Roche and P. Popper (2005). "Assessment of differential gene expression in vestibular epithelial cell types using microarray analysis." Brain Res Mol Brain Res **133**: 19-36.

Crouch, R. and M. Dirksen (1982). Ribonuclease H. Nucleases. S. Linn and R. Roberts. Cold Spring Harbor, NY, Cold Spring Harbor Laboratory Press**:** 211-241.

Darvasi, A. (1997). "The effect of selective genotyping on QTL mapping accuracy." Mamm Genome **8**: 67-8.

Darvasi, A. and M. Soller (1994). "Selective DNA pooling for determination of linkage between a molecular marker and a quantitative trait locus." Genetics **138**: 1365-73.

Darvasi, A., A. Weinreb, V. Minke, J. I. Weller and M. Soller (1993). "Detecting marker-QTL linkage and estimating QTL gene effect and map location using a saturated genetic map." Genetics **134**: 943-51.

Davis, A., S. Wood, R. Healy, H. Webb and S. Rowe (1995). "Risk factors for hearing disorders: epidemiologic evidence of change over time in the UK." J Am Acad Audiol **6**: 365-70.

Dememes, D. and A. Sans (1985). "Pathological-Changes During the Development of the Vestibular Sensory and Ganglion-Cells of the Bronx Waltzer Mouse - Scanning and Transmission Electron-Microscopy." Dev Brain Res **18**: 285-295.

Deol, M. S. (1981). "The Inner-Ear in Bronx Waltzer Mice." Acta Otolaryngol **92**: 331-336.

Deol, M. S. and S. Gluecksohn-Waelsch (1979). "The role of inner hair cells in hearing." Nature **278**: 250-2.

Di Cunto, F., E. Calautti, J. Hsiao, L. Ong, G. Topley, E. Turco and G. P. Dotto (1998). "Citron rho-interacting kinase, a novel tissue-specific ser/thr kinase encompassing the Rho-Rac-binding protein Citron." J Biol Chem **273**: 29706-11.

Di Cunto, F., S. Imarisio, E. Hirsch, V. Broccoli, A. Bulfone, A. Migheli, C. Atzori, E. Turco, R. Triolo, G. P. Dotto, L. Silengo and F. Altruda (2000). "Defective neurogenesis in citron kinase knockout mice by altered cytokinesis and massive apoptosis." Neuron **28**: 115-27.

Di Palma, F., R. H. Holme, E. C. Bryda, I. A. Belyantseva, R. Pellegrino, B. Kachar, K. P. Steel and K. Noben-Trauth (2001). "Mutations in Cdh23, encoding a new type of cadherin, cause stereocilia disorganization in waltzer, the mouse model for Usher syndrome type 1D." Nat Genet **27**: 103-107.

Dick, T., K. Ray, H. K. Salz and W. Chia (1996). "Cytoplasmic dynein (ddlc1) mutations cause morphogenetic defects and apoptotic cell death in Drosophila melanogaster." Mol Cell Biol **16**: 1966-77.

Dietrich, W. F., J. Miller, R. Steen, M. A. Merchant, D. DamronBoles, Z. Husain, R. Dredge, M. J. Daly, K. A. Ingalls, T. J. Oconnor, C. A. Evans, M. M. DeAngelis, D. M. Levinson, L. Kruglyak, N. Goodman *et al.* (1996). "A comprehensive genetic map of the mouse genome." Nature **380**: 149-152.

Dobson, C. M., T. Wai, D. Leclerc, H. Kadir, M. Narang, J. P. Lerner-Ellis, T. J. Hudson, D. S. Rosenblatt and R. A. Gravel (2002). "Identification of the gene responsible for the cblB complementation group of vitamin B12-dependent methylmalonic aciduria." Hum Mol Genet **11**: 3361-9.

Donaudy, F., A. Ferrara, L. Esposito, R. Hertzano, O. Ben-David, R. E. Bell, S. Melchionda, L. Zelante, K. B. Avraham and P. Gasparini (2003). "Multiple mutations of MYO1A, a cochlear-expressed gene, in sensorineural hearing loss." Am J Hum Genet **72**: 1571-7.

Donaudy, F., R. Snoeckx, M. Pfister, H. P. Zenner, N. Blin, M. Di Stazio, A. Ferrara, C. Lanzara, R. Ficarella, F. Declau, C. M. Pusch, P. Nurnberg, S. Melchionda, L. Zelante, E. Ballana *et al.* (2004). "Nonmuscle myosin heavy-chain gene MYH14 is expressed in cochlea and mutated in patients affected by autosomal dominant hearing impairment (DFNA4)." Am J Hum Genet **74**: 770-6.

Dou, H., A. E. Vazquez, Y. Namkung, H. Chu, E. L. Cardell, L. Nie, S. Parson, H. S. Shin and E. N. Yamoah (2004). "Null mutation of alpha1D Ca2+ channel gene results in deafness but no vestibular defect in mice." J Assoc Res Otolaryngol **5**: 215-26.

Draper, B. W., P. A. Morcos and C. B. Kimmel (2001). "Inhibition of zebrafish fgf8 pre-mRNA splicing with morpholino oligos: A quantifiable method for gene knockdown." Genesis **30**: 154-156.

Dumont, R. A., Y. D. Zhao, J. R. Holt, M. Bahler and P. G. Gillespie (2002). "Myosin-I isozymes in neonatal rodent auditory and vestibular epithelia." J Assoc Res Otolaryngol **3**: 375-89.

Ekker, S. C. (2000). "Morphants: A new systematic vertebrate functional genomics approach." Comp Funct Genomics **17**: 302-306.

Erkman, L., R. J. McEvilly, L. Luo, A. K. Ryan, F. Hooshmand, S. M. O'Connell, E. M. Keithley, D. H. Rapaport, A. F. Ryan and M. G. Rosenfeld (1996). "Role of transcription factors Brn-3.1 and Brn-3.2 in auditory and visual system development." Nature **381**: 603-6.

Ernest, S., G.-J. Rauch, P. Haffter, R. Geisler, C. Petit and T. Nicolson (2000). "Mariner is defective in myosin VIIA: A zebrafish model for human hereditary deafness." Hum Mol Genet **9**: 2189-2196.

Eskildsen, S., J. Justesen, M. H. Schierup and R. Hartmann (2003). "Characterization of the 2'-5'-oligoadenylate synthetase ubiquitin-like family." Nucleic Acids Res **31**: 3166-73.

Fay, R. and A. Simmons (1999). The sense of hearing in fishes and amphibians. Comparative hearing: fish and amphibians. R. Fay and A. Popper. New York, Springer Verlag**:** 269-318.

Fekete, D. M. (1996). "Cell fate specification in the inner ear." Curr Opin Neurobiol **6**: 533-41.

Flicek, P., E. Keibler, P. Hu, I. Korf and M. R. Brent (2003). "Leveraging the mouse genome for gene prediction in human: from whole-genome shotgun reads to a global synteny map." Genome Res **13**: 46-54.

Force, A., M. Lynch, A. Amores, Y.-L. Yan, J. Postlethwait and F. B. Pickett (1999). "Preservation of duplicate genes by complementary, degenerative mutations." Genetics **151**: 1531-1545.

Fortnum, H. M., A. Q. Summerfield, D. H. Marshall, A. C. Davis and J. M. Bamford (2001). "Prevalence of permanent childhood hearing impairment in the United Kingdom and implications for universal neonatal hearing screening: questionnaire based ascertainment study." BMJ **323**: 536-40.

Frengen, E., D. Weichenhan, B. H. Zhao, K. Osoegawa, M. van Geel and P. J. de Jong (1999). "A modular, positive selection bacterial artificial chromosome vector with multiple cloning sites." Genomics **58**: 250-253.

Friedman, T. B. and A. J. Griffith (2003). "Human nonsyndromic sensorineural deafness." Annu Rev Genomics Hum Genet **4**: 341-402.

Fritzsch, B., V. A. Matei, D. H. Nichols, N. Bermingham, K. Jones, K. W. Beisel and V. Y. Wang (2005). "Atoh1 null mice show directed afferent fiber growth to undifferentiated ear sensory epithelia followed by incomplete fiber retention." Dev Dyn **233**: 570-83.

Fritzsch, B., S. Pauley, V. Matei, D. M. Katz, M. Xiang and L. Tessarollo (2005). "Mutant mice reveal the molecular and cellular basis for specific sensory connections to inner ear epithelia and primary nuclei of the brain." Hear Res **206**: 52-63.

Frye, R. A. (1999). "Characterization of five human cDNAs with homology to the yeast SIR2 gene: Sir2-like proteins (sirtuins) metabolize NAD and may have protein ADP-ribosyltransferase activity." Biochem Biophys Res Commun **260**: 273-9.

Fujisawa, K., P. Madaule, T. Ishizaki, G. Watanabe, H. Bito, Y. Saito, A. Hall and S. Narumiya (1998). "Different regions of Rho determine Rho-selective binding of different classes of Rho target molecules." J Biol Chem **273**: 18943-9.

Gajiwala, K. S. and S. K. Burley (2000). "Winged helix proteins." Curr Opin Struct Biol **10**: 110-6.

Gallagher, B. C., J. J. Henry and R. M. Grainger (1996). "Inductive processes leading to inner ear formation during Xenopus development." Dev Biol **175**: 95-107.

Gallagher, P. G., D. G. Nilson, C. Wong, J. L. Weisbein, L. J. Garrett-Beal, S. W. Eber and D. M. Bodine (2005). "A dinucleotide deletion in the ankyrin promoter alters gene expression, transcription initiation and TFIID complex formation in hereditary spherocytosis." Hum Mol Genet **14**: 2501-9.

Garcia, J. A., A. G. Yee, P. G. Gillespie and D. P. Corey (1998). "Localization of myosin-Ibeta near both ends of tip links in frog saccular hair cells." J Neurosci **18**: 8637-47.

Gibbs, D., S. M. Azarian, C. Lillo, J. Kitamoto, A. E. Klomp, K. P. Steel, R. T. Libby and D. S. Williams (2004). "Role of myosin VIIa and Rab27a in the motility and localization of RPE melanosomes." J Cell Sci **117**: 6473-83.

Gibson, F., J. Walsh, P. Mburu, A. Varela, K. A. Brown, M. Antonio, K. W. Beisel, K. P. Steel and S. D. M. Brown (1995). "A type VII myosin encoded by the mouse deafness gene shaker-1." Nature **374**: 62-64.

Gong, T. W., L. Huang, S. J. Warner and M. I. Lomax (2003). "Characterization of the human UBE3B gene: structure, expression, evolution, and alternative splicing." Genomics **82**: 143-52.

Good, P., A. Yoda, S. Sakakibara, A. Yamamoto, T. Imai, H. Sawa, T. Ikeuchi, S. Tsuji, H. Satoh and H. Okano (1998). "The human Musashi homolog 1 (MSI1) gene encoding the homologue of Musashi/Nrp-1, a neural RNA-binding protein putatively expressed in CNS stem cells and neural progenitor cells." Genomics **52**: 382-4.

Goodhill, V. (1979). Ear diseases, deafness and dizziness. New York, Harper Collins.

Gouge, A., J. Holt, A. P. Hardy, J. C. Sowden and H. K. Smith (2001). "Foxn4--a new member of the forkhead gene family is expressed in the retina." Mech Dev **107**: 203-6.

Granato, M., F. J. M. Van Eeden, U. Schach, M. Brand, M. Furutani-Seiki, P. Haffter, M. Hammerschmidt, C.-P. Heisenberg, Y.-J. Jiang, D. A. Kane, R. N. Kelsh, M. C. Mullins, J. Odenthal, C. Nüsslein-Volhard, T. Trowe *et al.* (1996). "Genes controlling and mediating locomotion behavior of the zebrafish embryo and larva." Development **123**: 399-413.

Gratton, M. A. and A. E. Vazquez (2003). "Age-related hearing loss: current research." Curr Opin Otolaryngol Head Neck Surg **11**: 367-71.

Greene, C. C., P. M. McMillan, S. E. Barker, P. Kurnool, M. I. Lomax, M. Burmeister and M. M. Lesperance (2001). "DFNA25, a novel locus for dominant nonsyndromic hereditary hearing impairment, maps to 12q21-24." Am J Hum Genet **68**: 254-60.

Gregory, S. G., M. Sekhon, J. Schein, S. Y. Zhao, K. Osoegawa, C. E. Scott, R. S. Evans, P. W. Burridge, T. V. Cox, C. A. Fox, R. D. Hutton, I. R. Mullenger, K. J. Phillips, J. Smith, J. Stalker *et al.* (2002). "A physical map of the mouse genome." Nature **418**: 743-U3.

Grigorenko, A. P., Y. K. Moliaka, G. I. Korovaitseva and E. I. Rogaev (2002). "Novel class of polytopic proteins with domains associated with putative protease activity." Biochemistry (Mosc) **67**: 826-35.

Haas, B. J., N. Volfovsky, C. D. Town, M. Troukhan, N. Alexandrov, K. A. Feldmann, R. B. Flavell, O. White and S. L. Salzberg (2002). "Full-length messenger RNA sequences greatly improve genome annotation." Genome Biol **3**: RESEARCH0029.

Haddon, C., Y.-J. Jiang, L. Smithers and J. Lewis (1998). "Delta-Notch signalling and the patterning of sensory cell differentiation in the zebrafish ear: Evidence from the mind bomb mutant." Development **125**: 4637-4644.

Haddon, C. M. and J. H. Lewis (1991). "Hyaluronan as a propellant for epithelial movement: the development of semicircular canals in the inner ear of Xenopus." Development **112**: 541-50.

Haeseleer, F., I. Sokal, C. L. Verlinde, H. Erdjument-Bromage, P. Tempst, A. N. Pronin, J. L. Benovic, R. N. Fariss and K. Palczewski (2000). "Five members of a novel Ca(2+)-binding protein (CABP) subfamily with similarity to calmodulin." J Biol Chem **275**: 1247-60.

Haffter, P., M. Granato, M. Brand, M. C. Mullins, M. Hammerschmidt, D. A. Kane, J. Odenthal, F. J. M. Van Eeden, Y.-J. Jiang, C.-P. Heisenberg, R. N. Kelsh, M. Furutani-Seiki, E. Vogelsang, D. Beuchle, U. Schach *et al.* (1996). "The identification of genes with unique and essential functions in the development of the zebrafish, Danio rerio." Development **123**: 1-36.

Hagel, M., E. L. George, A. Kim, R. Tamimi, S. L. Opitz, C. E. Turner, A. Imamoto and S. M. Thomas (2002). "The adaptor protein paxillin is essential for normal development in the mouse and is a critical transducer of fibronectin signaling." Mol Cell Biol **22**: 901-15.

Hamada, H., M. G. Petrino and T. Kakunaga (1982). "A Novel Repeated Element With Z-Dna-Forming Potential Is Widely Found In Evolutionarily Diverse Eukaryotic Genomes." Proc Natl Acad Sci U S A **79**: 6465-6469.

Han, C. S., R. D. Sutherland, P. B. Jewett, M. L. Campbell, L. J. Meincke, J. G. Tesmer, M. O. Mundt, J. J. Fawcett, U. J. Kim, L. L. Deaven and N. A. Doggett (2000). "Construction of a BAC contig map of chromosome 16q by two-dimensional overgo hybridization." Genome Res **10**: 714-21.

Hardisty, R. E., D. C. Hughes and K. P. Steel (1997). "The characterization of the head bobber mouse mutant." Br J Audiol **31**: 83-84.

Harland, M., S. Mistry, D. T. Bishop and J. A. Bishop (2001). "A deep intronic mutation in CDKN2A is associated with disease in a subset of melanoma pedigrees." Hum Mol Genet **10**: 2679-86.

Hartmann, E. and R. K. Hartmann (2003). "The enigma of ribonuclease P evolution." Trends Genet **19**: 561-9.

Henikoff, S., B. J. Till and L. Comai (2004). "TILLING. Traditional mutagenesis meets functional genomics." Plant Physiol **135**: 630-636.

Hertzano, R., M. Montcouquiol, S. Rashi-Elkeles, R. Elkon, R. Yucel, W. N. Frankel, G. Rechavi, T. Moroy, T. B. Friedman, M. W. Kelley and K. B. Avraham (2004). "Transcription profiling of inner ears from Pou4f3(ddl/ddl) identifies Gfi1 as a target of the Pou4f3 deafness gene." Hum Mol Genet **13**: 2143-53.

Hildebrand, J. D., M. D. Schaller and J. T. Parsons (1995). "Paxillin, a tyrosine phosphorylated focal adhesion-associated protein binds to the carboxyl terminal domain of focal adhesion kinase." Mol Biol Cell **6**: 637-47.

Holzman, L. B., S. E. Merritt and G. Fan (1994). "Identification, molecular cloning, and characterization of dual leucine zipper bearing kinase. A novel serine/threonine protein kinase that defines a second subfamily of mixed lineage kinases." J Biol Chem **269**: 30808-17.

Hudziak, R. M., E. Barofsky, D. F. Barofsky, D. L. Weller, S.-B. Huang and D. D. Weller (1996). "Resistance of Morpholino phosphorodiamidate oligomers to enzymatic degradation." Antisense Nucleic Acid Drug Dev **6**: 267-272.

Hudziak, R. M., J. Summerton, D. D. Weller and P. L. Iversen (2000). "Antiproliferative effects of steric blocking phosphorodiamidate morpholino antisense agents directed against c-myc." Antisense Nucleic Acid Drug Dev **10**: 163-76.

Hulander, M., W. Wurst, P. Carlsson and S. Enerback (1998). "The winged helix transcription factor Fkh10 is required for normal development of the inner ear." Nat Genet **20**: 374-6.

Hunter-Duvar, I. M. (1978). "A technique for preparation of cochlear specimens for assessment with the scanning electron microscope." Acta Otolaryngol Suppl **351**: 3-23.

Ikeda, A., Q. Y. Zheng, A. R. Zuberi, K. R. Johnson, J. K. Naggert and P. M. Nishina (2002). "Microtubule-associated protein 1A is a modifier of tubby hearing (moth1)." Nat Genet **30**: 401-5.

Itoh, M., C.-H. Kim, G. Palardy, D. Maust, S.-Y. Yeo, A. B. Chitnis, T. Oda, S. C. Chandrasekharappa, Y.-J. Jiang, G. J. Wright, L. Ariza-McNaughton, J. Lewis, K. Lorick and A. M. Weismann (2003). "Mind bomb is a ubiquitin ligase that is essential for efficient activation of notch signaling by delta." Dev Cell **4**: 67-82.

Jacobson, A. G. (1963). "The Determination And Positioning Of The Nose, Lens And Ear. I. Interactions Within The Ectoderm, And Between The Ectoderm And Underlying Tissues." J Exp Zool **154**: 273-83.

Jacobson, A. G. (1963). "The Determination And Positioning Of The Nose, Lens And Ear. Ii. The Role Of The Endoderm." J Exp Zool **154**: 285-91.

Jacobson, A. G. (1963). "The Determination And Positioning Of The Nose, Lens And Ear. Iii. Effects Of Reversing The Antero-Posterior Axis Of Epidermis, Neural Plate And Neural Fold." J Exp Zool **154**: 293-303.

Jaffrey, S. R. and S. H. Snyder (1996). "PIN: an associated protein inhibitor of neuronal nitric oxide synthase." Science **274**: 774-7.

Jarman, A. P., E. H. Grell, L. Ackerman, L. Y. Jan and Y. N. Jan (1994). "Atonal is the proneural gene for Drosophila photoreceptors." Nature **369**: 398-400.

Jockusch, B. M., P. Bubeck, K. Giehl, M. Kroemker, J. Moschner, M. Rothkegel, M. Rudiger, K. Schluter, G. Stanke and J. Winkler (1995). "The molecular architecture of focal adhesions." Annu Rev Cell Dev Biol **11**: 379-416.

Johnson, K. R., Q. Y. Zheng, Y. Bykhovskaya, O. Spirina and N. Fischel-Ghodsian (2001). "A nuclear-mitochondrial DNA interaction affecting hearing impairment in mice." Nature Genetics **27**: 191-4.

Kappe, G., P. Verschuure, R. L. Philipsen, A. A. Staalduinen, P. Van de Boogaart, W. C. Boelens and W. W. De Jong (2001). "Characterization of two

novel human small heat shock proteins: protein kinase-related HspB8 and testis-specific HspB9." Biochim Biophys Acta **1520**: 1-6.

Keats, B. J. and D. P. Corey (1999). "The usher syndromes." Am J Med Genet **89**: 158-66.

Keithley, E. M. and M. L. Feldman (1983). "The spiral ganglion and hair cells of Bronx waltzer mice." Hear Res **12**: 381-91.

Kelley, J. M., C. E. Field, M. B. Craven, D. Bocskai, U. J. Kim, S. D. Rounsley and M. D. Adams (1999). "High throughput direct end sequencing of BAC clones." Nucleic Acids Res **27**: 1539-1546.

Kiernan, A. E., N. Ahituv, H. Fuchs, R. Balling, K. B. Avraham, K. P. Steel and M. H. de Angelis (2001). "The Notch ligand Jagged1 is required for inner ear sensory development." Proc Natl Acad Sci U S A **98**: 3873-3878.

Kim, J., Y. D. Chung, D. Y. Park, S. Choi, D. W. Shin, H. Soh, H. W. Lee, W. Son, J. Yim, C. S. Park, M. J. Kernan and C. Kim (2003). "A TRPV family ion channel required for hearing in Drosophila." Nature **424**: 81-4.

Kimmel, C. B., W. W. Ballard, S. R. Kimmel, B. Ullmann and T. F. Schilling (1995). "Stages of embryonic development of the zebrafish." Dev Dyn **203**: 253-310.

King, S. M. (2000). "The dynein microtubule motor." Biochim Biophys Acta **1496**: 60-75.

Korf, I., P. Flicek, D. Duan and M. R. Brent (2001). "Integrating genomic homology into gene structure prediction." Bioinformatics **17 Suppl 1**: S140-8.

Kubisch, C., B. C. Schroeder, T. Friedrich, B. Lutjohann, A. El-Amraoui, S. Marlin, C. Petit and T. J. Jentsch (1999). "KCNQ4, a novel potassium channel expressed in sensory outer hair cells, is mutated in dominant deafness." Cell **96**: 437-46.

Kuivenhoven, J. A., H. Weibusch, P. H. Pritchard, H. Funke, R. Benne, G. Assmann and J. J. Kastelein (1996). "An intronic mutation in a lariat branchpoint sequence is a direct cause of an inherited human disorder (fish-eye disease)." J Clin Invest **98**: 358-64.

Kumar, S., W. H. Kao and P. M. Howley (1997). "Physical interaction between specific E2 and Hect E3 enzymes determines functional cooperativity." J Biol Chem **272**: 13548-54.

Lagziel, A., Z. M. Ahmed, J. M. Schultz, R. J. Morell, I. A. Belyantseva and T. B. Friedman (2005). "Spatiotemporal pattern and isoforms of cadherin 23 in

wild type and waltzer mice during inner ear hair cell development." Dev Biol **280**: 295-306.

Lander, E. and L. Kruglyak (1995). "Genetic dissection of complex traits: guidelines for interpreting and reporting linkage results." Nat Genet **11**: 241-7.

Lander, E. S. and D. Botstein (1989). "Mapping mendelian factors underlying quantitative traits using RFLP linkage maps." Genetics **121**: 185-99.

Lander, E. S., P. Green, J. Abrahamson, A. Barlow, M. J. Daly, S. E. Lincoln and L. Newburg (1987). "MAPMAKER: an interactive computer package for constructing primary genetic linkage maps of experimental and natural populations." Genomics **1**: 174-81.

Lander, E. S., L. M. Linton, B. Birren, C. Nusbaum, M. C. Zody, J. Baldwin, K. Devon, K. Dewar, M. Doyle, W. Fitzhugh, R. Funke, D. Gage, K. Harris, A. Heaford, J. Howland *et al.* (2001). "Initial sequencing and analysis of the human genome." Nature **409**: 860-921.

Lander, E. S. and N. J. Schork (1994). "Genetic dissection of complex traits." Science **265**: 2037-48.

Larsen, W. (1997). Human Embryology. New York, Churchill Livingston.

Lee, A., R. E. Westenbroek, F. Haeseleer, K. Palczewski, T. Scheuer and W. A. Catterall (2002). "Differential modulation of Ca(v)2.1 channels by calmodulin and Ca2+-binding protein 1." Nat Neurosci **5**: 210-7.

Lee, H., T. Iida, A. Mizuno, M. Suzuki and M. J. Caterina (2005). "Altered thermal selection behavior in mice lacking transient receptor potential vanilloid 4." J Neurosci **25**: 1304-10.

Lee, J. W., H. S. Choi, J. Gyuris, R. Brent and D. D. Moore (1995). "Two classes of proteins dependent on either the presence or absence of thyroid hormone for interaction with the thyroid hormone receptor." Mol Endocrinol **9**: 243-54.

Lenoir, M. and R. Pujol (1984). "Age-Related Structural Investigation of the Bronx-Waltzer Mutant Mouse Cochlea - Scanning and Transmission Electron- Microscopy." Hear Res **13**: 123-134.

Leung, T., X. Q. Chen, E. Manser and L. Lim (1996). "The p160 RhoA-binding kinase ROK alpha is a member of a kinase family and is involved in the reorganization of the cytoskeleton." Mol Cell Biol **16**: 5313-27.

Li, S., Z. Mo, X. Yang, S. M. Price, M. M. Shen and M. Xiang (2004). "Foxn4 controls the genesis of amacrine and horizontal cells by retinal progenitors." Neuron **43**: 795-807.

Libby, R. T., J. Kitamoto, R. H. Holme, D. S. Williams and K. P. Steel (2003). "Cdh23 mutations in the mouse are associated with retinal dysfunction but not retinal degeneration." Exp Eye Res **77**: 731-9.

Libby, R. T. and K. P. Steel (2000). "The roles of unconventional myosins in hearing and deafness." Essays Biochem **35**: 159-74.

Liedtke, W., Y. Choe, M. A. Marti-Renom, A. M. Bell, C. S. Denis, A. Sali, A. J. Hudspeth, J. M. Friedman and S. Heller (2000). "Vanilloid receptor-related osmotically activated channel (VR-OAC), a candidate vertebrate osmoreceptor." Cell **103**: 525-35.

Lim, D. and J. Rueda (1992). Structural development of the cochlea. Development of auditory and vestibular systems 2. R. Romand. New York, Elsevier**:** 33-58.

Lin, X., P. Mattjus, H. M. Pike, A. J. Windebank and R. E. Brown (2000). "Cloning and expression of glycolipid transfer protein from bovine and porcine brain." J Biol Chem **275**: 5104-10.

Liu, H. L., C. W. Chen and J. C. Lin (2005). "Homology models of the tetramerization domain of six eukaryotic voltage-gated potassium channels Kv1.1-Kv1.6." J Biomol Struct Dyn **22**: 387-98.

Liu, P., N. A. Jenkins and N. G. Copeland (2003). "A highly efficient recombineering-based method for generating conditional knockout mutations." Genome Res **13**: 476-84.

Liu, S., W. Lu, S. Kuida, D. R. Beier, T. Obara, I. A. Drummond, J. Lehoczky and K. Dewar (2002). "A defect in novel Nek-family kinase causes cystic kidney disease in the mouse and in zebrafish." Development **129**: 5839-5846.

Liu, S., S. E. Smith, J. Julian, L. H. Rohde, N. J. Karin and D. D. Carson (1996). "cDNA cloning and expression of HIP, a novel cell surface heparan sulfate/heparin-binding protein of human uterine epithelial cells and cell lines." J Biol Chem **271**: 11817-23.

Liu, X.-Z., J. Walsh, P. Mburu, J. Kendrick-Jones, M. J. T. V. Cope, K. P. Steel and S. D. M. Brown (1997). "Mutations in the myosin VIIA gene cause non-syndromic recessive deafness." Nat Genet **16**: 188-190.

Liu, X. Z., J. Walsh, Y. Tamagawa, K. Kitamura, M. Nishizawa, K. P. Steel and S. D. M. Brown (1997). "Autosomal dominant non-syndromic deafness caused by a mutation in the myosin VIIA gene." Nat Genet **17**: 268-269.

Lomax, M. I., L. Huang, Y. Cho, T. L. Gong and R. A. Altschuler (2000). "Differential display and gene arrays to examine auditory plasticity." Hear Res **147**: 293-302.

Lufkin, T., A. Dierich, M. LeMeur, M. Mark and P. Chambon (1991). "Disruption of the Hox-1.6 homeobox gene results in defects in a region corresponding to its rostral domain of expression." Cell **66**: 1105-19.

Madaule, P., M. Eda, N. Watanabe, K. Fujisawa, T. Matsuoka, H. Bito, T. Ishizaki and S. Narumiya (1998). "Role of citron kinase as a target of the small GTPase Rho in cytokinesis." Nature **394**: 491-4.

Madaule, P., T. Furuyashiki, T. Reid, T. Ishizaki, G. Watanabe, N. Morii and S. Narumiya (1995). "A novel partner for the GTP-bound forms of rho and rac." FEBS Lett **377**: 243-8.

Marra, M. A., T. A. Kucaba, N. L. Dietrich, E. D. Green, B. Brownstein, R. K. Wilson, K. M. McDonald, L. W. Hillier, J. D. McPherson and R. H. Waterston (1997). "High throughput fingerprint analysis of large-insert clones." Genome Res **7**: 1072-1084.

Marsh, D. J., G. Theodosopoulos, V. Howell, A. L. Richardson, D. E. Benn, A. L. Proos, C. Eng and B. G. Robinson (2001). "Rapid mutation scanning of genes associated with familial cancer syndromes using denaturing high-performance liquid chromatography." Neoplasia **3**: 236-44.

Martin, P. and G. J. Swanson (1993). "Descriptive and experimental analysis of the epithelial remodellings that control semicircular canal formation in the developing mouse inner ear." Dev Biol **159**: 549-58.

Marton, M. J., C. R. Vazquez de Aldana, H. Qiu, K. Chakraburtty and A. G. Hinnebusch (1997). "Evidence that GCN1 and GCN20, translational regulators of GCN4, function on elongating ribosomes in activation of eIF2alpha kinase GCN2." Mol Cell Biol **17**: 4474-89.

Mathe, C., M. F. Sagot, T. Schiex and P. Rouze (2002). "Current methods of gene prediction, their strengths and weaknesses." Nucleic Acids Res **30**: 4103-17.

Mazaki, Y., S. Hashimoto, K. Okawa, A. Tsubouchi, K. Nakamura, R. Yagi, H. Yano, A. Kondo, A. Iwamatsu, A. Mizoguchi and H. Sabe (2001). "An ADP-ribosylation factor GTPase-activating protein Git2-short/KIAA0148 is

involved in subcellular localization of paxillin and actin cytoskeletal organization." Mol Biol Cell **12**: 645-62.

Michel, V., R. J. Goodyear, D. Weil, W. Marcotti, I. Perfettini, U. Wolfrum, C. J. Kros, G. P. Richardson and C. Petit (2005). "Cadherin 23 is a component of the transient lateral links in the developing hair bundles of cochlear sensory hair cells." Dev Biol **280**: 281-94.

Milisav, I. (1998). "Dynein and dynein-related genes." Cell Motil Cytoskeleton **39**: 261-72.

Minokoshi, Y., T. Alquier, N. Furukawa, Y. B. Kim, A. Lee, B. Xue, J. Mu, F. Foufelle, P. Ferre, M. J. Birnbaum, B. J. Stuck and B. B. Kahn (2004). "AMP-kinase regulates food intake by responding to hormonal and nutrient signals in the hypothalamus." Nature **428**: 569-74.

Mizuno, A., N. Matsumoto, M. Imai and M. Suzuki (2003). "Impaired osmotic sensation in mice lacking TRPV4." Am J Physiol Cell Physiol **285**: C96-101.

Morris, K. A., E. Snir, C. Pompeia, I. V. Koroleva, B. Kachar, Y. Hayashizaki, P. Carninci, M. B. Soares and K. W. Beisel (2005). "Differential Expression of Genes within the Cochlea as Defined by a Custom Mouse Inner Ear Microarray." J Assoc Res Otolaryngol **6**: 75-89.

Morrison, A., C. Hodgetts, A. Gossler, M. Hrabe de Angelis and J. Lewis (1999). "Expression of Delta1 and Serrate1 (Jagged1) in the mouse inner ear." Mech Dev **84**: 169-72.

Morton, C. C. (2002). "Genetics, genomics and gene discovery in the auditory system." Hum Mol Genet **11**: 1229-40.

Murphy, P. and R. E. Hill (1991). "Expression of the mouse labial-like homeobox-containing genes, Hox 2.9 and Hox 1.6, during segmentation of the hindbrain." Development **111**: 61-74.

Neyroud, N., F. Tesson, I. Denjoy, M. Leibovici, C. Donger, J. Barhanin, S. Faure, F. Gary, P. Coumel, C. Petit, K. Schwartz and P. Guicheney (1997). "A novel mutation in the potassium channel gene KVLQT1 causes the Jervell and Lange-Nielsen cardioauditory syndrome." Nat Genet **15**: 186-9.

Nicolson, T., M. Granato, C. Nüsslein-Volhard, A. Rüsch, J. P. Ruppersberg and R. W. Friedrich (1998). "Genetic analysis of vertebrate sensory hair cell mechanosensation: The zebrafish circler mutants." Neuron **20**: 271-283.

Nishikura, K. (1992). "Modulation of double-stranded RNAs in vivo by RNA duplex unwindase." Ann N Y Acad Sci **660**: 240-250.

Niwa, N., Y. Hiromi and M. Okabe (2004). "A conserved developmental program for sensory organ formation in Drosophila melanogaster." Nat Genet **36**: 293-7.

Nobes, C. D. and A. Hall (1995). "Rho, rac and cdc42 GTPases: regulators of actin structures, cell adhesion and motility." Biochem Soc Trans **23**: 456-9.

Nobes, C. D. and A. Hall (1995). "Rho, rac, and cdc42 GTPases regulate the assembly of multimolecular focal complexes associated with actin stress fibers, lamellipodia, and filopodia." Cell **81**: 53-62.

Nogueira, C. S. (2000). Modifiers of the bronx waltzer mutation. MRC Institute of Hearing Research. Nottingham, University of Nottingham. **Ph.D. Thesis:** 330.

Noramly, S. and R. M. Grainger (2002). "Determination of the embryonic inner ear." J Neurobiol **53**: 100-28.

Oh, W., L. Abu-Elheiga, P. Kordari, Z. Gu, T. Shaikenov, S. S. Chirala and S. J. Wakil (2005). "Glucose and fat metabolism in adipose tissue of acetyl-CoA carboxylase 2 knockout mice." Proc Natl Acad Sci U S A **102**: 1384-9.

Osoegawa, K., M. Tateno, P. Y. Woon, E. Frengen, A. G. Mammoser, J. J. Catanese, Y. Hayashizaki and P. J. de Jong (2000). "Bacterial artificial chromosome libraries for mouse sequencing and functional analysis." Genome Res **10**: 116-128.

Ou-Yang, H., L. Hua, Q. H. Mo and X. M. Xu (2004). "Rapid, accurate genotyping of the common -alpha(4.2) thalassaemia deletion based on the use of denaturing HPLC." J Clin Pathol **57**: 159-63.

Perrigo, G., L. Belvin, P. Quindry, T. Kadir, J. Becker, C. van Look, J. Niewoehner and F. S. vom Saal (1993). "Genetic mediation of infanticide and parental behavior in male and female domestic and wild stock house mice." Behav Genet **23**: 525-31.

Petek, E., C. Windpassinger, M. Mach, L. Rauter, S. W. Scherer, K. Wagner and P. M. Kroisel (2003). "Molecular characterization of a 12q22-q24 deletion associated with congenital deafness: confirmation and refinement of the DFNA25 locus." Am J Med Genet A **117**: 122-6.

Petit, C. (2001). "Usher syndrome: from genetics to pathogenesis." Annu Rev Genomics Hum Genet **2**: 271-97.

Pickart, C. M. (2000). "Ubiquitin biology: an old dog learns an old trick." Nat Cell Biol **2**: E139-41.

Pickles, J. O. (1988). An Introduction to the Physiology of Hearing. San Diego, Academic Press.

Pompeia, C., B. Hurle, I. A. Belyantseva, K. Noben-Trauth, K. Beisel, J. Gao, P. Buchoff, G. Wistow and B. Kachar (2004). "Gene expression profile of the mouse organ of Corti at the onset of hearing." Genomics **83**: 1000-11.

Popper, A. N. and R. R. Fay (1997). "Evolution of the ear and hearing: issues and questions." Brain Behav Evol **50**: 213-21.

Postlethwait, J., A. Amores, A. Force and Y. L. Yan (1999). "The zebrafish genome." Methods Cell Biol **60**: 149-163.

Postlethwait, J. H., Y.-L. Yan, M. A. Gates, S. Horne, A. Amores, A. Brownlie, A. Donovan, E. S. Egan, A. Force, Z. Gong, C. Goutel, A. Fritz, R. Kelsh, E. Knapik, E. Liao *et al.* (1998). "Vertebrate genome evolution and the zebrafish gene map." Nat Genet **18**: 345-349.

Premont, R. T., A. Claing, N. Vitale, S. J. Perry and R. J. Lefkowitz (2000). "The GIT family of ADP-ribosylation factor GTPase-activating proteins. Functional diversity of GIT2 through alternative splicing." J Biol Chem **275**: 22373-80.

Resendes, B. L., R. E. Williamson and C. C. Morton (2001). "At the speed of sound: gene discovery in the auditory system." Am J Hum Genet **69**: 923-35.

Ridley, A. J. and A. Hall (1992). "The small GTP-binding protein rho regulates the assembly of focal adhesions and actin stress fibers in response to growth factors." Cell **70**: 389-99.

Riley, B. B., M.-Y. Chiang, L. Farmer and R. Heck (1999). "The deltaA gene of zebrafish mediates lateral inhibition of hair cells in the inner ear and is regulated by pax2.1." Development **126**: 5669-5678.

Robertson, N. G., U. Khetarpal, G. A. Gutierrez-Espeleta, F. R. Bieber and C. C. Morton (1994). "Isolation of novel and known genes from a human fetal cochlear cDNA library using subtractive hybridization and differential screening." Genomics **23**: 42-50.

Rossetti, S., D. Chauveau, D. Walker, A. Saggar-Malik, C. G. Winearls, V. E. Torres and P. C. Harris (2002). "A complete mutation screen of the ADPKD genes by DHPLC." Kidney Int **61**: 1588-99.

Rozen, S. and H. Skaletsky (2000). "Primer3 on the WWW for general users and for biologist programmers." Methods Mol Biol **132**: 365-86.

Rzadzinska, A. K., M. E. Schneider, C. Davies, G. P. Riordan and B. Kachar (2004). "An actin molecular treadmill and myosins maintain stereocilia functional architecture and self-renewal." J Cell Biol **164**: 887-97.

Schadt, E. E., S. A. Monks, T. A. Drake, A. J. Lusis, N. Che, V. Colinayo, T. G. Ruff, S. B. Milligan, J. R. Lamb, G. Cavet, P. S. Linsley, M. Mao, R. B. Stoughton and S. H. Friend (2003). "Genetics of gene expression surveyed in maize, mouse and man." Nature **422**: 297-302.

Schafer, B. L., R. W. Bishop, V. J. Kratunis, S. S. Kalinowski, S. T. Mosley, K. M. Gibson and R. D. Tanaka (1992). "Molecular cloning of human mevalonate kinase and identification of a missense mutation in the genetic disease mevalonic aciduria." J Biol Chem **267**: 13229-38.

Schrott, A., J. L. Puel and G. Rebillard (1991). "Cochlear origin of 2f1-f2 distortion products assessed by using 2 types of mutant mice." Hear Res **52**: 245-53.

Schrott, A., K. Stephan and H. Spoendlin (1989). "Hearing with selective inner hair cell loss." Hear Res **40**: 213-9.

Schrott, A., K. Stephan and H. Spoendlin (1989). "Hearing with Selective Inner Hair Cell Loss." Hearing Research **40**: 213-220.

Schuknecht, H. F. (1974). Pathology of the ear. Cambridge, MA, Harvard University Press.

Schuler, G. D. (1997). "Sequence mapping by electronic PCR." Genome Res **7**: 541-550.

Seilhamer, J. J., T. L. Randall, M. Yamanaka and L. K. Johnson (1986). "Pancreatic phospholipase A2: isolation of the human gene and cDNAs from porcine pancreas and human lung." DNA **5**: 519-27.

Seki, N., A. Hattori, S. Sugano, M. Muramatsu and T. Saito (2000). "cDNA cloning, expression profile, and genomic structure of human and mouse RNF10/Rnf 10 genes, encoding a novel RING finger protein." J Hum Genet **45**: 38-42.

Self, T., M. Mahony, J. Fleming, J. Walsh, S. D. Brown and K. P. Steel (1998). "Shaker-1 mutations reveal roles for myosin VIIA in both development and function of cochlear hair cells." Development **125**: 557-66.

Seri, M., R. Cusano, S. Gangarossa, G. Caridi, D. Bordo, C. Lo Nigro, G. M. Ghiggeri, R. Ravazzolo, M. Savino, M. Del Vecchio, M. d'Apolito, A. Iolascon, L. L. Zelante, A. Savoia, C. L. Balduini *et al.* (2000). "Mutations in MYH9 result in the May-Hegglin anomaly, and Fechtner and Sebastian

syndromes. The May-Hegglin/Fechtner Syndrome Consortium." Nat Genet **26**: 103-5.

Shih, D. Q., M. Bussen, E. Sehayek, M. Ananthanarayanan, B. L. Shneider, F. J. Suchy, S. Shefer, J. S. Bollileni, F. J. Gonzalez, J. L. Breslow and M. Stoffel (2001). "Hepatocyte nuclear factor-1alpha is an essential regulator of bile acid and plasma cholesterol metabolism." Nat Genet **27**: 375-82.

Siemens, J., A. Reynolds, U. Müller, C. Lillo, D. S. Williams, R. A. Dumont and P. G. Gillespie (2004). "Cadherin 23 Is a component of the tip link in hair-cell stereocilla." Nature **428**: 950-955.

Silver, L. M. (1995). Mouse Genetics. New York, Oxford University Press Inc.

Skarnes, W. C., H. von Melchner, W. Wurst, G. Hicks, A. S. Nord, T. Cox, S. G. Young, P. Ruiz, P. Soriano, M. Tessier-Lavigne, B. R. Conklin, W. L. Stanford and J. Rossant (2004). "A public gene trap resource for mouse functional genomics." Nat Genet **36**: 543-4.

Smith, C. W., J. G. Patton and B. Nadal-Ginard (1989). "Alternative splicing in the control of gene expression." Annu Rev Genet **23**: 527-77.

Sobkowicz, H. M., J. E. Rose, C. V. Levenick and G. L. Scott (1988). "Morphology of the cochlea in the bronx waltzer mouse." Assoc. Res. Otolaryngol. Abstracts: 353.

Soderlund, C., S. Humphray, A. Dunham and L. French (2000). "Contigs built with fingerprints, markers, and FPCV4.7." Genome Res **10**: 1772-1787.

Sokal, I., N. Li, C. L. Verlinde, F. Haeseleer, W. Baehr and K. Palczewski (2000). "Ca(2+)-binding proteins in the retina: from discovery to etiology of human disease(1)." Biochim Biophys Acta **1498**: 233-51.

Sokal, R. R. and F. J. Rohlf (1995). Biometry: the principles and practice of statistics in biological research. San Francisco, W.H. Freeman and Company.

Söllner, C., T. Nicolson, G.-J. Rauch, R. Geisler, S. C. Schuster, J. Stemens and U. Müller (2004). "Mutations in cadherin 23 affect tip links in zebrafish sensory hair cells." Nature **428**: 955-959.

Solovyev, V. V., A. A. Salamov and C. B. Lawrence (1995). "Identification of human gene structure using linear discriminant functions and dynamic programming." Proc Int Conf Intell Syst Mol Biol **3**: 367-75.

Spoendlin, H. (1972). "Innervation densities of the cochlea." Acta Otolaryngol **73**: 235-48.

Steel, K. P. and S. D. M. Brown (1994). "Genes and Deafness." Trends Genet **10**: 428-435.

Steel, K. P. and D. Harvey (1992). Development of auditory function in mutant mice. Development of auditory and vestibular systems 2. R. Romand. New York, Academic Press**:** 221-242.

Steel, K. P. and C. J. Kros (2001). "A genetic approach to understanding auditory function." Nat Genet **27**: 143-9.

Steel, K. P., P. Moorjani and C. Barkway (1987). "The Role of Melanocytes in the Development of the Inner-Ear, Studied Using the Viable Dominant Spotting Mouse Mutant." Genet Res **49**: 255-255.

Steinmetz, M., Y. Uematsu and K. Fischer-Lindahl (1987). "Hotspots of homologous recombination in mammalian genomes." Trends Genet **7**: 7-10.

Stoss, O., F. W. Schwaiger, T. A. Cooper and S. Stamm (1999). "Alternative splicing determines the intracellular localization of the novel nuclear protein Nop30 and its interaction with the splicing factor SRp30c." J Biol Chem **274**: 10951-62.

Su, S. and R. C. Bird (1995). "Cell cycle, differentiation and tissue-independent expression of ribosomal protein L37." Eur J Biochem **232**: 789-97.

Summerton, J. and D. Weller (1997). "Morpholino antisense oligomers: Design, preparation, and properties." Antisense Nucleic Acid Drug Dev **7**: 187-195.

Suzuki, M., A. Mizuno, K. Kodaira and M. Imai (2003). "Impaired pressure sensation in mice lacking TRPV4." J Biol Chem **278**: 22664-8.

Svare, B., C. Kinsley, M. Mann and J. Broida (1984). "Infanticide: accounting for genetic variation in mice." Physiol Behav. **33**: 137-52.

Tabuchi, K., M. Suzuki, A. Mizuno and A. Hara (2005). "Hearing impairment in TRPV4 knockout mice." Neurosci Lett **382**: 304-8.

Tafti, M., B. Petit, D. Chollet, E. Neidhart, F. de Bilbao, J. Z. Kiss, P. A. Wood and P. Franken (2003). "Deficiency in short-chain fatty acid beta-oxidation affects theta oscillations during sleep." Nat Genet **34**: 320-5.

Takeno, S., R. V. Harrison, D. Ibrahim, M. Wake and R. J. Mount (1994). "Cochlear function after selective inner hair cell degeneration induced by carboplatin." Hear Res **75**: 93-102.

Tanksley, S. D. (1993). "Mapping polygenes." Annu Rev Genet **27**: 205-33.

Tasic, B., C. E. Nabholz, K. K. Baldwin, Y. Kim, E. H. Rueckert, S. A. Ribich, P. Cramer, Q. Wu, R. Axel and T. Maniatis (2002). "Promoter choice determines splice site selection in protocadherin alpha and gamma pre-mRNA splicing." Mol Cell **10**: 21-33.

Thalmann, I. and R. Thalmann Washington University Inner Ear Protein Database.

Thornton, C., M. A. Snowden and D. Carling (1998). "Identification of a novel AMP-activated protein kinase beta subunit isoform that is highly expressed in skeletal muscle." J Biol Chem **273**: 12443-50.

Torres, M. and F. Giraldez (1998). "The development of the vertebrate inner ear." Mech Dev **71**: 5-21.

Tsai, H., R. E. Hardisty, C. Rhodes, A. E. Kiernan, P. Roby, Z. Tymowska-Lalanne, P. Mburu, S. Rastan, A. J. Hunter, S. D. M. Brown and K. P. Steel (2001). "The mouse slalom mutant demonstrates a role for Jagged1 in neuroepithelial patterning in the organ of Corti." Hum Mol Genet **10**: 507-512.

Turner, C. E., J. R. Glenney, Jr. and K. Burridge (1990). "Paxillin: a new vinculin-binding protein present in focal adhesions." J Cell Biol **111**: 1059-68.

Turner, C. E. and J. T. Miller (1994). "Primary sequence of paxillin contains putative SH2 and SH3 domain binding motifs and multiple LIM domains: identification of a vinculin and pp125Fak-binding region." J Cell Sci **107 (Pt 6)**: 1583-91.

Tyson, J., L. Tranebjaerg, S. Bellman, C. Wren, J. F. Taylor, J. Bathen, B. Aslaksen, S. J. Sorland, O. Lund, S. Malcolm, M. Pembrey, S. Bhattacharya and M. Bitner-Glindzicz (1997). "IsK and KvLQT1: mutation in either of the two subunits of the slow component of the delayed rectifier potassium channel can cause Jervell and Lange-Nielsen syndrome." Hum Mol Genet **6**: 2179-85.

Van Gelder, R. N., M. E. von Zastrow, A. Yool, W. C. Dement, J. D. Barchas and J. H. Eberwine (1990). "Amplified RNA synthesized from limited quantities of heterogeneous cDNA." Proc Natl Acad Sci U S A **87**: 1663-7.

van Kuijk, F. J. and E. A. Dratz (1987). "Detection of phospholipid peroxides in biological samples." Free Radic Biol Med **3**: 349-54.

vom Saal, F. and L. Howard (1982). "The regulation of infanticide and parental behavior: implications for reproductive success in male mice." Science **215**: 1270-2.

Wallis, D., M. Hamblen, Y. Zhou, K. J. Venken, A. Schumacher, H. L. Grimes, H. Y. Zoghbi, S. H. Orkin and H. J. Bellen (2003). "The zinc finger transcription factor Gfi1, implicated in lymphomagenesis, is required for inner ear hair cell differentiation and survival." Development **130**: 221-32.

Walsh, T., V. Walsh, S. Vreugde, R. Hertzano, H. Shahin, S. Haika, M. K. Lee, M. Kanaan, M. C. King and K. B. Avraham (2002). "From flies' eyes to our ears: mutations in a human class III myosin cause progressive nonsyndromic hearing loss DFNB30." Proc Natl Acad Sci U S A **99**: 7518-23.

Waterston, R. H., A. T. Chinwalla, L. L. Cook, K. D. Delehaunty, G. A. Fewell, L. A. Fulton, R. S. Fulton, T. A. Graves, L. W. Hillier, K. Lindblad-Toh, P. An, E. Berry, B. Birren, T. Bloom, D. G. Brown *et al.* (2002). "Initial sequencing and comparative analysis of the mouse genome." Nature **420**: 520-562.

Weil, D., S. Blanchard, J. Kaplan, P. Guilford, F. Gibson, J. Walsh, P. Mburu, A. Varela, J. Levilliers, M. D. Weston, P. M. Kelley, W. J. Kimberling, M. Wagenaar, F. Levi-Acobas, D. Larget-Piet *et al.* (1995). "Defective myosin VIIA gene responsible for Usher syndrome type 1B." Nature **374**: 60-61.

Weil, D., P. Kussel, S. Blanchard, G. Levy, F. Levi-Acobas, M. Drira, H. Ayadi and C. Petit (1997). "The autosomal recessive isolated deafness, DFNB2, and the Usher 1B syndrome are allelic defects of the myosin-VIIA gene." Nature Genetics **16**: 191-193.

Westerfield, M. (2000). The zebrafish book. A guide for the laboratory use of zebrafish (Danio rerio). Eugene, University of Oregon Press.

Whitfield, T. T., B. B. Riley, M.-Y. Chiang and B. Phillips (2002). "Development of the zebrafish inner ear." Dev Dyn **223**: 427-458.

Wilkinson, D. (1992). In Situ Hybridisation: A Practical Approach. New York, Oxford University Press.

Wilson, S. M., D. B. Householder, V. Coppola, L. Tessarollo, B. Fritzsch, E.-C. Lee, D. Goss, G. A. Carlson, N. G. Copeland and N. A. Jenkins (2001). "Mutations in Cdh23 cause nonsyndromic hearing loss in waltzer mice." Genomics **74**: 228-233.

Wong-Riley, M., A. Guo, N. J. Bachman and M. I. Lomax (2000). "Human COX6A1 gene: promoter analysis, cDNA isolation and expression in the monkey brain." Gene **247**: 63-75.

Wood, J. D., S. J. Muchinsky, A. G. Filoteo, J. T. Penniston and B. L. Tempel (2004). "Low endolymph calcium concentrations in deafwaddler2J mice suggest that PMCA2 contributes to endolymph calcium maintenance." J Assoc Res Otolaryngol **5**: 99-110.

Wu, Q. and T. Maniatis (2000). "Large exons encoding multiple ectodomains are a characteristic feature of protocadherin genes." Proc Natl Acad Sci U S A **97**: 3124-9.

Yamaguchi, K., F. Yamaguchi, O. Miyamoto, K. Sugimoto, R. Konishi, O. Hatase and M. Tokuda (1999). "Calbrain, a novel two EF-hand calcium-binding protein that suppresses Ca2+/calmodulin-dependent protein kinase II activity in the brain." J Biol Chem **274**: 3610-6.

Yanase, S. and N. Ishi (1999). "Cloning of the oxidative stress-responsive genes in Caenorhabditis elegans." J Radiat Res (Tokyo) **40**: 39-47.

Zeng, C. J., N. Kouprina, B. Zhu, A. Cairo, M. Hoek, G. Cross, K. Osoegawa, V. Larionov and P. de Jong (2001). "Large-insert BAC/YAC libraries for selective re-isolation of genomic regions by homologous recombination in yeast." Genomics **77**: 27-34.

Zhang, T., P. Haws and Q. Wu (2004). "Multiple variable first exons: a mechanism for cell- and tissue-specific gene regulation." Genome Res **14**: 79-89.

Zhang, W., L. Vazquez, M. Apperson and M. B. Kennedy (1999). "Citron binds to PSD-95 at glutamatergic synapses on inhibitory neurons in the hippocampus." J Neurosci **19**: 96-108.

Zhao, S. Y., S. Shatsman, B. Ayodeji, K. Geer, G. Tsegaye, M. Krol, E. Gebregeorgis, A. Shvartsbeyn, D. Russell, L. Overton, L. X. Jiang, G. Dimitrov, K. Tran, J. Shetty, J. A. Malek *et al.* (2001). "Mouse BAC ends quality assessment and sequence analyses." Genome Res **11**: 1736-1745.

Zhao, Z., Y. Cao, M. Li and A. Meng (2001). "Double-stranded RNA injection produces nonspecific defects in zebrafish." Dev Biol **229**: 215-223.

Zheng, J. L. and W. Q. Gao (2000). "Overexpression of Math1 induces robust production of extra hair cells in postnatal rat inner ears." Nat Neurosci **3**: 580-6.

Zheng, J. L., J. Shou, F. Guillemot, R. Kageyama and W. Q. Gao (2000). "Hes1 is a negative regulator of inner ear hair cell differentiation." Development **127**: 4551-60.

Zheng, Q. Y., D. Yan, X. M. Ouyang, L. L. Du, H. Yu, B. Chang, K. R. Johnson and X. Z. Liu (2005). "Digenic inheritance of deafness caused by mutations in genes encoding cadherin 23 and protocadherin 15 in mice and humans." Hum Mol Genet **14**: 103-11.

Zine, A., A. Aubert, J. Qiu, S. Therianos, F. Guillemot, R. Kageyama and F. De Ribaupierre (2001). "Hes1 and Hes5 activities are required for the normal development of the hair cells in the mammalian inner ear." Journal of Neuroscience **21**: 4712-4720.

Zine, A., A. Aubert, J. Qiu, S. Therianos, F. Guillemot, R. Kageyama and F. de Ribaupierre (2001). "Hes1 and Hes5 activities are required for the normal development of the hair cells in the mammalian inner ear." J Neurosci **21**: 4712-20.